



SWEET ANSWERS TO THE DECADES- LONG DEBATES ON THE SUCROSE RETARDATION

Author: Weiqing, Xu

Dissertation number: 29902

DISS. ETH NO. 29902

SWEET ANSWERS TO THE DECADES-LONG DEBATES ON THE SUCROSE RETARDATION

A thesis submitted to attain the degree of

DOCTOR OF SCIENCES

(Dr. sc. ETH Zurich)

presented by

WEIQING XU

Master, spécialité matériaux innovants, Université Claude Bernard Lyon I

Master de sciences, technologies, santé. Mention chimie. Université Paris VI, Membre de la COMUE
SORBONNE UNIVERSITES

born on 10.04.1991

accepted on the recommendation of

Prof. Dr. Robert J. Flatt

Prof. Dr. Jean-Baptiste d'Espinose de Lacaillerie

Dr. Marta Palacios Arevalo

Dr. Tongbo Sui

2024

Contents

ABSTRACT	I
RÉSUMÉ	III
1 INTRODUCTION	1
1.1 GENERAL INTRODUCTION	1
1.2 OBJECTIVE OF THE THESIS	4
1.3 STRUCTURE OF THE MANUSCRIPT	5
2 STATE OF THE ART	7
2.1 GENERAL CONSIDERATIONS	7
2.1.1 <i>Hydration reactions</i>	7
2.1.2 <i>Hydration of alite</i>	8
2.1.3 <i>Hydration of C₃A</i>	15
2.1.4 <i>Hydration of OPC</i>	17
2.2 HYDRATION RETARDATION	18
2.2.1 <i>Retardation caused by chemical admixtures</i>	18
2.2.2 <i>Retardation induced by sugars</i>	19
2.3 IMPLICATIONS	27
3 MATERIALS AND METHODS	29
3.1 MATERIAL SYNTHESIS AND GRINDING	29
3.1.1 <i>Synthesis of C₃S and ²⁹Si enriched C₃S</i>	29
3.1.2 <i>Grinding of C₃S</i>	30
3.2 METHODS AND SAMPLE PREPARATIONS	31
3.2.1 <i>Paste preparation</i>	31
3.2.2 <i>Isothermal calorimetry</i>	32
3.2.3 <i>Phase separation</i>	36
3.2.4 <i>Hydration stoppage and specific surface area measurement</i>	37
3.2.5 <i>Sucrose concentration in solution</i>	38
3.2.6 <i>¹H/¹³C NMR</i>	38
4 IMPACT OF SUCROSE ON INITIAL HYDRATION KINETICS OF TRICALCIUM SILICATE	44
4.1 INTRODUCTION.....	44
4.2 RESULTS	45
4.2.1 <i>Calorimetry</i>	45
4.2.2 <i>Initial Adsorption</i>	47
4.2.3 <i>Time dependent Adsorption</i>	53
4.2.4 <i>Temperature dependence of initial adsorption</i>	56
4.3 DISCUSSION.....	58
4.3.1 <i>Evolution of adsorption in the induction period</i>	58
4.3.2 <i>Impact of sucrose on the induction period rate</i>	58
4.3.3 <i>Impact of temperature on hydration</i>	62
4.3.4 <i>Changes in the acceleration period</i>	64
4.4 CONCLUSIONS	64
4.5 ACKNOWLEDGEMENTS	65

5	IMPACT OF PORTLANDITE ON C₃S RETARDATION BY SUCROSE	66
5.1	INTRODUCTION	66
5.2	RESULTS	66
5.2.1	Calorimetry	66
5.2.2	Initial adsorption	68
5.2.3	Adsorption from Langmuir isotherm and mass balance	70
5.2.4	Impact of CH on the maximum slope of the acceleration period	72
5.2.5	Impact of CH on the velocity of hydration in induction period	74
5.3	DISCUSSION	77
5.3.1	Impact of CH on the induction period of C ₃ S without sucrose	77
5.3.2	Impact of CH on the induction period of C ₃ S with sucrose	78
5.3.3	A critical look at the proposed mechanism	80
5.4	CONCLUSIONS	81
6	IMPACT OF SUCROSE ON INITIAL HYDRATION KINETICS OF ORDINARY PORTLAND CEMENT	83
6.1	INTRODUCTION	83
6.2	RESULTS	84
6.2.1	Calorimetry	84
6.2.2	Initial adsorption	88
6.2.3	Time dependent Adsorption	94
6.3	DISCUSSION	96
6.3.1	Adsorption	96
6.3.2	Impact of temperature on hydration in absence of sucrose	99
6.3.3	Impact of sucrose on the induction period rate	104
6.3.4	Reasons of getting high saturation plateau from Langmuir isotherm	107
6.4	CONCLUSIONS	111
6.5	ACKNOWLEDGEMENTS	112
7	IMPACT OF PORTLANDITE ON OPC RETARDATION CAUSED BY SUCROSE	113
7.1	INTRODUCTION	113
7.2	RESULTS	113
7.2.1	Calorimetry	113
7.2.2	Initial adsorption	114
7.2.3	Adsorption from Langmuir isotherm and mass balance	116
7.2.4	Impact of CH on the maximum slope of the acceleration period	119
7.2.5	Impact of CH on the hydration rate in induction period	119
7.3	DISCUSSION	122
7.3.1	Impact of CH on OPC induction period without sucrose	122
7.3.2	Impact of CH on the OPC induction period with sucrose	125
7.3.3	Considerations on possible transfer from OPC to CH	126
7.3.4	Comparison with Reiter's results	127
7.4	CONCLUSIONS	130
7.5	ACKNOWLEDGEMENTS	130
7.6	APPENDIX A	131
8	CONCLUSIONS AND OUTLOOK	132
8.1	CONCLUSIONS	132
8.1.1	Main results for systems with pure C ₃ S phase	133
8.1.2	Main results for systems with OPC	134
8.2	OUTLOOK	136
9	REFERENCES	138

Abstract

In the cement and concrete industry, the use of chemical admixtures is essential to improve either the properties for fresh pastes or the hardened concrete. However, many chemical admixtures cause cement hydration retardation in addition to their main effects. Among them, sugars are a family of retards which work specifically to extend the open time by delaying the onset of cement hydration. According to early studies, sucrose is a very effective retarder in the family of sugars.

Many researchers have studied mechanisms of hydration retardation caused by sugars. Despite different hypothesis being proposed, the retardation mechanism of sucrose is still not fully understood. This can be attributed to the complexity of cement system which contains different phases, and the coupled chemical reactions taking place during each hydration period. In presence of sugars, the interaction between these molecules with different mineral surfaces as well as their behaviors at the solid-liquid interfaces adds more difficulties to such research.

In this thesis, synthetic tricalcium silicate was used as the first step to simplify cementitious systems. Due to its good ability in delaying hydration, sucrose was chosen as an example of chemical admixture for studying the mechanism of hydration retardation. Isothermal calorimetry measurements were performed *in situ* to follow hydration processes in a more reliable way. Different models were proposed for estimating sucrose adsorption from its dosage, which gave the possibility to build up the relation between rate of hydration in the induction period and sucrose adsorption, the latter being best described in terms of surface coverage.

It was shown that the hydration velocity of tricalcium silicate in the induction period decreases linearly with surface coverage of sucrose. Better said, that rate is proportional to the fraction of surface not covered by sucrose. In case where portlandite was mixed with tricalcium silicate, the hydration rate in the induction period of this blended material is enhanced by the increase surface area, which we interpret as allowing faster deposition of hydrates. Sucrose however does not seem to modify this, or to be displaced from tricalcium silicate to portlandite.

With understanding on hydration kinetics for tricalcium silicate, the second step in this work was to apply the same experimental and analytical methods to an industrial cement.

It was found that the temperature dependence of sucrose adsorption behaves differently on cement as on tricalcium silicate. As to the impact of sucrose on the rate of hydration in induction period, it was interesting to notice that in the low dosage range, it only depends on the surface coverage of sucrose on tricalcium silicate. Regarding the hydration of cement in presence of portlandite and sucrose, it seems that sucrose preferably adsorbs on the surface of tricalcium silicate phase, the transfer of sucrose molecules from this surface to portlandite surface does not take place.

In addition to these works, we also wanted to achieve direct “observations” for sucrose behaviors during hydration with NMR measurements, because of their selective and high

sensitivity on NMR active isotopes. For detecting the sucrose in pore solution, ^1H refocused INEPT NMR was successfully developed with largely enhanced sensitivity together with a quantification method. This opens the possibility of detecting mobile sucrose from a paste. However, monitoring sucrose adsorption during hydration of tricalcium silicate with this method posed many problems. Observations of sucrose in hydrated tricalcium silicate system were successful. But we failed in seeing the interaction of sucrose with this mineral surface, even though 2D HETCORE NMR and some pulse sequences based on different covalent pulse transfer were tried. For this question, maybe other surface enhanced NMR techniques can be tried in the future, such as dynamic nuclear polarization (DNP) may be more appropriate.

Résumé

Dans l'industrie du ciment et du béton, l'utilisation d'adjuvants chimiques est essentielle pour améliorer les propriétés du béton tant à l'état frais que durci. Cependant, de nombreux adjuvants chimiques retardent l'hydratation du ciment en plus de leurs effets principaux. Parmi ces adjuvants, les sucres constituent une famille de retardateurs qui agissent spécifiquement pour allonger la durée d'ouvrabilité en retardant l'hydratation du ciment. Selon les premières études, le sucrose est un retardateur très efficace dans la famille des sucres.

De nombreux chercheurs ont étudié les mécanismes de retard de l'hydratation causés par les sucres. Bien que différentes hypothèses aient été proposées, le mécanisme de retard du sucrose n'est toujours pas entièrement élucidé. Cela peut être attribué à la complexité du système cimentaire qui contient différentes phases, et aux réactions chimiques couplées qui ont lieu pendant chaque période d'hydratation. En présence de sucres, l'interaction entre ces molécules et les différentes surfaces minérales ainsi que leur comportement aux interfaces solide-liquide complexifie cette problématique encore davantage.

Dans cette thèse, le silicate tricalcique synthétique a été utilisé comme première étape pour simplifier les systèmes cimentaires. En raison de sa capacité à retarder l'hydratation, le sucrose a été choisi comme un exemple d'adjuvant chimique pour étudier le mécanisme de retard de l'hydratation. Des mesures de calorimétrie isotherme ont été effectuées *in situ* pour suivre le processus d'hydratation de manière plus fiable. Différents modèles ont été proposés pour estimer l'adsorption du sucrose à partir de son dosage, ce qui a permis d'établir la relation entre le taux d'hydratation pendant la période d'induction et l'adsorption du sucrose, qui est par ailleurs plus judicieusement décrite en termes de couverture de surface.

Il a été démontré que la vitesse d'hydratation du silicate tricalcique pendant la période d'induction diminue linéairement avec l'adsorption du sucrose. Mieux encore, cette vitesse est proportionnelle à la fraction de la surface non couverte par le sucrose. Lorsque de la portlandite est ajoutée au silicate tricalcique, la vitesse d'hydratation pendant la période d'induction de ce matériau composé est accélérée par l'augmentation de la surface, ce que nous interprétons comme résultat d'une plus ample possibilité de dépôt d'hydrates. Le sucrose ne semble pas modifier ce phénomène, ni être déplacé du silicate tricalcique vers la portlandite.

Avec la compréhension de la cinétique d'hydratation du silicate tricalcique, la deuxième étape de ce travail a consisté à appliquer les mêmes méthodes expérimentales et analytiques à un ciment industriel.

Il a été constaté que la dépendance de l'adsorption du sucrose à la température est différente entre le ciment et le silicate tricalcique. En ce qui concerne l'impact du sucrose sur la vitesse d'hydratation pendant la période d'induction, il est intéressant de noter qu'à bas dosage, celle-ci dépend uniquement de la couverture de surface du sucrose sur le silicate tricalcique. En ce qui concerne l'hydratation du ciment en présence de portlandite et de sucrose, il semble que le

sucrose s'adsorbe préférentiellement sur les surface du silicate tricalcique, le transfert des molécules de sucrose de cette surface à la surface de la portlandite n'ayant pas lieu.

En plus de ces travaux, nous voulions également obtenir des "observations" directes des comportements du sucrose pendant l'hydratation grâce à des mesures RMN, en raison de leur sélectivité et de leur grande sensibilité pour les isotopes actifs de la RMN. Pour détecter le sucrose dans la solution interstitielle, la ^1H INEPT RMN a été développée avec succès, avec une sensibilité largement améliorée et une méthode de quantification. Cela ouvre la possibilité de détecter le sucrose mobile à partir d'une pâte. Cependant, le suivi de l'adsorption du sucrose pendant l'hydratation du silicate tricalcique à l'aide de cette méthode a posé de nombreux problèmes. Les observations du sucrose dans le système de silicate tricalcique hydraté ont été couronnées de succès. Mais nous n'avons pas réussi à observer l'interaction du sucrose avec cette surface minérale, même si nous avons essayé la 2D HETCORE RMN et certaines séquences basées sur différents transferts d'impulsions covalentes. Pour traiter cette question, d'autres approches de RMN améliorée par la surface peuvent être essayées à l'avenir, comme la polarisation nucléaire dynamique (DNP), qui pourrait être plus appropriée.

1 Introduction

1.1 General introduction

Concrete is the most important building material all over the world. As a main constituent of concrete with special binding properties, Portland Cement (PC) makes it a durable material that can bear heavy loads and thus explains its wide use. PC is the most used type of cement in civil engineering and billion tons is produced per year all over the world. It is currently increasingly manufactured as a blend of Ordinary Portland Cement (OPC) and supplementary cementitious materials. However, OPC remains the most important active part of such cements and therefore is still considered as the most relevant reference system when looking at the broader picture of contemporary Portland Cement. The main content in OPC is clinker, which is composed of four main phases: Alite (pure form is C_3S), Belite (pure form is C_2S), tricalcium aluminate (C_3A) and calcium aluminate ferrite (C_4AF). The hydration products of Alite and Belite are calcium-silicate-hydrate (C-S-H) and Portlandite (CH), with C-S-H accounting for most of the binding properties.

Despite its widespread applications, concrete still faces several problems regarding its use such as shrinkage and cracking, freezing, sulphate attack, etc. Reducing the use of water without losing too much workability is also an important issue in improving the durability of this material. Apart from these issues, another problem arises from the huge consumption of this material and the associated CO_2 emissions. It is reported that the production of Portland cement contributes 5-8% of all man-made CO_2 [1]. This mainly comes from two aspects: the decarbonation of limestone during clinker production (60%) and the fossil fuels used to power the high temperature process (40%). The reason why global emissions are so high is however mainly due the very large amounts of clinker produced.

Since clinker is essential to the chemistry of Portland cement, research on reducing CO_2 emission during cement production mainly focus on blended cements, in which the clinker is partially replaced by supplementary cementitious material (SCMs) such as flay ash, silica fume, slag, calcined clays and/or limestone. Such substitutions affect not only chemical and physical properties of blended cement, but also its overall reactivity and thereby rate of strength development as well as durability.

Chemical admixtures (CAs) of different natures are therefore used in the cement and concrete industry. They refer to a group of organic compounds that play an important role in concrete design and the formulation of concrete with a low environmental impact [2]. Their importance shows on aspects of modifying properties of fresh pastes and/or hardened concrete. For example, superplasticizers change rheological behaviors of fresh concrete [3]; retarders and accelerators modify the hydration kinetics of cement [4], [5], which helps in adjusting the opening window for concrete placing; other chemical admixtures such as shrinkage reducers [6] and air entrainers [7] work for improving durability of structures.

Chemical admixtures act at the interfaces in the system. This is the reason for their big impact at low dosage [2]. Interfaces of greatest interest are those between solids and liquids (Figure 1.1), where most of the important processes regarding cement hydration takes place. The working mechanism of many chemical admixtures, such as superplasticizers and retarders, involves the adsorption of those compounds at a solid-liquid interface. Therefore, understanding the processes that takes place at that interface, and the interactions between chemical admixtures and solid surfaces are of great importance, with significant practical implications.

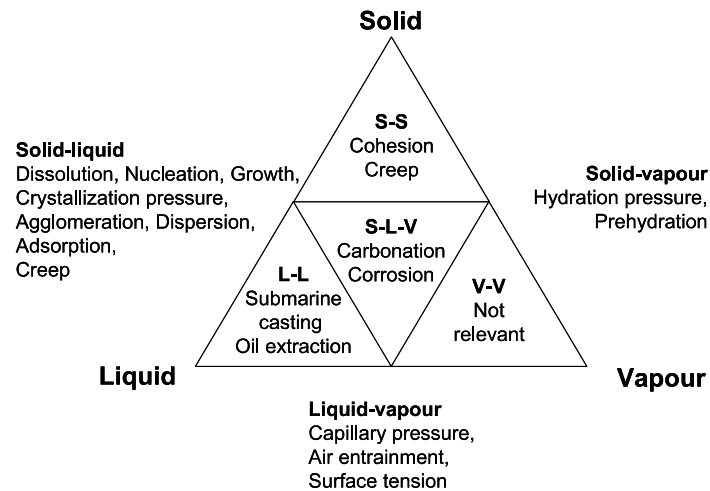


Figure 1.1. Illustration of the role played by different surfactant in the system. S-S: solid-solid; L-L: liquid-liquid; V-V: vapor-vapor and S-L-V: solid, liquid-vapor [2].

Despite their high effectiveness, chemical admixtures may lead to serious side-effects in causing undesired retardation of cement hydration. Many researchers have studied this effect since decades. However, as illustrated in Figure 1.2 with a model cement [8], the hydration of cement is a very complex process that includes several chemical reactions which dominate different stages of hydration in a coupled way. This makes studying how chemical admixtures interfere with these reactions challenging. In addition, the presence of different reactive minerals phases renders understanding the adsorption behaviors of chemical admixtures during cement hydration more complex. Therefore, although several mechanisms have been proposed to explain the cause of hydration retardation by chemical admixtures, there are still many questions that remain debated. Importantly also, owing to the diversity in the chemical structure of chemical admixtures, it can be expected that not all may affect cement hydration in the same way.

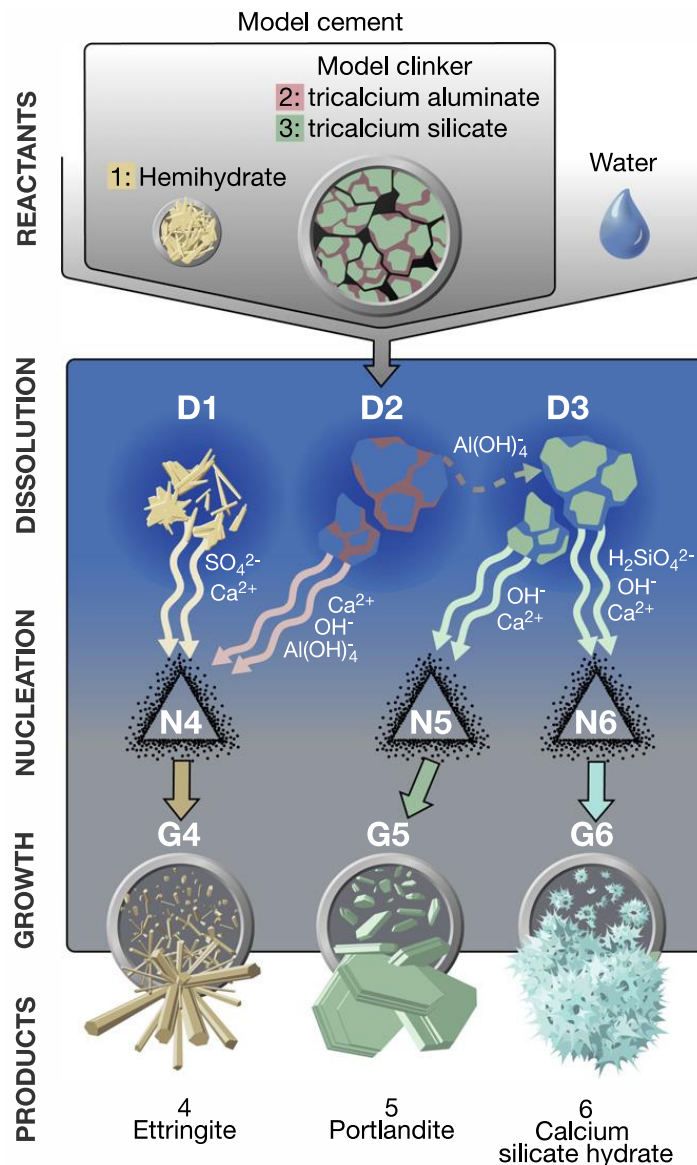


Figure 1.2 Schematic representation of the reaction in water for a model cement, coupled of hemihydrates and the model clinker that contains 20 wt.% tricalcium aluminate and 80 wt.% tricalcium silicate [8].

To simplify the problem, many studies regarding to retardation caused by chemical admixtures targets on one of the pure clinker phases (alite or C_3S in most of the cases) and with one kind of chemical admixtures (family of sugar or sucrose). However, such studies often may oversimplify the system, raising concerns about the relevance of results to real systems. For example, studying C_3S dissolution in a highly diluted system to prevent precipitation of hydrates, provides useful though only partial information that must be contextualized with respect to denser systems that are relevant to practice.

Beyond the simplification of systems to pure components, it should not be forgotten that cement includes many reactive phases that influence each other through the pore solution.

Therefore, while the value of simplified hydration systems should be appreciated, keeping conclusions in check with real cement should not be overlooked.

1.2 Objective of the thesis

The objective of this thesis is to better understand how sucrose retards the hydration of cement. It places a specific focus on the impact of sucrose dosage and temperature on hydration kinetics in the induction period. This is of particular relevance to practice as this period relates to one during which only low advancement of the hydration reaction occur.

It has been our objective to shed light into the mechanisms controlling the hydration rate in that period, and in particular how they may be modified by sucrose. In this sense, we chose to study our systems at different temperatures because this can provide activation energies that may help to identify the nature of the reactions at stake. In particular, it can help to position the relevance of our findings on C_3S for cement.

Indeed, as a first step we decide to simplify the system by using pure C_3S instead of cement (chapter 4). We did this at pH 13 to obtain similar dissociation degrees of sucrose than in OPC. Even if this constitutes an important step to make our model system more representative of question, it was clear that a reality check would be needed. In this sense, temperature dependence and activation energies were seen as a useful way of probing how relevant the behavior of pure C_3S is with respect to that of OPC (chapter 4 and 6).

Another founding aspect of this PhD was the desire to investigate the role of adsorption of sucrose and in particular its potential ability to inhibit dissolution of C_3S . In this sense, we saw the possibility of using CH to consume sucrose as a potential to test hypothesis relating to those mechanisms. This motivated the additions of CH to C_3S and to cement, respectively reported in chapters 5 and 7.

This PhD has innovated in terms of experimental protocols but establishing the systematic use of in-situ mixing, within calorimetry cells, a step that was crucial to obtain meaningful results. Further to this particular care concerning temperature was found to be essential and turned out to be another key factor in obtaining meaningful data resolving long-standing open questions from the literature.

Beyond this, a key finding of this PhD was achieved through the data analysis path followed. This constituted first deciding to analyze average hydration velocities in the induction period and then to normalize them by the velocity in absence of sucrose. The most important finding here is that this normalized velocity decreases linearly with the surface coverage of C_3S by sucrose. In other words, the average velocity in the induction period is controlled by the fraction of C_3S surface left free to react. This very simple and elegant conclusion could however only be reached thanks to the long and often painful method developments summarized above and that included:

- Massive production of pure C_3S and reliable grinding processes, with material characterizations by X-ray diffraction for quality control, laser diffraction for particle size distribution and BET measurement for the specific surface area.
- Well-controlled protocol for sucrose adsorption measurements on different mineral surfaces, including mixing, phase separation, filtering pore solution, stopping hydration and drying of the paste.
- Unique and controlled way for paste preparation being used in all experiments.
- For calorimetry measurements, a reliable way for mixing is used. Regarding to analysis based on hydration curve, a method of baseline correction is defined and applied regarding to the need.
- A new NMR pulse sequence designed to detect sucrose in pore solution from a paste with enhanced sensitivity. A method for quantification from this measurement is also developed.

1.3 Structure of the manuscript

The manuscript is structured as follows:

Chapter 2 presents the state-of-the-art in two main parts, respectively covering hydration and its retardation by chemical admixtures. The first part contains 4 sub sections relating to the general hydration process, hydration of Alite (C_3S), hydration of C_3A and hydration of OPC where aluminate-silicate-sulfate balance is involved. The second main part reviews hydration retardation caused by chemical admixtures. It starts by a general introduction, then focuses on retardation caused by sugars and related hypotheses on underlying retardation mechanisms.

Chapter 3 presents the materials and methods. It includes protocols for massive production of C_3S and grinding, which contribute the basis of this work. Sample preparations related to main characterization methods are also presented. Additionally, according to the special working conditions of some instruments or methods, strategies are developed for getting reliable data. These strategies include in-situ calorimetry measurements, baseline corrections for heat flow curve, and quantifying ^{13}C labeled sucrose in pore solutions by liquid state NMR with enhanced sensitivity.

Chapter 4 includes works on pure C_3S hydration. The key idea in this chapter is to understand how the hydration kinetics of C_3S is affected by sucrose dosages and temperatures. Sucrose adsorption isotherms are obtained at different temperatures. We establish procedure to reliably estimate the surface coverage by sucrose in all calorimetry experiments. With careful analysis of calorimetry curve, the rate of hydration in the induction period is defined using the hydration onset time and the degree of hydration at the onset. A key finding is that the normalized velocity

decreases linearly with the surface coverage. The simple and elegant result is expected to have a major impact in the field.

Chapter 5 followed up on chapter 4 by adding Portlandite to pure C_3S and applying the same experimental protocols. A first important finding is that the addition of CH appears to accelerate the hydration of C_3S proportionally to the increase in the surface to liquid ratio. More importantly for our overall objective, sucrose does not appear to transfer from C_3S to CH, contrary to previous reports in the literature.

Chapter 6 and 7 present work being done on cement and blended cement/portlandite system as we did in chapter 4 and 5, respectively.

In Chapter 6, the adsorption of sucrose on cement at different temperatures is analyzed with the same models developed in chapter 4. It is observed that sucrose has a much lower affinity for cement than it does for C_3S . However, when analyzing the impact of adsorbed sucrose on hydration kinetics, we find a behavior of similar nature to that observed on C_3S , namely that hydration rate decreases linearly with adsorption. Interestingly, the adsorption plateau that can be extrapolated from that regime is compatible with adsorption on pure C_3S . However, that value is much lower than the adsorption plateau measured on cement, suggesting that at higher dosages other phases are consuming the sucrose. This is supported by the fact that at high dosage incremental retardation decreases. This paints a consistent picture of how sucrose causes retardation both on pure C_3S and on OPC, but it also highlights that a much more careful analysis is required with OPC. In fact, without our previous work on pure C_3S it would probably not have been possible to reach very meaningful conclusions about the mechanism underlying the retardation caused by sucrose to OPC.

In chapter 7, we study the hydration of cement in presence of CH and sucrose as in chapter 5. This represents a further step in adding complexity to our system and testing our hypothesis. Globally, our analysis indicates that this system can be well rationalized by our conclusions about cement from chapter 6 and those on CH from chapter 5, with the basic analysis from chapter 4 remaining valid and appearing as a main result of this thesis.

In chapter 8, summarizes the main conclusions of this PhD. Then in the second part of that chapter, some thoughts for possible directions in future research are given as outlook

2 State of the Art

2.1 General considerations

This state of the art chapter is divided into two main parts, both of central importance to this PhD, namely cement hydration, and the retardation of that hydration by chemical admixtures.

We adopt the cement chemistry notation whereby C = CaO, S = SiO₂, A = Al₂O₃, F = Fe₂O₃ and H = H₂O.

2.1.1 Hydration reactions

Ordinary Portland Cement (OPC) is the product of co-grind Portland cement clinker with a source of calcium sulfate. It contains various mineral phases that react with water through dissolution of anhydrous phases and precipitation of hydrates. This PhD aims at understanding how sucrose delays the hydration of OPC, which is why we first need to examine the hydration of OPC taken alone. In doing so we successively examine the hydration of the pure phases tricalcium silicate (C₃S) and tricalcium aluminate (C₃A), as well as their combined reaction and the role played by calcium sulfate therein.

The hydration of Ordinary Portland Cement (OPC) is a complex process due to its chemical composition and numerous simultaneous reactions. Indeed, its hydration involves a collection of chemical processes that may occur in series, in parallel or in more complex sequence or coupling. These chemical processes are defined by Bullard et al. [9] as summarized below:

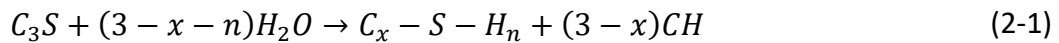
- a) Dissolution/dissociation of molecular units from the surface of solid in contact with water.
- b) Diffusion that describes the transport of solution components through the pore solution or along the solid surface in the adsorption layer.
- c) Nucleation that refers to the precipitation of hydrates on solid surfaces or in solution.
- d) Growth of hydrates that involves surface attachment.
- e) Complexation between simple ions to form complexes or adsorbed molecular complexes on solid surfaces.
- f) Adsorption of ions or other molecular units at the surface of solid.

In what follows, the bibliographic overview on OPC hydration will start with the hydration of alite, the most abundant phase that dominates OPC hydration. It is followed by a section dedicated to the hydration of C₃A, the most reactive phase in OPC clinker. Finally, we examine how OPC hydration is affected by the combined effects of aluminate and silicate phases.

2.1.2 Hydration of alite

Alite is the most abundant phase (50-70%) in OPC clinker, the pure form of this phase is tricalcium silicate, noted as C_3S . Because of its importance it has often been studied alone to elucidate in a simpler system the reaction mechanisms controlling OPC hydration. This approach is also used in this PhD, as we examine the effect of sucrose on C_3S hydration (chapter 4).

The hydration of C_3S dominates the overall hydration kinetics of OPC and results in the formation of two hydrates: calcium-silicate-hydrate (C-S-H) and portlandite (CH). The former is an amorphous or poorly crystallized phase with variable stoichiometry, which is responsible for binding properties and long-term strength development of cement, while the latter is a crystallized phase. The hydration reaction of C_3S can be describe by equation (2-1):



where n represents the water to silica ratio in C-S-H, while x is the calcium to silica ratio in that phase and varies between 1.2 and 2.1.

The hydration of C_3S can be followed by isothermal calorimetry. Results plotted as heat flow versus hydration time provide insights into the hydration kinetics. Figure 2.1 shows a typical calorimetry curve measured for alite hydration. It shows that the whole process includes different stages which are related to different rate-limiting mechanisms: 1) initial reaction; 2) period of slow reaction or induction; 3) acceleration and 4) deceleration period.

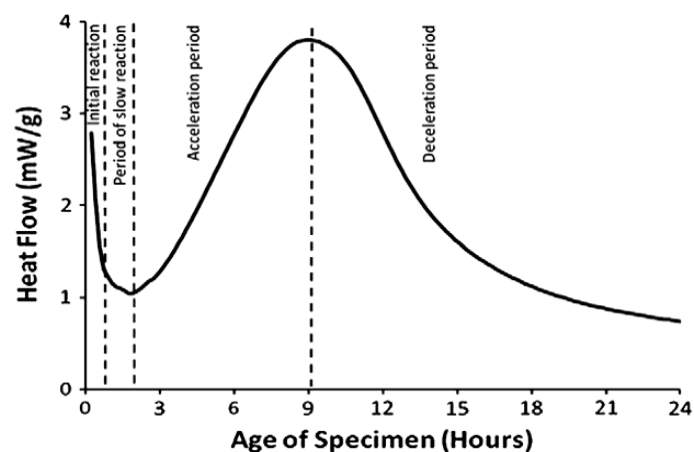


Figure 2.1. Rate of alite hydration in function of time given by an isothermal calorimetry measurement [9].

The main focus of this PhD is placed on the induction period and the extent to which sucrose may extend it. For this reason we place more emphasis in discussing factors controlling it, and in particular what triggers its end.

2.1.2.1 Initial reaction and the induction period

The first peak that occurs in the first hour refers to a rapid reaction between C_3S and water that takes place immediately after wetting. In this period, the dissolution of C_3S is the main contributor to this highly exothermic peak. However, the reason why the rapid deceleration happens is still under debate. Several hypotheses were proposed in previous works [10]. Here, we only present the protective membrane theory and dissolution control theory. The protective membrane theory used to be the most discussed ones in the past, but the dissolution control theory takes its place in recent research [9], [11], [12].

Protective membrane

This hypothesis refers to the formation of protective membrane on the surface of alite that hinder its dissolution, which further slows down the hydration. Stein [13] and Jennings [14] argued for the existence of a continuous but thin metastable C-S-H layer. Jennings [15] reviewed the solution composition data from literatures covering several decades and found out that they distributed along two master curves as shown in Figure 2.2. A later work from the same person [16] proposed that at first a metastable C-S-H layer forms that is characterized by a high solubility and protective properties for C_3S surface. This layer would then transform into a more stable but permeable C-S-H with low solubility.

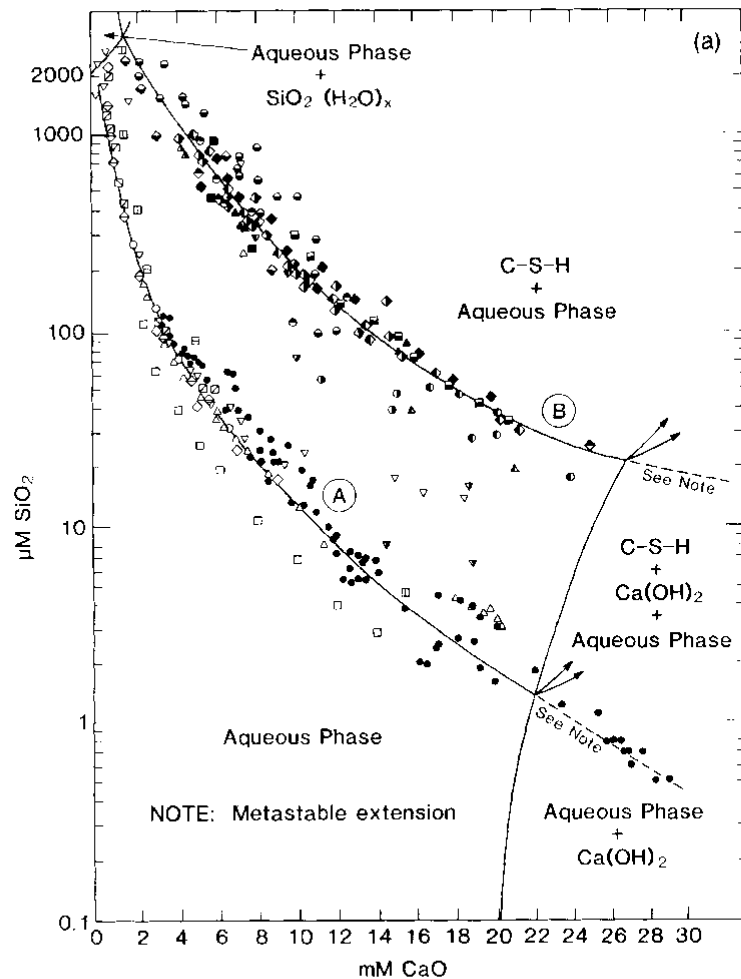


Figure 2.2. Concentrations of silica (y-axis in $\mu\text{mol/L}$) and calcium (x-axis in mmol/L) reported for cement paste pore solution. The logarithmic scale is used in y-axis to help to separate the point at high CaO concentrations [15].

Among these works, there has always no direct experimental evidence for the existence of such metastable layer, which poses the major difficulty in the protective membrane theory. This mechanism has greatly lost in popularity over the past decade at the expense of dissolution control.

Dissolution control

The second widely discussed hypothesis that explains the first deceleration and induction period is the slow dissolution step.

Under this hypothesis, Barret et al. [17], [18] firstly proposed that a “superficially hydroxylated layer” forms on C_3S once it is in contact with water, and that the slow dissociation rate of ions from this layer slows down the hydration. Nonat et al. [19], [20], [21] support the appearance of hydroxylated layer on C_3S surface, but they explained the slow dissolution of C_3S based on the steady state balance between C_3S dissolution and initial growth of C-S-H. They stated that the apparent solubility of this hydroxylated layer is much lower than that for C_3S , and the

dissolution rate decreases with the increasing of calcium hydroxide concentration. Once the supersaturation degree for C-S-H nucleation is reached, C-S-H precipitates on C_3S surface. In 2016, the existence of the hydroxylated layer is experimentally confirmed by 2D NMR measurement on a C_3S sample where the hydration is stopped at induction period [22].

Juilland et al. [23] proposed another theory under dissolution control mechanism. It is based on crystal dissolution from geochemistry to explain the first deceleration and induction period. They concluded that the dissolution is highly dependent on solution concentration. When alite is “just” in contact with water, the undersaturation level is very high, the dissolution is favored because etch pits could also form on plain surfaces. The undersaturation level will then quickly decrease and move into a regime where the etch pits can only form at surface defects (Regime II in Figure 2.3). As the concentration of ions keep increasing, the undersaturation continues to decrease until it is lower than the activation energy for the creation of etch pits. The dissolution is therefore largely slowed down compared to the very beginning of hydration because it is limited to step retreat at the pre-existing roughness.

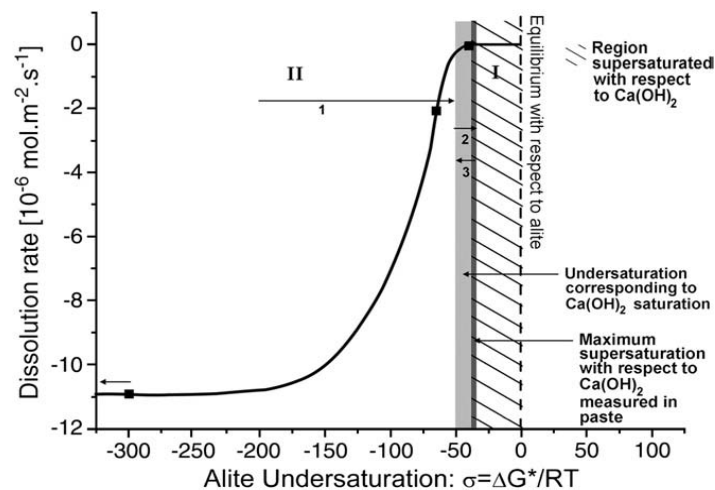


Figure 2.3. Schematic representation of dissolution rate as a function of undersaturation level. Zone II represents fast dissolution regime controlled by etch pits formation. Zone I is the slow dissolution regime where only step retreat takes place [23].

This non-linear decrease of the dissolution rate in function of decreasing undersaturation has also been proven in many other works [24], [25], [26], [27], [28], [29], [30], [31]. However, it should be pointed out that those studies were performed under very diluted conditions in order to prevent precipitation of hydrates. So, the dissolution rate obtained from these works are not representative of the dissolution rate in real pastes from a quantitative point of view [32].

Another important conclusion obtained by Juilland et al. [23] is that the rate of reaction depends on the density of defects, which strongly affects the dissolution in the induction period and its length. This can be modified by post-thermal annealing treatment of alite to decrease the density of surface defects. Figure 2.4 shows that the calorimetry curve of such an annealed

sample has a longer induction period. The same trend was also observed by Pustovgar et al. [33].

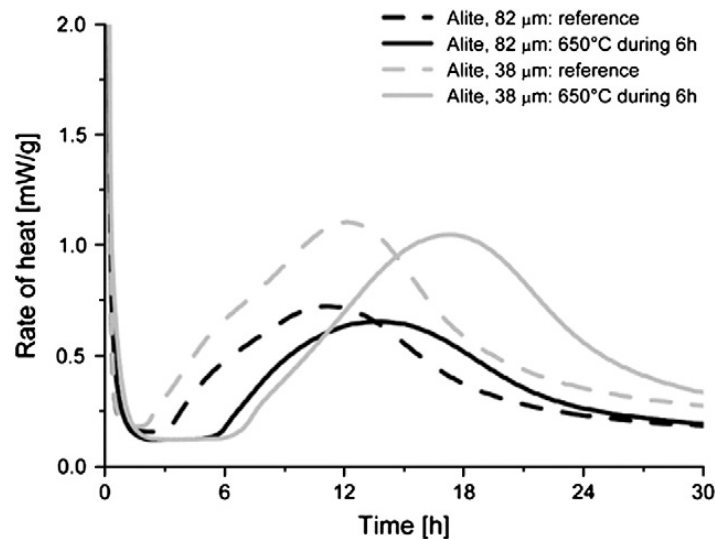


Figure 2.4. Heat evolution of alite untreated in discontinuous curve and treated at 650 °C for 6h in continuous curve [23].

Let us return to the initial reaction of C_3S with water and the rapid drop of silicate concentration in solution. This goes along with C-S-H nucleation, a process that continues during the induction period. At some point the reaction accelerates, putting an end to the induction period and a start to the onset for the acceleration period. The cause for this change in rates remains debated, but available growth surfaces appear to play a role. For example, Mantellato et al. [34] proved that the heat rate for an OPC hydration in this transition period is proportional to the specific surface area, which very likely implies a process of nucleation and growth [35], but analysis of the pore solution is needed to support this conclusion. Thomas et al. [36] added C-S-H seeds to hydrating C_3S suspensions and observed a significant acceleration of hydration with shortened induction periods and increased slopes in the acceleration period. Moreover, the effect of acceleration is proportional to the amount of C-S-H seeds added. This raises the importance of available surfaces of C-S-H nuclei for ending the induction and stepping into acceleration period.

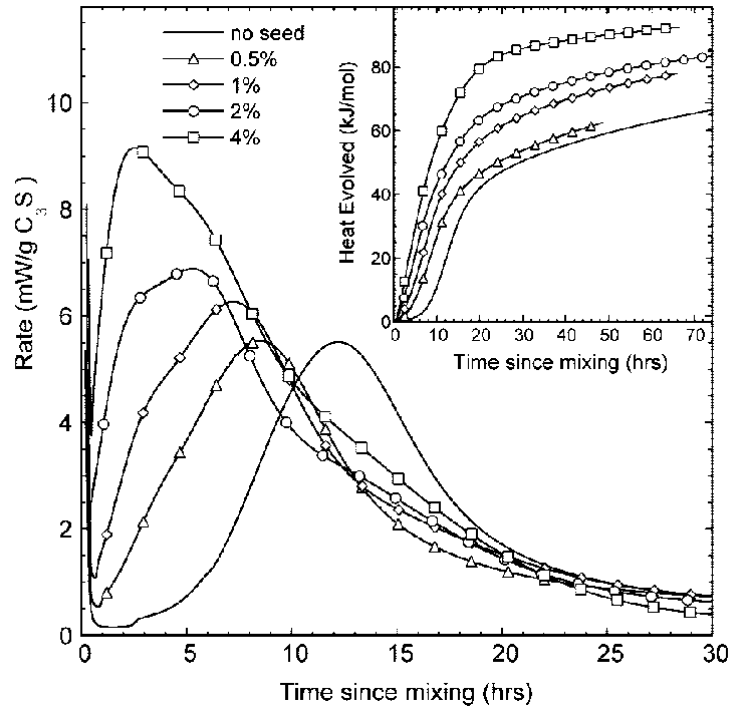


Figure 2.5. Effect of C-S-H seed on the early C_3S hydration. [36].

2.1.2.2 Acceleration period

The start of acceleration period is considered by some researchers just as the end of a slow reaction. But it is generally accepted that it is the moment when the system reaches a critical point for the rate of nucleation and growth of hydrates to increase [9]. There are a lot of works supporting the idea that the rate-controlling step for hydration in this period is the nucleation and growth of C-S-H on mineral surfaces [10], [17], [19], [35], [37], [38]. Therefore, studies on the growth mechanism of C-S-H and its structure become important.

The growth mechanism of C-S-H is still much debated. Regarding the structural arrangement, there are different views described in the literature: aggregation of nanoparticles [39], [40], [41], large but defective sheets of silicate layers [42].

According to the first theory, C-S-H particles grow until a characteristic size of several nanometers. Then, they remain stable for an extended period during which they could act as new surfaces for further nucleation, or form aggregates with other C-S-H nanoparticles [36].

Regarding to the second theory, Gartner [42] proposed a mechanism for the growth of branching sheets. The works mentioned the formation of multilayer tobermorite-like structure by the attachment of silicate tetrahedra at growing silicate chains on preformed single layer silicate sheets, with calcium and hydroxyls incorporate between layers. This mechanism is compatible with observed kinetics of hydration, and it may explain the high cohesive strength of C-S-H.

2.1.2.3 Transition from induction period to acceleration period

The moment when hydration transits from the induction period to the acceleration period is called the onset. Gartner et al. [10] summarized four mechanisms being proposed to explain the onset:

- a) Nucleation and growth of C-S-H firstly form a metastable protective layer on the surface of anhydrous C_3S . The end of induction period refers to a destabilization of this layer and a transformation of it to a more permeable phase [16], [43], [44].
- b) The nuclei of stable C-S-H formed during initial reaction grow at a nearly exponential rate, which is the rate controlling step for the start of acceleration period [17], [21].
- c) Initial hydration products form a semipermeable membrane which encloses the inner solution, it is then destroyed by osmotic pressure [45].
- d) The nucleation and growth of CH are poisoned by silicates during induction period. Once the supersaturation level is sufficient to overcome this effect, the induction period ends [44].

A previously mentioned the passivation layer theory has lost credibility, so the case a) does not appear a credible argument. Mechanism b) is widely adapted and is actively under discussion as we presented shortly before. Mechanism c) has not received much attention and it appears quite unrealistic for solution to remain trapped in a hydrate layer as proposed. Mechanism d) has been debated a lot in the literature. A case can clearly be made for the fact that when CH precipitates it benefits the dissolution rate of C_3S . However, this does not imply that CH precipitation triggers the end of the acceleration period. There are certainly cases where this can be the case, but there have also been cases reported where it isn't. A key question is to determine what the situation is for normal cementitious systems. For this thesis in particular a central question is to see how sucrose may affect such a mechanism.

2.1.2.4 Deceleration period

In deceleration period, the rate of hydration decreases. While it is not considered in this PhD, a brief summary of its main features is provided for completeness. Based on the Avrami equation, the deceleration happens when the growing region for hydrate starts to impinge and the available surface for growing decreases. Bishnoi and Scrivener [46] indicated that if C-S-H in early age paste has a similar density as in mature pastes, then impingement is very limited at the peak and deceleration should not happen. Therefore, they proposed that the growth of C-S-H occurs firstly in a diffuse manner and then densifies. Bazzoni [47] showed that the increase of water to cement ratio does not affect much the position of the main peak. This is in agree with the prediction by using a densification mechanism. In the same work, Bazzoni observed C-S-H with well-defined needle-shape outside the grains and proposed that once the C-S-H reaches a complete coverage of the C_3S surface, there is a transition from outer product to inner product growth, meaning that C-S-H precipitates at the interface of anhydrous grains. This leads to a densification of the system with decreased rate of reaction.

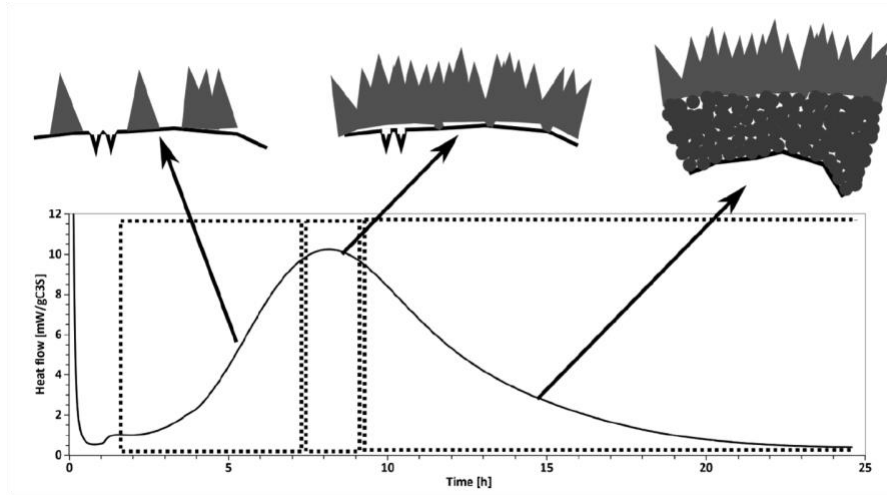
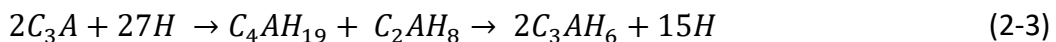
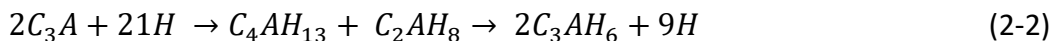


Figure 2.6. Representation of the hydration mechanisms during hydration kinetics. C-S-H firstly grow as outer product. Once the surface is completely covered by needles, a second growth model which refers to inner growth initiate [47].

2.1.3 Hydration of C₃A

Tricalcium aluminate is one of the main phases and the most reactive phase in OPC clinker. It plays an important role in the very early hydration, workability, setting and durability of cement. The hydration of C₃A in the absence of calcium sulfate is very fast and leads to the formation of various of aluminate hydrates such as C₄AH₁₃, C₄AH₁₉ and C₂AH₈ [48], [49], [50]. Those hydrates are poorly crystallized and will transform to hydrogarnet, noted as C₃AH₆. The transformation from these metastable phases to the stable one happens with in 25 min at room temperature and the rate of transformation increases with temperature [48]. This whole process leads to a rapid loss of workability, which is called “flash set” and is normally undesired in most applications. The hydration reactions of pure C₃A in the absence of any other anions can be summarized as the followings:



To avoid this rapid setting and therefore extend the open window for manipulation, a source of calcium sulfate is added to control the reaction of C₃A. It is normally added in the form of Gypsum (CaSO₄ · 2H₂O) and/or anhydrate (CaSO₄), but hemihydrate is often also presenting due to dehydration of Gypsum during the grinding step in clinker production.

The hydration of C₃A in presence of Gypsum to form ettringite is expressed in equation (2-4):



Figure 2.7 shows a typical heat release curve of C₃A hydration with gypsum [51]. The whole curve can be divided into 3 stages. Stage 1 corresponds firstly to a rapid heat release in very short time then followed by a low level of heat release. The main hydration product in this period is ettringite. The activation energy of this stage is found to be around 40-80 kJ/mol [52] as presented in Table 2.1. As these values are much higher than 20 kJ/mol, which is a typical value reported by Lasaga to differentiate surface controlled (> 20 kJ/mol) and transfer controlled (< 20 kJ/mol) reaction [53], the mechanism of hydration in this stage is unlikely to be diffusion controlled. This is in agreement with the finding of Minard et al. [54], who suggested that the hydration during this first stage is controlled by the dissolution of C₃A, and this dissolution is slowed down by the adsorption of sulfate and calcium ions on the active sites on C₃A surface but not by the formation of barrier layer of hydrate on its surface [55]. This theory is also supported by several other authors who reported that the C₃A hydration is effectively controlled by the specific surface area of C₃A, which implies that it is controlled by surface mechanisms [9], [56], [57]

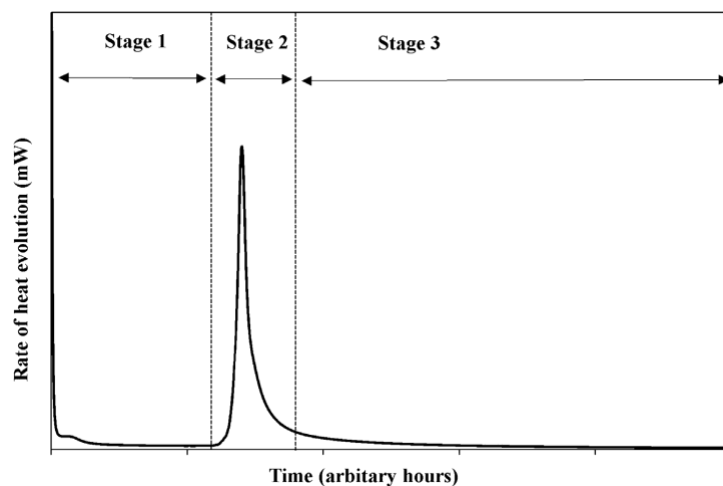


Figure 2.7. A typical heat release curve of C₃A hydration in presence of Gypsum [51].

Table 2.1. Activation energy calculated for C₃A-gypsum systems with 3 different gypsum replacements: 10%, 20% and 35% gypsum. First stage of the reaction: in the presence of gypsum. Second stage: acceleration after gypsum depletion [52].

	E_a first stage (kJ/mol)	E_a second stage (kJ/mol)
C ₃ A_10G	44 ± 11	21 ± 12
C ₃ A_20G	79 ± 1	59 ± 8
C ₃ A_35G	80 ± 2	44 ± 9

If gypsum is insufficiently available or fully consumed, where the latter is the case for the end of stage 1 on the hydration curve, ettringite will further react with the excess of C₃A to form calcium aluminosulfate according to equation (2-5). And the hydration curve moves forward to stage 2 with the appearance of a hydration peak that includes fast acceleration and

deceleration periods. The nature of the mechanism controlling hydration in this period is under debate. Minard et al. [54] proposed that this stage is controlled by dissolution as the stage 1 and the sharp increase in heat release is resulted from the desorption of calcium and sulfate ions. However, Quennoz and Scrivener [52] found that the shape of the hydration peak is not representative of a dissolution-controlled mechanism.



Stage 3 shows low heat release in long term, which is continuous until the end of reaction.

In some situations, such as an under-sulfated system, the hydration of C_3A and Gypsum can directly cause the precipitation of monosulfate without ettringite formation (Equation (2-6)).



2.1.4 Hydration of OPC

2.1.4.1 Stages of hydration

As mentioned before, OPC clinker is mainly composed of silicate and aluminate phases, co-ground with a small amount of calcium sulfate. The heat release of OPC hydration can also be divided into different stages as shown in Figure 2.8 [58].

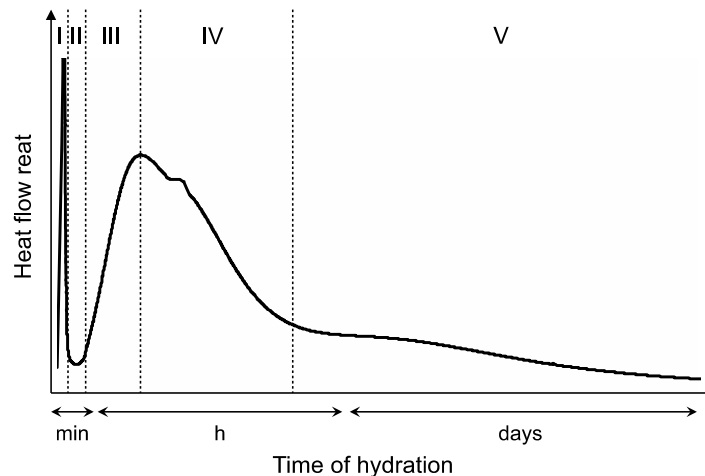


Figure 2.8. Schematic representation of the OPC heat release and illustration of different stages during hydration of OPC [58].

As for alite, stage I refers to the wetting of cement surface and a fast dissolution of anhydrous phases. The formation of ettringite from reaction of aluminate phase with calcium sulfate also takes place in the same period. In stage II, the hydration is largely slowed down, and it is followed by the start of main hydration peak that corresponds to the massive production of C-

S-H and CH. The reaction is then slowing down in stage IV. A small peak appears on the shoulder of main hydration peak, which is related to the sulfate depletion point. The stage V is a period where the material continues to harden, but at a much slower rate. A low, broad peak can be seen because of the formation of AFm [9].

2.1.4.2 Silicate-Aluminate-sulfate balance

With understanding on hydration of pure phases and a general view on cement hydration process, it is necessary to investigate how the different hydration reaction may influence each other.

A work from Tenoutasse [59] illustrates the importance of silicate-aluminate-sulfate balance. In this work, isothermal calorimetry measurements were done on mixtures containing 80 wt.% alite and 20 wt.% C_3A . When such a mix hydrates without gypsum, it is observed that the silicate hydration peak is almost fully suppressed by hydration of C_3A . When gypsum is added into the system, the sulfate depletion point is shifted to later time. Moreover, with increasing of gypsum content, the extent of C_3S hydration increases. With 4 wt.% gypsum addition, the peak for the aluminate reaction and the one for C_3S hydration revert their order of appearance, with the sulfate depletion point then appearing after the main silicate peak. When further increasing the gypsum content, the sulfate depletion point is further delayed but the position of silicate main peak does not change.

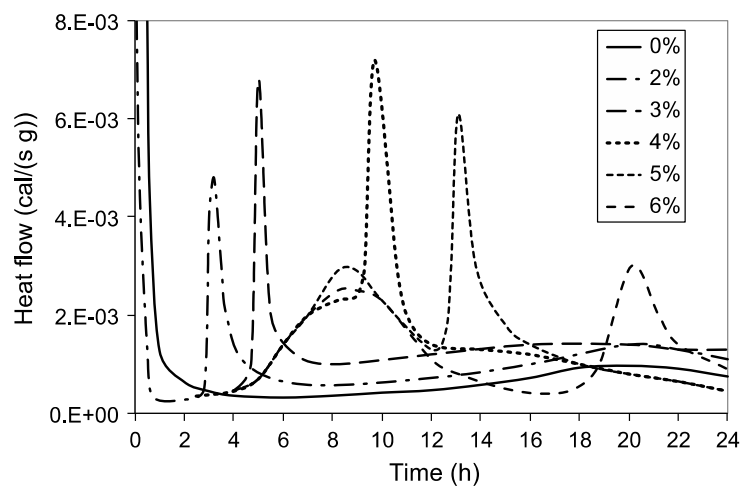


Figure 2.9. Calorimetry measurements performed on mixtures of 80 wt.% alite and 20 wt.% C_3A , with variable amount of gypsum [59].

2.2 Hydration retardation

2.2.1 Retardation caused by chemical admixtures

Chemical admixtures are nowadays widely used in application for modifying the properties of fresh or hardened concrete and for modifying the rate of cement hydration. Beside of their main effects, many chemical admixtures also cause undesired retardation, which can be affected by their dosage, chemical nature, molecular structure, time of addition, as well as the characteristics of cement.

The retardation is normally shown as prolonged induction period on a calorimetry curve. However, the retardation caused by chemical admixtures is not always only reflected as a delay of the onset, but it may also translate as a change of slope in the acceleration period and/or the displacement of the sulfate depletion peak [60].

The mechanism of hydration retardation caused by chemical admixtures is still unclear [61]. Different hypotheses have been proposed to explain it and are summarized in the following [62]:

- a) Complexation of calcium ions
- b) Hindering the dissolution of anhydrous phases
- c) Hindering nucleation and growth of hydrates
- d) Perturbation of the aluminate-silicate-sulfate balance

Since we only focus on the hydration retardation caused by sugar in our study, the bibliographic review for the mechanisms of retardation only focuses on that topic and is presented in more detail in the next section.

2.2.2 Retardation induced by sugars

Sugars are used as retarders for cement hydration. However, their effectiveness in causing retardation can be different from one to the other, depending on their nature as well as the molecular structure. Thomas and Birchall [63] classified sugars based on their retarding capacity into three categories as presented in Table 2.2. The reducing sugars being studied in their work are all good retarders. But the non-reducing sugars behave very differently to the two extents. Among them, sucrose – the sugar we will use in our study – is categorized as excellent retarder.

Table 2.2. Classification of sugars based on their retarding capacity [63].

Non-retarding	Good retarders	Excellent retarders
α -Methyl glucoside ^b	Glucose ^a	Sucrose ^b
Thehalose ^b	Maltose ^a	Raffinose ^b
	Lactose ^a	
	Cellobiose ^a	

a: reducing sugar.

b: non-reducing sugar

Zhang et al. [64] worked on the impact of molecular structure of sugars on retardation. They found that aliphatic sugar alcohols retard setting of C₃S and OPC. The effectiveness of these aliphatic sugars increases with the number of threo-hydroxy pairs and with the total number of hydroxy groups on the molecule.

Moving towards mechanisms possibly controlling the retardation by sugars we next review the four possibilities listed in section 2.2.1.

2.2.2.1 Complexation of calcium ions in solution

Since sugars are considered to form complexes with salts and metal hydroxides, several researchers believe that the retarding effect is associated to the complexation of sugar with Ca²⁺ ions.

The reducing sugars show higher binding properties because they suffer from chemical modifications through ring-opening reaction and degradation at high pH [65], [66]. However, Young [67] underlined the poor stability of these complexes. Lothenbach et al. [68] measured the change of calcium concentration in presence of different sugars. They also determined the strength of complexes formed between Ca²⁺ and these sugars by thermodynamic modelling. Their results showed that although pH played a role, sugars only containing hydroxide groups do not cause big changes in Ca²⁺ concentration. The strength of complexes they form are also much lower compared to others (i.e: D-Gluconate) containing at least one carboxylic group. So, with low stability constants and low concentrations of sugars in solution, the complexing reaction should not significantly affect the Ca²⁺ ions equilibrium. For this reason, this effect can be neglected in our study, contributing to our decision to mainly focus on the adsorption of sucrose on mineral surfaces.

Thomas and Birchall [63] found that there is no correlation between calcium binding capacity of different sugars and their retarding effects. ¹³C and ²⁹Si NMR were used for the sucrose/silicate solutions in alkaline conditions, no sucrose-silicate complexes were detected but a chemical shift in ¹³C NMR was observed for both sucrose and raffinose at high pH (>10.5). According to Popov et al. [69], this is caused by the deprotonation of the alcohol group on C8 carbon at high pH (higher than 11) with a pKa measured to be 13.1. This deprotonation probably makes these sugars good complexing agents [70]. It could also enhance their ability of adsorption. The relation between charge density and the ability of complexing Ca²⁺ was studied by Nalet and Nonat [71] in solutions at equilibrium with portlandite. They showed that non-charged sugar molecules caused almost no difference in Ca²⁺ concentration. For organic molecules containing different amounts of charged functional groups, their ability in forming complexes increased with the number of charges in the molecule. Besides, in the previously mentioned work from Thomas and Birchall [63], the complexes formed by non-reducing sugar (sucrose) were argued to poison the growth of portlandite and/or C-S-H.

The charge density in an organic molecule also influences adsorption, as demonstrated by Nalet and Nonat [71], and thereby retardation. It is true that a higher charge density in an organic molecule favors both the complexation and adsorption. But, in the same system, complexation and adsorption compete, as a too strong complexation could a priori make adsorption unfavorable. From our perspective the complexation of ions matters in as much as it affects adsorption, thereby triggering one or the other of the mechanisms discussed in the next subsections.

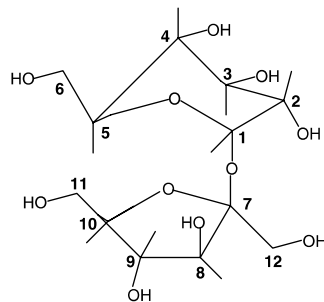


Figure 2.10. Molecular structure of sucrose with labeled carbons being used in the research of Popov et al. [69].

2.2.2.2 Hindering nucleation and growth of hydrates portlandite

Adsorption of sugar on mineral surfaces

In the study of Reiter et al. [72], [73], showed a strong adsorption of sucrose on a commercial portlandite. Langmuir isotherm was established with an adsorption plateau of 7.5 mg sucrose per gram of portlandite (CH in cement chemistry). Considering the SSA of portlandite is 15 m²/g, this plateau is converted to 0.5 mg sucrose per m² of portlandite surface and it does not change while increasing the pH. More interestingly, those authors found that the addition of portlandite to a cement paste reduces the retardation caused by sucrose (Figure 2.11). This retardation reducing effect is proportional to the portlandite dosage, with the retardation being fully cancelled when the total surface of portlandite can be saturated by the amount of sucrose in the system (adsorption plateau). This implies a stronger affinity of sucrose for portlandite than for other mineral surfaces in the paste. Moreover, a transfer of sucrose from cement surfaces to portlandite may be suspected to underlie this cancellation of retardation.

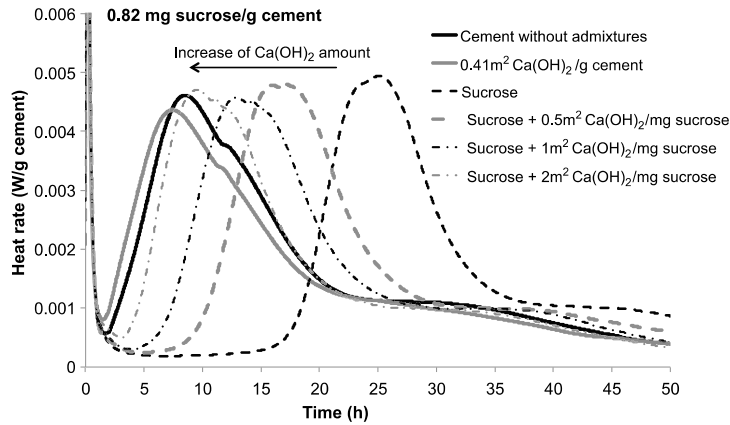


Figure 2.11. Rate of heat released for cement pastes containing 0.82 mg of sucrose per gram of cement and different dosages of Ca(OH)_2 [72].

Nalet and Nonat [71], [74] studied the adsorption of different sugars on CH in suspension as well as the impact of molecular structures on retardation. A first point made in that study is the difference between the adsorption of various sugars and other small organic compounds, as shown in Figure 2.12. It shows for example that D-gluconate has a higher affinity for CH with much stronger initial adsorption and higher adsorption plateau compared to D-glucitol. The molecular structures of these two sugars and their ability of retardation are presented in Figure 2.13. It is obvious that the presence of sugar acid anion in molecular enhances the adsorption, which also translates as a stronger C_3S hydration retardation even at very low sugar dosage. Furthermore, Figure 2.13 also shows that D-galactarate that carries two carboxylic groups leads to more substantial retardation than D-gluconate. So clearly that acid groups appear to promote both adsorption and retardation. Moreover, adsorption behavior of non-charged sugar molecules was studied separately with D-mannitol, D-galactitol and D-glucitol [75]. These sugar molecules have the same chemical composition but a different stereochemistry. Thereby, it was demonstrated that D-glucitol adsorbs more on C_3S surface compared to the other two sugars at the same dosage. The adsorption of D-galactitol was only slightly higher than D-mannitol but appear to reach the same saturation plateau. Retardation of C_3S hydration caused by these three sugars followed the same relation as their adsorption. Therefore, in general, retardation can be directly related to adsorption. In case of having one type of sugar in a hydrating system, the role of surface coverage of the mineral caused by adsorption of sugar becomes crucial. In this thesis, we paid special attention on the impact of this factor on hydration kinetics.

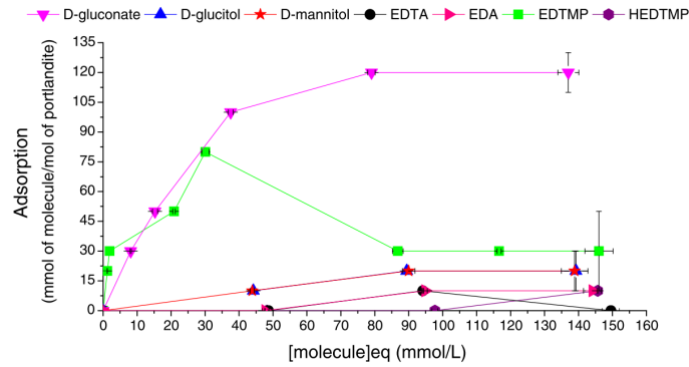


Figure 2.12. Adsorption isotherms of the organic molecules on portlandite in suspension [71].

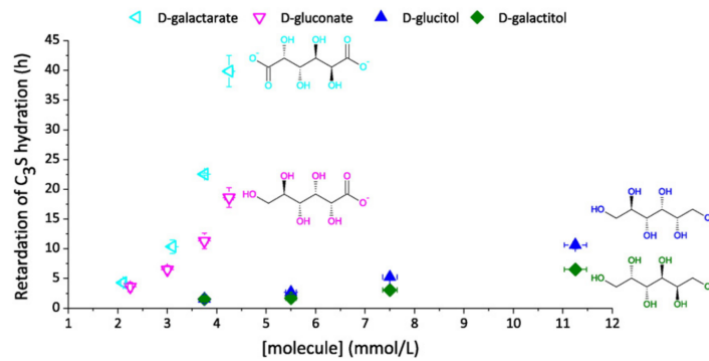


Figure 2.13. Retardation of C_3S hydration as a function of the concentration of sugar alcohols and of some of their corresponding sugar acid anions [74].

Impact of sucrose on the nucleation and growth of portlandite

The study of Juenger and Jennings [76] suggested that sucrose would poison portlandite nucleation, which is the reason why retardation takes place. However, they unfortunately did not report on whether sucrose adsorbs on mineral phases and if so which one. While other studies indicate this takes place, the extent may vary depending on the pore solution composition and specific mineralogy of the cement.

Juilland and Gallucci [77] studied the nucleation and growth of C-S-H with co-precipitation experiments from dilute sodium metasilicate and calcium chloride solutions. The initial pH of the sodium metasilicate solution was adjusted with NaOH to reach defined values, whereby pH and calcium selective electrodes were used to monitor the reaction. With initial pH increasing from 12.5 to 13.2, with or without sucrose, a decrease of the maximum calcium concentration was observed (Figure 2.14). This was considered to reflect a favored precipitation of C-S-H with higher Ca/Si ratio [78]. However, in presence of sucrose, these authors found that these processes are only affected to a very limited extent (10% increase) at pH 12.5 and 12.7. It appeared that the calcium concentration increases 25% at pH 13.2, but this pH value is higher compared to a real cement pore solution. Therefore, the impact of sucrose on C-S-H precipitation is very limited. However, also based on precipitation from solution, the same authors found that both the nucleation and growth of CH are extremely sensitive to the presence

of sucrose at all pH values used. Thus, they proposed that the retardation of cement hydration caused by sucrose is due to the hindrance of CH nucleation and growth.

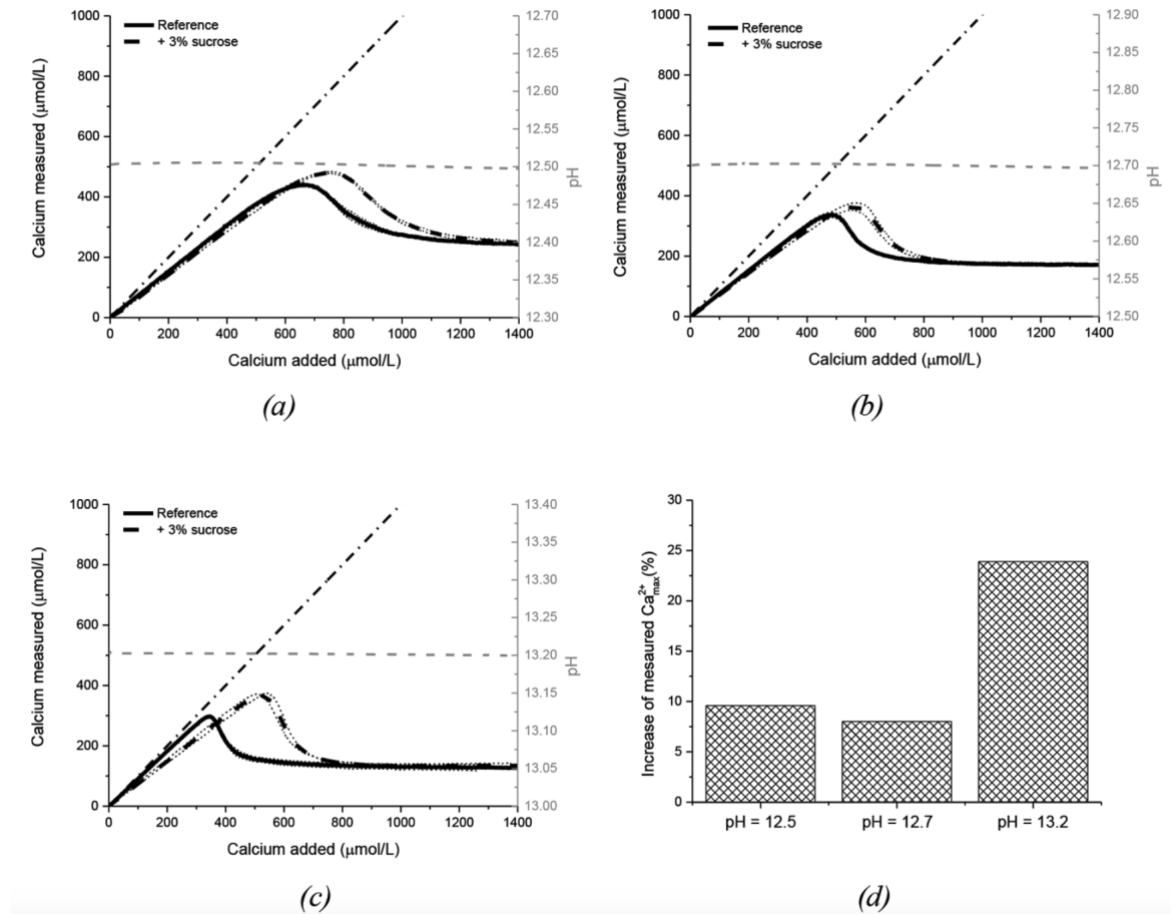


Figure 2.14. C-S-H nucleation experiments with/without sucrose at (a) pH 12.5, (b) pH 12.7 and (c) pH 13.2. (d) represents the increase of saturated Ca^{2+} with its respective reference [77].

Their argument joins a theoretical conjecture by Bullard and Flatt [38], based on a critical comparison of two hydration models. While both models could capture the basic kinetics of cement hydration, they led to very different predictions in terms of the consequence of inhibiting the formation of Portlandite. In particular, the model based on the induction period being controlled by a hydroxylate C_3S surface (as described in 2.1.2.1), indicated that inhibiting portlandite formation would rise the concentrations of calcium and hydroxide in solution enough to severely penalize the dissolution of C_3S . Exactly how reliable that conjecture is depends on the reliability of solution thermodynamics and the equilibrium constant of the hydroxylated layer, a topic that may still require further refinement [79].

2.2.2.3 Hindering the dissolution of anhydrous phase

Adsorption of sugar on calcium aluminate and calcium silicate

Since adsorption of sugar on cementitious surfaces plays an important role in causing retardation, advanced techniques have been applied in order to achieve more direct insight into adsorption behavior and to “see” this interaction at molecular level. Smith et al. [80], [81] studied the behaviors of sucrose, glucose and maltodextrin for a wet cement at 95 °C. By using 2D HETCOR NMR, they could observe a complete degradation of glucose and a non-selective adsorption of degradation products on aluminate and silicate hydrates. Sucrose remains stable at this temperature and adsorbs selectively on C₃A and C₃S surfaces. Additionally, with quantitative surface force apparatus (SFA) measurements on molecularly smooth aluminosilicate mica sheets immersed in alkaline solutions (pH 12.7, 25 °C), they observed that the distance between a so-called “hard wall” (where the repulsive force increases rapidly in short distance, observed at approximately 1nm for mica surfaces in alkaline solution alone) increased to 7 nm with 0.2 wt.% sucrose dosed in system. Based on this effect, they proposed that sucrose molecules adsorb strongly in multilayers on the mica surface.

Chmelka et al. [82] worked on the interaction of sucrose molecules with hydroxylated C₃S surface by using dynamic nuclear polarization (DNP) surface-enhanced solid-state NMR techniques. With longer contact time, they observed in Figure 2.15b a small spot above the red frame, which refers to the correlation of ¹³C on sucrose molecule and ¹H from -Ca-OH group on the hydroxylated C₃S surface. This appears to be the first experimental observation for this interaction. However, we noticed that the chemical shift for ¹H from -Ca-OH group (-2.5 ppm) is lower than what it should be (1ppm). One cannot therefore refer this signal to ¹H in -Ca-OH. This suggests that their judgement on the correlation from surface interaction between sucrose molecule and hydrated C₃S surface may be questionable.

Although NMR techniques face a lot of difficulties during their applications in cement research, we are still interested in their good selective sensitivity on target isotopes at molecular level. So, in this thesis, we also attempted to apply such techniques to our problem. To overcome the low signal sensitivity caused by low natural abundance and in case of using sucrose, low dosage as well, using isotope enriched materials (ex. ²⁹Si enriched C₃S and ¹³C labelled sucrose) is considered.

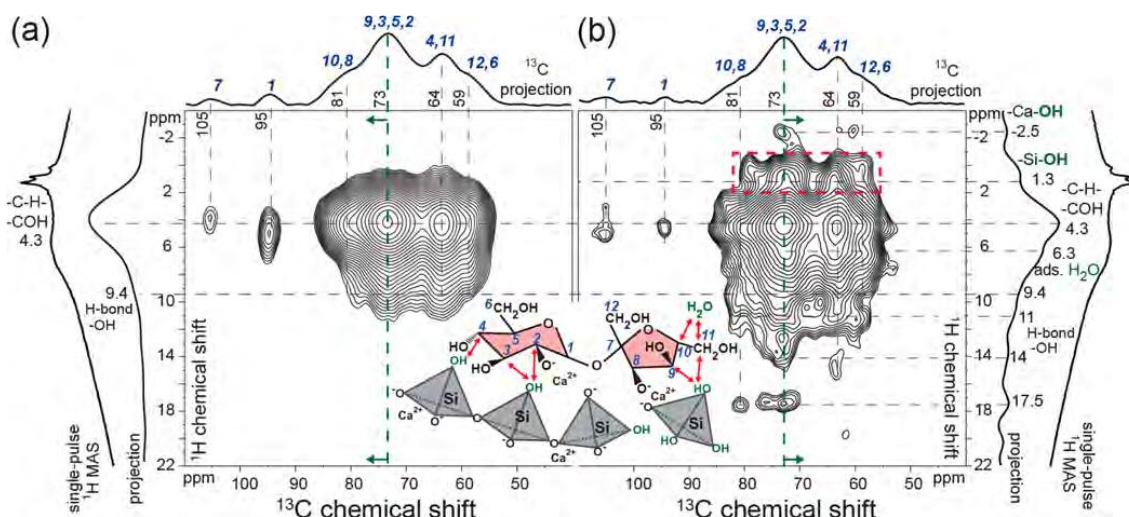


Figure 2.15. Solid-state surface-enhanced 2D $^{13}\text{C}\{^1\text{H}\}$ DNP HETCOR spectra of hydrated tricalcium silicate (4 h, 90 °C) with 0.1% bwos ^{13}C -labeled sucrose acquired with different contact times of (a) 0.5 ms and (b) 1.5 ms. The 2D spectra were acquired with 4 mM bCTbK (biradical) in frozen 1,2-dichlorobenzene (the DNP solvent), with continuous microwave irradiation at 263 GHz, at 9.4 T, 105 K, and 12.5 kHz MAS. The measurement times for the 2D spectra were (a) 3.4 h and (b) 2 h. Quantitative 1D single pulse 1H MAS NMR spectra acquired at 11.7 T, 25 °C, and 10 kHz MAS are shown along the vertical axes for comparison with the 1D projections of the 2D spectra.

Impact of sucrose on hindering C_3S dissolution

Juilland and Gallucci [77] studied the dissolution rate of synthetic impure C_3S in presence of sucrose. With sucrose dissolved in deionized water, the rate of dissolution showed no difference to the case where sucrose is not present. However, the pH in this experiment was much lower than in real cement or C_3S pore solutions, which will strongly impact the deprotonation of sucrose molecules. The adsorption of sucrose on C_3S surfaces is indirectly supported by a study from Suraneni and Flatt [83], in which they focused on the dissolution kinetic of C_3S in presence of sucrose by using a microreactor. It is reported that adding sucrose to a KOH solution of pH 13 completely blocks the dissolution, while the dissolution takes place if sucrose is added to pure water. The experiment in question implies a high dilution, so that the pH of water will not be changed much by any dissolution of the C_3S from the microreactor. The difference between pure water and the highly alkaline solution raises the possibility that sucrose adsorbs more strongly on C_3S surface at high pH. It however remains to be seen if C_3S dissolution inhibition by surface adsorption is indeed a main factor in delaying cement hydration. Should this be the case, a follow-up question is whether the progressive formation of portlandite in the induction period may consume sucrose, depleting it from the C_3S surface and thereby letting dissolution resumes.

2.2.2.4 Disturbing aluminate-silicate-sulfate balance

It is widely accepted that sugar also affects C_3A hydration [5]. For cement retardation caused by sugar, the retardation of C_3S can be altered because of a consumption of sugar by C_3A and/or its reaction products. When talking about the impact of sugars on C_3A hydration, Bishop and Barron [84] found that the addition of sucrose to a C_3A with an excess gypsum leads to accelerated ettringite formation. A similar behavior was observed by Meyer and Perenchio [85] in Portland cements systems with largely increased sulfate consumption rate in presence of sucrose. They supposed that in this system, the consumption of calcium ions by sucrose favors the dissolution of calcium sulfate, which leads to the amount of free sulfate ions in solution increasing. The ettringite formation is therefore favored and the sulfate depletion point appears earlier. In contrast, Reiter [73] found that for case when sucrose is added directly or delayed to OPC hydration, the aluminate peak in the heat flow curve remains unchanged. This contrasts with an expected change in hydration kinetics in cases where and admixture modifies the aluminate reactions. Therefore, the similitude of behavior between direct and delayed addition suggest that the aluminate reaction is not affected by sucrose.

2.3 Implications

Sucrose is a very powerful retarder, with an important effect being to delay the onset of the acceleration period. The mechanism through which this happens is however unclear, which is further challenged by the fact that even in absence of sucrose the factors controlling the duration of the induction period have not been fully resolved.

In this sense, studying the effect of sucrose on retardation may not only resolve the question of retardation but also provide further clues into the nature of rate limiting mechanisms of the induction period in absence of chemical admixtures.

Among the various mechanisms proposed, sucrose adsorption onto anhydrous phases and/or hydrates appears most credible to account for retardation. A simplified system is C_3S , that avoids additional complication linked to the fast reactivity of C_3A in OPC. This lays the ground for chapter 4, that focusses on the impact of sucrose on C_3S . Further to this we note that charged groups appear to influence both adsorption and retardation, which for sucrose may happen at high pH owing to the deprotonation of hydroxyl. This is why our experiments in chapter 4 and 5 are carried out at pH 13.

Among the different mechanism explaining the role of sucrose, we have underlined the possibility that portlandite may mobilize sucrose. For the hydration of OPC, this would imply that adsorption onto forming CH may control the overall duration of retardation. One objective of this thesis has been to test this hypothesis and explains the work presented in chapters 5 and 6 where CH is added respectively to C_3S and OPC.

Finally, the reactivity of C_3A in OPC is known to affect the behavior of many chemical admixtures. In the case of sucrose, the literature includes contradictory statements. On the one

hand some results suggest that sucrose barely interferes with C₃A reactivity, while others point to a change in its kinetics that indirectly modifies its impact on C₃S hydration. Shedding light onto this question is another objective of this thesis and motivates chapters 6 and 7. The question however rapidly includes numerous possible parameters of influence, so that this part of the work should be seen as bringing clues rather than definitive answers. Overall, however, it will be shown that a clear link can be established between the effects of sucrose both C₃S and OPC. Thereby, this PhD makes an important contribution to the state-of-the-art presented in this chapter, even if open questions remain concerning details of how sucrose interacts with C₃A reactivity.

3 Materials and methods

3.1 Material synthesis and grinding

As this thesis firstly focus on studying the C₃S hydration retardation induced by sucrose, obtaining C₃S with well-controlled properties is of great important. From this aspect, we carefully choose the protocol based on our requirements.

3.1.1 Synthesis of C₃S and ²⁹Si enriched C₃S

The C₃S and ²⁹Si enriched C₃S were firstly produced following the protocol developed by Pustovgar [86], based on the solid-state reaction.

For ²⁹Si enriched C₃S, CaCO₃ (> 99% pure, Sigma Aldrich) and SiO₂ powder (99.9% enriched in ²⁹Si, Cortecnet) were mixed stoichiometrically for 24h (Turbula T2F, WAB) and then pressed into approximately 0.5 g pellets under 550 bars load (VLP-Serise, Enerpac). The pellets were fired afterwards in a platinum crucible at 1600 °C (Nabertherm LHT 08/16) for 8 h then quenched by compressed air until it cooled to room temperature. To ensure the full transformation of starting materials into product, the whole procedure was repeated 4 times until no free lime could be detected by X-ray diffraction.

The same protocol is applicable to produce non-enriched C₃S as well but with pellets of 10 g for each. However, since large amount of non-enriched C₃S was required (from several hundred grams to kilos) in the study, the productivity of the above protocol became problematic. Specifically for the efficiency of sintering. Once the pellets were piled up in the crucible, the homogeneity of the product after sintering turned out to be very bad, not only in aera where pellets were in touch, but also within each pellet. Therefore, several rounds of repetitions were needed to ensure the quality of product, which would have excessively prolonged the whole sintering process.

Based on this consideration, a massive production method published by Li at al.[87] was followed for producing non-enriched C₃S.

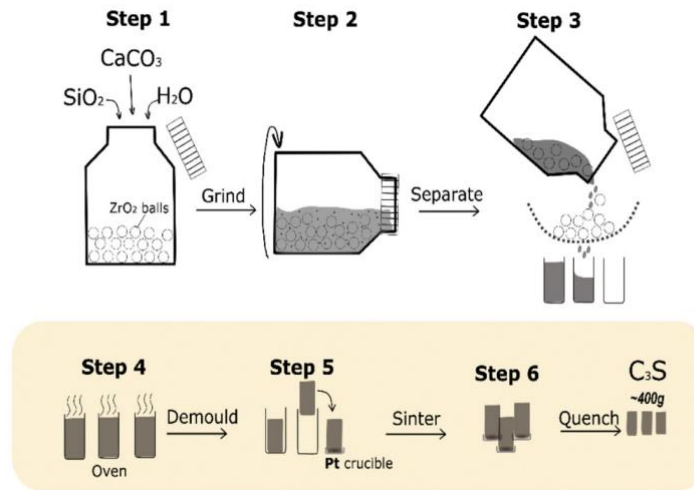


Figure 3.1. Schematic representation of the sequences for massive production of C_3S [87].

This protocol includes mixing, homogenizing, shaping, sintering and quenching steps as shown in Figure 3.1. In our lab, the $CaCO_3$ (> 99% pure, Sigma Aldrich) and SiO_2 (> 98% pure, Sigma Aldrich) powder were put stoichiometrically in a container together with 5 silica milling medias. Water was added with a water to solid ratio of 2. The container was then well closed and homogenized for 24h (Turbula T2F, WAB). Afterwards, the suspension was poured into beakers and dried at 100 °C until no water remained. The homogenized powder sedimented during drying with water evaporation, it was shaped by the beakers as cylinders which were not very dense but could be easily took out from the beakers with their shape. Those cylinders were then placed in the platinum crucible and fired at 1600 °C (Nabertherm LHT 08/16) for 10 h. In the end of sintering, the crucible was quickly taken out from the oven and the product was quenched by blowing it with compressed air continuously until it reached room temperature. With this procedure, no lime or C_2S reflection was observed with XRD even after one round of sintering. Therefore, the repetition was not necessary and the C_3S product was much easier to be broken into small pieces compared to those as pellets, which eases further grinding.

3.1.2 Grinding of C_3S

The non-enriched C_3S was ground by following a protocol that Marchon used for model clinker [8]:

- Coarse C_3S was broken into small pieces by hands (<1.5 cm).
- 30 g of small C_3S grains was distributed between the layers of a disk mill (Retsch) and ground 45 s at 700 rpm.
- 15 g of ground powder was then put into a jar in the planetary mill (Pulverisette 5, Fritsch) for fine grinding with zirconia beads.
- Equilibrated the sample jar, then ground 4 min at 400 rpm.

- Cleaned the jar and the grinding balls for the planetary mill after each round of grinding with water. In case a lot of powder stucked on wall, a diluted HCl solution could be used.

The ^{29}Si enriched C_3S was ground in different way [88]:

- The produced ^{29}Si enriched C_3S pellets was firstly ground by hands in an agate mortar into powder.
- As it is reactive with water and very valuable with small amount, 0.5 g of powder was further ground in a micronizing mill (McCrone) for 10 min with 15 ml absolute ethanol.
- The mixture of powder and ethanol was collected and dried at 65 °C until no solvent remained.

Particle size distributions of ground C_3S and ^{29}Si enriched C_3S were measured in isopropanol by a Malvern MasterSizer S diffractometer. Results are shown in Figure 3.2. The D_{v50} is 6.17 μm for C_3S and 6.09 μm for ^{29}Si enriched C_3S .

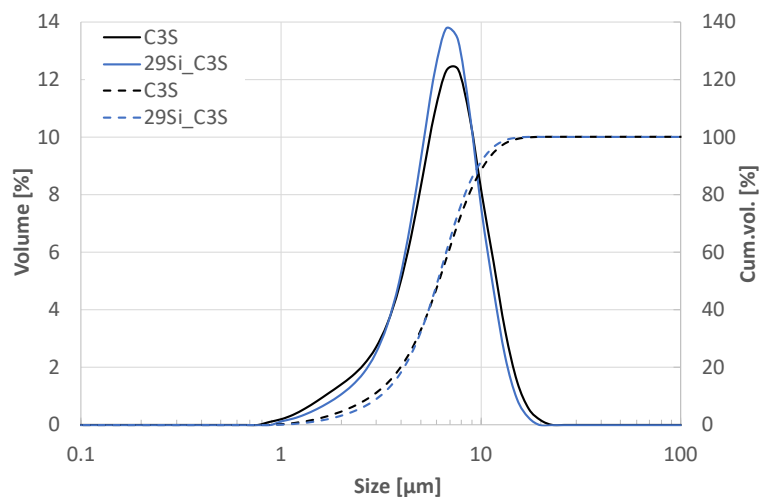


Figure 3.2. Particle size distribution of ground C_3S and ^{29}Si enriched C_3S .

3.2 Methods and sample preparations

3.2.1 Paste preparation

This thesis includes two main modes of paste preparation: ex-situ and in-situ. The ex-situ method follows procedures used by Pustovgar [88], using a vortex mixer to enable the mixing of small amounts of samples. Unless mentioned otherwise, this method was used for pastes reported in this thesis. The in-situ measurement was used for a series of calorimetry measurements, as we realized that this was needed to more accurately determine the onset point.

In particular, this eliminates some source of randomness between samples and made it easier to establish the impact of factors as sucrose dosage, portlandite additions and temperature.

The ex-situ pastes were prepared by adding powder into the corresponding amount of liquid. In case of working with blended systems, powders were firstly mixed by hands then added to liquid. As most of the pastes were prepared in small amount (below 20 g), a mixing method of using a Vortex mixer for 1.5 min at 3500 rpm (VWR standard heavy-duty Vortex mixer) was selected. Table 3.1 summarizes the mixing method used in different experiments.

Table 3.1. The mixing method used for different experiment.

Experiment	Calorimetry for OPC or C ₃ S	Calorimetry for blended powder	Calorimetry with delayed sucrose addition	Adsorption	NMR
Mixing method	In-situ	Ex-situ	In-situ	Ex-situ	Ex-situ

3.2.2 Isothermal calorimetry

As mentioned above for calorimetry we started by preparing samples ex-situ and then for several cases, in particular OPC, we used an in-situ mixing procedure.

3.2.2.1 Ex situ sample preparation

For each test, about 5 g of paste was prepared and inserted into the measurement channel in the isothermal calorimeter (TAM Air, TA Instruments). The calorimeter was pre-stabilized at target temperature for 24 h, gain calibration was then proved with references. Before the measurement, a baseline was acquired for 30 min to get a stable and low heat level close to 0.

Regarding experiments at other temperatures, the solution and powder were stored at the selected temperature for at least 2 h before mixing, but the mixing was always at room temperature (23 °C).

Calorimetry samples were pastes mostly prepared as mentioned before. Specially, for sucrose being added shortly after hydration starts, so called delayed addition, half of the total required liquid without sucrose was firstly weighed in a sample vial and powder was mixed with it as presented previously. After 3 min 30 s, the other half of the total required liquid contains sucrose was added into the vial and mixed again for 1 min at 3500 rpm. The delay is considered as 5 min in total.

It has to be mentioned that for those measurements, the sample was inserted in the measuring position of the calorimeter after final mixing. It is therefore named as ex-situ mixing refers to reactions ongoing in calorimeter. Since the software starts data recording when the sample is in the measuring position, an external timer was used to record the time loss between mixing and the start of data recording. This time loss was also considered when plotting data.

3.2.2.2 *In situ* sample preparation

The inconvenience in data recording at the beginning of hydration was particularly problematic for reference samples without sucrose, for which the onset time is very short. Because those samples play a big role in all our data analysis, we came to realize that it was important to mix samples *in situ*. It provides more consistent measurements on the initial heat as well, which also plays a role in our data analysis as we calculate the rate of hydration to the onset taking a ratio between the degree of hydration at the onset to the time of the onset.

A problem with the in-situ mixing is that the commercial devices are very expensive and that their motors are very weak. We thus moved to producing ourselves additional copies of the mixing devices and selecting a more powerful and easy to use motor. This work was carried out by M. Martin Keller, a technician at our institute. Having multiple such mixers gave a completely new turn to this thesis, with data suddenly making more sense without their scatter, in particular thanks to better measurements of the references. For consistency, all experiments with C₃S and OPC, without CH, were repeated (chapters 4 and 6).

Details of the mixing devices are shown in Figure 3.3. The set is mainly composed of three parts: a glass sample vial, syringes for liquid injection with needles entering the vial once it is closed, and a shaft in the middle of the whole set which is connected with a plastic stirrer that almost touches the bottom of the vial when it closes. The vial is closed by connecting the syringe part on top of the glass vial.

For sample preparations, powder was placed in the vial and solution in syringes. After closing, the set was inserted in the measuring position in the calorimeter for 30 min to stabilize the temperature and for the background signal to level off. Solutions were injected into the vial at once for direct addition and separately for delayed addition. The mixing was performed by connecting the bar to an external motor (a cordless screwdriver, Bosch GO professional) and running it for 1.5 min at 360 rpm. The data recording started together with the mixing.

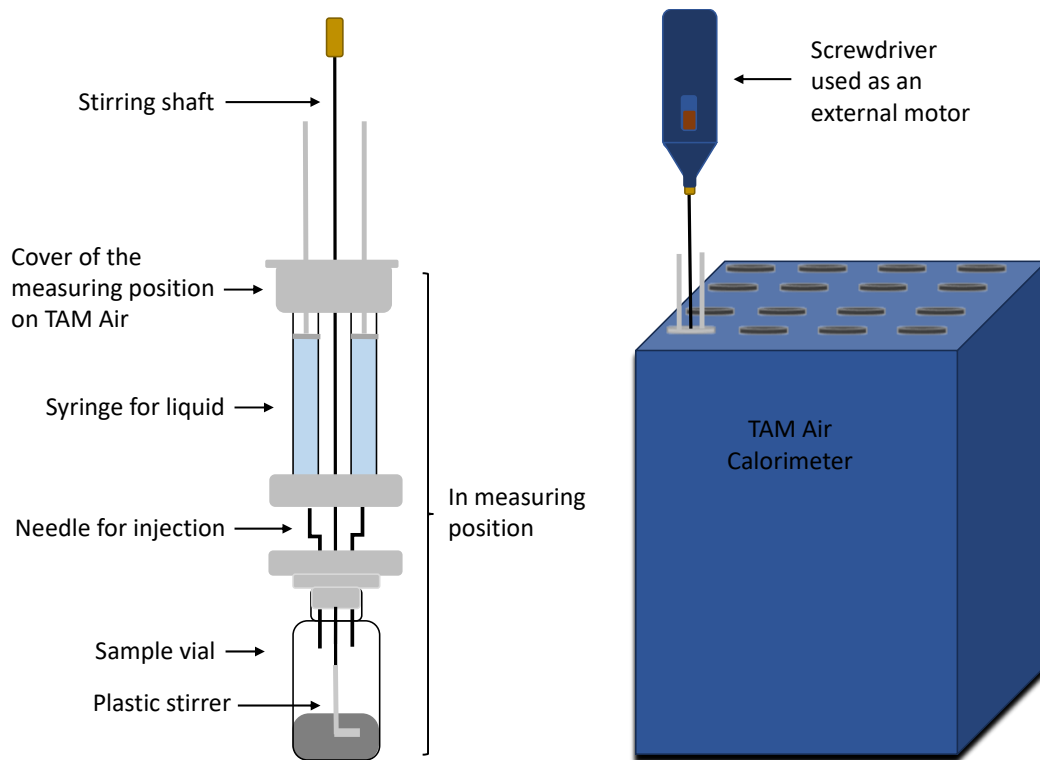


Figure 3.3. Graphic illustration of the devices used to mix the solution and powder inside the calorimeter, with in-situ set shown on the left.

Concerning other analysis than calorimetry, described in the following sub-sections, samples were prepared *ex situ*. This is not considered to be problematic versus the *in situ* samples for two reasons: 1) Only the calorimetry is concerned by heat losses prior to insertion in the calorimeter, 2) Those measurements are less concerned with an analysis normalizing by a reference value without sucrose, which in any case is not affected by pre-insertion heat losses.

Comparisons between in-situ and ex-situ mixing for cement and C_3S are given in Figure 3.4a and b. For cement, large differences can be observed for all temperatures. This may partially come from the pre-insertion heat loss, and for cement hydration at 23 °C (no baseline correction), it may also come from the fact that we define hydration onset with the abscissa of the maximum rate in the acceleration period, the heat flow rate in the induction period is not 0, this definition will lead to an earlier onset. For C_3S , the mixing method brings almost no difference to the estimation of hydration onset. However, if we compare the degree of hydration at the onset for C_3S hydration with in-situ and ex-situ mixing, without sucrose, large difference appears for all temperatures especially for hydration at high temperature, where a big negative value was obtained from ex-situ mixed experiment (Figure 3.5a). This came from the fact that the sample had to reach environmental temperature by adsorbing heat after the measurement started (Figure 3.5b). Although we pre-stabilized the temperature of powder and liquid before mixing, the temperature of the sample dropped quickly during ex-situ mixing due to its small volume. Generally speaking, in-situ mixing provides more reliable heat release evolution for hydration without sucrose.

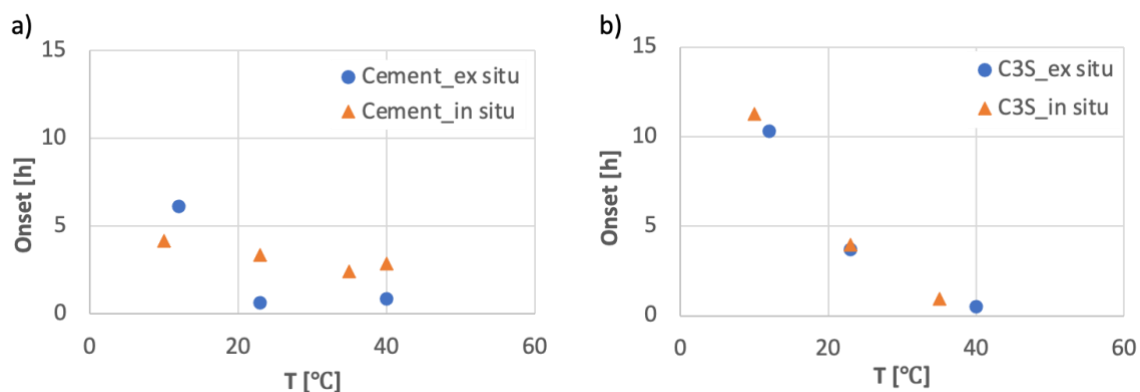


Figure 3.4. Comparing onsets for hydrations without sucrose mixed with ex-situ or in-situ method, a) for cement and b) for C₃S. Same Cement and C₃S were used in these experiments, and hydration onsets for all experiments were obtained with the same method.

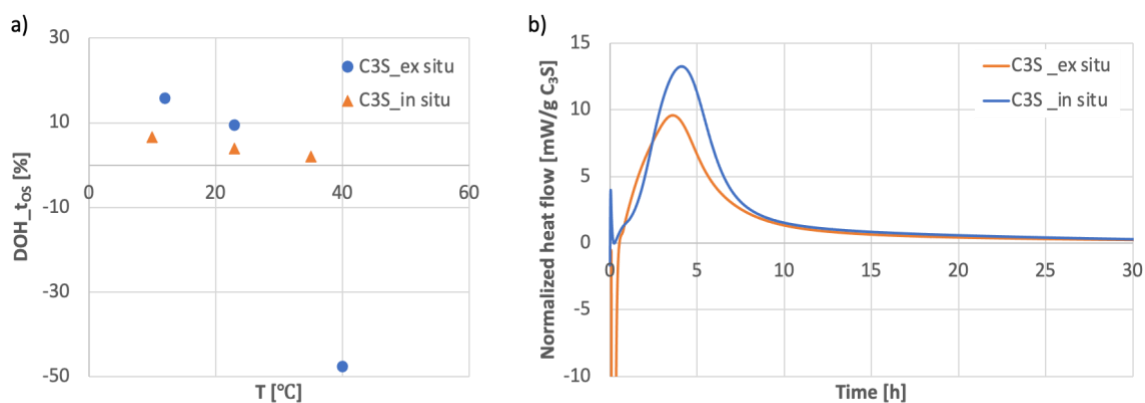


Figure 3.5. Comparing a) degree of hydration at the onset and b) heat flow curves for C₃S hydration without sucrose mixed with ex-situ or in-situ method. In graph b, the ex-situ curve was obtained for hydration at 40 °C, and the in-situ curve was obtained from hydration at 35 °C. Baseline correction was applied on both curves.

3.2.2.3 Baseline correction

Some problems happened during the analysis of calorimetry data. Figure 3.6a shows the evolution of heat flow rate for C₃S hydration at 40 °C with sucrose dosage of 0.27 mg/m². The calorimetry measurement of this reaction was carried out with ex-situ mixing. The first thing to notice is that the peak related to initial dissolution peak is endothermic, which is not correct. This happens because of the temperature at which mixing place is lower than that at the measuring position, the sample takes time to reach 40 °C during data recording. With in-situ mixing, this issue disappears.

The second problem refers to the shifting of baseline. It happened whatever in-situ or ex-situ mixing was used, specifically for experiments at temperatures other than room temperature, and it is more pronounced while using in-situ mixing method. The reason for this remains unclear, but we developed a way to correct it in 2 steps. Firstly, we defined a new baseline, using data in the linear ranges both of the induction period and after the main peak (shown in

red continuous line in Figure 3.6b). In case where the induction period was too short, only the linear range after the main peak was considered. Correcting for the slope of that baseline, essentially rotated the curve around the ordinate at the origin of the baseline, giving an appearance close to what is expected (step 1 in Figure 3.6b). In some cases, this still leaves negative values in this induction period, which we corrected for in a second step, shifting the curve upwards so the lowest value would lie on the horizontal axis (step 2 in Figure 3.6). This second step appeared more reliable than using the ordinate at the origin of the baseline, owing to its error. A combination of the use of different mixing methods in calorimetry measurements with the need of baseline correction is presented in Table 3.2.

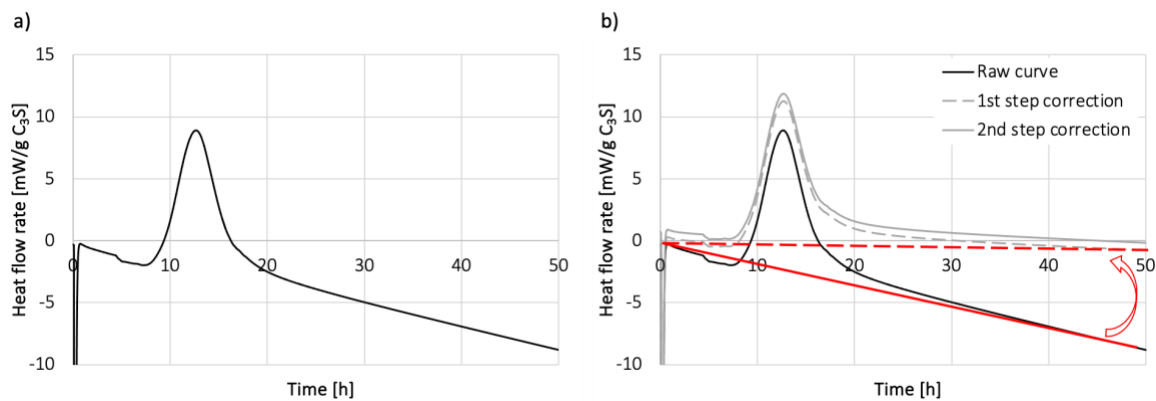


Figure 3.6. Illustration problems during data analysis based on calorimetry measurements, with an raw heat flow curve achieved from C_3S hydration at 40 °C with sucrose dosage 0.27 mg/m². Calorimetry measurement for this reaction was carried out with ex-situ mixing. a) error in initial dissolution peak; b) baseline correction by two steps, black curve is the raw curve as in a), discontinuous grey curve is the result after first step correction and the grey continuous line is the final result after second step correction. Red lines represent the new baseline initially defined and after turning, with an arrow indicates the turning direction.

Table 3.2. Requirement on baseline correction regarding to the mixing method being used, temperature and composition of powder for hydration.

Mixing method	Ex-situ 23 °C	Ex-situ other temperatures	In-situ 23 °C	In-situ other temperatures	Ex-situ C_3S/CH	Ex-situ OPC/CH
Baseline correction	No	Yes	Yes	Yes	No	Yes

3.2.3 Phase separation

Phase separation can be done either by air extrusion, through pressure or centrifugation. In case of using a centrifuge, the paste was centrifuged for 4 min at 10000 rpm and the supernatant was withdrawn with a syringe. Regarding to quantifying sucrose in pore solution, solutions containing sucrose from the same paste obtained with these two methods did not show significant difference in sucrose content. But with centrifuge, it allows to work with smaller amount of paste, which matches better our needs in preparing NMR samples containing isotope enriched species (ex. ¹³C). To ensure consistency in sample preparations, we adopted this method for all phase separations during this PhD work.

3.2.4 Hydration stoppage and specific surface area measurement

The specific surface area (SSA) is well known to have great impact on hydration kinetics of cement [89]. It also strongly affects the amount of sucrose that can be adsorbed on cement particles. For our study of impact of sucrose on initial hydration kinetics, measuring specific surface area at different moments during the induction period and at least until the start of acceleration period is necessary. Since SSA are measured on dry powders, the hydration must be stopped at determined times and the paste must be dried for further sample preparations.

There are different methods to stop hydration such as oven drying, vacuum drying, freeze-drying and solvent exchange by using an organic solvent to “wash out” the free water. Collier et al. [90] found that none of these techniques caused major difference to the composition and microstructure of hardened cement pastes. But regarding the early hydrated cement pastes, a study in our lab proved that solvent exchange by cold isopropanol is the most adequate method compared to freeze-drying, because it introduces less impact to the sensitive ettringite phase from a microscopic point of view and does not cause significant differences in the SSA of ettringite whereas freeze-drying slightly increases it from 8.8 to 9.3 m²/g [91].

As for our study, the use of C₃S is free from ettringite formation during the hydration. We decided to keep the same protocol on cement pastes, assuming the changes to SSA would not be critical and would not change the trend of their evolution over time in the induction period. Therefore, we used freeze-drying, which is also more practical when dealing with 2 samples of short time interval.

For doing freeze-drying, fresh paste was firstly centrifuged to remove the liquid phase as much as possible, this part was stored for solution analysis. The rest of the paste was immersed into liquid nitrogen (-196 °C) directly in the sample tube for centrifugation for 2 min. The tube was then taken out from liquid nitrogen, the frozen paste was transferred immediately to a round bottom flask and freeze-fried with a freeze-dryer (Alpha 1-2 LDplus) for 24 h at 4 mbar. In case of having small sample about 0.5 g, the drying process can be shortened to 4 h under the same conditions. This allowed us to obtain well dispersed dry powder for SSA measurement. But in some cases, specifically for pastes hydrated longer, particles agglomerated due to the formation of hydrates. The agglomerations were then dispersed manually within a grinding bowl, without applying too much pressure.

The SSA of anhydrous and hydrated cement can be measured by three methods: laser diffraction, Blaine test and nitrogen adsorption. The last one is mostly used in laboratories for academic research. And it is based on quantifying the nitrogen molecules adsorbed on powder surfaces, the SSA can be then calculated with the BET (Brunauer-Emmett-Teller) model [92]. From its basis, an effective and non-destructive degassing step is required in sample preparation. Mantellato [93] studied carefully on degassing conditions for anhydrous as well as hydrated cement pastes during her PhD, and she proposed reliable protocol for sample preparation [93], [94]. We adapted this protocol in our work, as it is described as follow:

The samples after freeze-drying were degassed in an external degassing station (VacPrep 061 from micromeritics) at 40 °C under N₂ flow with a flux of about 3 · 10⁻³ m³/h for 16 h. The BET specific surface area measurements were carried out by using a BET multi-point nitrogen physisorption device (Micromeritics Tristar II 3020), with nitrogen adsorption measured from a 6 points isotherm.

3.2.5 Sucrose concentration in solution

The Total organic carbon (TOC) is a technique for quantifying the organic carbon concentration in a solution. TOC measurements (Shimadzu TOC-V CSH) were used to determine the sucrose concentrations either in mother solutions before mixing them with C₃S or cement powder, or in pore solutions obtained by phase separation from pastes. It is valid because sucrose is the only source of organic carbon in our cases. Regarding to sample preparation, the pore solution was firstly filtered with a 0.45 µm filter and then diluted with 0.05 M HCl solution by a factor of at least 20 times to ensure a pH lower than 4. The diluted pore solution was then analyzed. Before measuring samples, standard solutions with well-defined carbon concentrations were tested to check the accuracy of calibration methods, which would be used to determine the organic carbon concentrations in our samples.

Unfortunately, our experience showed that the TOC can only detect sucrose with natural abundant carbon. For ¹³C labelled sucrose, the calibration appeared to be totally off, and the method turned out to be unreliable because the IR bands are not the same as those the instrument measures. The manufacturer could not offer a valid alternative.

3.2.6 ¹H/¹³C NMR

¹³C labelled sucrose was used to study the interaction of sucrose molecules with mineral surfaces by solid state NMR. This interaction is mainly through adsorption. We are therefore also interested in looking at the adsorption of sucrose during C₃S hydration. Although TOC measurements provide information on sucrose concentration, it cannot detect ¹³C labelled sucrose owing to a shift in IR bands. This is problematic as the labelled sucrose can slightly change the hydration kinetics. From this aspect, using liquid state NMR techniques to detect sucrose concentration is required. It will be even better if we can quantify sucrose in pore solution directly from a paste sample. As preliminary experiments for this purpose, detecting liquid samples with a solid NMR probe is necessary.

3.2.6.1 From static single-pulse NMR to INEPT NMR

We prepared a solution with ^{13}C labeled sucrose dissolved in D_2O for an initial sucrose concentration of 8 mM, which corresponds to a ^{13}C labeled sucrose dosage of 1.60 mg/g C_3S , for a paste prepared with L/S 0.7. Although this concentration is much higher than what we used in calorimetry measurements, we took this sample to test signal sensitivities under this special situation.

NMR experiments were performed with 4 mm ZrO_2 rotor using a Bruker Avance-500 spectrometer (magnetic field is 11.7 T). A ^{13}C single-pulse NMR experiment was firstly done without spinning (Figure 3.7a). During this experiment, the radio frequency was applied directly on ^{13}C after a pulse delay. ^{13}C spectrum was collected [95] with 256 scans and presented very poor signal intensities and broadband. Since we were using solid-state NMR equipment, we applied magic angle spinning (MAS) to the previous experiment. The MAS is usually used in solid-state NMR measurements but not in liquid- state NMR to overcome the line boarding of the signals with a spinning angle of the probe at 54.7° with respect to the external magnetic field [96]. After spinning our sample at 550 Hz, the same ^{13}C single-pulse experiment gave a ^{13}C spectrum with much better resolved peaks (Figure 3.7b) without improvement of signal intensity. To improve this, heteronuclear decoupling was added to the pulse sequence to remove all ^1H - ^{13}C couplings. As shown in Figure 3.7c, the two peaks caused by ^1H - ^{13}C coupling with doublets (due to ^{13}C - ^{13}C coupling) between 85 and 80 ppm collapsed together with the decoupling step. This helps to clean up the spectrum and most importantly to concentrate all the ^{13}C resonance intensities together. As a result, it provides a good increase in signal intensity. However, since we used much lower sucrose concentrations in calorimetry experiments and solution sucrose concentration even decreases due to adsorption, we needed further enhancement to the signal with short experimental time. The latter can be critical for in-situ measurements.

For this reason, we used refocused INEPT NMR (Pulse sequence is shown in Figure 3.7e). The basic INEPT [97] (Insensitive Nuclei Enhanced by Polarization Transfer) begins with excitation of all protons and heteronuclear coupling to the ^{13}C -spin. After a period of delay ($\tau_1=1/4J_{\text{H-C}}$), the proton vectors experience a 180 degrees pulse which serves to refocus chemical shift evolution during the second delay period. Simultaneous application of a 180 degrees (^{13}C) pulse ensures heteronuclear coupling continues to evolve by inverting the proton vectors' sense of precession. For an H-C pair, a total delay of $1/2J$ leaves the two proton vectors opposed or anti-phase. So, a further delay ($\tau_2=1/6J_{\text{H-C}}$) [98] after polarization transfer allows the ^{13}C -spin magnetization to refocus under the influence of the H-C coupling, giving the refocused INEPT sequence [98], [99]. In Figure 3.7d, a significant signal enhancement was achieved on the same sample used before with refocused INEPT NMR, MAS and heteronuclear decoupling were also applied.

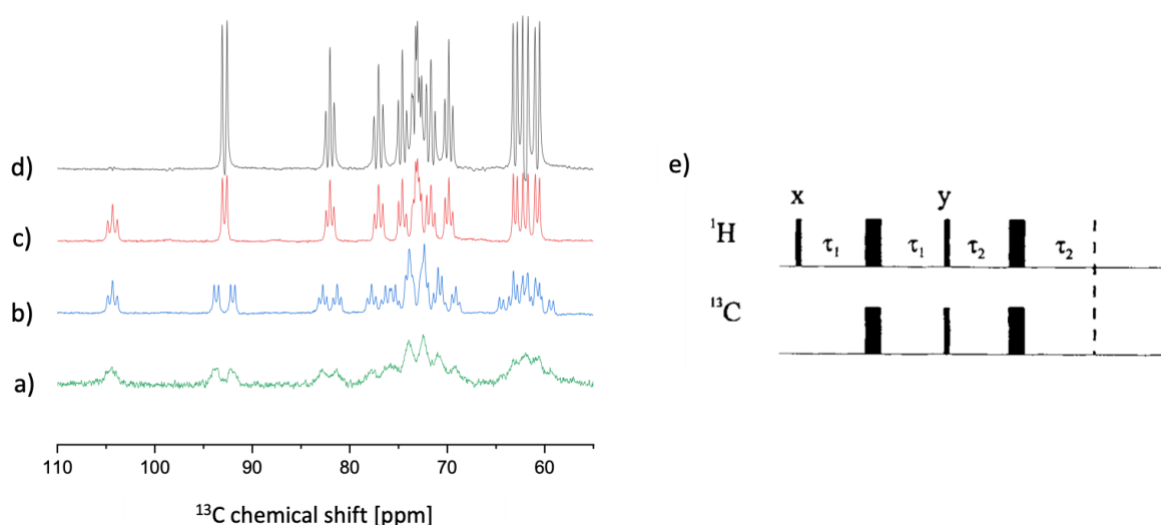


Figure 3.7. Step-by-step illustration on ^{13}C signal enhancement with an 8 mM ^{13}C labelled sucrose sample being measured in a solid-state NMR probe. a) Static single-pulse NMR without spinning; b) static single-pulse NMR with MAS at 550 Hz; c) Static single-pulse NMR with MAS at 550 Hz and heteronuclear decoupling; d) Refocused INEPT, with initial delay $d_1=1\text{s}$ and $\tau_1=1.6\text{ ms}$ ($J_{\text{H-C}}=150\text{ Hz}$); e) Schematic presentation of the pulse sequence for refocused INEPT [98].

Refocused INEPT NMR detected ^{13}C in a ^{13}C labeled sucrose molecule. Since a sucrose molecule consists of more H than C atoms, we therefore added reversed pulse transfer steps to transfer the polarization from ^{13}C to chemically bound ^1H and to obtain ^1H detected INEPT pulse sequence (Figure 3.8). The time evolution of the ^{13}C polarization was kept to a minimum with τ_2 set to $3\ \mu\text{s}$. ^{13}C was decoupled from ^1H during acquisition through a waltz16 composite pulse.

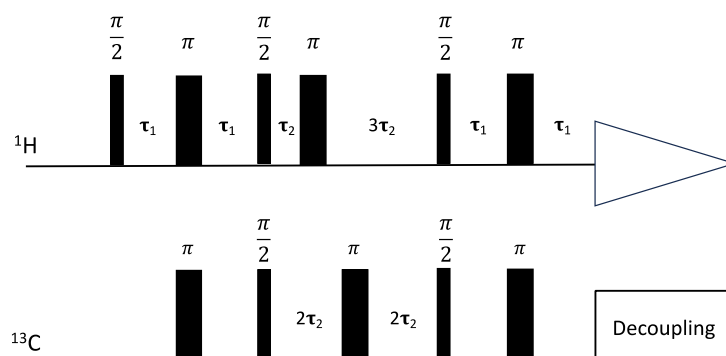


Figure 3.8. Chronogram of the ^1H detected INEPT NMR sequence.

A long-weak pulse selectively for ^1H signal from water was applied on ^1H channel before other resonance, it helps to suppress ^1H signal from solvent, so that the impact of environmental water on detecting sucrose is reduced. The spectrum from ^1H detected INEPT NMR on the 8 mM ^{13}C labelled sucrose solution is shown in Figure 3.9. Signals in the red frame correspond to ^1H from sucrose [95], the random peaks on the left are due to the water suppression [98]. We do not observe all ^1H from sucrose under the impact of water suppression, but this pulse

sequence still allows us to distinguish sucrose from solvent, with the linewidth for the most intensive signal peak about 22 Hz.

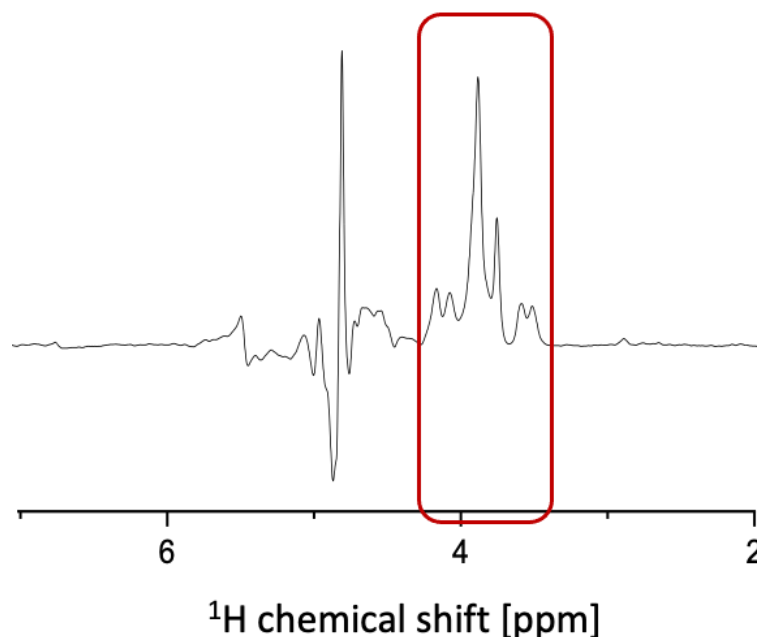


Figure 3.9. ^1H detected INEPT NMR spectrum on an 8 mM ^{13}C labelled sucrose sample, with an initial delay time $d_1=1\text{s}$ and $\tau_1=1.6\text{ ms}$ ($J_{\text{H-C}}=150\text{ Hz}$) as for refocused INEPT. Spectrum obtained with 256 scans. Peaks in red frame are ^1H signal of sucrose.

3.2.6.2 Refocused INEPT vs ^1H detected INEPT

To compare the abilities of the two pulse sequences on detecting sucrose in very diluted conditions, we progressive diluted the 8 mM ^{13}C labeled sucrose solution to 4 mM, 2 mM, 1 mM, 0.25 mM, 0.12 mM, and 0.03 mM, then using two NMR techniques to measure them. We found that both of them worked out similarly for all solutions, although a detection time was increased to about 1 h 30 min for obtaining relatively good signal to noise ratio on the 0.03 mM sample.

The signal intensities were obtained from each spectrum. For refocused INEPT NMR, ^{13}C signals between 95 and 55 ppm was considered. For ^1H detected INEPT NMR, we only selected the most intensive peak in the frame of Figure 3.9, which is in the range of 4.00 - 3.70 ppm. These intensities were normalized by the number of scans and mass of solution being used in related experiment. Normalized intensities from refocused INEPT NMR measurements were plotted in Figure 3.10a, those from ^1H detected INEPT NMR measurements were in Figure 3.10b. Both techniques behave identically for ^{13}C labelled sucrose dissolved in D_2O . The regression line serves also as a calibration line for solution samples with unknown concentrations, such as sucrose contained pore solutions extracted during hydration.

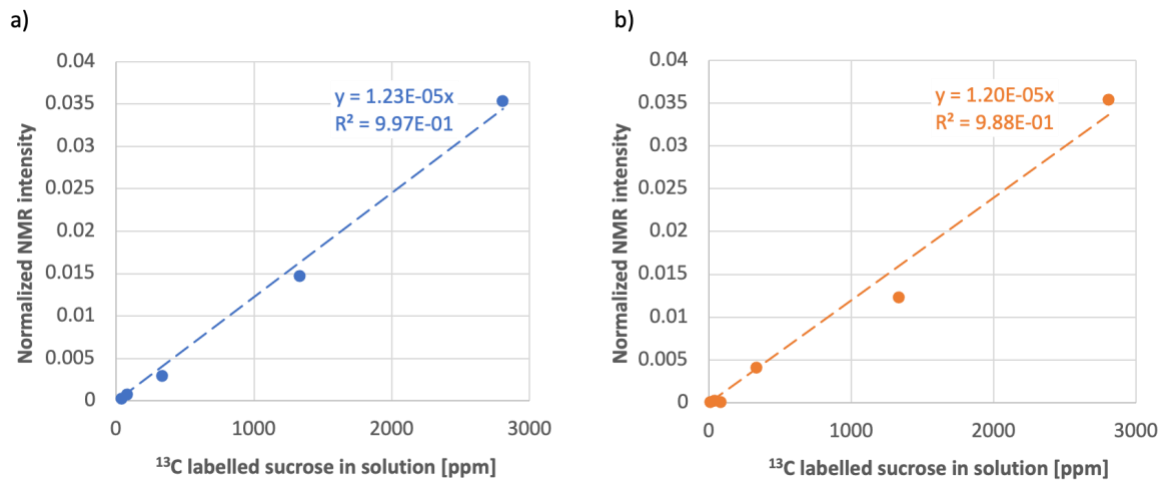


Figure 3.10. Normalized NMR signal intensities versus ^{13}C labelled sucrose concentrations, basing on a) ^{13}C signal obtained by refocused INEPT and b) ^1H signal obtained by ^1H detected INEPT NMR. The discontinuous line in each graph is the regression line, it is later used as calibration line for quantitative analysis.

With these in hand, we tested both techniques with real pore solutions containing ^{13}C labelled sucrose. Different from before, the ^{13}C labelled sucrose was dissolved in UPW instead of D_2O for an initial concentration of about 5 mM. C_3S powder with natural abundant Si was mixed to this solution with Vortex mixer for 1 min 30 s at 3500 ppm, for L/S 0.7. Calorimetry measurement for 5 g of the same paste was started after mixing. Figure 3.11a shows the heat flow curve from calorimetry measurement, Figure 3.11b and c indicate the moments when pore solutions were extracted as described in section 3.2.3.

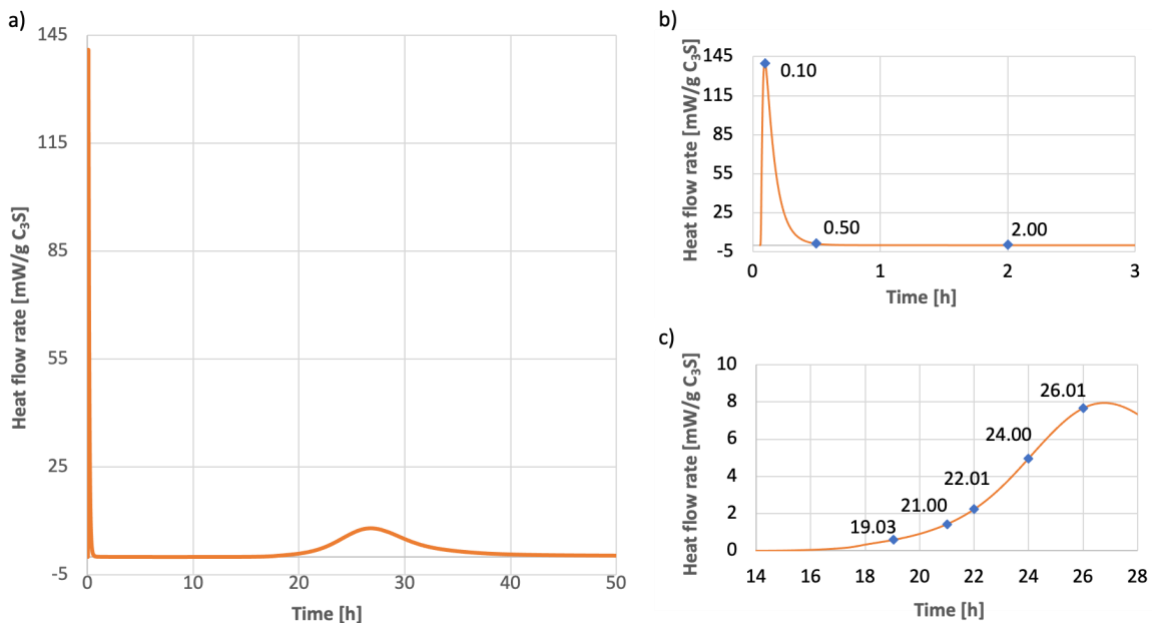


Figure 3.11. a) Heat flow curve of calorimetry measurement for C_3S hydrated with 5 mM ^{13}C labelled sucrose solution, L/S 0.7. b) and c) represent the first 2 h and the acceleration period of the same hydration curve, respectively, with time indications to show the moments when pore solutions were extracted.

With refocused INEPT, no ^{13}C signal was obtained for pore solution extracted at 19 h and later, with 50'000 scans (total experimental time 17 h). However, ^1H detected INEPT still worked until the pore solution being extracted at 24 h. The signal intensity was integrated from each spectrum and normalized as stated previously. Concentration of ^{13}C labelled sucrose for each pore solution was defined with the regression line in Figure 3.10b. Results are plotted in Figure 3.12, with narrower concentration range for experiments after 19 h shown on top-right (sucrose concentration at 24 h is marked as 0). These results demonstrated the ability of ^1H detected INEPT in measuring ^{13}C labelled sucrose for very low concentrations. Therefore, we chose this technique to follow the evolution of ^{13}C labelled sucrose in pore solution during C_3S hydration in our later works. Results are reported in chapter 4 and play an important part in consolidating our interpretation on the mechanism through which cement delays the hydration of this phase.

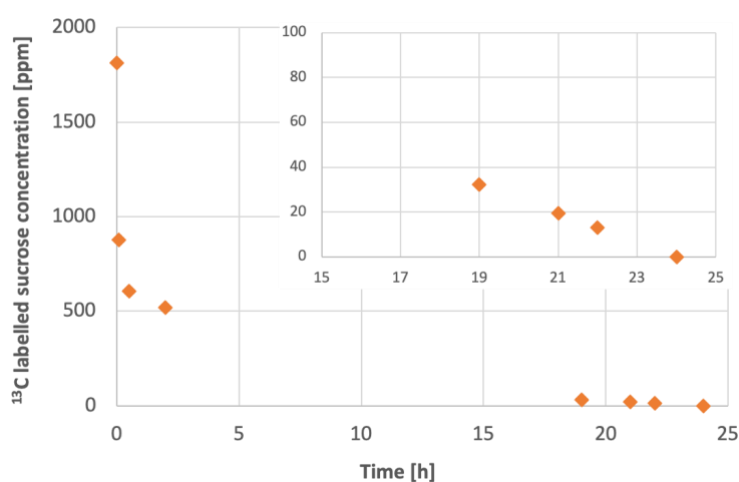


Figure 3.12. ^{13}C labelled sucrose concentrations in pore solutions during hydration of C_3S . Pore solutions were extracted at different moments from the beginning of hydration until 26 h. ^{13}C labelled sucrose concentration was defined by using ^1H detected INEPT NMR.

4 Impact of sucrose on initial hydration kinetics of tricalcium silicate

Foreword: This chapter represents original research performed by and written up by the author of this thesis under the guidance of Prof. Robert J. Flatt. The NMR work received additional guidance by Dr. René Verel (ETHZ) and Prof. Jean-Baptiste d’Espinose (ESPCI). The ^1H detected INEPT method reported here was suggested by Dr. Deni Mance. Most calorimetry measurements were performed using a series of in-situ mixing cells produced by M. Martin Keller.

This chapter has formed the basis for a paper submitted to Cement and Concrete Research on 11 February 2024. The data analysis is improved but conclusions remain the same.

4.1 Introduction

In this chapter, we focus on the impact of sucrose on C_3S hydration kinetics. To this end, the main method used is the calorimetry measurement, which allows to identify different period of hydration and to follow the heat production during whole hydration process. Our focus is placed on understanding how the related kinetics are modified by sucrose, a question that has a long history, dating back at least to year in the paper by Thomas and Birchall in 1983 [63]. There are also a variety of opinions on the nature of the rate combining mechanisms.

To resolve this open question, our initial intention was to directly measure sucrose on the surface of C_3S by NMR using ^{29}Si enriched C_3S and ^{13}C labelled sucrose. Thereby, we were hoping to see if the sucrose might be displaced from solution to surface or surface to surface during hydration. Unfortunately, these attempts were unsuccessful. Thereby, we did however find a novel procedure to follow the concentration of sucrose in solution with largely enhanced sensitivity using ^1H detected INEPT NMR. The advantage of this technique is that it mainly measures the target ^1H in liquid phase and the effect of water ^1H doesn’t affect the following quantification from ^1H signal intensity.

These results together BET specific surface area measurements (SSA) helped us to determine the evolution of sucrose over time up to the first stages of the acceleration period. They helped us decide to focus on initial adsorption to studying the induction period. Consequently, for the rest of our adsorption measurements, we used the simpler method of Total Organic Carbon analysis (TOC).

In the face of this debated topic, one strategy developed in this chapter has been to run calorimetry experiment at different temperatures, because this provides insight into the activation energy of the process which can help understand the rate controlling step with or without sucrose. Such measurements turned out to be very sensitive on the quality of the temperature control, which led us having to mix samples within the calorimeter and place the

calorimeter itself within a climate-controlled room. The combination of calorimetry and adsorption measurements at different temperatures leads to a simple new insight into the impact of sucrose on the initial hydration of C₃S.

In what follows, the chapter first presents the results obtained (calorimetry, adsorption, SSA and time evolution of sucrose both adsorbed and in solution). It is followed by a discussion section that established a very simple model accounting for how sucrose delays the emergence of the acceleration period in C₃S hydration. Implications and limitations of these findings are then discussed more broadly before presenting our final conclusions on this topic.

4.2 Results

4.2.1 Calorimetry

This section reports systematic measures of hydration kinetics of C₃S as a function of sucrose dosage and temperature. It turned out that for a sufficient stability of the instrument and reproducibility of the measurements at low temperatures, samples had to be mixed *in situ* (within the calorimeter). The in-situ setups and sample preparation are presented in chapter 3. Additionally, in particular for the lowest temperature we had to place the instrument in a room regulated at an even lower temperature to insure good stability. The rationalization of the impact of sucrose that is derived in our work only became possible once we eliminated artifacts thanks to both those measures.

As for the adsorption measurements, the sucrose was dissolved in a 0.1 M NaOH solution. The C₃S powder has a specific surface area of 1.82 m²/g. It is therefore slightly lower than for the samples used for adsorption (2.06 m²/g C₃S). This is due to different milling batches and is something that we will be considering in our data analysis by reporting dosages and adsorption with respect to the surface of C₃S in a suspension, rather than its mass.

4.2.1.1 Definitions of the hydration onset and the slope in the acceleration period

A single hydration curve contains a lot of information, which for our purpose we will reduce to two main features: the onset and the maximum rate. As shown schematically in Figure 4.1, we use the maximum rate (slope), R_{max} , to also define the onset time, t_{OS} , taking the intercept with the abscissa. There are different views on whether C₃S does or not have a true onset of the main hydration peak. However, additions of sucrose (and many other chemical admixtures) tend to shift the acceleration period to later times, without substantially changing its slope or the height of the peak Figure 4.2. From this perspective the effect of sucrose on C₃S hydration appears to involve delaying the occurrence of a critical event. From a data analysis point of view, the effect of sucrose “is just” a shift in time of the acceleration period and does not depend on the heat rate taken to define it.

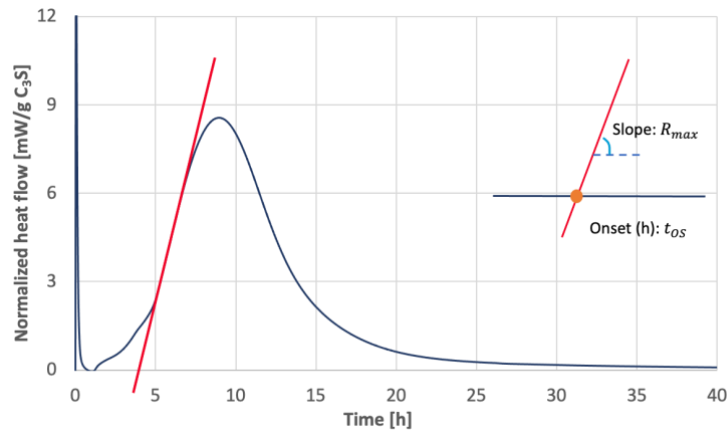


Figure 4.1. An example of the C_3S hydration curve to show the definitions of t_{OS} and R_{max} .

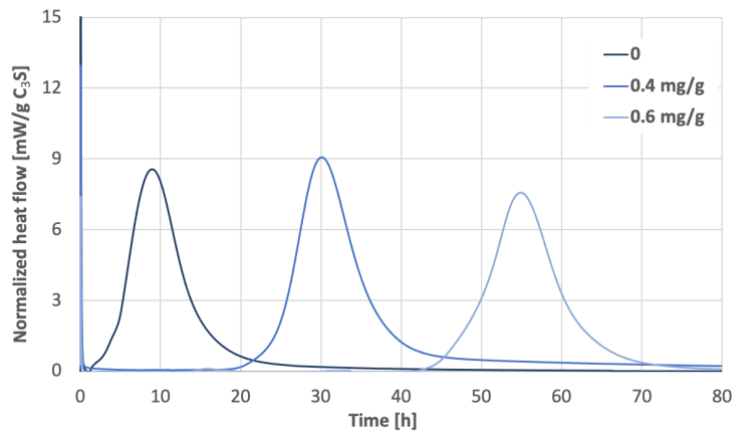


Figure 4.2. Effect of sucrose dosage on the hydration retardation of C_3S . The different curves show that up to 0.6 mg/g sucrose, the sucrose dosage does not cause significant changes in slope of acceleration period and the maximum heat rate. C_3S used in these experiments has the same SSA of 1.82 m²/g.

4.2.1.2 Change of hydration onset and slope in the acceleration period with sucrose

Based on the above definitions, t_{OS} and R_{max} are extracted from each calorimetry measurement and plotted versus sucrose dosage in Figure 4.3a and b. This shows that t_{OS} increases with decreasing temperature regardless of the sucrose dosage and that this increase is nonlinear.

As to R_{max} , it increases with temperature, but shows different trends with respect to sucrose dosage depending on the temperature. For the measurements at 10 °C and 23 °C, values remain relatively stable up to sucrose dosage of 0.15 mg/m² C_3S .

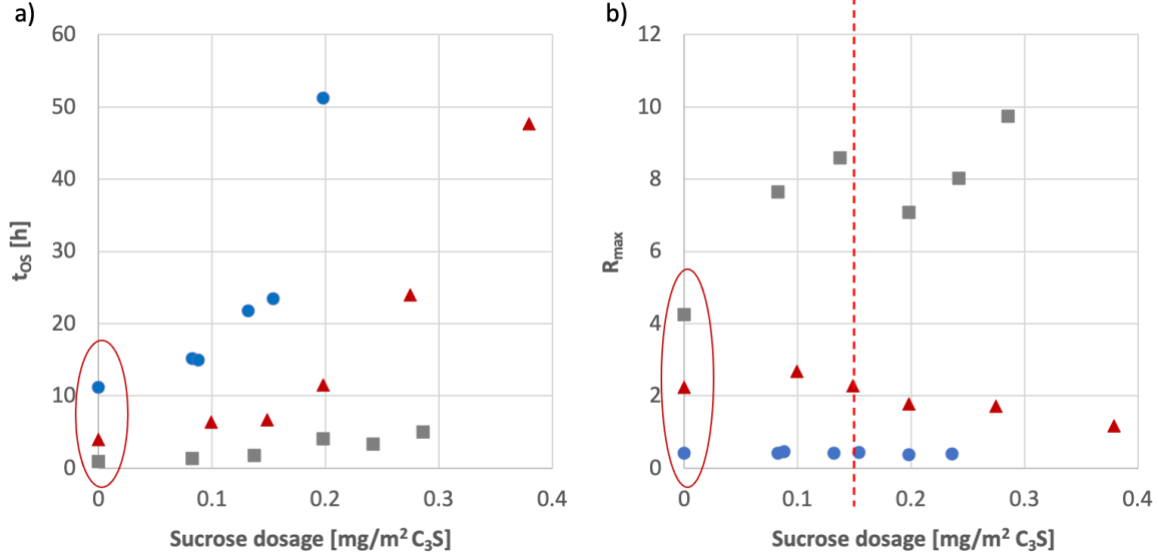


Figure 4.3. a) t_{os} and b) R_{max} extracted from calorimetry experiments containing different sucrose dosages and at different temperatures. (Circles: 10 °C, triangles: 23 °C, squares: 35 °C).

4.2.2 Initial Adsorption

4.2.2.1 Langmuir isotherm

The adsorption of sucrose on the surface of synthetic C_3S was measured at 10 °C, 23 °C and 40 °C in a solution of 0.1 M NaOH to mimic the pH of cementitious systems. The adsorbed amount is obtained by deducting the sucrose remaining in solution from total one dosed. Values are then normalized by the mass of C_3S . Results reported in Figure 4.4 show a sharper initial increase in adsorption at lower temperatures. Data points appear to outliers are marked with empty symbols. Leaving those data points aside, we find that the data at each temperature can be relatively well fitted by a Langmuir isotherm [100] (lines in Figure 4.4):

$$c_{ads} = \frac{K_T c_{sol} c_{\infty}}{1 + K_T c_{sol}} \quad (4-1)$$

which is linearized as:

$$\frac{1}{c_{ads}} = \frac{1}{c_{sol} c_{\infty} K_T} + \frac{1}{c_{\infty}} \quad (4-2)$$

The corresponding plots have high correlation coefficients, as shown in Figure 4.5. The ordinate of the fit gives $1/c_{\infty}$ while the slope is $1/K_T c_{\infty}$. Because K_T represents an equilibrium constant between the solution and the surface, it makes sense to use molar fraction units for the concentration c of sucrose in solution. Thereby the value of K_T can be subsequently used in a thermodynamic analysis.

The fitting parameters obtained are summarized in Table 4.1. They also highlight a decrease in the adsorption plateau as the temperature is increasing (0.52 mg/g, 0.43 mg/g and 0.35 mg/g at 10 °C, 23 °C and 40 °C respectively). Values are also reported per unit surface area of C₃S, which is the most adequate representation for powders. The specific surface area used in sucrose adsorption measurements is 2.06 m²/g C₃S.

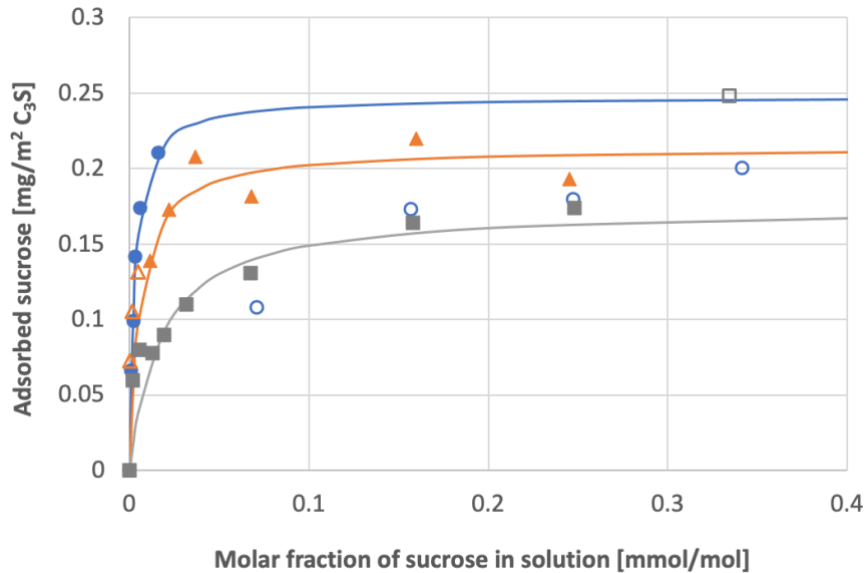


Figure 4.4. Adsorption of sucrose on C₃S at different temperatures (Circles: 10 °C; triangles: 23 °C; squares: 40 °C). The continuous lines indicate the Langmuir fits of which the parameters are reported in Table 4.1. Filled symbols were used for the regression, while open symbols were considered as outliers and left out.

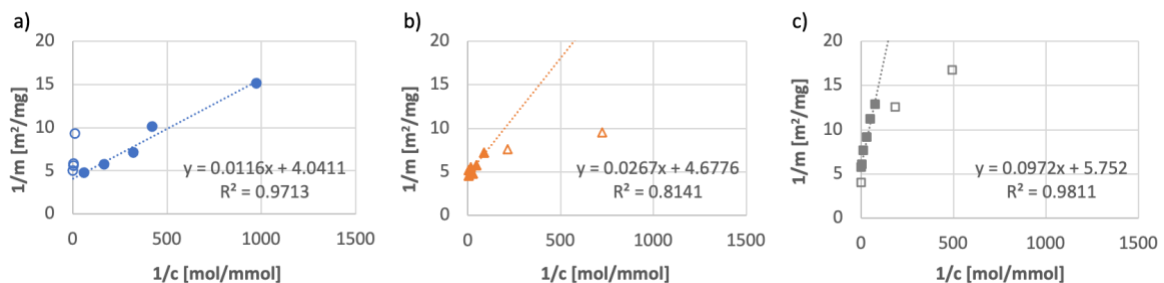


Figure 4.5. Adsorption data plots with linearized Langmuir equation of sucrose on C₃S at different temperatures (Circles: 10 °C; triangles: 23 °C; squares: 40 °C). Filled symbols were used for the regression, while open symbols were considered as outliers and left out.

Table 4.1. Parameters describing adsorption K_T and c_∞ correspond to values obtained for a Langmuir isotherm, while c_∞^* comes the empirical fit described by equation (4-12). K_T^* is the equilibrium constant which is obtained when sucrose concentration in solution was used in ppm instead of molar concentration.

Temperature (°C)	$K_T \cdot 10^3$	K_T^*	c_∞ (mg/g)	c_∞ (mg/m ²)	c_∞^* (mg/m ²)
10	348.37	2.47E-02	0.52	0.25	0.46
23	175.19	9.20E-03	0.43	0.21	0.32
40	59.18	2.55E-03	0.35	0.17	0.15

4.2.2.2 Adsorption in relation to dosage

In calorimetry experiments we use a certain dosage of admixtures and will wish to know what extent of adsorption this leads to. Therefore, in what follows we present means to predicting adsorption from dosage, since the Langmuir isotherm only gives the link between solution concentration and adsorption.

Adsorption from Langmuir isotherm and mass balance

For this, we need a mass balance on the dosed sucrose mass, m_{dos} is:

$$m_{dos} = c_{ads} \cdot S + c_{sol} \cdot L \quad (4-3)$$

S is the total surface of solid in m² and L is the liquid volume in liter.

The dosage c_{dos} expressed in mass per surface of adsorbate is:

$$c_{dos} = \frac{m_{dos}}{S} = c_{ads} + c_{sol} \cdot \frac{L}{S} \quad (4-4)$$

Let us now use Equation (4-1) to express c_{sol} as a function of c_{ads} . For this we rearrange it as follows:

$$c_{ads}(1 + K_T^* \cdot c_{sol}) = K_T^* \cdot c_{sol} \cdot c_{\infty} \quad (4-5)$$

$$c_{ads} = c_{sol} \cdot (K_T^* \cdot c_{\infty} - K_T^* \cdot c_{ads}) \quad (4-6)$$

And we obtain

$$c_{sol} = \frac{c_{ads}}{K_T^* \cdot (c_{\infty} - c_{ads})} \quad (4-7)$$

Substitution equation (4-7) into (4-4) gives:

$$c_{dos} = c_{ads} + \frac{c_{ads}}{K_T^* \cdot (c_{\infty} - c_{ads})} \cdot \frac{L}{S} \quad (4-8)$$

which can be rearranged to obtain a second order equation:

$$c_{dos} \cdot K_T^* \cdot (c_\infty - c_{ads}) = c_{ads} \cdot K_T^* \cdot (c_\infty - c_{ads}) + c_{ads} \cdot \frac{L}{S}$$

$$c_{ads}^2 \cdot K_T^* - c_{ads} \cdot \left(K_T^* \cdot c_\infty + \frac{L}{S} + c_{dos} \cdot K_T^* \right) + c_{dos} \cdot K_T^* \cdot c_\infty = 0 \quad (4-9)$$

For which the solution is:

$$c_{ads} = \frac{\left(K_T^* \cdot c_\infty + \frac{L}{S} + c_{dos} \cdot K_T^* \right) - \sqrt{\Delta}}{2 \cdot K_T^*} \quad (4-10)$$

with

$$\Delta = \left(K_T^* \cdot c_\infty + \frac{L}{S} + c_{dos} \cdot K_T^* \right)^2 - 4 K_T^{*2} \cdot c_{dos} \cdot c_\infty \quad (4-11)$$

and where c_{ads} is the adsorption obtained from the Langmuir isotherm for a selected dosage c_{dos} of sucrose.

As c_{ads} is a function of c_{dos} , we can solve the above equation to find the value of c_{ads} for a given dosage. As already mentioned, the C₃S used in calorimetry measurements has different SSA than the adsorption measurement, which we factor in by expressing dosages in mg/ m².

Adsorption from empirical relation

The second option to determine adsorption from dosage builds upon the fact that our adsorption measurements were done at the same L/S ratio than the calorimetry measurements. Therefore, it also makes most sense to plot adsorption versus dosage and use a best fit to determine adsorption at the dosages used in our calorimetry tests. With respect to using the normal Langmuir fit, this has the advantage of not forcing a physical model that contains intrinsic limitations. A shortcoming of this is that the result is specific to the selected L/S value used, which for our purpose however is perfectly acceptable.

When plotting adsorption versus dosage, it is interesting to see that the adsorption is close to linear at low dosage range, which is a normal result for a Langmuir isotherm (Figure 4.6). It is also seen that values appear to plateau-off at higher dosages. Therefore, to simplify the previous solution, we consider empirically fitting our adsorption data with a Langmuir type-equation using however dosage rather than solution concentration. While this does not have a physical meaning, it would capture both an initial linear range and a plateau.

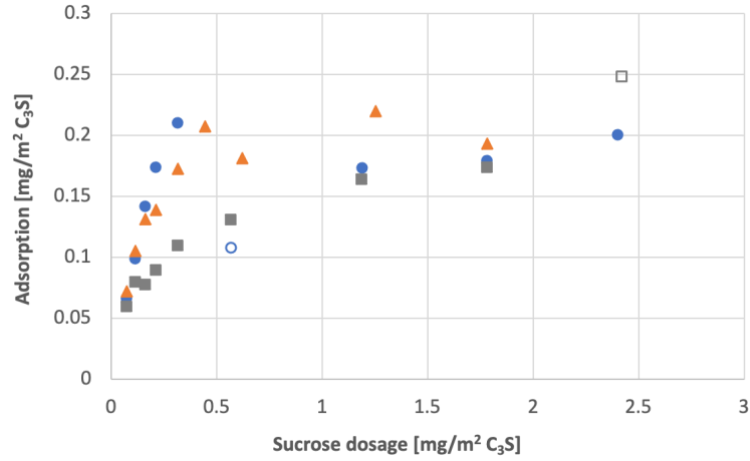


Figure 4.6. Adsorption of sucrose on C₃S at different temperatures (Circles: 10 °C; triangles: 23 °C; squares: 40 °C).

Therefore, we empirically consider that adsorption may be fitted to dosage according to:

$$c_{ads} = \frac{c_{dos}c_{\infty}^*K_T^{\#}}{1 + c_{dos}K_T^{\#}} \quad (4-12)$$

where c_{∞}^* the plateau and $c_{\infty}^*K_T^{\#}$ is the slope at low dosage (between adsorption and dosage)

Because all curves appear to have a similar behavior at low dosage, it is worth reexamining the fitting procedure by rewriting Equation (4-12) as:

$$\frac{1}{c_{ads}} = \frac{1}{c_{\infty}^*} + \frac{1}{c_{\infty}^*K_T^{\#}c_{dos}} \quad (4-13)$$

and plotting $\frac{1}{c_{ads}}$ versus $\frac{1}{c_{dos}}$.

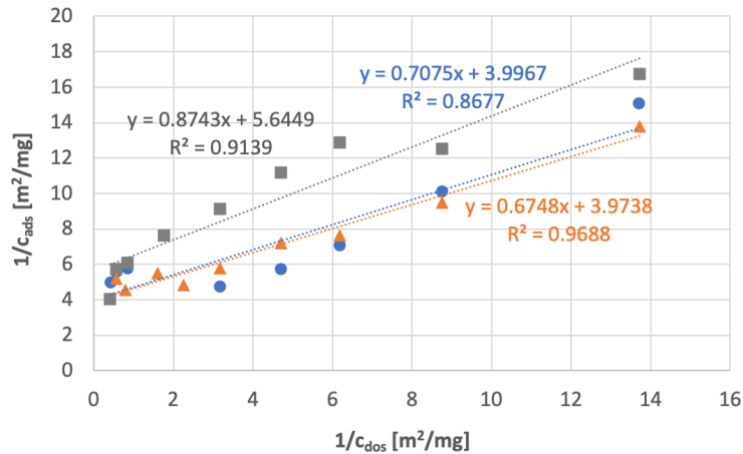


Figure 4.7. Linearized form of equation (4-12) (circles: 10 °C, triangles: 23 °C, squares: 40 °C).

As shown in Figure 4.7, such plots are roughly linear at all temperatures and have very similar slopes (term $1/c_{\infty}^* K_T^{\#}$ in (4-12)). This points to similar slopes in the linear regime of adsorption at different temperatures, implying that a fixed fraction of sucrose would adsorb at low dosage. Accepting this as a fact, we refit all data assuming of a common value of $c_{\infty}^* K_T^{\#}$ at all temperatures. This gives the general value of 1.24 for $c_{\infty}^* K_T^{\#}$, while for c_{∞}^* , we get 0.46 mg/m² (10 °C), 0.32 mg/m² (23 °C) and 0.15 mg/m² (40 °C) depending on the temperature.

It is clear that all $c_{\infty}^* K_T^{\#}$ values are larger than 1. From a physical point of view, having a value of $c_{\infty}^* K_T^{\#}$ larger than 1 does not make sense, because it implies that more sucrose would adsorb than is actually added. However, this only concerns extremely low dosages, below our range of interest. Moreover, as shown in Figure 4.8, the obtained fits (solid lines) match the experimental data very well in the dosage range considered for our calorimetry experiments. To highlight this, the discontinuous lines show the maximum dosages (vertical) used in calorimetry measurements. The horizontal discontinuous line identifies plateau values obtained by taking the average of adsorption data from the last few data points at each temperature in Figure 4.6 (not the c_{∞}^* from Figure 4.7).

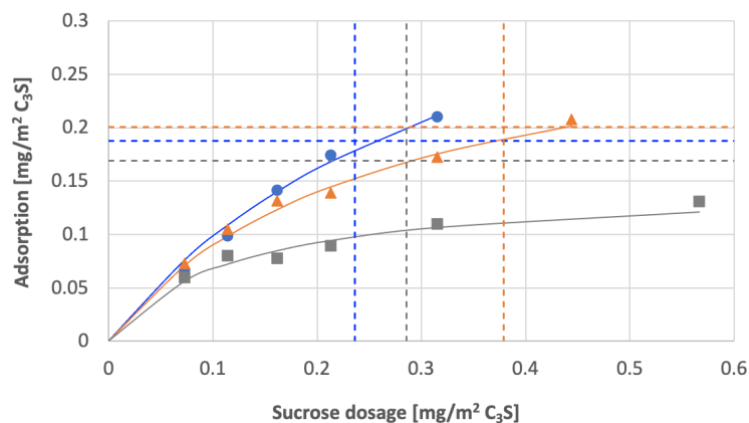


Figure 4.8. Zoom-in in low dosage range for the Adsorption of sucrose on C₃S at different temperatures (Circles: 10 °C; triangles: 23 °C; squares: 40 °C).

We now examine the dependence of c_{∞}^* , on temperature. As shown in Figure 4.9, we find that it varies linearly with temperature. The linear regression in that figure allows us to estimate the plateau value of c_{∞}^* to be used in equation (4-12), which further allows to estimate adsorption in relation to dosage at various temperatures (keeping $c_{\infty}^* K_T^{\#}$ as 1.24).

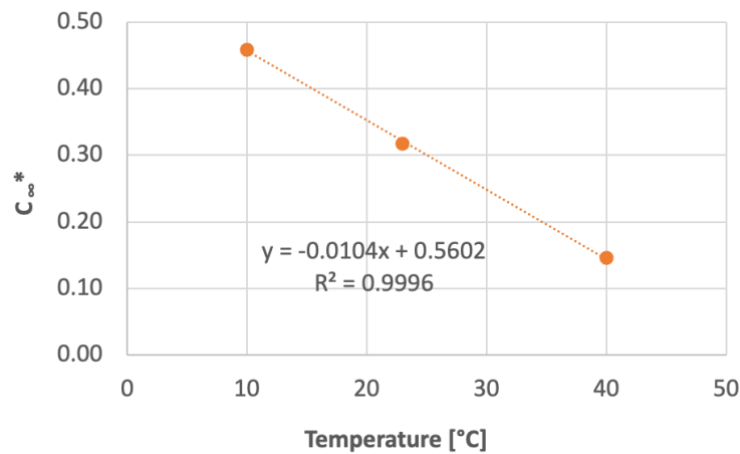


Figure 4.9. Relation of c_{∞}^* from equation (4-12) with respect to temperature.

Concerning the adsorption plateau value estimated with this procedure, c_{∞}^* , we note that they are substantially higher than those obtained from the Langmuir isotherm (Table 4.1). Hereby, we must however underline that values obtained from the Langmuir isotherm are constrained (for good or for bad) to the underlying assumption of its physical model. In contrast, values of c_{∞}^* should simply be considered as fitting parameters that provide a good match to experimental observations over the range of dosages of interest.

4.2.3 Time dependent Adsorption

The free C₃S surface is an important factor when considering the adsorption. Therefore, we study the evolution of SSA and adsorption during the hydration of C₃S. Many of these experiments derived from our initial and unfortunately unsuccessful attempts to directly measure sucrose on the surface of C₃S by NMR using ²⁹Si enriched C₃S and ¹³C labelled sucrose.

In our experiments aimed at following the adsorption of C₃S over time, we thought to minimize errors from sample variability. Therefore, we prepared a large amount of C₃S paste (L/S 0.7 in 0.1 M NaOH solution) that was split into small portions of which the hydration was stopped later at different times. Additionally, a calorimetry measurement was run on the same paste.

In order to enhance the NMR sensitivity on sucrose, ^{13}C labelled sucrose was used with an initial dosage of $0.49 \text{ mg/m}^2 \text{ C}_3\text{S}$. The small portions of paste were stored at room temperature then centrifuged at selected times during either the induction or the acceleration period. The solid part obtained after centrifugation was freeze-dried and then used to measure the SSA with BET.

The evolution of SSA over time is plotted in Figure 4.10a, along with the corresponding calorimetry curve. The onset of the hydration estimated from calorimetry curve is 13.67 h, estimated with the same method as described in section 4.2.1.1. The SSA increases slightly in the induction period, from $1.24 \text{ m}^2/\text{g}$ to $2.03 \text{ m}^2/\text{g}$ during the first 15 h (64%). Then, the quick increase happens not immediately at the onset but after 17 h, changing from $2.15 \text{ m}^2/\text{g}$ to $14.91 \text{ m}^2/\text{g}$ in the following 6 h. This is probably because the lab temperature for storing the pastes is slightly different from that of the calorimeter ($23 \text{ }^\circ\text{C}$).

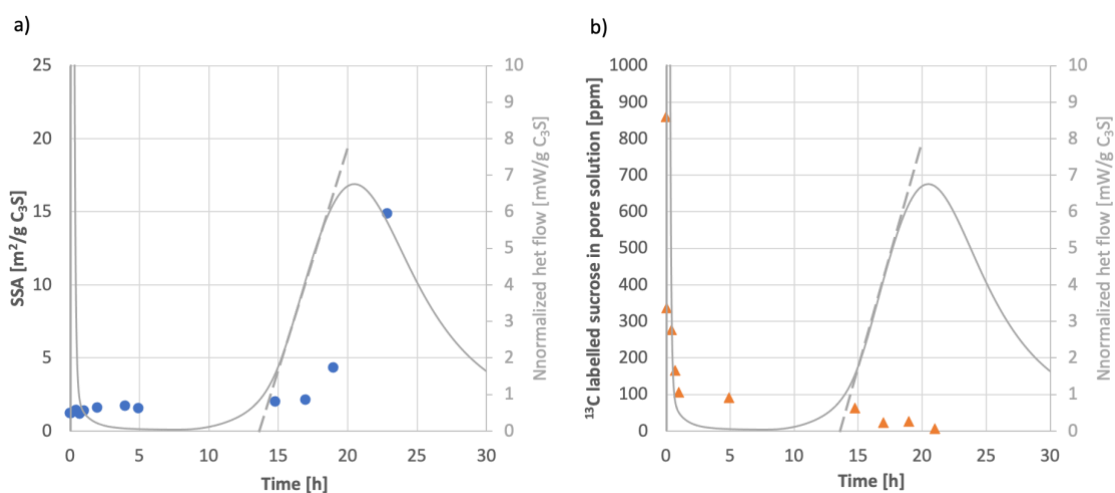


Figure 4.10. Evolution of a) SSA and b) sucrose concentration in pore solution during the hydration of C_3S in presence of sucrose. The discontinuous line is the tangent in the linear range in acceleration period, the crossing point of this line with time axis represents the onset.

The evolution of sucrose in pore solution during the same hydration process was measured by ^1H detected INEPT NMR due to its ability in detecting sucrose with low concentrations. The detail about this technique is described in chapter 3. Due to the use of insert (prepared for measuring paste) in NMR rotor, the speed of MAS was increased to 1500 Hz so that the calibration line was measured again with new set-ups.

We must note that with ^1H detected INEPT NMR, we selected the ^1H signal from sucrose in solution after several pause transfers. Therefore, this technique does not allow a direct quantification from signal intensity. For our purpose of analyzing the evolution of sucrose during hydration, a relative quantification method was developed based on establishing a calibration line.

For doing so, we diluted the 3 mM ^{13}C labelled sucrose/ D_2O solution in several steps and each time measured ^1H spectrum with ^1H detected INEPT NMR. Since the small signal peaks were rarely visible for low concentrations, we only focused on the most intense ^1H peak between 4.05 and 3.70 ppm in spectrum (Figure 4.11). Taking the intensity of this peak from spectrum obtained from each sample and normalizing it by the mass of the relative NMR sample and the number of scans, a calibration line could be obtained by plotting normalized NMR signal intensity versus ^{13}C labelled sucrose concentrations (Figure 4.12).

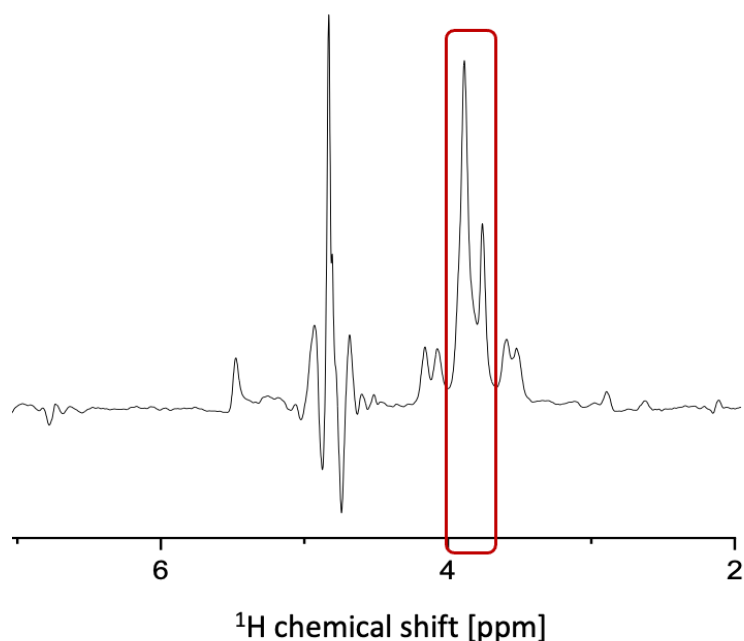


Figure 4.11. ^1H detected INEPT NMR spectrum on 3 mM ^{13}C labelled sucrose/ D_2O solution, MAS at 1500 Hz.

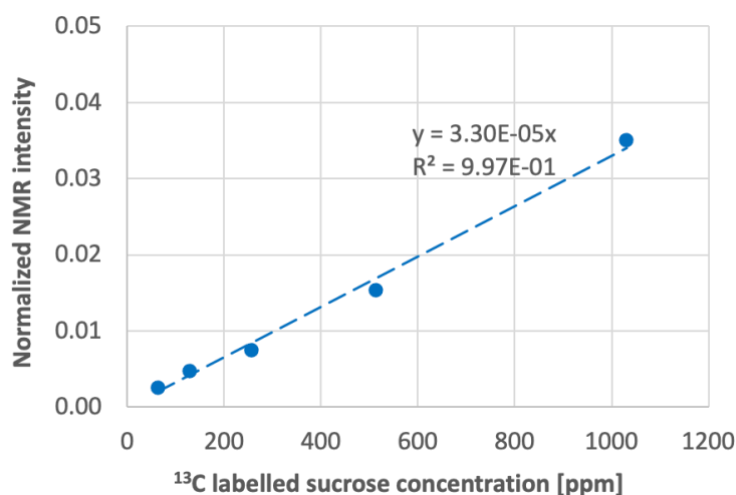


Figure 4.12. Establishment of calibration line from ^1H detected INEPT NMR.

For real pore solutions containing ^{13}C labelled sucrose and separated out at different hydration times, the ^1H detected INEPT NMR spectrums were collected. With normalized NMR

intensity between 4.05 and 3.70 ppm, the ^{13}C labelled sucrose concentration can be calculated from the calibration line as shown in Figure 4.12. The evolution of sucrose during the hydration is presented in Figure 4.10b. The first orange point at time 0 is obtained from the initial ^{13}C labelled sucrose solution used for preparing the paste, the second point corresponds to the pore solution extracted right after mixing (3 min). It shows that the sucrose concentration in pore solution sharply drops, in this case by 88%, after the mixing. Then, it decreases slowly in the induction period (another 5% in 14 h) and drops again but much slower than the initial one once the hydration passed the onset.

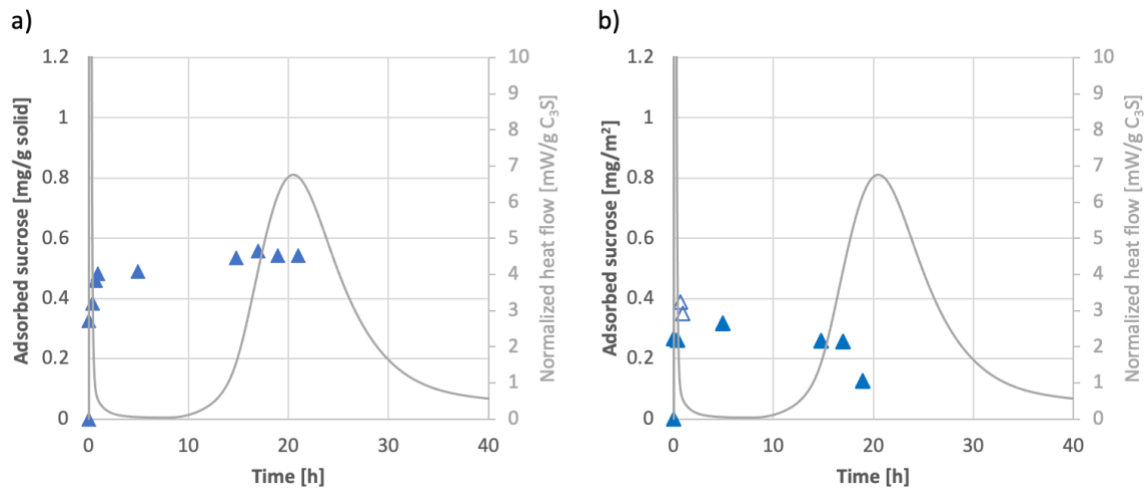


Figure 4.13. Evolution of sucrose adsorption during the hydration of C_3S . a) adsorption of sucrose per unit mass of solid; b) adsorption of sucrose per unit surface of solid.

Knowing the amount of sucrose that remains in pore solution, we determined the adsorption over time by deducting the remaining sucrose from its initial dosage. Figure 4.13a shows the evolution of adsorption during hydration expressed as sucrose mass by mass of C_3S . More meaningful for adsorption is to report such data by surface area rather than by mass of the solid. This is done in Figure 4.13b, and shows that adsorption (or better surface coverage) remains constant after mixing until the onset, with an average adsorption of 0.26 mg/m^2 , which is similar to the adsorption plateau estimated from Langmuir isotherm (Table 4.1).

4.2.4 Temperature dependence of initial adsorption

Figure 4.4 shows that the adsorption of sucrose on C_3S surface is temperature dependent. This reversible reaction can be written as [101]:



A represents sucrose, S refers to free surface site on C_3S surface and SA is the occupied surface site by sucrose.

With sucrose dosage high enough, we notice in Figure 4.13b that adsorption on C₃S reaches its saturation plateau right after mixing and remains unchanged when hydration is in the dormant period. We can therefore assume that the adsorption data used in Langmuir isotherm fitting at each temperature were obtained at equilibrium. The equilibrium constant of adsorption K_T from Langmuir fitting parameter is the same as the equilibrium constant of above reaction, and can be written as:

$$K_T = \frac{[SA]}{[A][S]} \quad (4-15)$$

where $[A]$ is the activity of sucrose molecule in solution, $[S]$ is the activity of free C₃S surface site and $[SA]$ is the activity of occupied C₃S surface site.

From a thermodynamic point of view, for adsorption at each temperature, the change of Gibbs free energy (ΔG) can be written as a function of the change of enthalpy (ΔH), the change of entropy (ΔS) and the absolute temperature T (in Kelvin):

$$\Delta G = \Delta H - T\Delta S = -RT \ln K_T \quad (4-16)$$

We have therefore

$$-R \ln K_T = \frac{\Delta H}{T} - \Delta S \quad (4-17)$$

Values for K_T at different temperatures are obtained from Langmuir isotherm parameter as shown in Table 4.1. R is universal gas constant with the value of 8.314 J/mol/K. We then plot ($-R \ln K_T$) as a function of $1/T$ in Figure 4.14. The slope gives ΔH and the intercept is ($-\Delta S$). This plot gives ΔH -44 KJ/mol, ΔS -106 J/mol and ΔG about -12 KJ/mol at 23 °C.

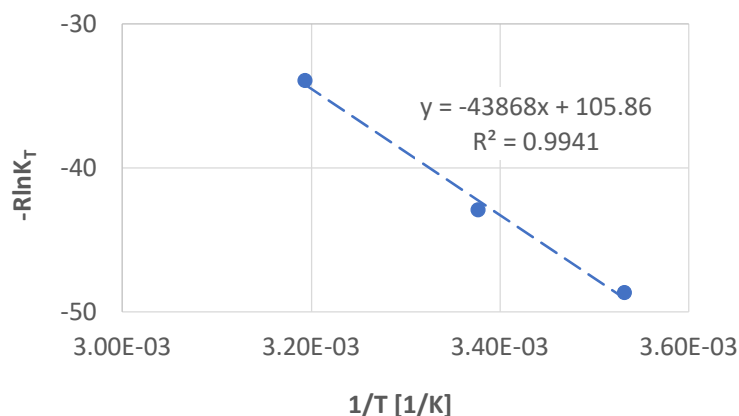


Figure 4.14. ($-R \ln K_T$) plotted in function of $1/T$.

4.3 Discussion

4.3.1 Evolution of adsorption in the induction period

Results from the previous section suggest that adsorption, expressed in terms of adsorbed sucrose per surface area of hydrating C₃S is constant during the induction period. Once the acceleration period begins, the sucrose in solution starts to drop, being adsorbed in precipitating hydrates, until no more sucrose is available. After that, surface coverage by sucrose drops rapidly as a direct result of the additional surfaces created.

This implies that the onset of the acceleration period may occur slightly before the drop in surface coverage by the sucrose. More importantly for the analysis that will follow, we argue that since the surface coverage is constant over the majority of the induction period, it is sufficient to examine initial adsorption to gain mechanistic insight on the role of surface coverage, which is the logic followed by our analysis below. First however, we examine the temperature dependence of C₃S hydration in absence of sucrose.

4.3.2 Impact of sucrose on the induction period rate

4.3.2.1 Degree of hydration at the onset

With the calorimetry data, we have the cumulative heat H_t at time t , and H_t / H_{total} gives the degree of hydration (DOH). As illustrated in Figure 4.15, the DOH remains almost constant until the onset. The DOH at the onset is noted as $DOH_{t_{os}}$ (Figure 4.15). Therefore, the hydration rate during the induction period, ν_{ind} , can also be defined as $DOH_{t_{os}}/t_{os}$

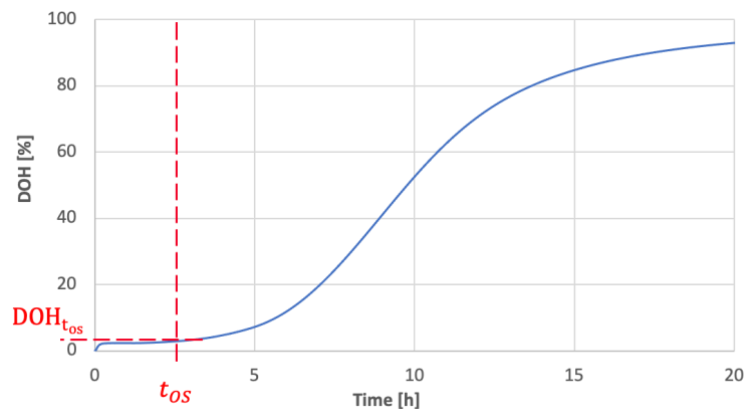


Figure 4.15. Definition of the degree of hydration at the onset.

Getting the $DOH_{t_{os}}$ for all calorimetry experiments and plotting their values versus sucrose dosages, it can be seen that for each temperature, $DOH_{t_{os}}$ is independent to the sucrose dosage (Figure 4.16). Besides, it also decreases while increasing the temperature, the average $DOH_{t_{os}}$ values are given in Table 4.2.

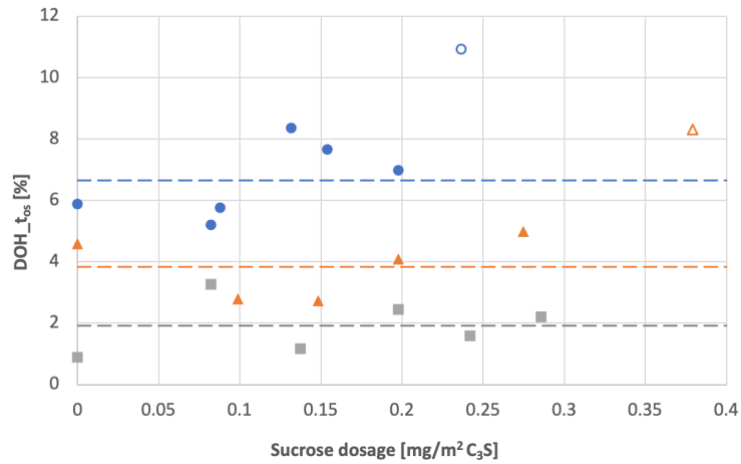


Figure 4.16. Evolution of DOH at the onset with sucrose dosages and at different temperatures. Circles: 10 °C; triangles: 23 °C; squares: 35 °C. The discontinuous line gives the average $DOH_{t_{0s}}$ value for the corresponding temperature.

Table 4.2. Average $DOH_{t_{0s}}$ at different temperatures

Temperature (°C)	Average $DOH_{t_{0s}}$ [%]
10	6.64
23	3.83
35	1.93

4.3.2.2 Hydration rate in the induction period

Since $DOH_{t_{0s}}$ appears to be independent of sucrose dosage, when calculating ν_{ind} we use the average $DOH_{t_{0s}}$ for the considered temperature and divide it by the individual t_{0s} of experiment in question. The reference rate ν_{ind}^0 is the ν_{ind} for the experiment without sucrose at the temperature considered.

In Figure 4.17, by normalizing all values of ν_{ind} at a given temperature by the rate ν_{ind}^0 obtained at the same temperature, rather surprisingly, we find that all points collapse together on a single master curve, which suggests that the impact of sucrose on C_3S hydration is not temperature dependent.

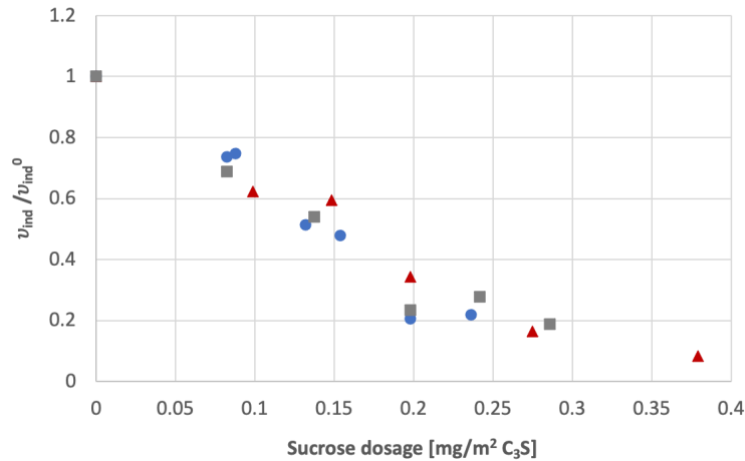


Figure 4.17. Normalized hydration speed in induction period in function of sucrose dosage. (Circles: 10 °C; triangles: 23 °C; squares: 35 °C)

Figure 4.17 shows an initial linear decrease of the normalized velocity as sucrose dosage increases. At higher dosages, the slope becomes less steep, indicating that v_{ind} probably tends asymptotically towards zero as dosage is increased. Importantly the most significant impact of sucrose on the induction rate occurs at low dosages, which is also when most of the added sucrose adsorbs (about 87%). This suggests that the adsorbed amount of sucrose may control retardation.

4.3.2.3 Impact of adsorption on induction period hydration rate

Based on results in section 4.3.2.1, hydration degrees reached at the onset are low, which implies assuming constant conditions during the induction period appears reasonable. This is further supported by the fact that adsorption per unit surface area is also constant during that period (section 4.2.3). Therefore, discussed in section 4.3.1, we mainly examine hydration kinetics in relation to initial adsorption. For this we need to determine the amount of sucrose adsorbed at the dosages used in the calorimetry experiments.

In section 4.2.2, we developed two methods to build up the relation between adsorption and dosage: 1) from Langmuir isotherm and mass balance, 2) from an empirical relation. With the first method, the equation (4-10) and (4-11) are used to calculate the adsorption for each dosage being used in calorimetry measurements. With the second method, equation (4-12) is used for this. With these adsorption estimates, our normalized velocities from Figure 4.17 can be replotted versus adsorption. As can be seen in Figure 4.18, no matter which method is used, data separate into different series that are linear over the whole adsorption range. This implies a linear decrease of v_{ind}/v_{ind}^0 down to zero, which would be reached for well-defined values of adsorption.

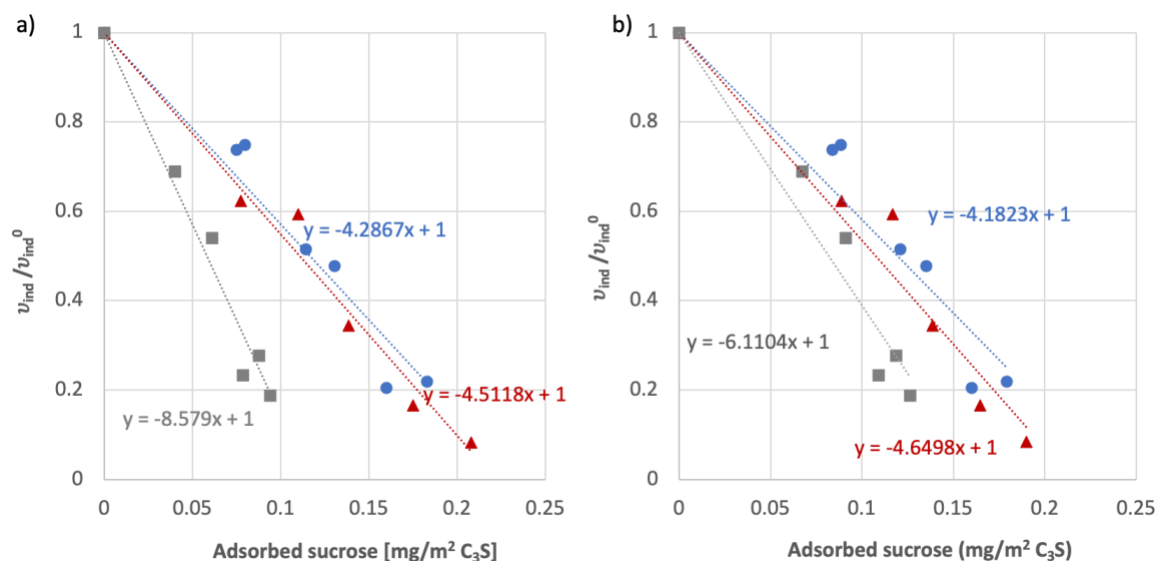


Figure 4.18. Normalized hydration speed in induction period in function of adsorbed sucrose. The adsorbed sucrose was calculated from a) Langmuir isotherm and mass balance; b) empirical relation. (Circle: 10 °; triangle: 23 °C; square: 35 °C). The discontinuously lines are linear regressions imposing the ordinate at the origin to be 1.

It is natural to wonder whether those critical adsorption values correspond to those of the plateau, as this would imply that the rate is zero when the surface is fully covered. To examine this hypothesis, we compare Langmuir adsorption plateau in mg/m^2 with the intercept of the regression lines in Figure 4.18 with the abscissa (also in mg/m^2). As shown in Table 4.3, these values are all very close to each other, particularly for 10 and 23 °C. For the values at 35 °C, we should note that this is the temperature at which calorimetry was measured, but that adsorption was measured at 40 °C. This is the value reported in Table 4.3, the column “Intercept 1” derives from using the 40 °C adsorption in Figure 4.18. But the last column “Intercept 2” uses the estimate for adsorption at 35 °C based on Figure 4.9 . In any case, all values are quite similar and the data analysis can be considered meaningful.

Table 4.3. Comparison of maximum adsorption from calorimetry analysis and Langmuir isotherm

Temperature (°C)	c_{∞} Langmuir (mg/m^2)	c_{∞} Intercept 1 (mg/m^2)	c_{∞} Intercept 2 (mg/m^2)
10	0.25	0.23	0.24
23	0.21	0.22	0.22
35	0.17*	0.12**	0.16

* The adsorption plateau at 40 °C.

** The c_{∞} at 35 °C is calculated by using the Langmuir fitting parameters for TOC data points at 40 °C.

Based on the above, we assume that the intercept of the regression lines corresponds to the adsorption plateau c_{∞} . We therefore replot our data as a function of the surface coverage θ taken as c/c_{∞} . As shown in Figure 4.19, this brings all data back onto a single master curve, which is linear between a relative velocity of 1 at zero surface coverage ($\theta=0$), and a velocity of zero for full surface coverage ($\theta=1$). The impact of sucrose may therefore be represented through the following equation:

$$\frac{v_{ind}}{v_{ind}^0} = 1 - \theta \quad (4-18)$$

which we can also write more generally to include the effect of temperature on C₃S hydration:

$$v_{ind} = A \exp\left(-\frac{Ea}{RT}\right) (1 - \theta) \quad (4-19)$$

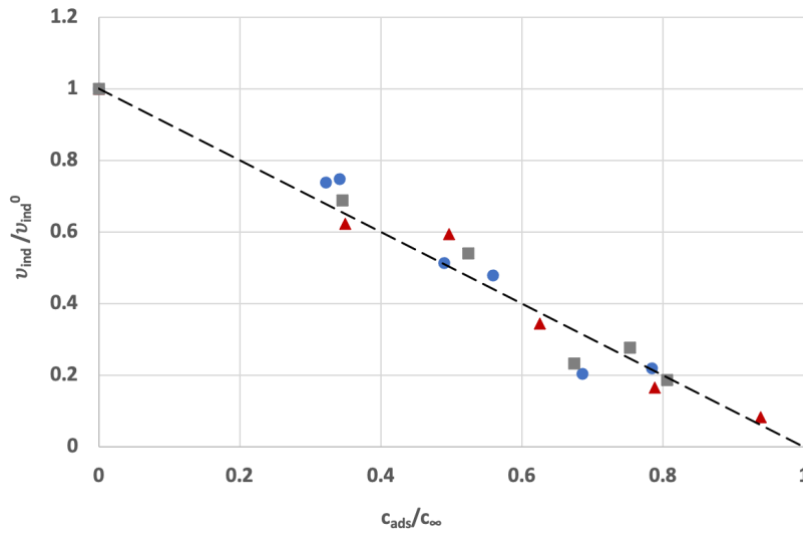


Figure 4.19. Normalized hydration speed in induction period in function of normalized sucrose adsorption. (circles: 10 °C, triangles: 23 °C, squares: 35 °C)

4.3.3 Impact of temperature on hydration

Our previous analysis suggests that the impact of temperature on C₃S hydration is independent on the presence of sucrose, at least in the induction period. To analyze this more generally, we examine how t_{OS} and R_{max} changing with the temperature and focus for this on data without sucrose (data in the red circles in Figure 4.3).

In terms of temperature dependence, we may assume that the Arrhenius equation holds, so that:

$$v_{ind} = A \cdot \exp\left(-\frac{Ea}{RT}\right) \quad (4-20)$$

where A is a frequency factor, Ea is an activation energy, R the universal gas constant and T the absolute temperature.

This equation can be linearized as:

$$\ln(v_{ind}) = \ln(A) - \frac{Ea}{RT} \quad (4-21)$$

so that plotting $\ln(v_{ind})$ versus $-1/RT$ would be linear with a slope of Ea if the Arrhenius equation holds. As shown in Figure 4.20a, this is the case, and the slope indicates the activation energy to be about 36 kJ/mol. However, as showing in Figure 4.20b, if the velocity is only approximated as being inversely proportional to the onset time, then a value about twice larger is obtained (72 kJ/mol). This underlines the important of considering the velocity in terms of a progress of the degree of hydration.

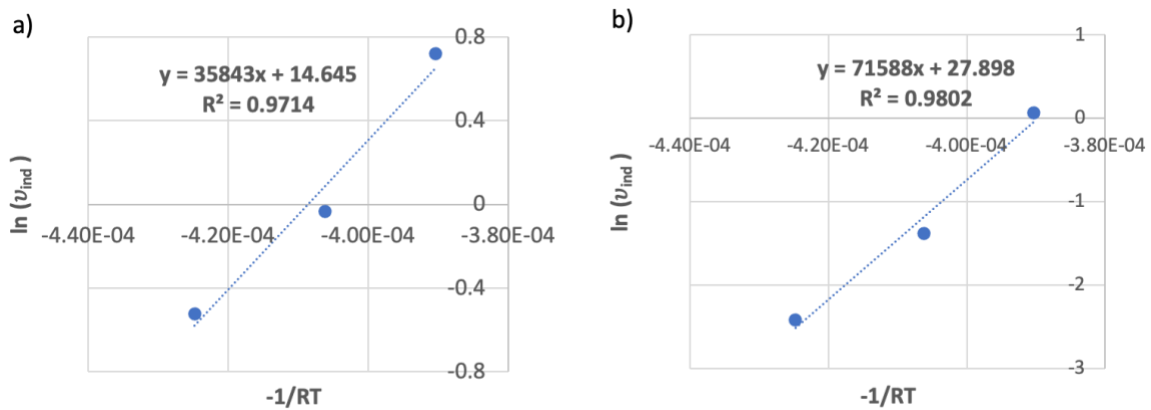


Figure 4.20. Linearized Arrhenius plots with different definitions of the velocity. a) $v_{ind} = DOH_{t_{os}}/t_{os}$; b) $v_{ind} = 1/t_{os}$.

The value of 36 kJ/mol is very close to what Juilland and Gallucci reported for direct dissolution measurements of alite. Those authors identified two regimes depending on the undersaturation conditions of the surface [102]. For low undersaturation conditions that are more representative of our pastes, they indicate the activation energy to be about 48 kJ/mol. While this work examined the role of varying solution compositions, it did not explore pH values as high as ours, which may account for the difference with respect to our study.

Using a scanning calorimetry on pastes similar to ours, Thomas inferred very similar activation energies to Juilland and Gallucci, both for C_3S and cement, 51 kJ/mol and 48 kJ/mol respectively [102], [103]. A previous study by the same author applied the boundary nucleation and growth theory to study the hydration kinetics of C_3S [35]. In that case, the data was fitted assuming the existence of an onset time, but these we later not analyzed. Of relevance to our study however is the fact that the model includes two rate constants, one of which defines the rate of transformation of the boundary (surface of particles) by the formation of nuclei on that boundary. This should a priori also control the very early hydration, before the acceleration period and interestingly found to be 31 kJ/mol.

It is unclear whether this should also be related to the dissolution of C_3S , the formation of C-S-H nucleation on its surface or some other form of surface modification. The fact that the rate

of hydration in the induction period should decrease linearly with the free surface, suggests rather that we are facing a problem of dissolution. However, we cannot exclude that nucleation of C-S-H is at stake. Unfortunately, we are not aware of published data on the activation energy of that process, which could a priori provide us some selection criteria between both hypotheses.

4.3.4 Changes in the acceleration period

The situation during the acceleration is more complex than during the induction period. Indeed, as seen in Figure 4.3, while t_{OS} increases with dosages regardless of temperature, R_{max} exhibits a more complex behavior. The fact that it is only slightly modified by sucrose at 10 and 23°C suggests that once the acceleration period has started, the reaction is no more affected by that admixture. However, the fact that the maximum rate should increase with sucrose at higher temperatures is more surprising. Furthermore, the analysis of kinetics during the acceleration period is more complex and requires a model that accounts for the acceleration. This rapidly leads to model dependent analysis, which is why in this thesis we decided to keep our main focus on the induction period.

For example, while it is worth pointing out that values of R_{max} also show an Arrhenius type behavior (Figure 4.21), it is difficult to know whether the activation energy obtained of (69 kJ/mol) has a mechanistic meaning.

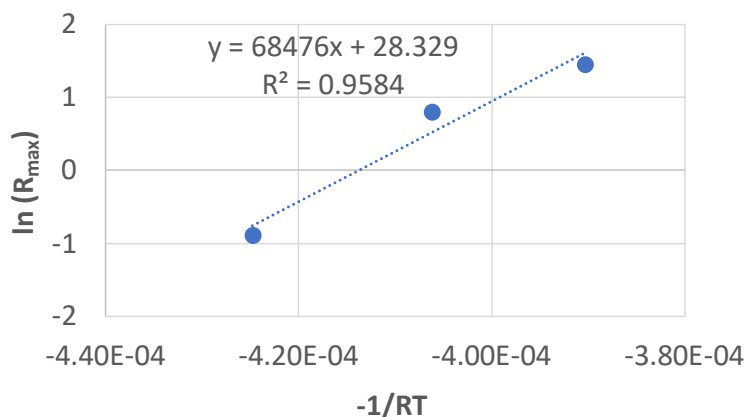


Figure 4.21 Linearized Arrhenius plot for the acceleration period of calorimetry measurements without sucrose at different temperatures.

4.4 Conclusions

Research on C₃S hydration often debates the existence or absence of a true onset for the main hydration peak. However, it is accepted that the addition of retarders, here sucrose, leads to a clear onset that increase with admixture dosage. In this chapter, rather than once again entering the debate on the onset in absence of admixtures, we have examined how sucrose addition may affect it.

Results show that they are very consistent whether or not sucrose is included, which point to the fact that considering an onset does make sense. In our case, this has been defined as the intersection between the line of maximum rate and the abscissa. Importantly, we found that the degree of hydration reached at that point is temperature dependent, which led us to a more robust definition of an average hydration rate in the induction period. This in turn led us to estimate an activation energy of about 36 kJ/mol, close to but not equivalent to that for the dissolution of C₃S (50 kJ/mol). This difference may result from our experiments using a higher pH solution, or from nucleation at the particle surfaces playing an important role.

Concerning the impact of sucrose on hydration kinetics, we found that this appears to vary linearly with the surface that is not occupied by sucrose. Interestingly that free surface depends on the temperature through a changing adsorption plateau. However, when this is taken into account, we find that the hydration rate in the induction period is given by the product between the hydration rate in absence of sucrose and the free surface fraction.

Considering the long-standing debate on the impact of sugars on C₃S hydration, this result appears extremely simple. However, obtaining this required to eliminate numerous misleading experimental errors. In particular, in situ mixing and placing the calorimeter in a climate-controlled room were essential. It should also be noted that adsorption measurements involved additional delicate data analysis, to get the best possible relation to the conditions of the pastes measured by calorimetry.

Finally, we underlined that our results detail the rate in the induction period, leaving aside the more complex question of the main peak. However, since changes in the onset time have the greatest significance for practice, this approach is well justified and it appears that an important enigma in cement hydration kinetics has now gained extra clarity.

4.5 Acknowledgements

Support for Ms. Weiqing Xu was provided by the SNF project (No. 172481) titled “Molecular control of cement hydration through tailored chemical admixtures”.

The authors would like to acknowledge the help of Dr. René Verel (ETHZ) and Dr. Deni Mance in setting-up the NMR experiments and designing the pulse sequence, and Prof. Jean-Baptiste d’Espinoise (ESPCI) for constructive discussions in NMR data analyzing. In addition, we would like to thank M. Martin Keller for producing a series of in-situ mixing cells to support the calorimetry measurements.

5 Impact of portlandite on C₃S retardation by sucrose

Foreword: This chapter represents original research performed by and written up by the author of this thesis under the guidance of Prof. Robert J. Flatt.

5.1 Introduction

In the previous chapter we studied the retarding impact that sucrose has on cement hydration. A main conclusion there was that adsorption plays a central role, whereby the hydration rate in the induction period is proportional to the C₃S surface not occupied by adsorbed sucrose. Our main conclusion was that this was probably reflective of an inhibition of C₃S dissolution, although we could not fully exclude an inhibition of C-S-H nucleation of on the C₃S surface.

Another mechanism that has been advanced concerning retardation by sucrose is that it inhibits the nucleation of portlandite [38], [102]. Indeed, it was argued that if CH nucleation is hindered, the concentration in solution should increase to the point where C₃S dissolution becomes very slow [38]. It follows, that addition of CH would be expected to decrease retardation by sucrose, which was demonstrated experimentally on OPC by Reiter et al [72]. In fact, those authors found that, in OPC pastes, adsorption of sucrose on CH was strongly favored, causing retardation to decrease in direct relation of the amount of sucrose that consumed by CH.

Such a behavior could help refine our hypothesis on the retardation mechanism by sucrose, which is why we study it in further detail in this chapter. Our focus here remains on C₃S in 0.1 M NaOH solution to keep the sucrose in a similar state of deprotonation that could be expected in OPC pastes. As a reference point, the work presented also examines as the impact that CH itself has on the hydration of C₃S, a topic that has a long debate regarding its possible role in the end of the induction period. While our purpose is not to revive that discussion. However, we do reveal that the hydration rate in the induction period is proportional to the combined surface of C₃S and CH. This finding underlines that kinetic models about sucrose in that period need to account for a possible change in availability of those surface by adsorbed sucrose. When taking this into account all observations can be rationalized, consolidating our basic principle model of how sucrose modifies hydration kinetics of the induction period.

5.2 Results

5.2.1 Calorimetry

To follow the hydration process, calorimetry experiments were done for C₃S hydrating with fixed amount of sucrose and different dosages of CH. The CH dosages used in this study were 0, 0.02, 0.04, 0.05, 0.06, 0.09 and 0.28 g/m² C₃S. At the same time, C₃S hydrating only with the same dosages of CH were also traced by calorimetry measurements to determine reference behaviors without sucrose.

Regarding sample preparation, the C₃S powder was firstly mixed by hand with different amounts of CH powder. Suspensions were prepared to reach a defined solid to liquid ratio of 0.7 and a sucrose dosage of 0.5 mg/g C₃S (0.27 mg/m² C₃S) in 0.1 M NaOH/UPW solution. For this, we used a stock solution of 710 ppm sucrose that added to C₃S for L/S 0.7 achieves the desired sucrose dosage. To keep L/S constant for samples additionally containing CH, an extra amount of a 0.1 M NaOH/UPW solution was added to reach the targeted L/S of 0.7. Different from the in-situ mixing that we described in C₃S chapter, here the paste was mixed *ex situ* by Vortex mixer for 1 min and 30 s before being introduced into the calorimeter.

In Figure 5.1, we notice that the addition of CH or sucrose alone does not substantially change the height or maximum slope of the main peak, but only shifts it to earlier or later times respectively. However, the combined addition of sucrose and CH largely increases the height of this peak, while not changing the maximum slope.

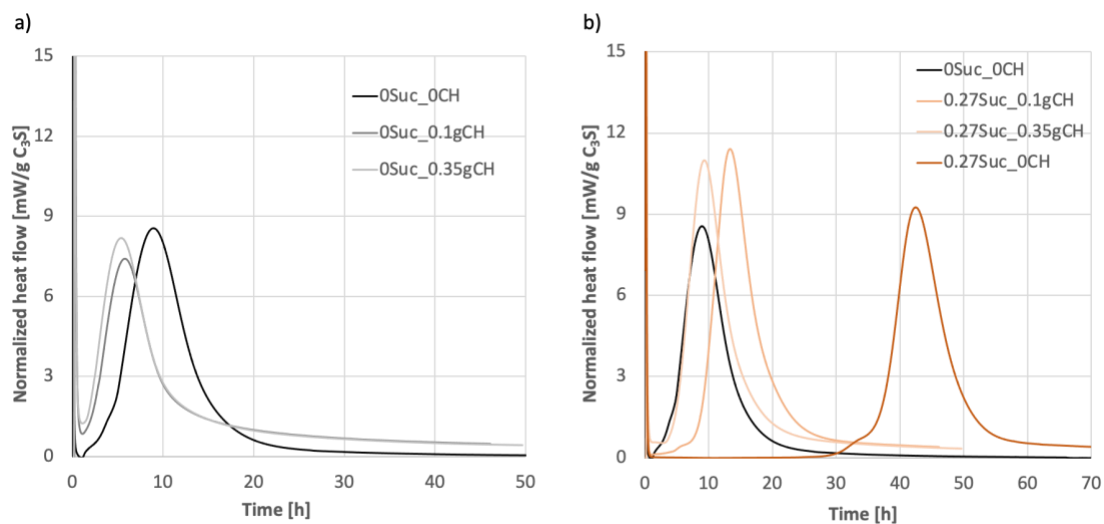


Figure 5.1. Acceleration of CH on C₃S hydration a) without sucrose; b) with sucrose.

We also tested the effect of direct and delay addition of CH on the C₃S hydration with sucrose. Calorimetry samples prepared for direct addition was prepared as described previously. For delayed addition, C₃S was firstly mixed with 0.1 M NaOH/UPW solution containing sucrose by Vortex mixer for 1 min and 30 s, with the stock solution added so as to reach L/S 0.7 with respect to C₃S. After another 3 min, 0.1 g CH (0.02 g/m² C₃S) was added along with the amount of stock solution needed to keep the total L/S to 0.7. Mixing again with Vortex mixer for 30 s before introducing the sample into the calorimeter. The delay time is counted from the first contact of liquid and solid and ends once the sample is introduced into the calorimeter, giving 5 min in total.

Results are plotted in Figure 5.2. The three samples had the same sucrose dosage. The one not containing CH shows the longest retardation, while to two others are very similar. This shows that the addition mode of CH does not play a role, in accordance with the findings of Reiter on OPC [73].

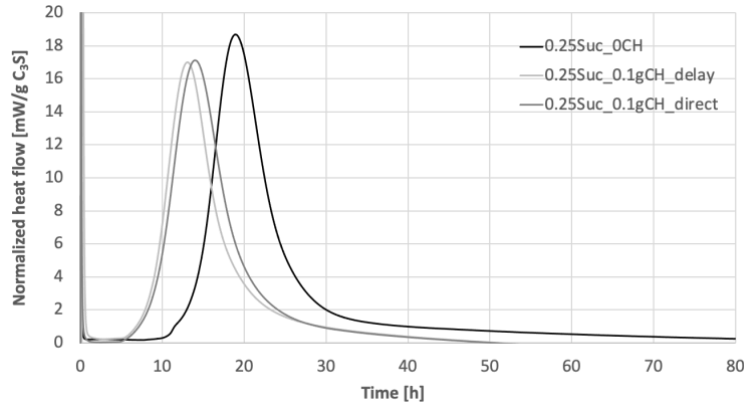


Figure 5.2. Effect of delay and direct addition of CH on C_3S hydration with sucrose.

5.2.2 Initial adsorption

The adsorption of sucrose on the commercial CH was measured at 23 °C in a solution containing 0.1 M NaOH to mimic the pH of cementitious systems. The liquid to solid ratio is 2. The adsorbed amount is obtained by deducting the sucrose remaining in solution from total one dosed. Values are then normalized by the total surface of CH, to obtain adsorption in mg/m^2 CH. Results reported in Figure 5.3a show a sharp initial increase in adsorption. This represents a linear regime with a slope of 0.81, indicating that up to high dosages about 81% of the added sucrose is adsorbed under these conditions (Figure 5.3b). However, our calorimetry experiments involve other liquid to solid ratios, in addition to the presence of C_3S . It is therefore preferable to examine sucrose adsorption with a model based on an equilibrium between surface and solution. For doing this, we preferably fit data in the range of interest by a Langmuir isotherm (solid line in Figure 5.3a):

$$c_{ads} = \frac{K_T c_{\infty} c_{sol}}{1 + K_T c_{sol}} \quad (5-1)$$

where c_{ads} is the adsorbed amount per unit surface area, c_{sol} is the solution concentration, c_{∞} is the adsorption plateau and K_T is the equilibrium constant.

This equation can be linearized as:

$$\frac{1}{c_{ads}} = \frac{1}{K_T c_{\infty}} \cdot \frac{1}{c_{sol}} + \frac{1}{c_{\infty}} \quad (5-2)$$

The corresponding plots have high correlation coefficients, as shown in Figure 5.4. The ordinate of the fit gives $1/c_{\infty}$ while the slope is $1/K_T c_{\infty}$. The concentration c_{sol} is in ppm, while c_{ads} is in mg/m^2 CH.

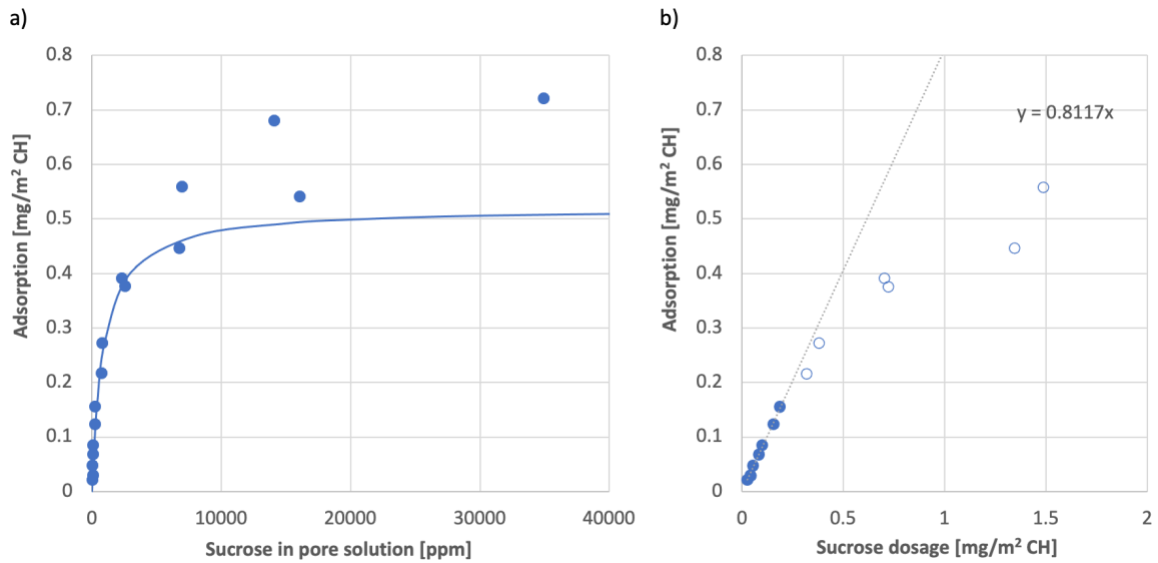


Figure 5.3. Adsorption of sucrose on the CH. a) TOC measurement points in circles and the Langmuir fitting curve in solid line. b) Adsorption versus sucrose dosage in the low dosage range.

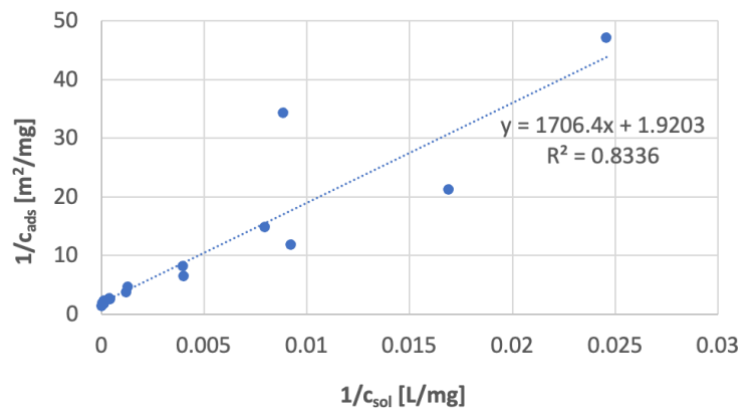


Figure 5.4. Plot of linearized Langmuir equation.

The sucrose adsorption on synthetic C₃S data was reported in the previous chapter. It was fitted with a Langmuir isotherm as shown in Figure 5.5. The data were measured at 23 °C with the same pH, but also the same liquid to solid ratio as used for preparing the paste for calorimetry measurement (0.7). That adsorption isotherm also shows a sharp initial increase in adsorption but the experimental data points in the very low dosage range were not taken into consideration when doing the fitting with the Langmuir equation.

The fitting parameters used for sucrose adsorption on CH and on C₃S are summarized in Table 5.1. They suggest that the affinity of sucrose for C₃S is much higher than for CH, contrary to what could be inferred from the work of Reiter on OPC pastes [73], a difference that could be due to the composition of the pore solution.

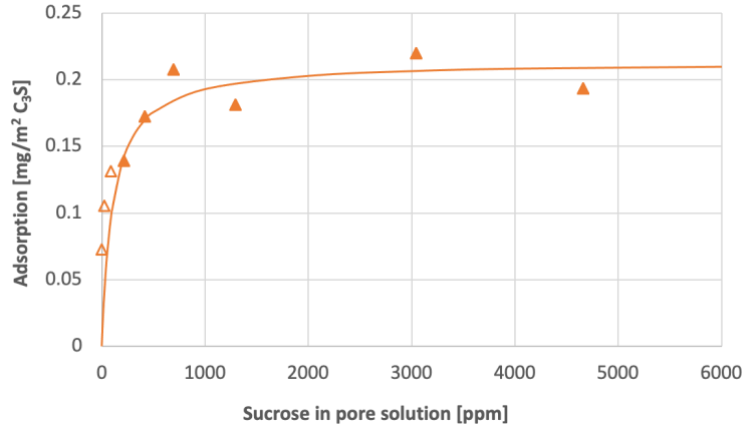


Figure 5.5. Adsorption of sucrose on C₃S. TOC measurement points in triangles and the Langmuir fitting curve in solid line. Empty points are not considered for fitting the data with Langmuir equation.

Table 5.1. Langmuir fitting parameters for sucrose adsorption on CH and C₃S surface. K_T is the equilibrium constant obtained when sucrose concentration in solution is used in ppm and adsorption in mg/m².

	K_T	c_∞ (mg/m ²)
Sucrose on CH	0.0011	0.52
Sucrose on C ₃ S	0.0092	0.21

5.2.3 Adsorption from Langmuir isotherm and mass balance

For C₃S hydration with sucrose and CH, we need to consider that sucrose could adsorb on both minerals. Therefore, in what follows we present a way to predict this for specified dosages. Our analysis begins by assuming that sucrose will reach equilibrium with both surfaces. Both Langmuir isotherm equations must then be satisfied for the same solution concentration.

Based on the Langmuir equation, we can write the coverage of sucrose on surface i as θ_i :

$$\theta_i = \frac{c_{ads,i}}{c_{\infty,i}} = \frac{K_{T,i} \cdot c_{sol}}{1 + K_{T,i} \cdot c_{sol}} \quad (5-3)$$

where $c_{ads,i}$ is the adsorbed amount on surface i (mg/m²), $c_{\infty,i}$ is the adsorption plateau on surface i (mg/m²), $K_{T,i}$ is the equilibrium constant with surface i (in L/mg) and c_{sol} is the solution concentration (in mg/L).

The mass balance on the dosed mass m of sucrose is:

$$m = c_{sol} \cdot L + \sum_i \theta_i \cdot c_{\infty,i} \cdot S_i \quad (5-4)$$

where S_i is the surface in m^2 of phase i and L is the liquid volume in units compatible with those of the solution concentration c_{sol} .

Noting the dosage c in mg per m^2 of solid 1 (C₃S), we have:

$$c = c_{sol} \cdot \frac{L}{S_1} + \sum_i \theta_i \cdot c_{\infty,i} \cdot \frac{S_i}{S_1} \quad (5-5)$$

Substitution of equation (5-3) into (5-5), we obtain

$$c = c_{sol} \cdot \frac{L}{S_1} + \sum_i \frac{K_{T,i} \cdot c_{sol} \cdot c_{\infty,i}}{1 + K_{T,i} \cdot c_{sol}} \cdot \frac{S_i}{S_1} \quad (5-6)$$

The general solution numerically solving this equation to obtain the value of c_{sol} that gives the value of c used as dosage. However, in our experiments, we have only two surfaces and for the case of CH (phase 2) we are in the linear range, which allows obtaining an analytical solution for c_{sol} . For such cases, we can rewrite (5-6) as:

$$c = c_{sol} \cdot \left(\frac{L}{S_1} + \frac{K_{T,1} \cdot c_{\infty,1}}{1 + K_{T,1} \cdot c_{sol}} + K_{T,2} \cdot c_{\infty,2} \cdot \frac{S_2}{S_1} \right) \quad (5-7)$$

which can be rearranged to

$$\begin{aligned} c(1 + K_{T,1} \cdot c_{sol}) = \\ \frac{L}{S_1} c_{sol} + \frac{L}{S_1} K_{T,1} c_{sol}^2 + K_{T,1} c_{\infty,1} c_{sol} + K_{T,2} c_{\infty,2} \frac{S_2}{S_1} c_{sol} \\ + K_{T,1} K_{T,2} c_{\infty,2} \frac{S_2}{S_1} c_{sol}^2 \end{aligned} \quad (5-8)$$

Giving the second order equation

$$\begin{aligned} c_{sol}^2 K_{T,1} \left(\frac{L}{S_1} + K_{T,2} c_{\infty,2} \frac{S_2}{S_1} \right) \\ + c_{sol} \left(K_{T,1} c_{\infty,1} + \frac{L}{S_1} + K_{T,2} c_{\infty,2} \frac{S_2}{S_1} - K_{T,1} c \right) - c = 0 \end{aligned} \quad (5-9)$$

For which the solution is

$$c_{sol} = \frac{-\left(K_{T,C_3S}c_{\infty,C_3S} + \frac{L}{S_{C_3S}} + K_{T,CH}c_{\infty,CH}\frac{S_{CH}}{S_{C_3S}} - K_{T,C_3S}c\right) + \sqrt{\Delta}}{2K_{T,C_3S}\left(\frac{L}{S_{C_3S}} + K_{T,CH}c_{\infty,CH}\frac{S_{CH}}{S_{C_3S}}\right)} \quad (5-10)$$

with

$$\Delta = \left(K_{T,C_3S}c_{\infty,C_3S} + \frac{L}{S_{C_3S}} + K_{T,CH}c_{\infty,CH}\frac{S_{CH}}{S_{C_3S}} - K_{T,C_3S}c\right)^2 + 4cK_{T,C_3S}\left(\frac{L}{S_{C_3S}} + K_{T,2}c_{\infty,2}\frac{S_{CH}}{S_{C_3S}}\right) \quad (5-11)$$

The surface coverage of sucrose on C₃S is:

$$\theta_{C_3S} = \frac{c_{ads,C_3S}}{c_{\infty,C_3S}} = \frac{K_{T,C_3S} \cdot c_{sol}}{1 + K_{T,C_3S} \cdot c_{sol}} \quad (5-12)$$

And the surface coverage of sucrose on CH is

$$\theta_{CH} = \frac{c_{ads,CH}}{c_{\infty,CH}} = \frac{K_{T,CH} \cdot c_{sol}}{1 + K_{T,CH} \cdot c_{sol}} \quad (5-13)$$

These equations very well match the exact numerical solutions as shown in Figure 5.6.

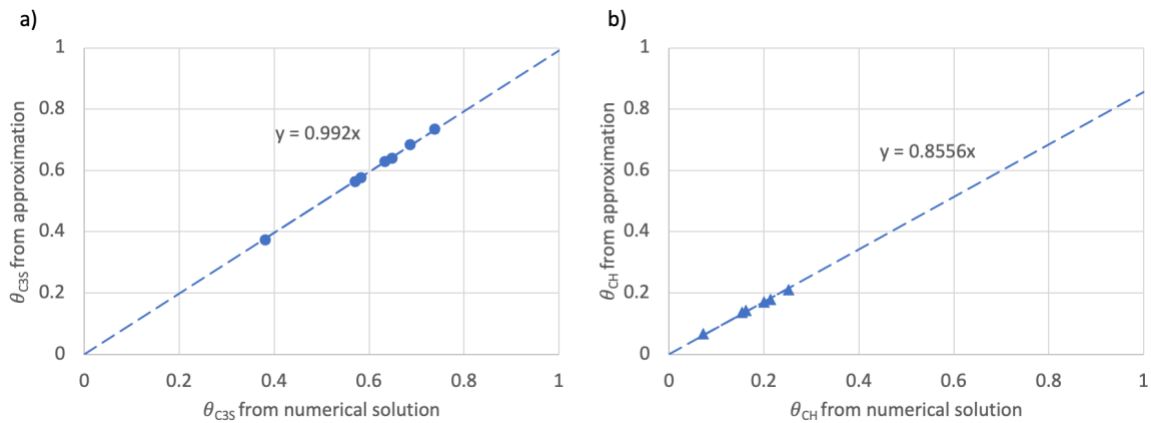


Figure 5.6. Comparison of surface coverage of sucrose on a) C₃S and on b) CH obtained by using the equations and from the numerical solutions.

5.2.4 Impact of CH on the maximum slope of the acceleration period

Based on the calorimetry curves, the onset (t_{os}) and the slope in the acceleration period (R_{max}) are extracted as described in the previous chapter. As shown in Figure 5.7, C_3S hydration with sucrose presents higher R_{max} in general except for the last one with CH dosage $0.28 \text{ g/m}^2 C_3S$. The addition of CH to the system causes an increase of R_{max} in both cases. This increase of R_{max} is 0.96 for hydration without sucrose and 0.97 for hydration with sucrose, which means the addition of CH increases the R_{max} in the same way for C_3S hydration with or without sucrose. Besides, it is clear that R_{max} does not change with CH dosage. The average slope for hydrations with both sucrose and CH give a small increase of 0.40 comparing to that for hydrations only with CH. Similarly, for hydrations without CH, the addition of sucrose also causes an increase in R_{max} of 0.39. This indicates that sucrose changes the slope in acceleration period in same way no matter CH is added or not. Also, it has much smaller effect on this issue than CH does.

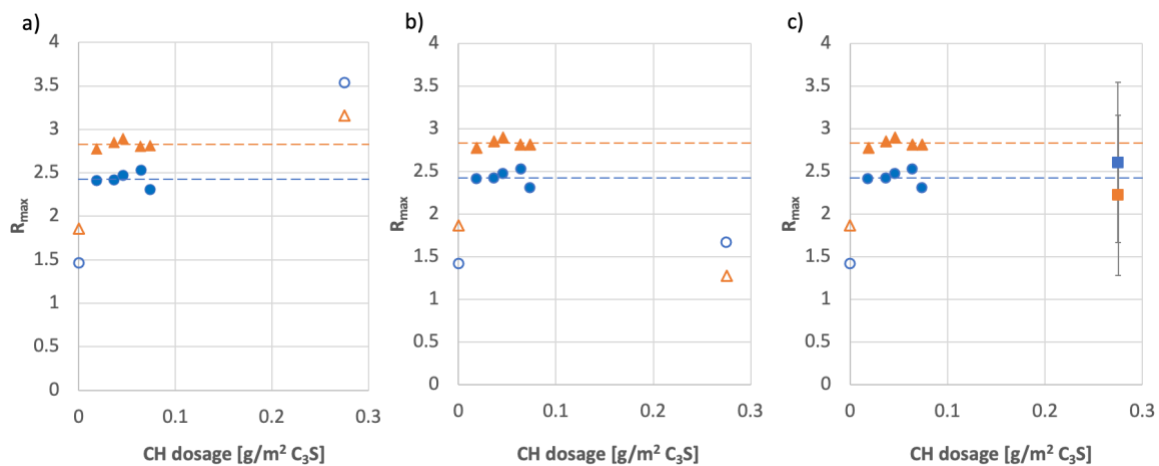


Figure 5.7. Slopes of the calorimetry curves. The discontinuous lines show the average slope where the empty points were not taken into consideration. For C_3S hydration with 1.5 g CH , a) slope in second range in Figure 5.8; b) slope in first range in Figure 5.8; c) average slope. Circles: C_3S hydration without sucrose but with CH; triangles: C_3S hydration with sucrose and CH; squares in plot c): average slope for hydration with or without sucrose, for hydration with maximum CH dosage of $0.27 \text{ mg/m}^2 C_3S$.

For the highest CH dosage (0.28 g CH per unit surface of C_3S), the slopes are much higher no matter sucrose is present or not (Figure 5.7a). For all CH dosages, R_{max} is higher for hydration with sucrose than without.

When looking at the calorimetry curves at high CH dosage, there are clearly two regimes in the acceleration period (Figure 5.8). This makes for an ambiguity about the way how to define R_{max} . Values in Figure 5.7a only take the second regime into account, while Figure 5.7b covers the second regime and Figure 5.7c gives their average. For the latter, error bars represent the distances between values in the previous two figures. Possibly out of coincidence, the average is similar to the average of the samples at lower CH dosages.

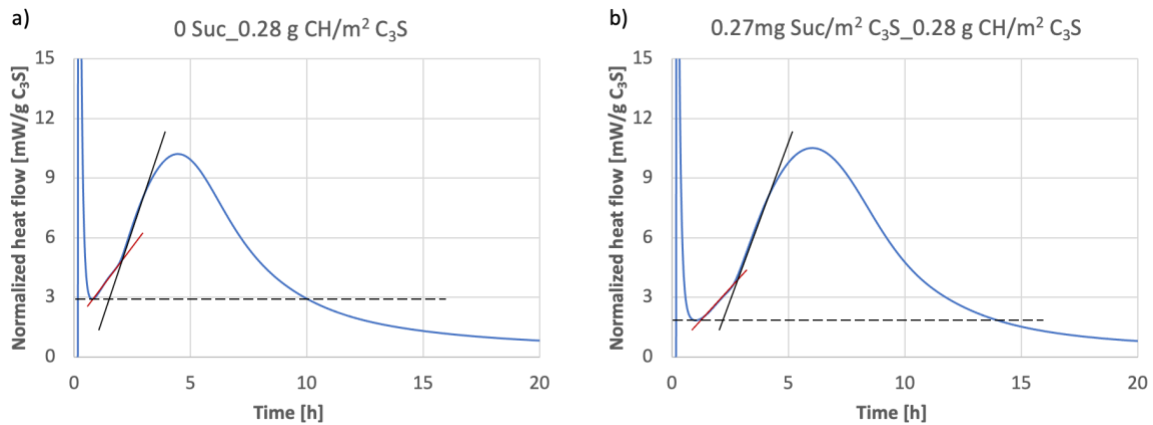


Figure 5.8. Calorimetry curves for C_3S hydration with CH dosage $0.28 \text{ g/m}^2 C_3S$, a) without sucrose; b) with sucrose. Straight lines are the tangents for the two regimes in the acceleration period, the discontinuous lines are the minimum heat flow in the induction period.

5.2.5 Impact of CH on the velocity of hydration in induction period

The calorimetry curve in Figure 5.8 suggests that in presence of CH, the definition of the onset may be more problematic. Indeed, in the previous chapter, the minimum heat flow came down roughly to zero, so taking the intercept of the line of maximum hydration rate with the abscissa was a simple choice. Here, not only do we have a change of slope at high CH dosage, but we also have hydration rates that do not drop to zero in the induction as illustrated in Figure 5.9. Therefore, we firstly look at the implications of different definitions of the onset. The first is our previous one (Figure 5.9a), while the second uses the line of minimum heat rate instead of the abscissa (Figure 5.9b).

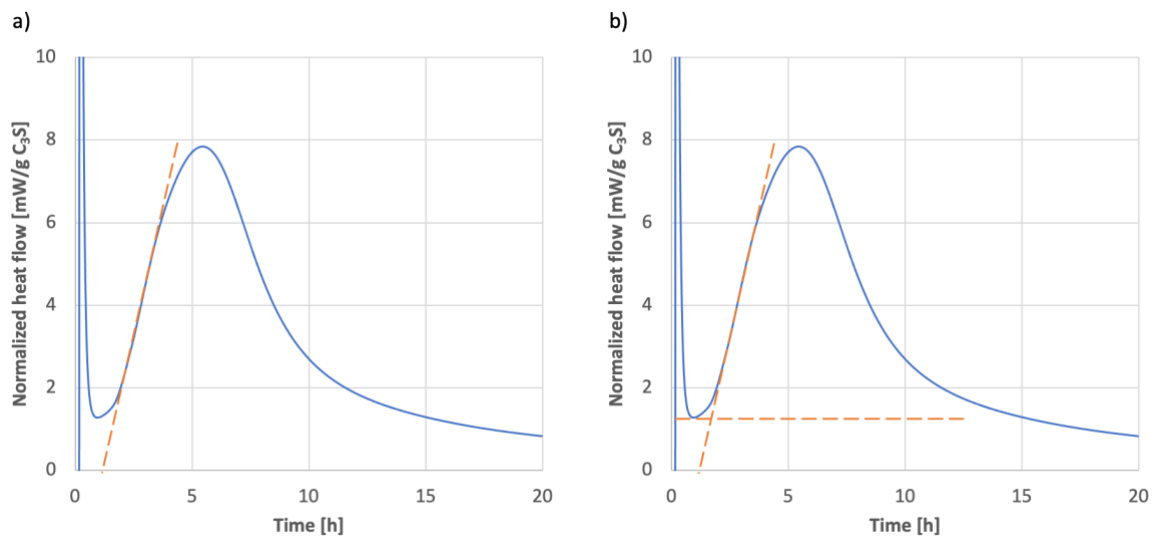


Figure 5.9. Different options in defining the onset. a) By the crossing point of the tangent in the linear range in the induction period with the abscissa; b) by the crossing point of the tangent in the linear range in the induction period with the minimum heat rate of the induction period.

Figure 5.10 and Figure 5.11 represent the results of $DOH_{t_{OS}}$ and t_{OS} from the two definitions. They show that whatever the definition is used, the $DOH_{t_{OS}}$ and t_{OS} are similar (a and b compared to c and d in both figures). The largest difference is found in absence of sucrose, which results from sucrose lowering the minimum hydration rate. This suggests that the first definition is the most meaningful, which is why it is mainly used in the discussion section.

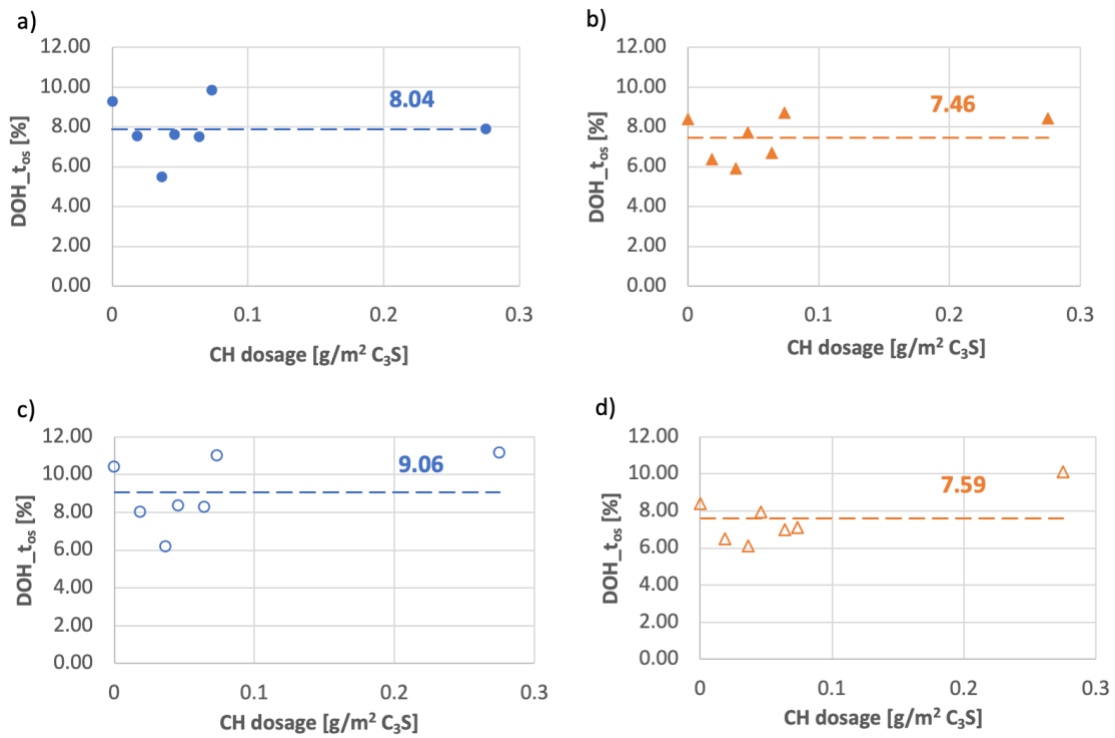


Figure 5.10. The $DOH_{t_{OS}}$ defined in different ways. a) and b) are by using the crossing point of the tangent in the linear range in acceleration period with the abscissa (filled symbols); c) and d) are by using the crossing point of the tangent in the linear range in acceleration period with the minimum of the induction period (open symbols). Circles represent the data from experiments with CH but without sucrose, triangles are the data from experiments with both CH and sucrose. Discontinuous lines are the average $DOH_{t_{OS}}$ with the value indicated above.

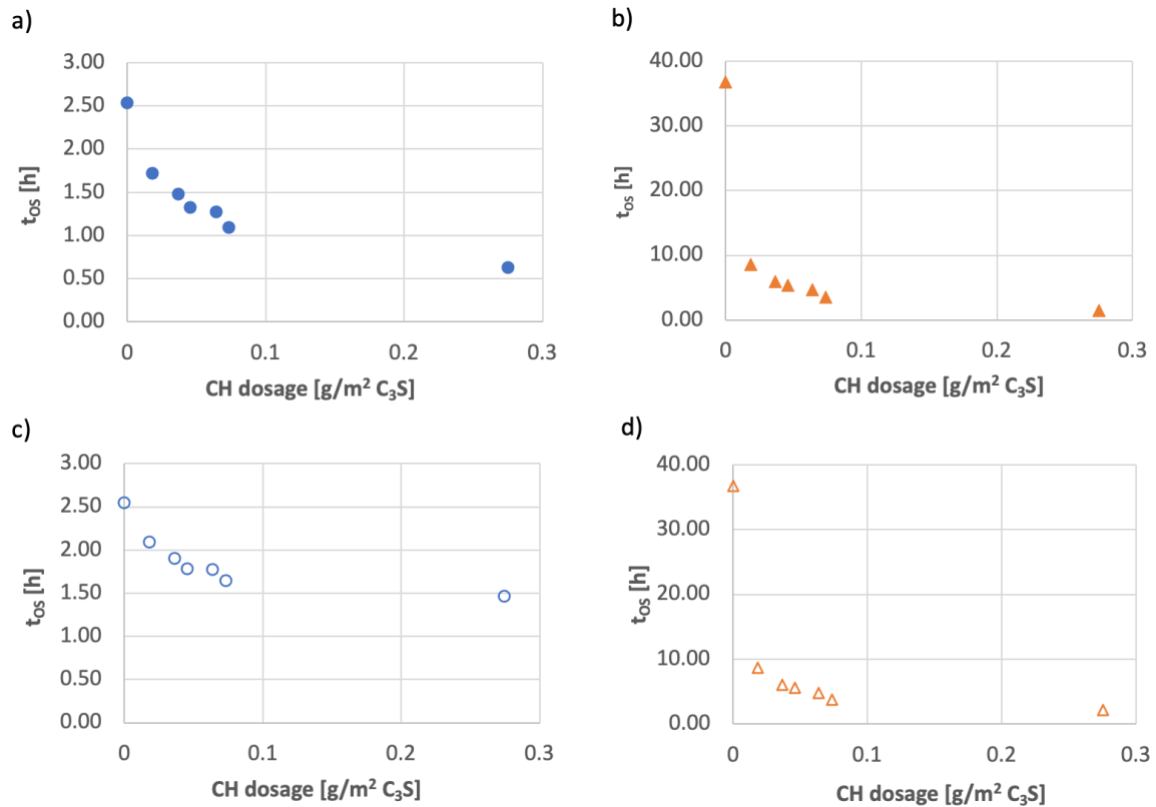


Figure 5.11. The onset defined in different ways. a) and b) are by using the crossing point of the tangent in the linear range in acceleration period with the abscissa (filled symbols); c) and d) are by using the crossing point of the tangent in the linear range in acceleration period with the minimum of the induction period (open symbols). Circles represent the data from experiments with CH but without sucrose, triangles are the data from experiments with both CH and sucrose.

The velocity in the induction period (v_{ind}) is defined as the average $DOH_{t_{os}}$ divided by t_{os} . Figure 5.12 shows that with both definitions for the onset, the general trend for the effect of sucrose and CH does not change. The effect of CH is roughly linear with the surface of CH added, although point at highest CH dosage does not line up well. The slopes of the corresponding regression lines from the two definitions for system with sucrose are almost the same, but for systems without sucrose, they are much lower when using the second definition. The reason for the effect of CH on C₃S hydration with and without sucrose will be further analyzed in the discussion section.

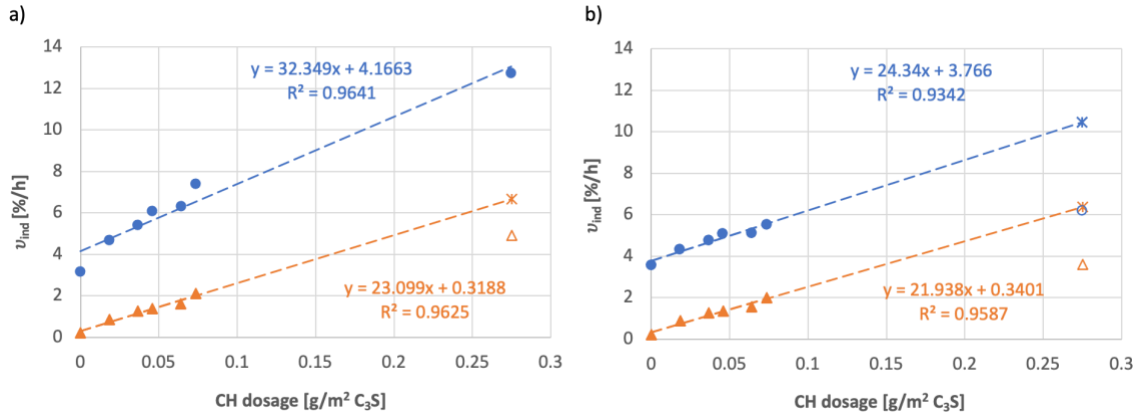


Figure 5.12. Evolution of the velocity in induction period versus CH dosage from different definitions of the onset and $DOH_{t_{OS}}$. a) from the crossing point of the tangent in the linear range in acceleration period with the abscissa; b) from the crossing point of the tangent in the linear range in acceleration period with the minimum of the induction period. Circles represents the data from experiments with CH but without sucrose, triangles are the data from experiments with both CH and sucrose. Discontinuous lines are the regression lines for different data series where the empty data points are not being considered.

5.3 Discussion

As alluded to in the previous section, our previous definition of the onset appears more robust than the one taking the minimum hydration rate in the onset. This is why we focus on those results in our further data analysis.

5.3.1 Impact of CH on the induction period of C₃S without sucrose

Regarding the general impact of CH on C₃S hydration without sucrose, the accelerating effect in the induction period must be contrasted with the absence of an effect on the maximum rate of hydration. This implies that whatever causes the acceleration in the induction period, it is no more rate controlling in the acceleration period.

This initial accelerating effect appears to be linked to the presence of additional surface area in the system as the velocity increases with the added surface of CH. This is probably linked to a consumption of released ions by available surfaces either through adsorption or nucleation. Therefore, we propose to look at this effect with respect to the combined surface of C₃S and CH per unit volume of liquid (5-16). This is represented in Figure 5.13 with velocity and surface being normalized by their respective values in absence of CH. The slope for data obtained from hydrations without sucrose (marked as circles in Figure 5.13a) is not unity as would be expected from normalization done in each axis. This suggests that C₃S and CH have different abilities of consuming ions from the solution. To capture this, we introduce an efficiency factor, f_{CH} , defining how much more efficient CH is at this than C₃S. Thereby we define an effective surface as:

$$S_L^\# = \frac{m_{C_3S} \cdot SSA_{C_3S} + f_{CH} \cdot m_{CH} \cdot SSA_{CH}}{V_L} \quad (5-14)$$

The reference surface in absence of both sucrose and CH is S_L^0 and is given by:

$$S_L^0 = \frac{m_{C_3S} \cdot SSA_{C_3S}}{V_L} \quad (5-15)$$

A value of 1.27 for the factor f_{CH} leads to a quasi-perfect linear relation with a slope of 1 between v_{ind}/v_{ind}^0 and $S_L^\#/S_L^0$ (circles in Figure 5.13b), with v_{ind}^0 the velocity in absence of both sucrose and CH. This supports our hypothesis that for C₃S hydrating with CH alone, the velocity in induction period is proportional to the surface available, probably reflecting a consumption of ions from the solution. Since C₃S is the source of those ions, it is not too surprising that its efficiency would be lower than that of CH. Moreover, if the acceleration effect indeed has to do with ion consumption from solution, then it makes sense to report the total surface in the system with respect to the volume of liquid.

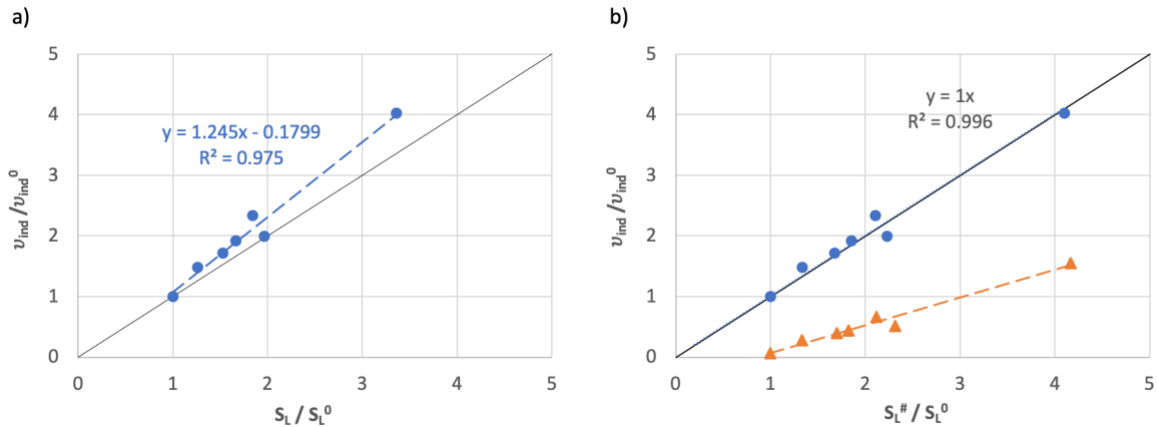


Figure 5.13. Change of relative velocity in the induction period with respect to the total surface area. The reference values of v_{ind}^0 and S_L^0 are taken for the pastes without CH and sucrose. a) S_L obtained from total solid surface normalized by volume of liquid, circles represents data from hydrations with CH but without sucrose; b) effective surfaces $S_L^\#$ as defined in equation (5-14) with a value of 1.27 for f_{CH} , circles represent the data from hydrations with CH but without sucrose, triangles refer to data from hydrations with both CH and sucrose.

5.3.2 Impact of CH on the induction period of C₃S with sucrose

Let us now consider what happens when sucrose is added in the system. First there is a retardation, which according to our findings from the previous chapter should be related to the surface coverage of C₃S. Second in presence of CH, we can expect that the accelerating effect linked to the total available surface may be reduced. This will also be driven by adsorption of

sucrose but will concern both surfaces. For this we need to return to our analysis of sucrose adsorption in the mixed system containing both C₃S and CH, using equations (5-10)-(5-13).

With the surface coverages by sucrose $\theta_{C_3S}^*$ and θ_{CH}^* respectively for C₃S and CH, the total available effective surface becomes:

$$S_L^* = \frac{m_{C_3S} \cdot SSA_{C_3S} \cdot (1 - \theta_{C_3S}^*) + f_{CH} \cdot m_{CH} \cdot SSA_{CH} \cdot (1 - \theta_{CH}^*)}{V_L} \quad (5-16)$$

With this in hand, we replot triangles in Figure 5.13b against S_L^*/S_L^0 multiplied by $(1-\theta_{C_3S}^*)$. In this way we account both for the total surface effect and the free C₃S surface controlling the hydration of samples without CH. For samples without sucrose, this new axis does not change anything as $\theta_{C_3S}^*$ is zero. For samples with sucrose, it leads to a good alignment of most points from samples with sucrose (filled triangles), as shown in Figure 5.14a. For the purpose of reference, the previous location of the sucrose sample data is shown with the open triangles.

At this point we come back to our observation that the affinity of sucrose of C₃S is much higher than for CH (see Table 5.1). Therefore, we may also consider that sucrose might adsorb almost exclusively on C₃S, despite the high surface area of CH. When taking up this hypothesis, we note the adsorption on C₃S as $\theta_{C_3S}^{\S}$ and the surface to liquid ratio as S_L^{\S} , given by:

$$S_L^{\S} = \frac{m_{C_3S} \cdot SSA_{C_3S} \cdot (1 - \theta_{C_3S}^{\S}) + f_{CH} \cdot m_{CH} \cdot SSA_{CH}}{V_L} \quad (5-17)$$

Thereby, we find that data points with sucrose align slightly better than before with the trend predicted by our model (continuous diagonal line).

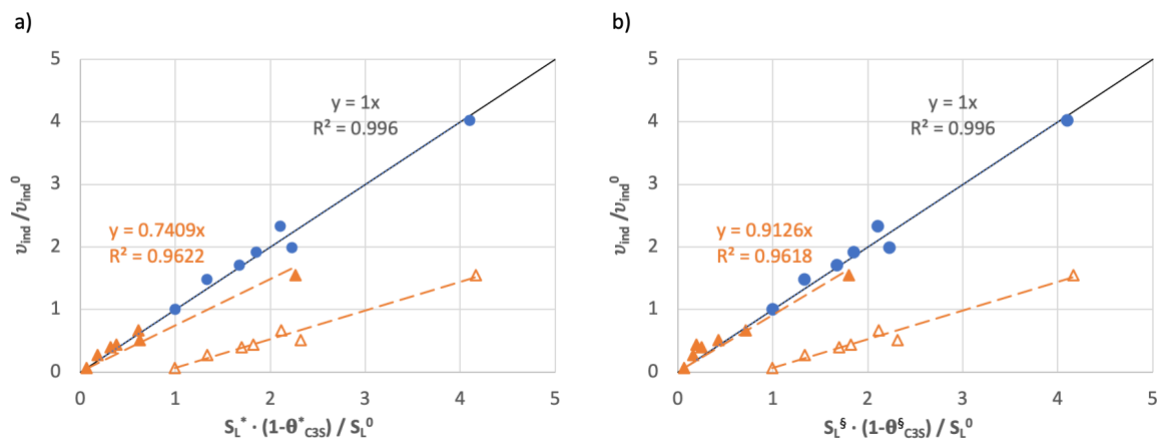


Figure 5.14. Plots of normalized velocity versus normalized effective surface. a) Sucrose adsorbs both on C₃S and CH; b) Sucrose only adsorbs on C₃S. Circles and empty triangles are plots from Figure 5.13b, solid triangles

are the calculated points considering the surface coverage of sucrose on different surfaces. Discontinuous lines are the regression lines.

5.3.3 A critical look at the proposed mechanism

Our previous analysis calls for a clarification concerning the reference velocity, v_{ind}^0 . For the previous chapter the question was relatively simple, as this was just the velocity in absence of sucrose. Here however, the velocity in absence of sucrose is influenced by CH. We have therefore taken as a reference C₃S in absence both of sucrose and CH.

Our results point to the fact that the normalized velocity of C₃S hydration in the induction period may be written as:

$$\frac{v_{ind}}{v_{ind}^0} = \frac{S_L^X}{S_L^0} (1 - \theta_{C_3S}^X) \quad (5-18)$$

where S_L^0 is ratio of the total solid surface to the liquid volume in absence of both CH and sucrose, as given in equation (5-15). S_L^X is the total available surface to liquid ratio in presence of both sucrose and CH. It depends on the distribution of sucrose between C₃S and CH surfaces. If both surfaces are considered, it is S_L^* as given (5-16), while if we only consider adsorption on C₃S it is S_L^{\S} as given in equation (5-17). Similarly, $\theta_{C_3S}^X$ is either $\theta_{C_3S}^*$ or $\theta_{C_3S}^{\S}$ depending on whether or not adsorption is considered to also take place on CH.

Figure 5.15 compares both these approaches, showing that they have an identical correlation coefficient, but that the slope of the curve is much closer to one when only adsorption on C₃S is considered. Because we are considering normalized data, the closeness of the slope to one is an important criteria in determining the validity of the model. This representation underlines the pertinence of our previous choice to neglect the adsorption on CH.

The same figure also shows an additional case (marked by squares), for which we also neglect adsorption on CH. Here however, we additionally consider that the available surface is not modified by sucrose adsorption on C₃S. Therefore, S_L^X is taken as $S_L^{\#}$ given in equation (5-14). This would correspond to a case where dissolution of C₃S would be hindered by adsorbed sucrose, but deposition of hydrates and/or adsorption of ions would not. Results in Figure 5.15 also show a very high correlation coefficient but a slope distinctly different from unity.

This leads us to conclude that the combined effect of sucrose is best described by considering a combination of dissolution inhibition and consumption of ions onto the total available surface under the assumption that sucrose only adsorbs on C₃S.

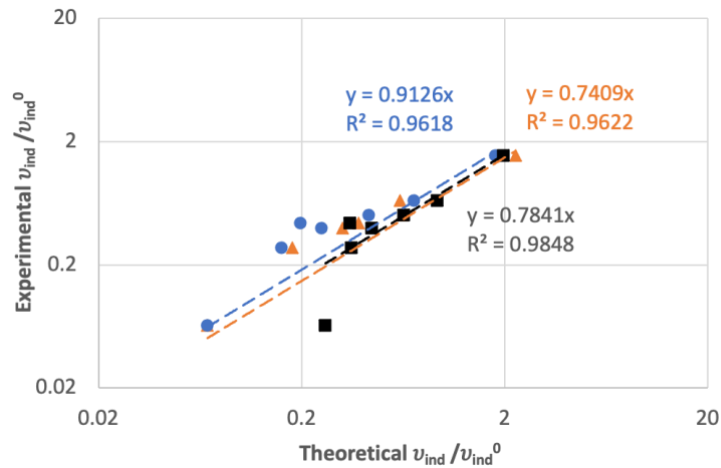


Figure 5.15. Comparison between theoretical prediction and experimental measurement on the relative velocity. Circles: for sucrose adsorbed both on C_3S and CH; triangles: for sucrose only adsorbs on C_3S ; squares: for sucrose only adsorbs on C_3S , but the surface coverage of sucrose on C_3S does not affect the deposition of hydrates. Discontinuous lines are the regression lines for the corresponding data series.

This conclusion is fully compatible with the finding from the previous chapter indicating that the rate in the induction period is proportional to the free surface area of C_3S still holds. In presence of CH, we must consider an additional change in hydration kinetics in the induction period relating to the total available surface, probably because of consuming ions from solution by adsorption and/or heterogenous nucleation. This view is however not consistent with a transfer of sucrose from C_3S to CH as an explanation of the impact of CH.

While these results also point to the system having to reach a defined degree of hydration for the onset to occur, they are not sufficient to determine the underlying mechanism causing that onset. From a pragmatic point of view however, the existence of such a critical DOH, along with our induction period kinetic model, allows to predict the impact of both CH and sucrose on the hydration of C_3S .

5.4 Conclusions

The addition of CH modifies the hydration kinetics of C_3S hydration, both in presence and absence of sucrose. In absence of sucrose, the hydration rate in the induction period is found to be proportional to the combined surface of C_3S and CH, an efficiency factor of 1.27 is introduced for CH. This impact of the total surface probably reflects the consumption of ions released into solution through adsorption and/or nucleation of hydrates. With C_3S being the source of those ions, it is understandable that it may have a lower effect in this mechanism than CH.

Concerning the impact of sucrose in systems containing both C_3S and CH, we find that this can be rationalized in a very similar way as for C_3S . This considers that only the free fractions of the surfaces contribute to the respective mechanisms. The rate of hydration of C_3S in the induction period is therefore proportional both to the free fraction of the total surface

(nucleation or adsorption) and to the free fraction of the C_3S surface (dissolution). Determining the exact surface coverage of both surfaces is delicate and appears to be a limiting factor in our analysis, even if results do overall show a very good match to these simple principles. Best results are obtained by neglecting the adsorption on CH, which is consistent with the much higher adsorption equilibrium constant for C_3S .

6 Impact of sucrose on initial hydration kinetics of Ordinary Portland Cement

Foreword: This chapter represents original research performed by and written up by the author of this thesis under the guidance of Prof. Robert J. Flatt. All calorimetry measurements were performed using a series of in-situ mixing cells produced by M. Martin Keller.

This chapter has formed the basis for a paper close to completion and that will be submitted after hearing back about the paper from chapter 4, as it used some important conclusions from that paper. The journal to which this will be submitted has not been decided yet.

6.1 Introduction

In this chapter, we focus on the impact of sucrose on hydration kinetics of Ordinary Portland Cement (OPC). Similar to the chapter dealing with the impact of sucrose of C_3S hydration, the main method used here is calorimetry. Following the same approach, our focus remains on the induction period. As OPC have an impure form of tricalcium silicate, called alite, we will refer to as such to avoid confusions with studies on the pure C_3S phase. When moving from pure C_3S to OPC, we add an important complexity linked to the hydration of tricalcium aluminate (C_3A), but also a role of alkali and/or alkali sulfates. Our model system of C_3S in a 0.1 M NaOH solution, should in principle recover the effect of alkali on the pH, but we do not capture a possible effect of sulfate ions.

Two cements from Holcim were used in this work. Their main active components were analyzed by XRD with Rietveld refinement and presented in Table 6.1. The use of each cement is specified at the beginning of the relative part of work.

Table 6.1. The main active components of cement type I 52.5 R and 42.5 R.

	C_3S (%)	C_2S (%)	C_3A (%)	C_4AF (%)	Anhydrate (%)	Gypsum (%)
CEM I 52.5R	62.1	9.7	4.5	18.3	0.2	3.1
CEM I 42.5R	63.0	4.1	2.7	21.4	2.4	1.1

Our main results show that key observations made on C_3S can be applied to OPC, but only up to limited dosages, after which the behavior becomes more complex. Additionally, the temperature dependence of OPC hydration is much less easy to rationalize than that of C_3S . For these reasons, and despite the similitude in approaches, results on OPC are presented in a separate chapter than those on C_3S .

Here also, the adsorption of sucrose during the hydration of cement up to first stages of the acceleration period was carried out by Total Organic Carbon analysis (TOC) combining with BET specific surface area measurements (SSA).

A main finding of this chapter is that at low dosages the retardation of OPC hydration is dictated by adsorption of sucrose on alite, probably involving an inhibition of its dissolution. Indeed, the rate of hydration in the induction period is proportional to the surface fraction of alite in the OPC not occupied by sucrose. However, at higher dosages, it appears that additional adsorbed sucrose becomes less effective, which may be due to formation of some form of organo-aluminate compounds.

In what follows, the chapter first presents the results obtained (calorimetry, adsorption, SSA and time evolution of sucrose both adsorbed and in solution). It is followed by a discussion section.

6.2 Results

6.2.1 Calorimetry

This section reports systematic measures of hydration kinetics of OPC (CEM I 52.5R) as a function of sucrose dosage and temperature. As for C₃S:

- for a sufficient stability of the instrument and reproducibility of the measurements at low temperatures, samples had to be mixed *in situ* (within the calorimeter).
- additionally for the lowest temperature we had to place the instrument in a room regulated at an even lower temperature to insure a good stability.
- our rationalization of the impact of sucrose only became possible once we eliminated artifacts thanks to both above points.

As for the adsorption measurements, the sucrose was firstly dissolved in UPW then mixed with cement powder with a liquid to solid ratio 0.7. The pH of the pore solution extracted 5 min after mixing at room temperature is 12.8, measured by a pH meter. The specific surface area (SSA) of cement was measured by BET and gave 1.72 m²/g OPC for powder without contacting with UPW or sucrose solution (dry SSA). But since we are more interested in the behavior of sucrose at the early age of hydration, measuring the SSA for cement paste after short contacting time with liquid (wet SSA) makes sense. For doing so, we immersed about 4 g of the cement paste prepared as described above in liquid nitrogen for 30 s then dried it with freeze-dryer. The use of wet SSA values is discussed in section 6.2.1.2.

6.2.1.1 Definitions of the hydration onset and the slope in the acceleration period

As pointed out in previous chapters, a single hydration curve contains a lot of information, which we reduce to two main features: the onset and the maximum rate. Since baseline corrections were performed on original calorimetry data, using the minimum heat rate of

induction period in defining the onset does not make sense. So, we illustrate again our definition of the maximum rate R_{max} and the onset time t_{OS} in the same ways as for C₃S (Figure 6.1).

Similar to the case with C₃S, additions of sucrose (and many other chemical admixtures) tend to shift the acceleration period to later times, without substantially changing its slope or the height of the peak (Figure 6.2). From this perspective the effect of sucrose on cement hydration once again appears to involve delaying the occurrence of a critical event responsible for ending the induction period. Therefore, from a data analysis point of view, the effect of sucrose “is just” a shift in time of the acceleration period and does not depend on the heat rate taken to define it.

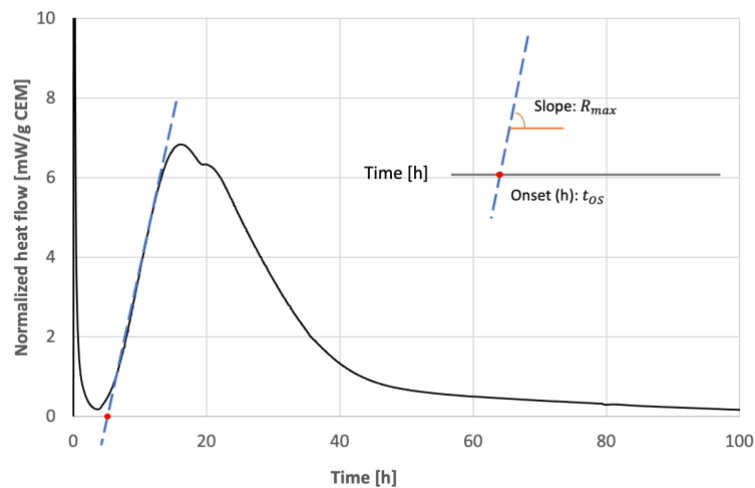


Figure 6.1. An example of the OPC hydration curve to illustrate definitions of t_{OS} and R_{max} .

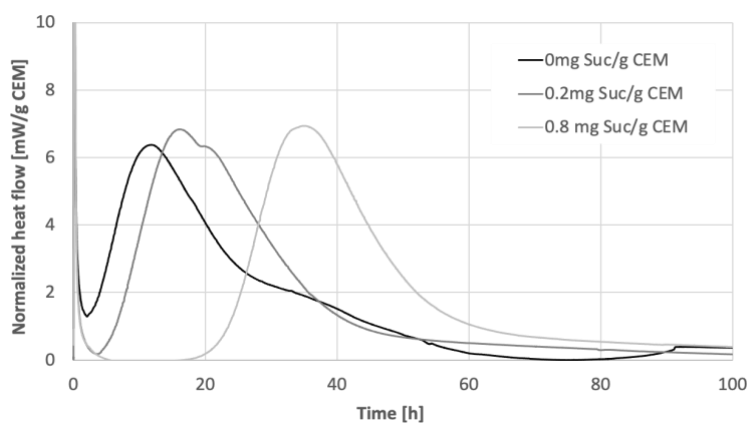


Figure 6.2. Effect of sucrose dosage on the hydration retardation of OPC. Different curves show that up to 0.8 mg sucrose per gram of cement, the slopes in the acceleration period are very similar.

6.2.1.2 Impact of direct addition and delay addition of sucrose on the onset

We also tested the effect of direct and delayed addition of sucrose on the OPC hydration. Since we used in-situ mixing for all calorimetry experiments, for direct addition, sucrose solutions with desired concentrations were injected first into the cell containing the cement powder and then mixed with our external motor for 1 min and 30 s. For delayed addition, UPW of ½ of the amount of total liquid was first injected into the cell containing the cement powder and then mixed in the same way for 1 min and 30 s. Following this, 3 min and 30 s later, a sucrose solution of ½ of the amount of total liquid and doubled desired sucrose concentration was injected and mixed again for 1 min (giving the same final sucrose dosage as in the direct addition). The total liquid to solid ratio in both cases was 0.7. The delay time is counted from the first contact of liquid and solid, and ends once the sucrose solution is added, giving 5 min in total.

Results in Figure 6.3 show that the order of sucrose addition does not change the onset when sucrose dosage is lower than 0.71 mg/g CEM. For higher dosages, the direct addition of sucrose causes a slightly longer retardation than delayed addition and this divergence increases with sucrose dosage. Above dosages of 0.71 mg/g sucrose, the slightly higher retardation in direct addition is the opposite to what one would expect if sucrose were being consumed by the hydration of C₃A. Rather it may suggest a better efficiency at preventing etch pit opening in direct addition, consistently with what has been suggested by Suraneni and Flatt [83].

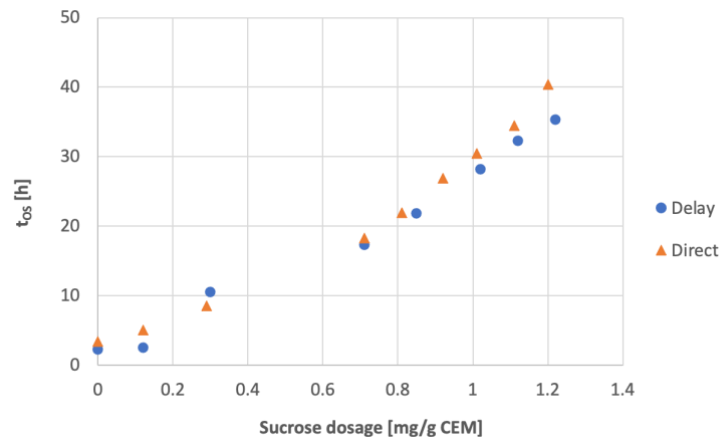


Figure 6.3. Effect of delay addition and direct addition of sucrose on the hydration retardation of OPC.

6.2.1.3 Change of hydration onset and slope in the acceleration period with sucrose

Values of t_{OS} and R_{max} extracted from each calorimetry measurement are plotted versus sucrose dosage in Figure 6.4a and b respectively. This shows that t_{OS} increases with decreasing

temperature regardless of the sucrose dosage and that this increase is nonlinear. Qualitatively, this is a similar observation than for C₃S.

As to R_{max} , it increases with temperature and remains relatively independent of sucrose dosage for all temperatures in the dosage range we studied except for at 35 °C. At that temperature, it shows a dramatic drop once the sucrose dosage is higher than 1 mg/m² CEM. This sudden change in R_{max} indicates a different process in the acceleration period. Therefore, in our following analysis, we only focus on data obtained at 35 °C with sucrose dosages lower than 1 mg/m² CEM.

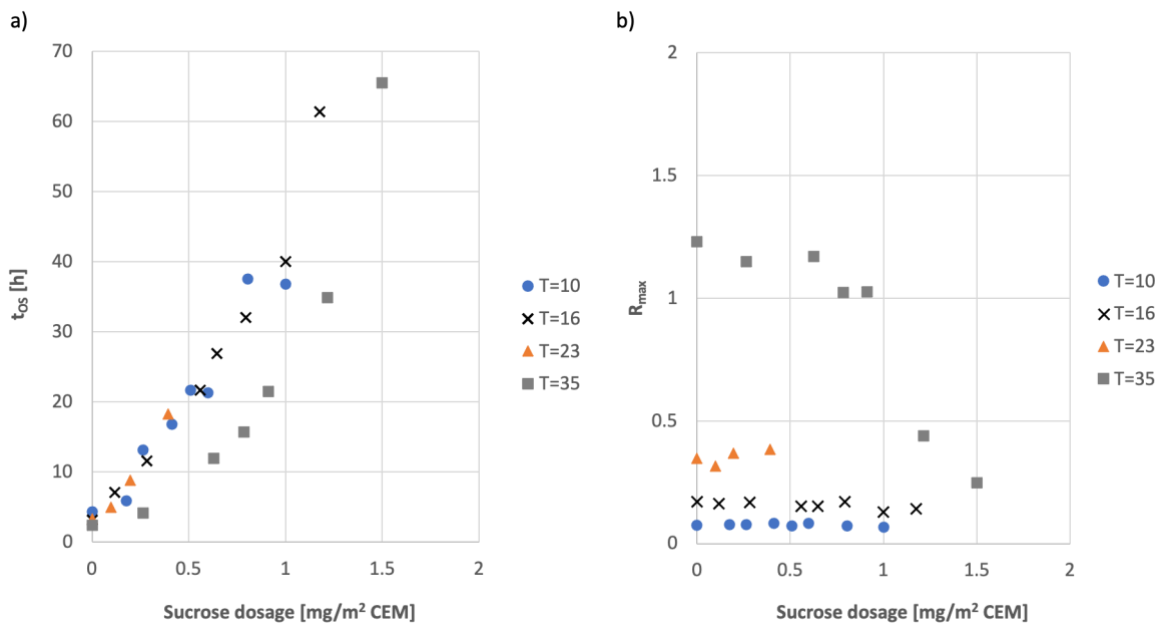


Figure 6.4. Evolution of a) hydration onset and the b) maximum slope in acceleration period versus sucrose dosages and their temperature dependences.

As far as experiments without sucrose are concerned, we would expect a decrease of t_{os} with temperature increases. But the t_{os} at 23 °C lies slightly out of the trend set by the other temperatures.

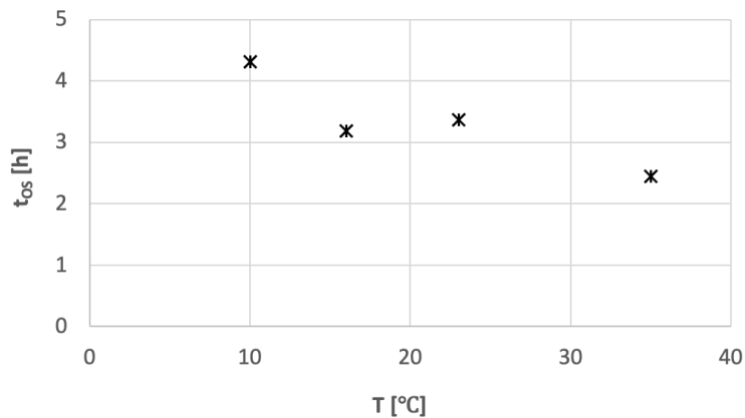


Figure 6.5. Temperature dependence of hydration onset for OPC hydration without sucrose.

6.2.2 Initial adsorption

6.2.2.1 Langmuir isotherm

The adsorption of sucrose on the surface of cement was measured at 10 °C, 23 °C and 40 °C in UPW. The adsorbed amount is obtained by deducting the sucrose remaining in solution from total one dosed. Values are then normalized by the total surface of cement, which is the amount of cement multiplied by the SSA after contact with water (see section 6.2.1.2). As for adsorption of sucrose on OPC, results in Figure 6.6b show a sharp initial increase in adsorption, which is the same at all temperatures. At high dosages data become more scattered (Figure 6.6a). Thereby however, 2 data points, one at 23 °C and one at 40 °C appear to be outliers and are marked with empty symbols. Leaving those two points aside, data can be relatively well fitted by a Langmuir isotherm (lines in Figure 6.6a):

$$c_{ads} = \frac{K_T c_{sol} c_{\infty}}{1 + K_T c_{sol}} \quad (6-1)$$

which is linearized as:

$$\frac{1}{c_{ads}} = \frac{1}{c_{sol} c_{\infty} K_T} + \frac{1}{c_{\infty}} \quad (6-2)$$

The corresponding plots have high correlation coefficients for 10 °C and 23 °C, as shown in Figure 6.7. The ordinate of the fit gives $1/c_{\infty}$ while the slope is $1/K_T c_{\infty}$. Because K_T represents an equilibrium constant between the solution and the surface, it makes sense to use molar fraction units for the concentration c of sucrose in solution. Thereby the value of K_T can be subsequently used in a thermodynamic analysis.

The fitting parameters obtained are summarized in Table 6.2. They also highlight a decrease in the adsorption plateau from 10 °C to 23 °C then an increase at 40 °C (0.73 mg/m², 0.92 mg/m² and 0.79 mg/m² at 10 °C, 23 °C and 40 °C respectively). Values are also reported per unit surface area of cement, which is the most adequate representation for powders. The specific surface area after 3 min in contact with the solutions is measured as 1.02 m²/g CEM.

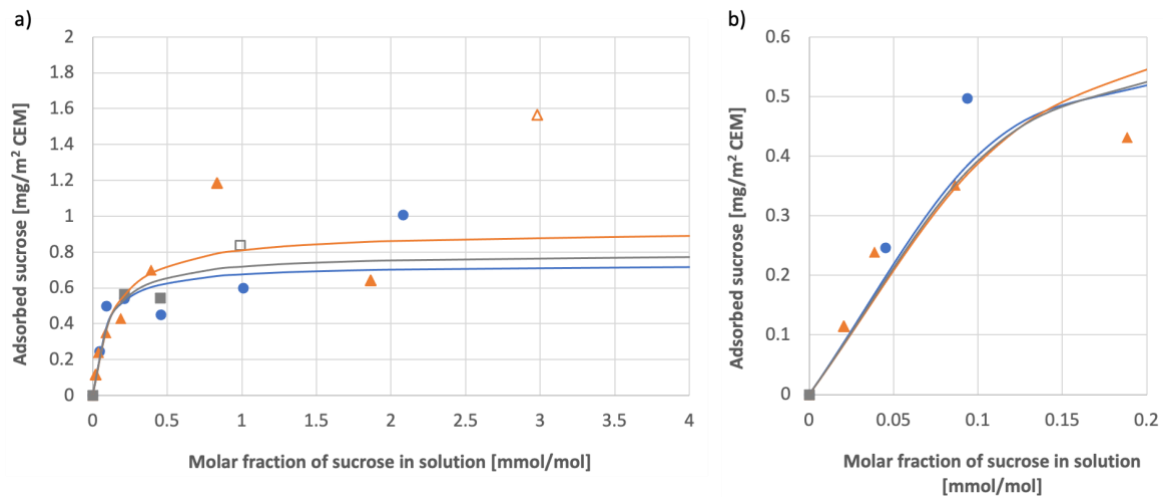


Figure 6.6. a) Overall plot of sucrose adsorption on cement at different temperatures (Circles: 10 °C; triangles: 23 °C; squares: 40 °C). The continuous lines indicate the Langmuir fits of which the parameters are reported in Table 6.2. Filled symbols were used for the regression, while open symbols were considered as outliers and left out. b) Zoom-in of the overall plot for sucrose molar fraction in solution below 0.2 mg/m² CEM.

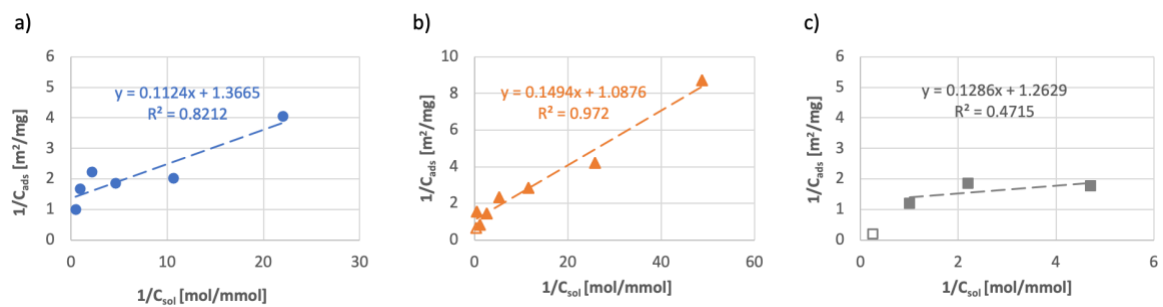


Figure 6.7. Adsorption data plots with linearized Langmuir equation of sucrose on OPC at different temperatures (Circles: 10 °C; triangles: 23 °C; squares: 40 °C). Filled symbols were used for the regression, while open symbols were considered as outliers and left out.

Table 6.2. Langmuir adsorption parameters. K_T and c_∞ correspond equilibrium constant and adsorption plateau values obtained when sucrose solution concentration was used in molar fraction and adsorption in mg/m² CEM. K_T^* is the equilibrium constant obtained when sucrose solution concentration was used in ppm. c_∞^* comes the empirical fit described by equation (6-5), without physical meaning.

Temperature (°C)	$K_T \cdot 10^3$	K_T^*	c_∞ (mg/g)	c_∞ (mg/m ²)	c_∞^* (mg/m ²)
10	12.16	6.39E-04	0.74	0.73	0.94
23	7.28	3.83E-04	0.94	0.92	1.37
40	9.82	5.16E-04	0.81	0.79	1.00

6.2.2.2 Adsorption in relation to dosage

Similar to what we did for C₃S, we wish to know the extent to which of sucrose adsorption in calorimetry experiments. For this we use both approaches introduced for C₃S and that are briefly recalled below.

Adsorption from Langmuir isotherm and mass balance

The first approach combines a Langmuir isotherm and a mass balance between the solution and the surface. It leads to the following solution for the adsorption c_{ads} as a function of dosage, c_{dos} :

$$c_{ads} = \frac{\left(K_T^* \cdot c_\infty + \frac{L}{S} + c_{dos} \cdot K_T^*\right) - \sqrt{\Delta}}{2 \cdot K_T^*} \quad (6-3)$$

with

$$\Delta = \left(K_T^* \cdot c_\infty + \frac{L}{S} + c_{dos} \cdot K_T^*\right)^2 - 4 K_T^{*2} \cdot c_{dos} \cdot c_\infty \quad (6-4)$$

where c_{ads} is the adsorption obtained from the Langmuir isotherm for a selected dosage c_{dos} of sucrose.

Adsorption from empirical relation

The second option to determine adsorption from dosage is empirical. It builds upon the observed linearity between adsorption and dosage, as well as on the assumption that a plateau is reached. It then uses a Langmuir-type equation to fit the data, replacing the solution concentration by dosage.

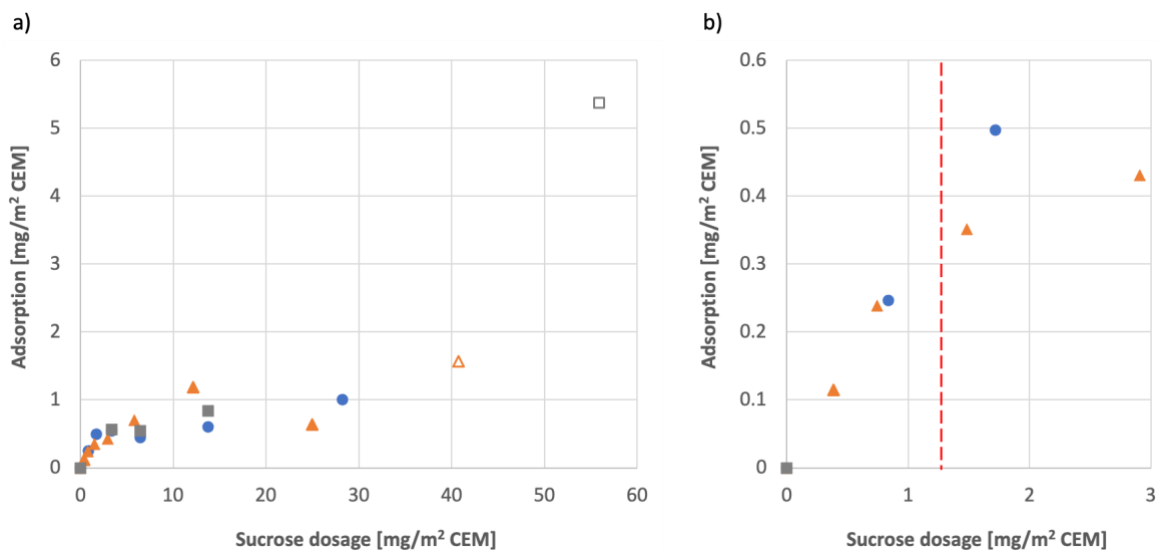


Figure 6.8. Adsorption of sucrose on cement at different temperatures (circles: 10 °C; triangles: 23 °C; squares: 40 °C). a) Overall plot; b) zoom-in in the low dosage range, where the discontinuous line represents the limit of dosage being used in calorimetry measurement (1.21 mg/m² CEM).

Thereby, we empirically consider that adsorption may be fitted to dosage according to:

$$c_{ads} = \frac{c_{dos}c_{\infty}^*K_T^{\#}}{1 + c_{dos}K_T^{\#}} \quad (6-5)$$

where c_{∞}^* the plateau and $c_{\infty}^*K_T^{\#}$ is the slope at low dosage (between adsorption and dosage).

Because all curves appear to have a similar behavior at low dosage, it is worth reexamining the fitting procedure by rewriting equation (6-5) as:

$$\frac{1}{c_{ads}} = \frac{1}{c_{\infty}^*} + \frac{1}{c_{\infty}^*K_T^{\#}c_{dos}} \quad (6-6)$$

and plotting $\frac{1}{c_{ads}}$ versus $\frac{1}{c_{dos}}$.

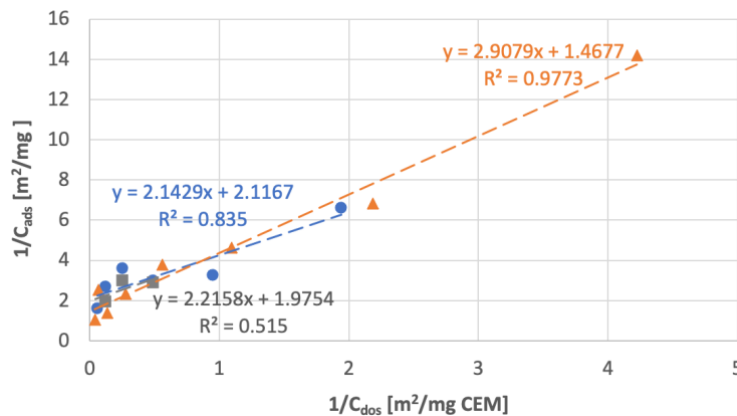


Figure 6.9. Linearized form of equation (6-5), (circles: 10 °C, triangles: 23 °C, squares: 40 °C).

As shown in Figure 6.9, these plots are roughly linear at all temperatures and have very similar slopes (term $1/c_{\infty}^*K_T^{\#}$ in equation (6-6)). As for C₃S, this points to similar slopes in the linear regime, implying that a fixed fraction of sucrose would adsorb at low dosage. Accepting this as a fact, we refit all data assuming of a common value of $c_{\infty}^*K_T^{\#}$ at all temperatures. This gives the general slope of 3.51 which corresponds to a general value of 0.29 for $c_{\infty}^*K_T^{\#}$, while for c_{∞}^* , we get 0.94 mg/m² (10 °C), 1.37 mg/m² (23 °C) and 1.00 mg/m² (40 °C) for OPC.

A first observation is that $K_T^{\#}$ values are much lower than for C₃S at equivalent temperature. For C₃S, the slope of initial adsorption ($c_{\infty}^*K_T^{\#}$) was larger than one, which although not making physical sense does point to most sucrose added being adsorbed. For OPC, the value obtained

points to only about 30% sucrose being adsorbed, which is very different from results reported by Reiter [73].

Similar to the case of C_3S , values of c_{∞}^* , are higher than the plateau values obtained from the Langmuir isotherm (Table 6.2). As before, we attribute this to the fact that c_{∞}^* , unlike c_{∞} , is obtained from an empirical fit.

Experimental adsorption data with empirical fitting curves is given in Figure 6.10. The discontinuous line shows the limit of sucrose dosage from calorimetry measurements that will be used in analysis: 0.80 mg/m² CEM for 10 °C, 0.40 mg/m² CEM for 23 °C and 0.58 mg/m² CEM for 40 °C. It can be seen that the fitting curve for 40 °C shows relatively large divergency from the other two. Apart of that, the empirical curves at 10 and 23 °C fit well their adsorption in the dosage range of interest for calorimetry.

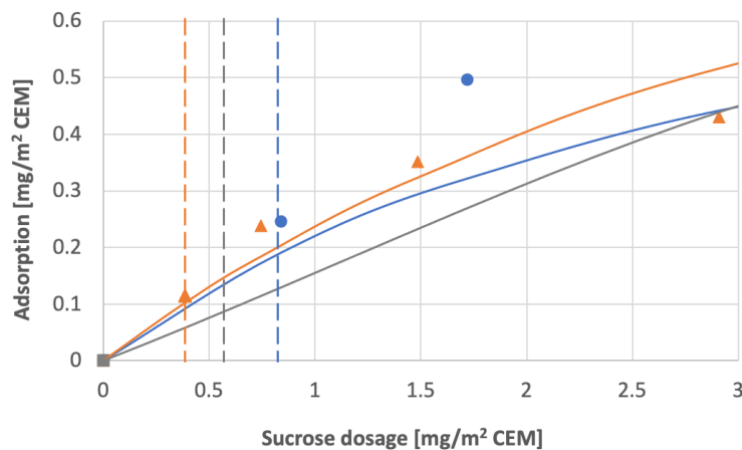


Figure 6.10. Empirical fits of adsorption data with equation (6-5). Circles: 10 °C, triangles: 23 °C, squares: 40 °C. Continuous line represents the empirical fitting curve, and the discontinuous line is the limit of sucrose dosage used in calorimetry measurement at relative temperature (0.80 mg/m² CEM for 10 °C, 0.40 mg/m² CEM for 23 °C, 0.58 mg/m² CEM for 40 °C).

We now examine the dependence of c_{∞}^* on temperature. As shown in Figure 6.11, we find that c_{∞}^* does not depend on temperature, which contrasts strongly with C_3S . Based on this, a common fit with dosage of a Langmuir equation can be used for all data collected at different temperatures. It gives a plateau value of 0.89 mg/m² and $K_T^{\#}$ of 0.47. It can be seen from Figure 6.12a that this common fit match the experimental data quite well. Figure 6.12b gives a closer view of the same plot for sucrose dosages lower than 8 mg/m². This shows that for sucrose dosages below 4 mg/m², regardless of temperature, all data are well matched by the common fit. Moreover, data increases almost linearly for sucrose dosages below 1.5 mg/m². Considering the sucrose dosages being used in calorimetry measurements, where the highest value is 1.21 mg/m² used for 35 °C, a linear fit with a single set of parameters can be taken for data at all temperatures. As shown in Figure 6.13, this single linear fit appears to predict adsorption well in the dosage range relevant to our calorimetry experiments.

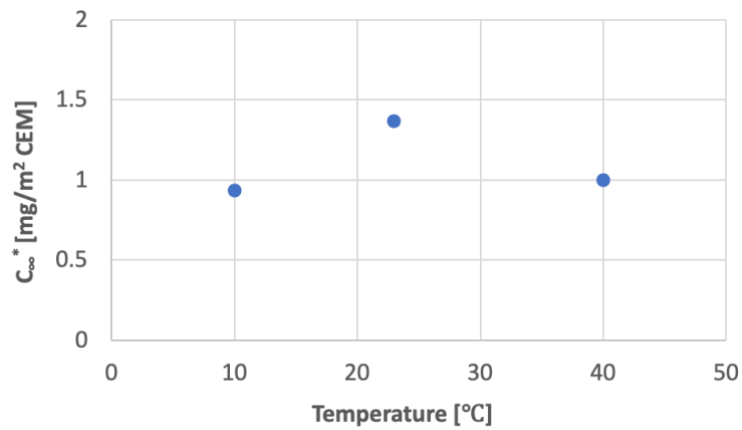


Figure 6.11. The temperature dependence of adsorption plateau from empirical fits.

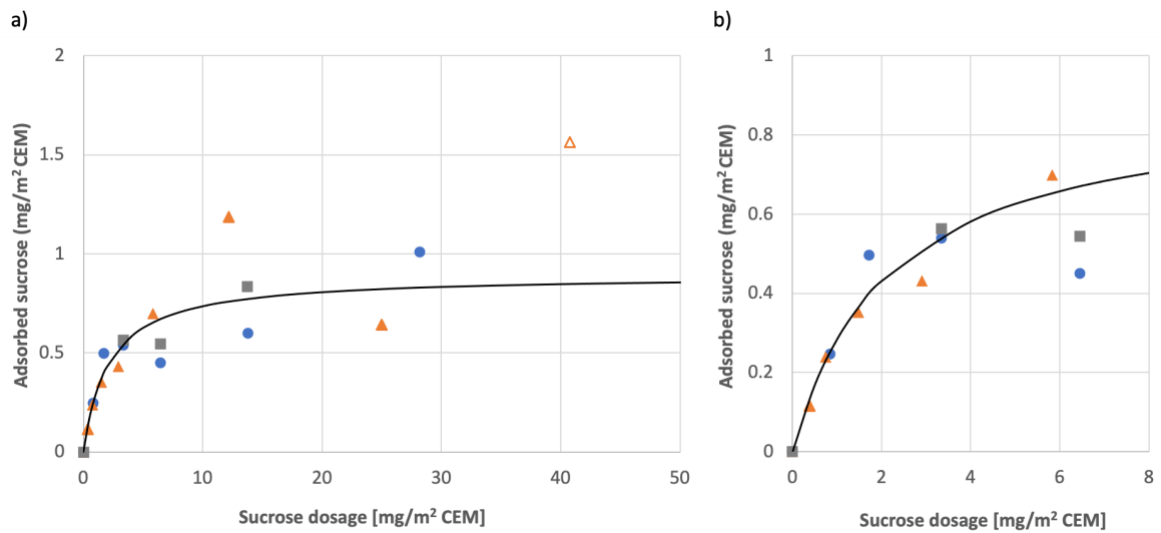


Figure 6.12. a) Common fit of all adsorption data points at different temperatures with dosage Langmuir equation. The plateau value is 0.89 mg/m^2 and $K_T^\#$ is 0.47 . b) A Zoom-in of the common fitting curve with adsorption data points in the low dosage range (below 8 mg/m^2).

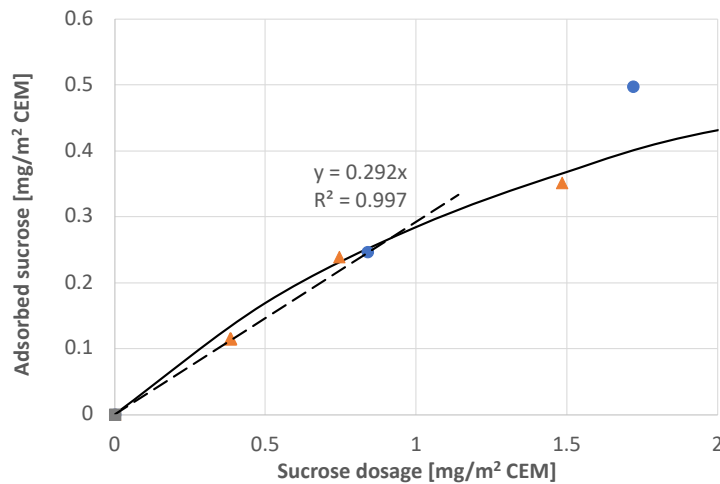


Figure 6.13. Linear fit of adsorption data for dosages below 1.2 mg/m² CEM for all temperatures (circles: 10 °C, triangles: 23 °C, squares: 40 °C). The solid curve is the common dosage Langmuir fit; the discontinuous line is the regression line for the linear fit.

6.2.3 Time dependent Adsorption

As we did for C₃S, we also investigated the time evolution of sucrose both in solution and adsorbed on solid phase during the hydration of OPC. The idea is to separate the liquid phase from the paste at different hydration ages then detect the sucrose content in each pore solution by TOC. The difference between initial sucrose dosage and sucrose remaining in pore solution gives the adsorption at corresponding hydration age.

To ensure the identity of the paste for all samples, a large amount of cement paste with an initial sucrose dosage of 0.29 mg/g CEM was prepared for a liquid to solid ratio 0.7. From this, 5 g of paste was transferred immediately to the pre-stabilized calorimeter after mixing. The rest was divided into several small portions for later use.

At each selected hydration age, one small portion of paste was centrifuged at 10'000 rpm for 4 min to separate the liquid from the solid phase. The liquid phase was then passed through a 0.45 μm filter and acidified, simultaneously diluting at least 20 times by using 0.5 M HCl solution to reach pH lower than 4. The solution is measured by TOC to obtain the concentration of total organic carbon in it, which can be converted to sucrose concentration because sucrose is the only source of organic carbon in these samples. The rest of the paste after centrifugation was immersed in liquid nitrogen for 30 s and dried in freeze-dryer. The SSA of the resulting powder was then measured by BET. We note that while freeze-drying leads to an amorphization of ettringite, it has only little effect on SSA.

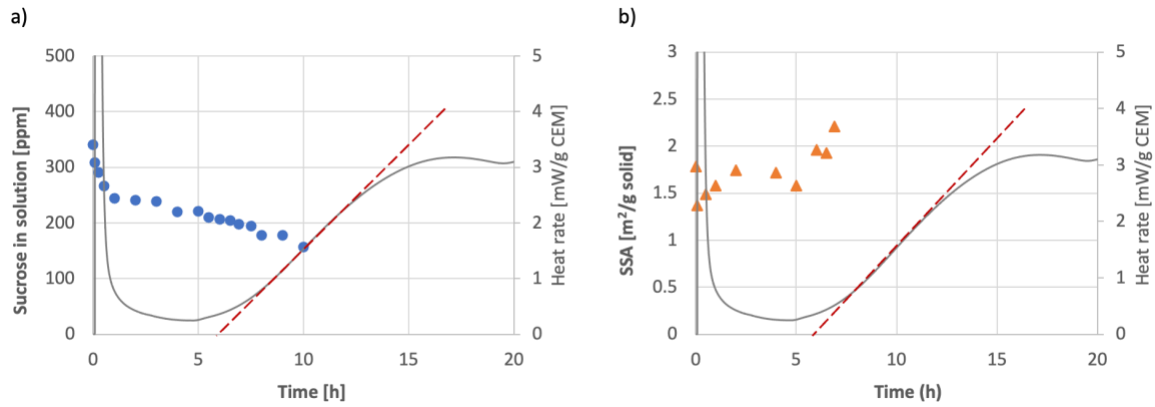


Figure 6.14. Evolution of a) sucrose in pore solution and b) SSA of solid phase during the hydration of OPC. The continuous curve is the calorimetry curve from the same initial paste, it follows a secondary axis for heat rate shown on the right side of the plot. The discontinuous line is the tangent in the acceleration period, it gives an onset of 6.01 h.

The evolution of sucrose in pore solution and the SSA of the solid phase is shown in Figure 6.14. Separating liquid phase by centrifugation was feasible until 11h, where the hydration reached almost to the middle of acceleration period. However, the freeze-dried paste after 7 h contains hard aggregates that cannot be broken by hands. Therefore, the BET measurements were only performed for dried powder obtained from samples younger than 7 h of hydration.

In Figure 6.14a, the sucrose in solution decreases suddenly after the mixing and during the first hydration peak which is dominated by the aluminat reaction. In the induction period, it slightly decreases until the acceleration starts then this decrease becomes more pronounced in the acceleration period. The trend of sucrose evolution in pore solution during hydration of OPC is the same as for C₃S. But evolution of SSA is different during the first hour of hydration. It decreases from the dry powder once in contact with sucrose solution then goes up quickly during the first hydration peak. In the induction period (between 2 to 6 h), it varies a bit but in general remains constant. In the acceleration period, it then increases dramatically (Figure 6.14b).

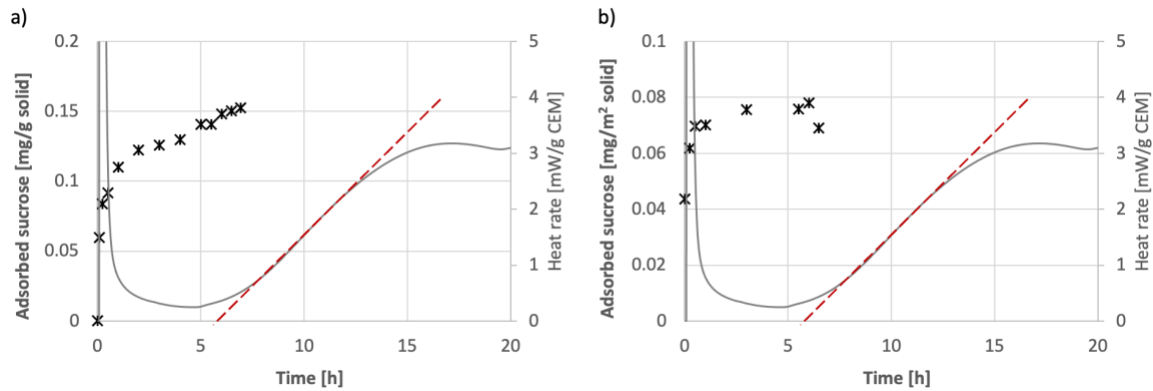


Figure 6.15. Evolution of a) adsorbed sucrose per gram of solid b) adsorbed sucrose per unit surface of solid during the hydration of OPC. The continuous curve is the calorimetry curve from the same initial paste, it is plotted with respect to the secondary axis for heat rate shown on the right side of the plot. The discontinuous line is the maximum slope in the acceleration period, it gives an onset of 6.01 h (taken as the interception of that line with the x-axis).

In Figure 6.15a, we plot the adsorption per gram of solid phase over time. Values are observed to keep rising during the time range over which measurements were performed. The most important increase happened during the first hydration peak, which includes initial dissolution and more intense reaction of tricalcium aluminate. Then, it slows down in the induction period followed by the faster sucrose consumption once acceleration period starts. Since the free surface created by these reaction offers sites for adsorption to happen, we normalize the adsorption per unit mass of solid by the SSA of corresponding solid phase. This gives us a new plot as shown in Figure 6.15b, where the adsorption remains constant in the induction period, implying that the newly formed adsorb sucrose, keeping a similar surface coverage as long as enough sucrose is available.

6.3 Discussion

6.3.1 Impact of sucrose on aluminate reaction

In Figure 6.3, we see that the direct and delayed addition of sucrose does not cause big change in hydration onset for sucrose dosages below 0.7 mg/g CEM, but that direct addition results in longer onset time at higher dosages. It is known that aluminate phase dominates the hydration in the first few minutes, but in our delay and direct addition experiments, the solid to liquid ratio is actually different in the first 5 min. To eliminate the effect of aluminate reaction at different liquid to solid ratio and to check the effectiveness in preventing etch pit opening, we measured the SSA of freeze-dried cement pastes containing different amounts of sucrose (0, 0.71, 0.92, 1.11 mg/g CEM). Different from the sample for calorimetry measurement, the mixing of these samples was done *ex situ* but followed the same procedure of liquid addition as for *in situ*, which is previously described. To ensure the mixing of sucrose solution with cement in case of delayed addition, pastes obtained from both delayed and direct addition were frozen 6 min after the first contact of cement powder and liquid.

As shown in Figure 6.16a, the SSA of cement paste from delayed addition is always higher than that from direct addition even in absence of sucrose. Joseph and co-authors [104] showed in their study on C₃A hydration that the DOH increases with liquid to solid ratio in the long-term, but it gave opposite correlation in the first few minutes. So, in our case of delayed addition, the higher SSA is probably caused by the lower initial liquid to solid ratio for aluminate reaction. Beside of that, we also see that the addition of sucrose increases the SSA regardless of the order of addition. However, for all dosages tested we then get the same SSA. The average value for delayed addition with sucrose gives 1.83 m²/g while it is 1.65 m²/g for direct addition. If we normalize these SSA values by the SSA from paste without sucrose (SSA₀), we see from Figure 6.16b that the order of sucrose addition makes no difference on normalized SSA.

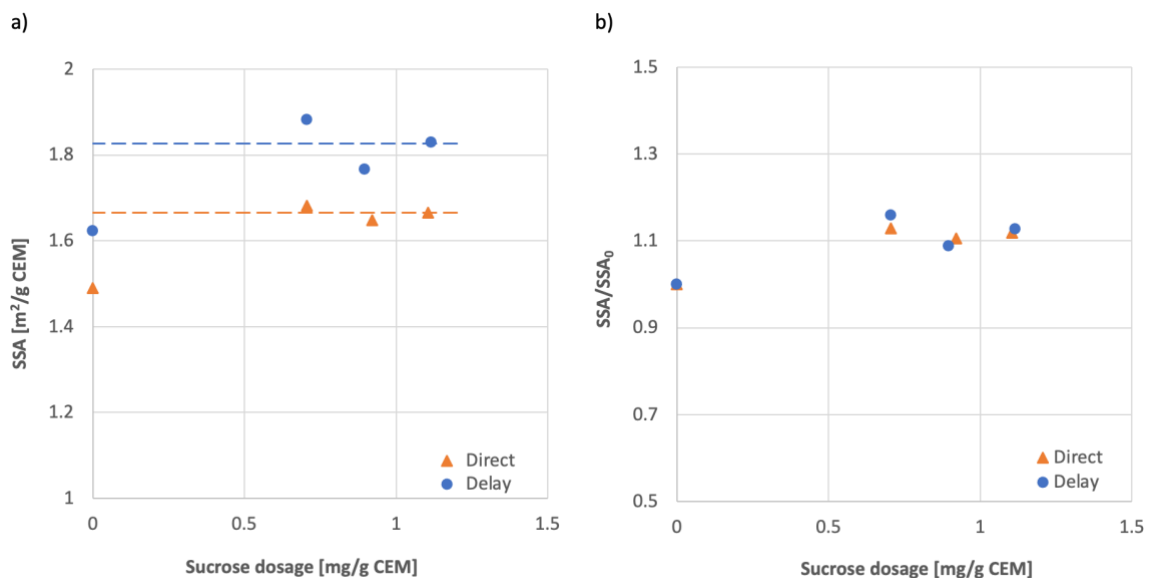


Figure 6.16. Effect of delay addition and direct addition of sucrose on the specific surface area of OPC paste for which the hydration was stopped 6 min after the first contact of liquid and solid. a) SSA versus sucrose dosage; b) normalized SSA versus sucrose dosage.

Considering the difference in SSA at early age for delayed and direct addition, for each series we normalize the sucrose dosage (x-axis) in Figure 6.3 by the corresponding average SSA from Figure 6.16a. New results are plotted in Figure 6.17, where we see the overlapping of two series of points. This indicates that the differences between direct and delayed addition can be brought back to the difference in the initial specific surface area. Most importantly, it can be concluded that the role of addition time on the onset time is minor. Therefore, sucrose should not be considered to have a strong effect on the hydration kinetics of C₃A in our dosage range. However, in the later section (6.3.5), we found that in the high dosage range, the interaction of sucrose with aluminate phase seems to reduce the incremental impact of sucrose on retardation of OPC, probably by then consuming part of it through adsorption onto aluminate hydrates.

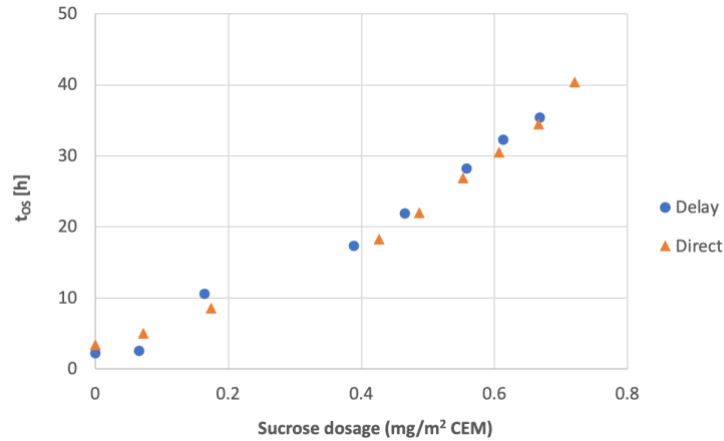


Figure 6.17. Effect of delay addition and direct addition of sucrose on the hydration retardation of OPC.

6.3.2 Adsorption

When using the first model to predict adsorption from the isotherm and mass balance, we assume the adsorption is temperature dependent and different K_T and c_∞ values are applied for each temperature. In contrast, with the empirical fitting model, adsorption appears independent of temperature. Since both models lead to very different conclusions, we calculate the correlation coefficient (R^2) for each model in order to figure out the better way to predict adsorption. This analysis is done for a sucrose dosage range lower than 2 mg/m^2 , which covers the dosage range we used in calorimetry works and also ensures having enough data points for these calculations.

As shown in Figure 6.18, the TOC adsorption data are presented by individual circles and triangles for 10 and 23 °C respectively. The data at 35 °C does not appear on the plot because no TOC data was collected in this dosage range. For each experimental dosage used in TOC measurements, the adsorption was calculated by using both models at 10 and 23 °C. The results are presented in continuous lines for the first model and discontinuous lines for the second model. It is obvious that both models work almost identically with high quality. But the second one shows a much easier relation for calculations. Therefore, in the following part, we only present results analyzed by using the second model.

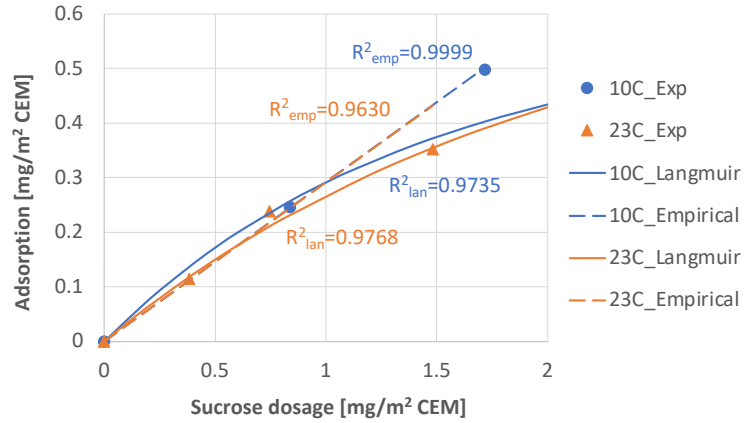


Figure 6.18. Comparing the two models for predicting adsorption at 10 and 23 °C, with coefficient of determination (R^2) for each model at each temperature. Solid lines are obtained from the prediction made with first model, using adsorption isotherm and mass balance. Discontinuous lines are the prediction lines from the second model by using an empirical dosage-based analogue to the Langmuir equation. The corresponding R^2 is marked next to the relative regression line. Circle points are the adsorptions measured by TOC at 10 °C, triangle points are the adsorptions measured by TOC at 23 °C.

Based on the second model, the fact that sucrose adsorption does not show a temperature dependence suggests a high affinity for the surface, that is adsorption would be dominated by heat of adsorption and barely sensitive to adsorption entropy. However, this assertion contrasts with the low fraction of sucrose that adsorbs on this cement at low temperature. It may suggest the existence of specific, but limited high energy sites for which sucrose has a strong affinity. The fact that cement shows this and not C_3S , is not due to pH, but could be due to sulfates. This question would deserve further investigation but could not be tested in the scope of this thesis. A simple experiment would be to add alkali sulfates to our high pH suspensions of C_3S .

6.3.3 Impact of temperature on hydration in absence of sucrose

As shown in Figure 6.4, t_{os} changes with the sucrose dosage and with the temperature while R_{max} changes only with temperature. To analyze these dependencies separately, we begin our analysis with the data obtained without sucrose.

In terms of temperature dependence, we may assume that the Arrhenius equation holds, so that:

$$v_{ind} = A \cdot \exp\left(-\frac{Ea}{RT}\right) \quad (6-7)$$

where A is a frequency factor, Ea is an activation energy, R the universal gas constant and T the absolute temperature.

This equation can be linearized as:

$$\ln(v_{ind}) = \ln(A) - \frac{Ea}{RT} \quad (6-8)$$

so that plotting $\ln(v_{ind})$ versus $-1/RT$ would be linear with a slope of Ea if the Arrhenius equation holds.

The case of C₃S highlighted that the best was to define a hydration rate in the induction period is to take the ratio between degree of hydration at the onset and its time of occurrence. As explained further the situation is more challenging for cement than C₃S, because the heat at the onset includes a non-negligible contribution from the aluminat reaction.

Concerning the temperature dependence of R_{max} , the situation is more delicate to analyze. Indeed, as already mentioned for C₃S the maximum rate in the acceleration period, corresponds to the second derivative of the heat rate being zero, which may be affected by any change in kinetic factors taking place during the acceleration period, as specific surface area and ionic concentrations. As these may also be temperature dependent, the problem is not trivial.

If the reaction follows Avrami type kinetics in the acceleration period, it can be shown that the slope of an Arrhenius plot is E_a/n , where n is the exponent in the Avrami equation.

Whatever the correct way to analyze this is, we note that the slope is about to be 78 kJ/mol, which is similar to the one we found for C₃S.

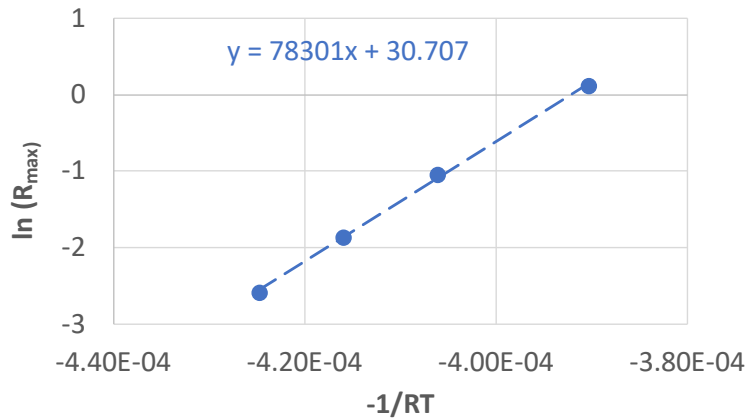


Figure 6.19. Linearized Arrhenius plots for the maximum slope of the acceleration period, R_{max} values are obtained from the calorimetry measurements without sucrose at different temperatures.

Defining the v_{ind} from degree of hydration at the onset

As mentioned above, with cement the heat of hydration at the onset includes a non-negligible part from the aluminat reaction. To highlight this difference, in Figure 6.20a and b, we plot the calorimetry curves for C₃S and OPC hydration with different amounts of sucrose at 23 °C respectively. The time scale is taken as logarithmic scale to better display simultaneously the

first and second peak. This shows that the maximum heat rate is higher in the initial peak for cement, but smaller in the second.

This difference is further highlighted in Figure 6.21 by the cumulative heat of both peaks as well as at the onset. This highlights that the initial peak is only of secondary importance for the case of C_3S , including with respect to the heat at the onset. This justifies our analysis in the C_3S chapter, which neglected the issue of the heat contributed by the first peak. However, for cement this is not possible.

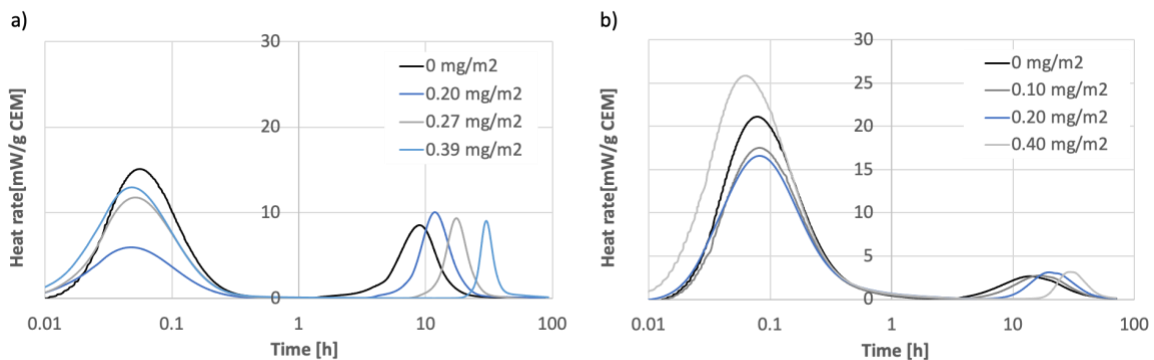


Figure 6.20. Calorimetry curves for a) C_3S and b) OPC hydration with different amount of sucrose at 23 °C. The time is plotted in logarithmic scale, but the heat rate remains in linear scale.

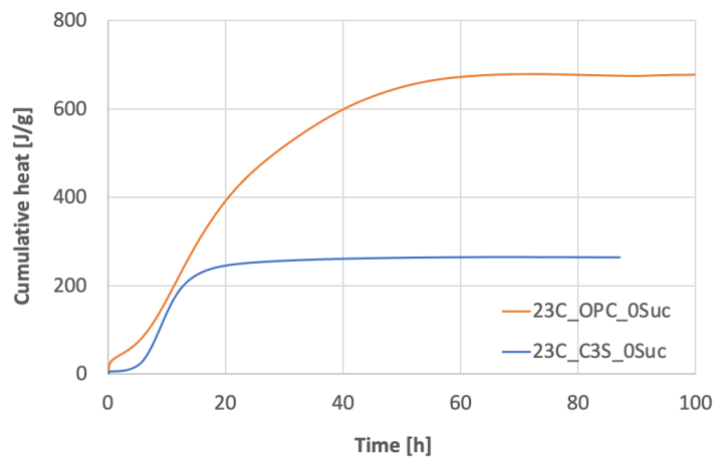


Figure 6.21. Cumulative heat for C_3S and OPC hydrating at 23 °C without sucrose.

Based on the difference of the initial peak between C_3S and cement, we can consider that most of the initial peak of cement is due to the aluminat reaction. Therefore, the heat associated to this peak should be deducted from the heat at the onset to get the heat that can be associated to the progress of alite hydration in cement samples.

The boundaries of integration for the initial peak are determined using Figure 6.22, in which we plot heat rates for all temperatures are plotted with the same linear-log representation as before. Based on these plots, we consider the end of aluminat reaction at the moment where all curves cross each other. For Figure 6.22a, b, c and d, this end was read to be 3.68 h for 10 °C, 1.22 for 16 °C (except for hydration without sucrose), 0.51 h for 23 °C and 0.48 h for 35 °C.

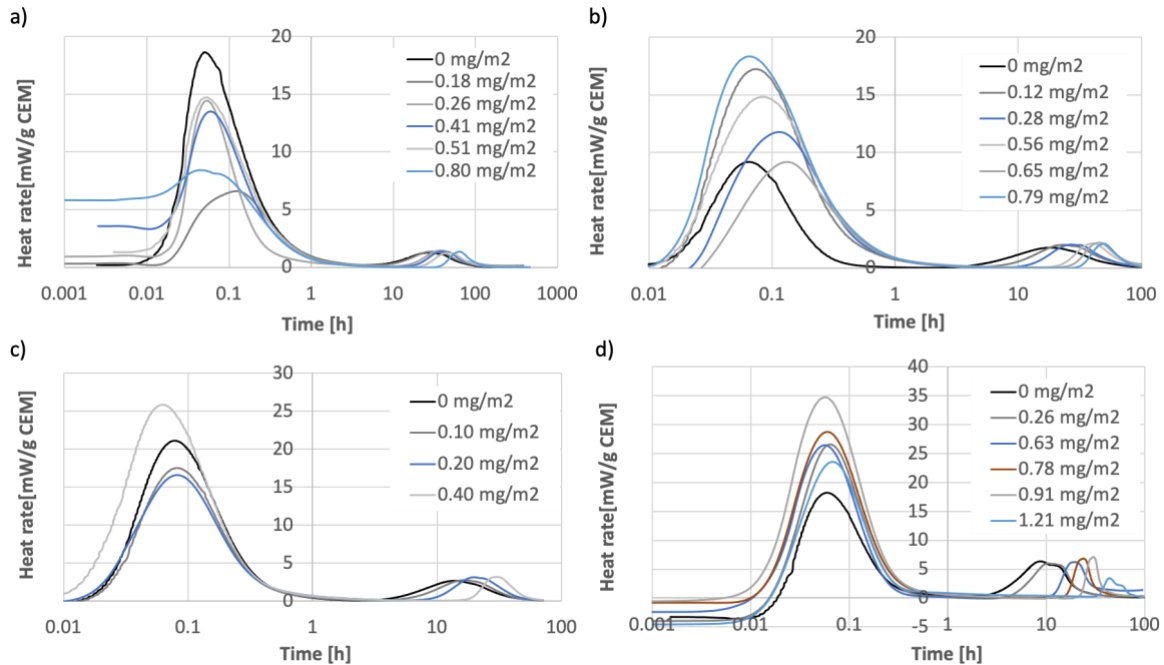


Figure 6.22. Calorimetry curves for OPC hydration with different amount of sucrose at a) 10 °C, b) 16 °C, c) 23 °C and d) 35 °C. The time is plotted in logarithmic scale, but the heat rate remains in linear scale.

Values obtained with this procedure are reported in Figure 6.23a, beside the cumulative heat at the onset in Figure 6.23b. Apart from the heat at the onset for the highest sucrose dosage, all data series seem to depend on temperature but not on sucrose dosage. Values are reported in Table 6.3. Interestingly, while neither $\overline{H_{tOS}}$ and $\overline{H_{Al}}$ do not show a clear evolution with temperature their difference $\overline{H_{tOS}} - \overline{H_{Al}}$ does and this represents the heat of hydration of alite in OPC at the onset $\overline{H_{alite}}$.

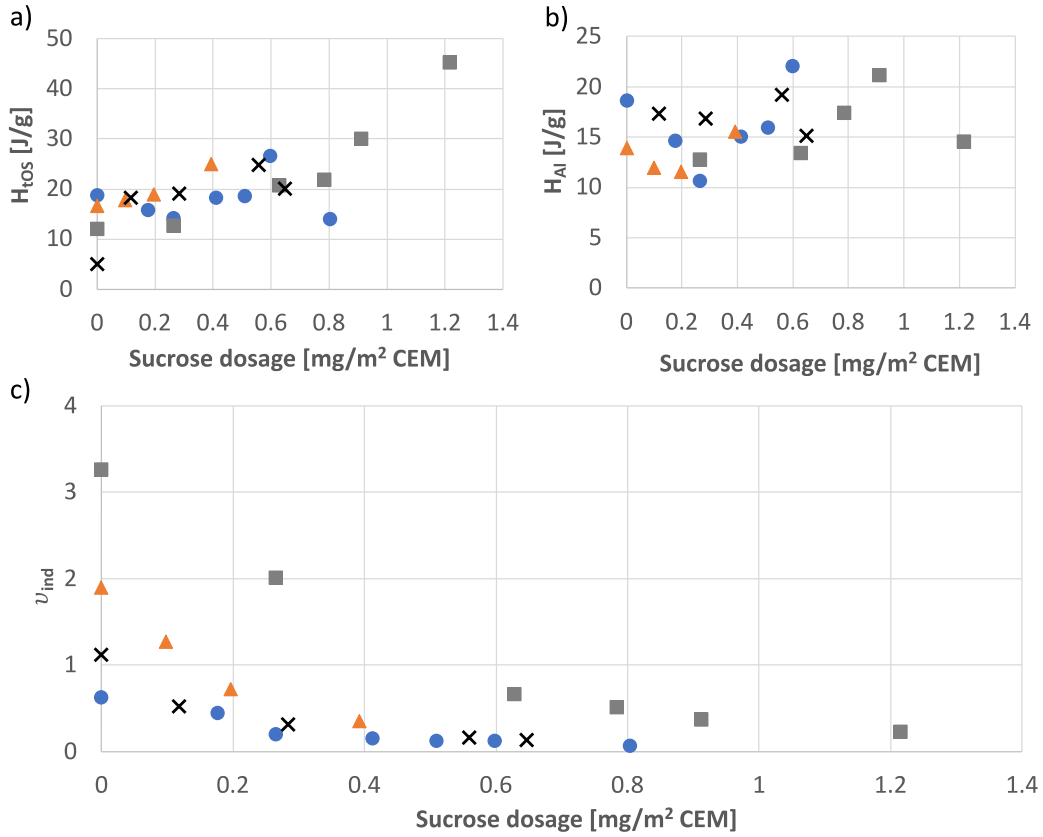


Figure 6.23. Characteristic of the onset at different temperatures (Circles: 10 °C, crosses: 16 °C, triangles: 23 °C, squares: 35 °C). a) Cumulative heat, b) Cumulative heat of initial (aluminite) peak, c) Hydration rate.

Table 6.3. Averaged heat at the onset, $\overline{H_{tOS}}$, and of the aluminite peak, $\overline{H_{Al}}$, obtained Figure 6.23a and b.

Temperature (°C)	End of aluminite reaction (h)	$\overline{H_{tOS}}$ (J/g CEM)	$\overline{H_{Al}}$ (J/g CEM)	$\overline{H_{alite}}$ (J/g CEM)
10	3.68	18.72	16.12	2.60
16	1.22	20.55	17.12	3.43
23	0.51	19.57	13.19	6.38
35	0.40	23.78	15.83	7.95

With this estimation of $\overline{H_{alite}}$, we calculate the hydration rate of alite in OPC during the induction period as: $v_{ind} = \overline{H_{alite}} / t_{OS}$. The corresponding linearized Arrhenius plot of these values is presented in Figure 6.24. Its slope indicates an activation energy of 47 KJ/mol, slightly higher than the 36 kJ/mol obtained for alite. The value obtained is however extremely similar to the activation energy of a dissolution in saturated CH system [102], suggestion that sucrose acts by inhibiting the dissolution of alite in cement.

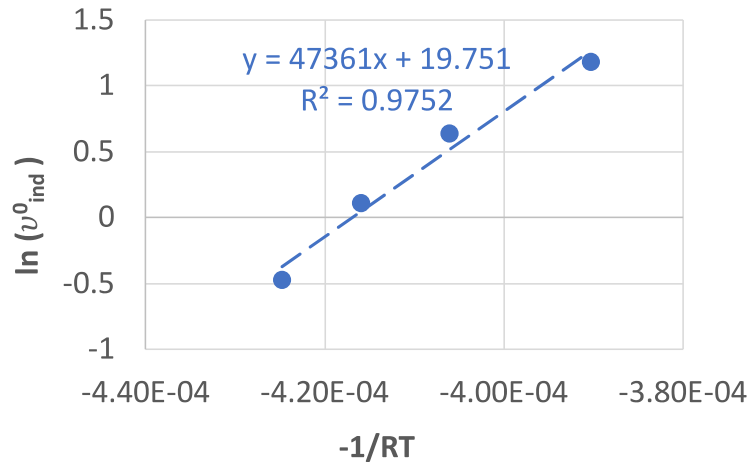


Figure 6.24. Linearized Arrhenius plots for the rate at induction period of OPC hydration without sucrose at different temperatures.

6.3.4 Impact of sucrose on the induction period rate

Having an adequate estimate of v_{ind} , we proceed its dependence of sucrose, in a similar way as in the previous chapters.

6.3.4.1 Hydration rate in the induction period

In Figure 6.25, we normalize all values of v_{ind} at a given temperature by the rate v_{ind}^0 obtained at the same temperature. The reference rate v_{ind}^0 is the v_{ind} for the experiment without sucrose at the temperature considered. As for C₃S, all points collapse on a single same master curve which is initially linear, but then approaches zero asymptotically.

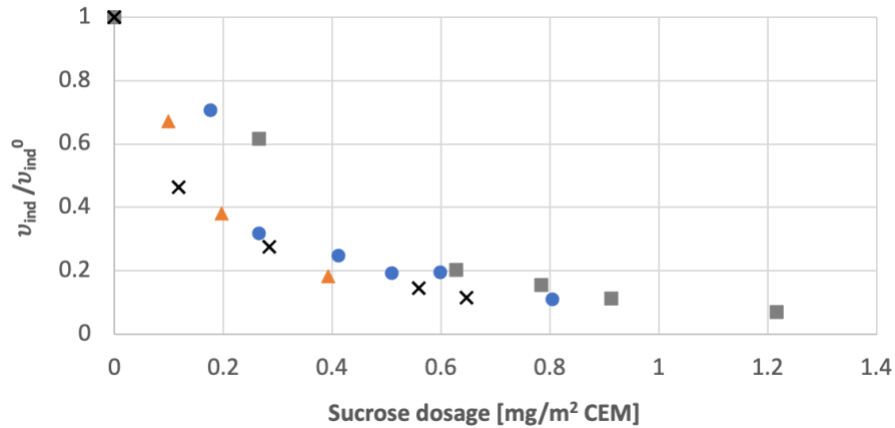


Figure 6.25. Normalized hydration speed in induction period in function of sucrose dosage. (Circles: 10 °C, crosses: 16 °C, triangles: 23 °C, squares: 35 °C).

The linear ranges go up to 0.42 mg/m² CEM for 10, 16 and 23 °C, 0.63 mg/m² CEM for 35 °C. In this range, adsorption is proportional to dosage, so we can infer that the hydration rate is proportional to adsorption. However, the proportion of sucrose adsorbing is only 29%, in this case versus the 87% for C₃S. We therefore proceed to examine the normalized velocity in relation to adsorption.

6.3.4.2 Impact of adsorption on induction period hydration rate

In section 6.2.2.2, we developed two methods to build up the relation between adsorption and dosage: 1) from Langmuir isotherm and mass balance, 2) from an empirical relation. With the first method, the equation (6-3) and (6-4) are used to calculate the adsorption for each dosage being used in calorimetry measurements. With the second method, the proportionality given in Figure 6.13 between dosage and adsorption is used. Then, in section 6.3.1, we proved that both methods work well for predicting adsorption from dosage in the range of interest for our calorimetry measurements. But the second one is simpler for calculations. Using this conclusion, our normalized velocities from Figure 6.25 are replotted versus adsorption calculated with empirical equation, the new plots are given in Figure 6.26.

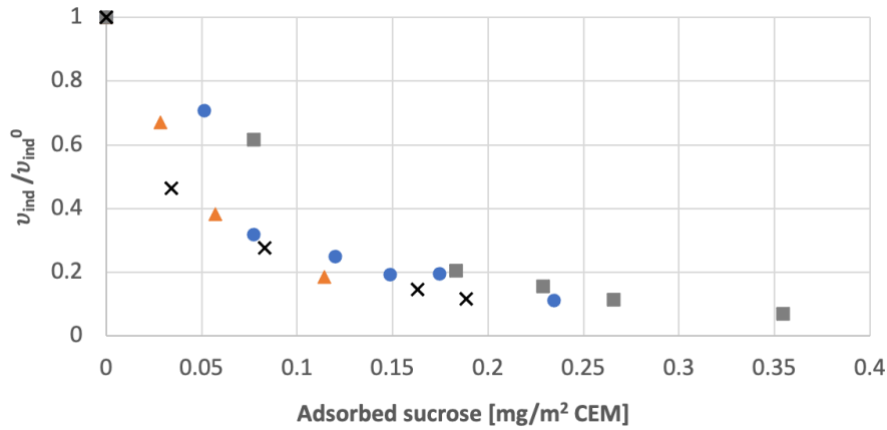


Figure 6.26. Normalized hydration speed in induction period in function of adsorbed sucrose. The adsorbed sucrose was calculated from empirical relation. (circle: 10 °C, crosses: 16 °C, triangle: 23 °C, square: 35 °C).

As can be seen in Figure 6.26, the temperature dependence is not obvious in the whole dosage range being used. In the first regime where the velocity decreases rapidly (adsorption below 0.14 mg/m² CEM), we apply a common linear fit as shown in Figure 6.27. The intercept of this regression line gives a critical adsorption value which is 0.13 mg/m² CEM. Based on chapter 4, this value can be thought to reflect a maximum adsorption on the alite of this cement.

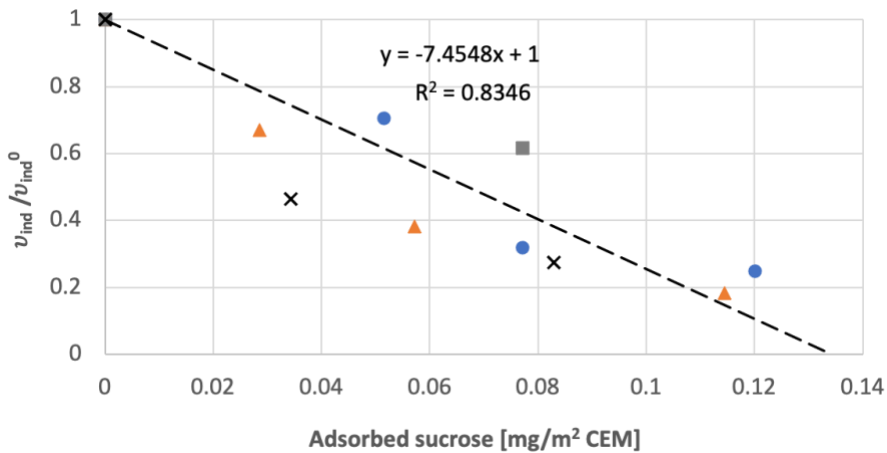


Figure 6.27. For adsorption in low dosage range, plotting normalized hydration speed in induction period in function of adsorbed sucrose. The adsorbed sucrose was calculated from empirical relation. (circle: 10 °C, crosses: 16 °C, triangle: 23 °C, square: 35 °C). The discontinuously line is the common linear regression for data at 4 temperatures imposing the ordinate at the origin to be 1.

It is natural to wonder whether this critical adsorption value corresponds to any of the adsorption plateau from Langmuir isotherm based on TOC measurements. To examine this, we compare Langmuir adsorption plateau in mg/m² with the intercept of the regression line in Figure 6.27 with the abscissa (also in mg/m²). Since a common fitting line was used for all data in low adsorption range, only one value is presented in **Error! Reference source not found.** for this critical adsorption value in the last column. Clearly, c_{∞}^{OPC} from the intercept of regression line is not comparable to any of the adsorption plateau from Langmuir isotherm.

Table 6.4. Comparison of maximum adsorption from calorimetry analysis and Langmuir isotherm. The value of c_{∞}^{alite} is estimated from c_{∞}^{OPC} obtained from the intercept of Figure 6.27 considering all sucrose adsorbs on alite. Values from c_{∞}^{C3S} come from our previous study on pure C_3S .

Temperature (°C)	c_{∞}^{OPC} Langmuir (mg/m ²)	c_{∞}^{OPC} Intercept (mg/m ²)	c_{∞}^{alite} Intercept (mg/m ²)	c_{∞}^{C3S} (mg/m ²)
10	0.73			0.24
16				---
23	0.92	0.13	0.22	0.22
35	0.79*			0.16

* The adsorption values were measured by TOC at 40 °C.

If however and as previously alluded to, we assume the surface fraction of alite in cement is equal to its mass fraction, we can estimate the adsorption plateau of sucrose on alite in cement (c_{∞}^{alite}), assuming that it does not adsorb on other phases at low dosages. Based on the plateau value for OPC in **Error! Reference source not found.** and with alite content in this cement (62% as presented in Table 6.1), the results of c_{∞}^{alite} are presented in Table 6.4. Since adsorption plateaus for pure C_3S obtained by different methods give very similar values, here we only present the one from empirical equation as c_{∞}^{C3S} . Interestingly, c_{∞}^{alite} from common regression line in Figure 6.27 gives very similar value as c_{∞}^{C3S} at 23 °C. This strongly suggests that the retardation of alite phase in OPC in this low dosage range is mainly caused by the sucrose coverage on the free alite surface, which is consistent to our conclusion in chapter 4. As hydration of tricalcium silicate is responsible for the appearance of hydration main peak when sucrose dosage is low, we also conclude that the retardation of OPC hydration is dominated by the surface coverage of sucrose on the alite phase in OPC clinker. As this maximum coverage is approached, other mechanisms start to contribute more significantly to sucrose consumption and delay the hydration less effectively. Luck and Luck [105] found that the evolution of Ca^{2+} , Al^{3+} , Si and SO_4^{2-} concentrations in pore solution for an OPC (type I) hydration depended on sucrose dosage. Between sucrose dosage 0.5% and 1%, clear difference in the trend of concentration evolution was observed for these species. These two dosages actually fall in the 2 regimes respectively in Figure 6.25, which very likely provide evidence for the different controlling step in hydration kinetics.

6.3.5 Reasons of getting high saturation plateau from Langmuir isotherm

In Table 6.4, we notice that the saturation plateau of sucrose adsorption on OPC at 23 °C is much higher than that on alite. Two scenarios are considered to explain this:

- 1) Sucrose forms complexes with other ions in pore solution, possibly some kind of aggregates. These would be filtered out by the solution depletion method and considered as adsorbed if they are larger than pore filter diameter of 0.45 μm , causing an overestimation of adsorption.

- 2) Other phases in OPC also consume sucrose but do not significantly change hydration kinetics. This would be the case for aluminate hydrates as AFm and Aft.

In what follows, we will discuss the possibility for having each scenario occur.

High adsorption plateau due to operation

To examine if our operation causes large errors in adsorption measurements, we made two series of adsorption measurements with same OPC (CEM I 42.5 R, Holcim, SSA = 1.41 m²/g CEM) and sucrose solutions. Pastes and pore solutions were prepared in same way. Then, one series of pore solutions was firstly filtered and then acidified by 0.05 M HCl for at least 20 times, which is the basic protocol we followed for TOC sample preparation. The other series of pore solutions was prepared by inverting the order of filtration and acidification. In this case, any aggregates present in the solution ought to be dissolved and would pass through the filter. For each series of samples, 3 repetitions for the lowest sucrose dosage and the highest sucrose dosages in each series were performed. All samples were finally measured in the same day by TOC device.

Results shown in Figure 6.28 show that sucrose adsorption measured from the two series of samples behave quite similarly. Repetitions for the highest sucrose dosage also gave almost identical adsorptions between both series with good reproducibility. Therefore, we can fit all these data with a single Langmuir isotherm, which gives a saturation plateau of 0.72 mg/m² CEM. This value is much higher than c_{∞}^{alite} (0.22 mg/m²), suggesting that the formation of complexes is not the issue causing the higher adsorption plateau with respect to c_{∞}^{alite} .

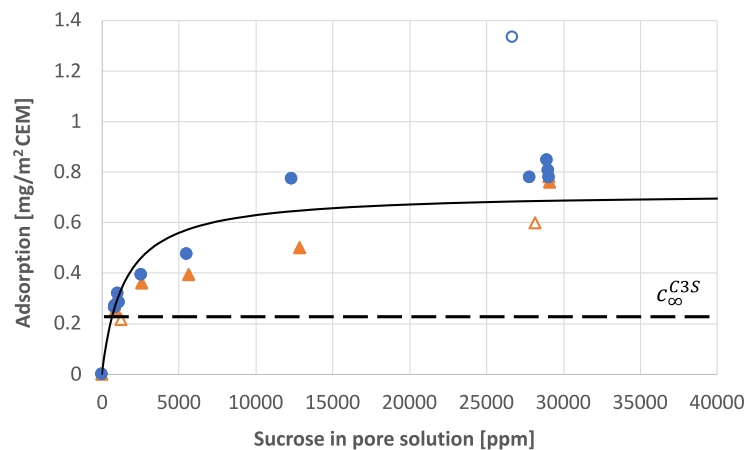


Figure 6.28. Adsorption measurements for TOC samples prepared differently. Circles: filtration before acidification; triangles: acidification before filtration.

Adsorption of sucrose on other phases

It is considered that other phases in OPC may also consume sucrose. Our adsorption results suggest that there is even more sucrose can be adsorbed/consumed by these phases than by alite phase in the first few minutes of hydration, but without causing big effect to hydration kinetics when sucrose dosage is low. Importantly however, at low dosages, sucrose appears to be mainly mobilized by alite. For higher sucrose dosages, the alite surface in OPC is almost fully covered while these other phases are still able to consume sucrose from pore solution, the sucrose adsorption falls in the second regime in Figure 6.26. There, we expect that only a small part of the incremental sucrose adsorption goes to alite and impact alite hydration kinetics, while the rest is consumed by other phases that do not impact kinetics in the induction period.

Regarding OPC clinker, C_3A and C_4AF are two phases which are active in early hydration period and forming ettringite. The consumption of sucrose by these phases were studied by Ivanova et al. [106], showing that C_3A consumes sucrose strongly and spontaneously with the start of hydration. C_4AF also consumes sucrose, less extensively than C_3A but much more than C_3S (Figure 6.29). Also, they observed the formation of $Fe(OH)_3$ hydrogels accompanied with C_4AF dissolution. From this aspect, they proposed that the strong sucrose adsorption was linked to those $Fe(OH)_3$ gels. The formation of this iron-rich amorphous phase was proposed in other works as well [107], [108], [109]. In another work, they found that sucrose retarded C_4AF hydration [107], the appearance of this gel took a certain time to occur because of the low solubility of $Fe(OH)_3$, which would be favored at high pH.

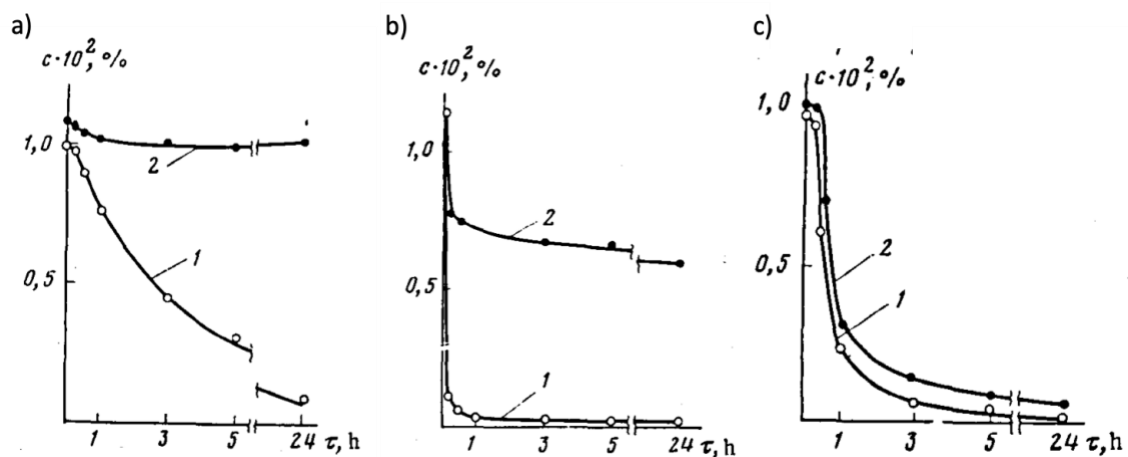


Figure 6.29. Changes in concentration in (1) sucrose and (2) trehalose during hydration of individual binders in suspensions of 2 g/100 ml of 0.01% carbohydrate solution. Binders: a) C_3S ; b) C_3A ; c) C_4AF .

To further test the impact of pH on adsorption in OPC, we carried out experiments with OPC using a pre-dissolved sucrose solution at pH 13.8 (rather than water). Results very likely support the formation of iron-rich gel with sucrose. Indeed, as can be seen in Figure 6.30, sucrose adsorption at high pH is much more extensive. And very interestingly, we observed the formation of a brownish phase (in Figure 6.31) from pore solutions with initial sucrose

dosages higher than 12 mg/m² CEM. This phase was still able to pass through the 0.45 μm filter but did not dissolve when adding 20 times 0.05 M HCl to it. With the increase of sucrose dosage, the color of this phase got darker, and the sedimentation appeared earlier. We hypothesize that most of this phase does not remain in the solution after centrifugation and, that even if it does, most particles do not pass through the filter, which would explain the increased adsorption at high pH reported in Figure 6.30.

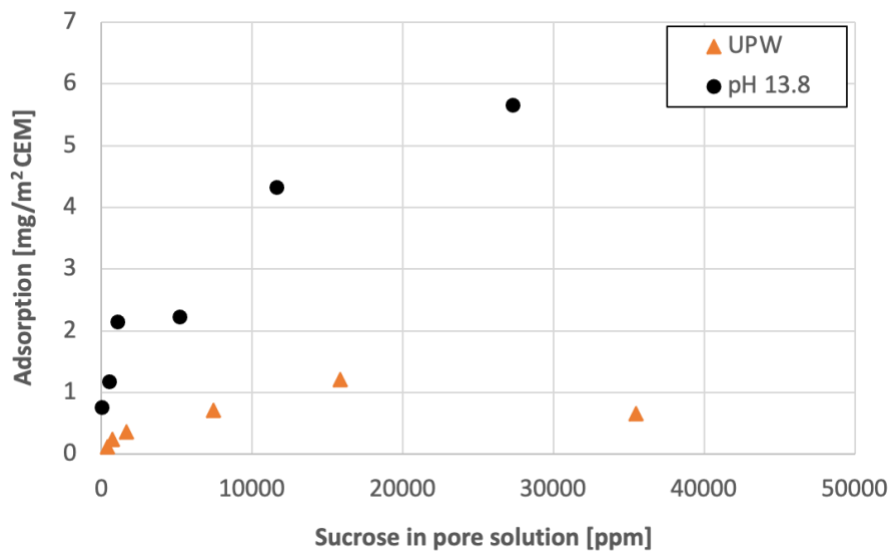


Figure 6.30. Sucrose adsorption at different initial pH. Circle: sucrose dissolved in a NaOH solution at pH 13.8; triangles: sucrose dissolved in UPW. Pastes were prepared with CEM I 52.5 R in the same way as those for all other adsorption measurements in this thesis.

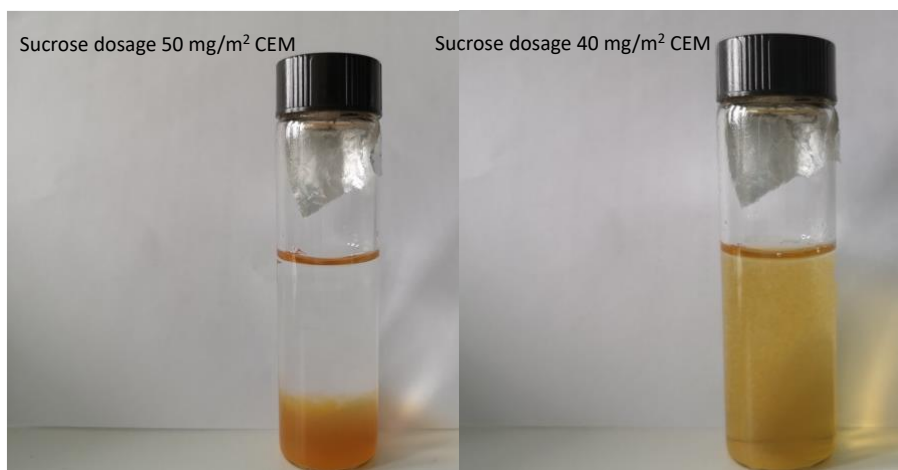


Figure 6.31. Observations of the iron-rich gel from OPC pore solutions, which are obtained at high pH, with high sucrose dosages.

To summarize, the formation of an iron-rich gel strongly consumes sucrose at high pH. Our results confirm the formation of such a gel at high pH. At lower pH the formation of this gel is not visible to the naked eyes, but nevertheless is likely to take place and probably impacts

solution depletion measurements of adsorption. We propose that the adsorption of sucrose by this gel may be the reason of having much higher sucrose adsorption plateau on OPC than on pure C₃S phase. More research on this topic would be needed but lies beyond not the scope of this thesis. Interesting approaches could be to use a white cement (non C₄AF) and pure phases.

6.4 Conclusions

In this part of work, we followed the same strategy as we did for C₃S in chapter 4. When looking at the initial adsorption of sucrose on OPC from TOC data, we find that the adsorption in low dosage range seems to be independent to temperature, but the plateau is much more difficult to be estimate compared to that for C₃S. Moreover, the two models for predicting adsorption from sucrose dosage work similarly with high quality. With the second and empirical model, we also infer that the adsorption plateau does not depend on temperature.

Another important finding is related to the definition of velocity in the induction period. For C₃S, we directly use the degree of hydration at the onset divided by onset. But for OPC, since the aluminate reaction produces a significant amount of heat in the first hour of hydration that cannot be neglected, the same definition is not representative anymore to the degree of hydration caused by alite. Therefore, we estimate the heat of the aluminate peak and deduct this from the total cumulative heat to estimate the heat released by alite hydration ($\overline{H_{tOS}} - \overline{H_{Al}}$). It is on this basis that we then determine heat of hydration of alite in OPC at the onset ($\overline{H_{alite}}$). It is with this heat and the onset time that we then calculate the average velocity of alite hydration in the induction period.

Regarding the relation between relative velocity in the induction period and adsorption, there are clearly two regimes. First there is a sharp decrease that does not depend on temperature and then there is a slower decrease of velocity that indicates a decreasing effectiveness of added sucrose in terms of retardation. This behavior is different from the case for C₃S where the relative velocity keeps decreasing with adsorption until it reaches zero at which point the surface is saturated. The intercept of the common regression line in the first regime gives a maximum adsorption that is much lower than any of the estimated adsorption plateau values. However, when including the alite content in OPC, this maximum value appears to be the same as determined on C₃S alone (chapter 4). This strongly suggests that in the low dosage range, it is the adsorption of sucrose on free alite surface in OPC that causes retardation. Conversely, as for C₃S, the hydration rate is governed by the amount of alite surface that is free to dissolve during the induction period.

The reason of having higher saturation plateau for sucrose adsorption on OPC than on pure C₃S phase is also discussed. With the observation of an iron-rich gel forming in pore solution with sucrose, together with its dependence on sucrose dosage, we propose that the adsorption of sucrose by this gel is possibly being the reason of higher adsorption plateau.

6.5 Acknowledgements

Support for Ms. Weiqing Xu was provided by the SNF project (No. 172481) titled “Molecular control of cement hydration through tailored chemical admixtures”. We would like to thank M. Martin Keller for producing a series of in-situ mixing cells to support the calorimetry measurements.

7 Impact of portlandite on OPC retardation caused by sucrose

Foreword: This chapter represents original research performed by and written up by the author of this thesis under the guidance of Prof. Robert J. Flatt.

7.1 Introduction

In chapter 4, we studied the impact of sucrose adsorption on C_3S retardation. This led us to conclude that the average velocity in the induction period is proportional to the free C_3S surface. Then, chapter 5 was dedicated to mixtures of C_3S and CH system. There, we came to two additional important conclusions. First that CH consumes ions in solution and/or allows deposition of hydrates more effectively than C_3S . Second, that the velocity in the induction period for a system containing both C_3S and CH is proportional both to the total surface in system and to the free C_3S surface to the system. In chapter 6, we moved on to studying the impact sucrose on OPC retardation, bringing in the additional complexity of an industrial cement, containing multiple phases in addition to soluble alkali. There, we found that in the low dosage range, the velocity in the induction is mainly related to the free alite surface, as we had found for that phase in chapter 4.

In the present chapter, following our path of increasing the complexity, we see whether the same principles can be applied to rationalize the effect of sucrose on a system containing both OPC and CH. In this regard, an interesting study by Reiter et al [72] reports that the addition of CH reduces the retardation of OPC caused by sucrose. These authors further found this to be linked to the surface area of CH and assume that a complete transfer of sucrose from OPC to CH surfaces takes place.

While very interesting and compelling, those conclusions contrast with our chapter 5, where we did not find that CH substantially reduced retardation induced by sucrose on C_3S . Rather we found that CH leads to an acceleration of C_3S hydration. In the present chapter, we therefore examine whether OPC and CH mixes behave similarly to what Reiter et al [72] reported. For a better comparison to our previous chapters, we focus on OPC hydrating in UPW with L/S 0.7. The impact of CH alone on OPC hydration is also studied as a reference point for hydration containing both CH and sucrose.

7.2 Results

7.2.1 Calorimetry

The hydration of OPC (CEM I 42.5R) was followed by calorimetry. To study the effect of CH on OPC hydration retarded by sucrose, a series of experiments were performed with fixed

amount of sucrose ($0.36 \text{ mg/m}^2 \text{ CEM}$) and different dosages of CH. The CH dosages used were 0, 0.02, 0.05 and $0.12 \text{ g/m}^2 \text{ CEM}$. In addition, OPC pastes hydrating with different amounts of CH, but without sucrose, were also measured as reference cases.

Regarding sample preparation, we used the same ex-situ mixing method as described in the chapter 5. The cement powder and relative amount of CH powder were firstly mixed by hand at room temperature. A stock solution of 714 ppm sucrose was prepared by dissolving sucrose in UPW and stored in a water bath set at $23 \text{ }^\circ\text{C}$. This solution was then added to mixed powder to reach a liquid to cement ratio (L/C) of 0.7. Additional UPW was also added along with the extra CH to maintain the overall L/S 0.7. The paste was mixed by Vortex mixer for 1 min and 30 s before being introduced into the calorimeter.

Figure 7.1a and b present the calorimetry curves for OPC hydration with different amounts of CH, respectively without and with sucrose. They show that the addition of CH does not significantly change the height or maximum slope of the main hydration peak, but only shift it to earlier time (Figure 7.1a). Moreover, the addition of sucrose also does not change the shape of this main peak but only delays the time of its occurrence (Figure 7.1b).

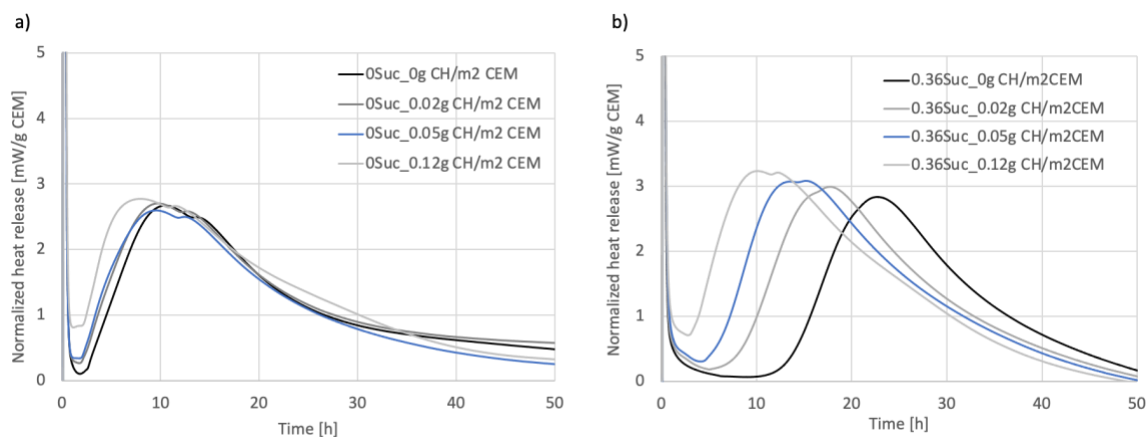


Figure 7.1. Acceleration of CH on OPC hydration a) without sucrose; b) with sucrose.

7.2.2 Initial adsorption

As sucrose adsorbs both on cement and portlandite surfaces, it is important to evaluate its adsorption on each mineral surfaces that we will note CEM and CH.

The same commercial CH was used in this part of work as for C_3S and CH system, and the cement pore solution extracted 5 min after mixing gave a pH of 12.78 which is very close to the value of 13 used when measuring sucrose adsorption on the CH. This probably explains why the initial adsorption of sucrose on the CH remains the same as presented in chapter 5. Therefore, we simply re-plot the sucrose adsorption data on CH from chapter 5, showing the

adsorption data fitted with a Langmuir isotherm (Figure 7.2), with the fitting parameters listed in Table 7.1.

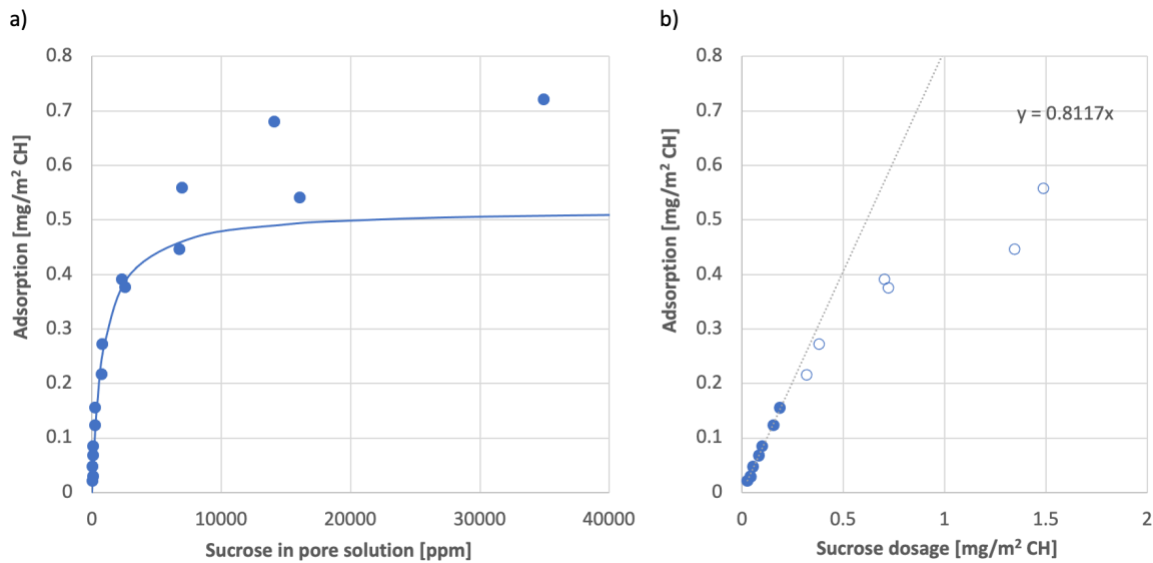


Figure 7.2. Adsorption of sucrose on the CH. a) TOC measurement points in circles and the Langmuir fitting curve in solid line. b) Adsorption versus sucrose dosage in the low dosage range.

The sucrose adsorption on CEM I 52.5 R was reported in the previous chapter. In the present chapter we use CEM I 42.5 R but the C₃S contents in both these OPC are similar, which are 62% for CEM I 52.5 R and 63% for CEM I 42.5 R. The dry SSA for CEM I 42.5 R is 0.82 g/m² and the wet SSA is 1.41 g/m². Here, we present adsorption data for CEM I 42.5 R at 23 °C. Adsorption measurements are carried out at the same L/S as the calorimetry (0.7). Results are shown in Figure 7.3a, along with the fitted Langmuir isotherm. This shows an initial linear increase in adsorption but not as sharp as for CH. As shown in Figure 7.3b, in the low sucrose dosage range, only 37% of dosed sucrose is adsorbed, which is much lower than the 81% adsorption as presented in Figure 7.2b for CH.

The fitting parameters used for sucrose adsorption on OPC are also summarized in Table 7.1. We notice that the K_7^* for CH is almost doubled compared to the value for OPC. This suggests that the affinity of sucrose for CH is much higher than for OPC, which agrees with the study from the work of Reiter on OPC pastes [73].

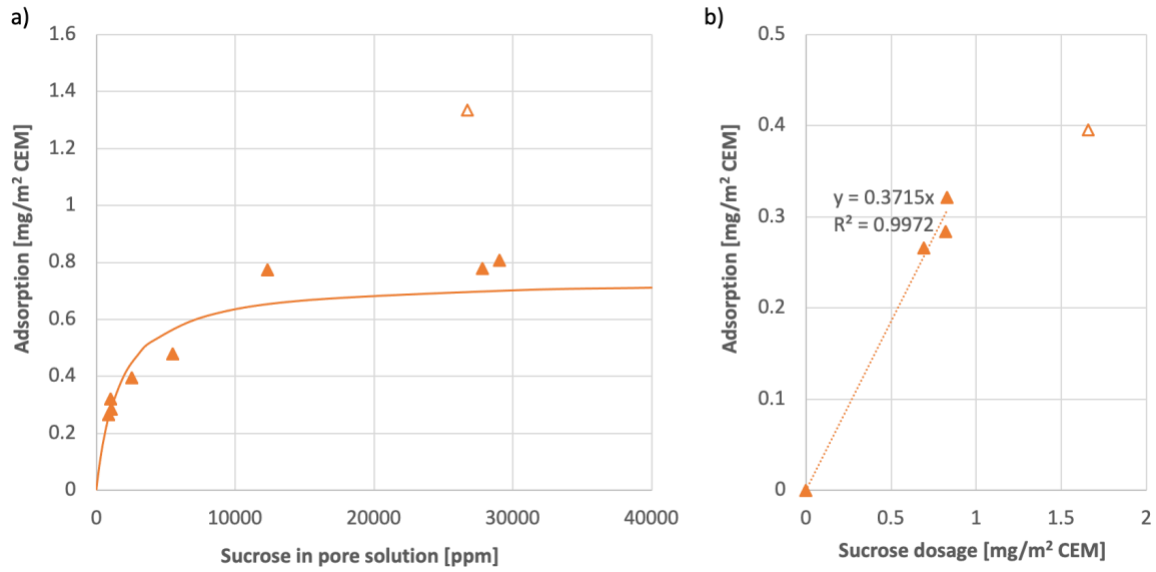


Figure 7.3. Adsorption of sucrose on the CH. a) adsorption isotherm with TOC measurement points in triangles and the Langmuir fitting curve in solid line; b) adsorption versus sucrose dosage in the low dosage range with empty points not being considered for linear regression.

Table 7.1. Langmuir fitting parameters for sucrose adsorption on CH and OPC surface. These values were obtained when sucrose concentration was used in ppm and adsorption in mg/m² of surface.

	K_T^*	c_∞ (mg/m ²)
Sucrose on CH	0.0011	0.52
Sucrose on OPC	0.0006	0.74

7.2.3 Adsorption from Langmuir isotherm and mass balance

Starting from individual sucrose adsorption isotherms, we need to evaluate the distribution of sucrose on different mineral surfaces for a system where both OPC and CH present. For this, we use the same approach as in chapter 5. For convenience, the needed equations are reproduced below.

The surface coverage of OPC by sucrose is:

$$\theta_{CEM} = \frac{c_{ads,CEM}}{c_{\infty,CEM}} = \frac{K_{T,CEM}^* \cdot c_{sol}}{1 + K_{T,CEM}^* \cdot c_{sol}} \quad (7-1)$$

And the surface coverage of CH by sucrose

$$\theta_{CH} = \frac{c_{ads,CH}}{c_{\infty,CH}} = \frac{K_{T,CH}^* \cdot c_{sol}}{1 + K_{T,CH}^* \cdot c_{sol}} \quad (7-2)$$

This should be combined with the mass balance below and solved numerically for each dosage:

$$m = c_{sol} \cdot L + \theta_{CEM} \cdot c_{\infty,CEM} \cdot S_{CEM} + \theta_{CH} \cdot c_{\infty,CH} \cdot S_{CH} \quad (7-3)$$

In chapter 5, the sucrose adsorption on CH is almost proportional to its concentration in pore solution, for the solution concentration range relevant to our experiments. At the same time, sucrose adsorption on C₃S is non-linear in the same range. This allowed simplifying the term $\theta_{CH} \cdot c_{\infty,CH} \cdot S_{CH}$ in equation (7-3).

However, for the system of OPC & CH studied here, adsorption on CH is no more linear in the concentration range of interest, while in contrast adsorption on OPC seems to be linear. As shown in Figure 7.4b, the non-linear behavior is obvious to the eye. In Figure 7.4d, no experimental data point falls in the concentration range of interest, a regression line was therefore made based on the Langmuir fitting curve by assuming that it also describes adsorption reasonably well at low dosages. Figure 7.4d suggests that adsorption is indeed proportional to solution concentration in the range of interest. Therefore, so we can simplify the term θ_{CEM} in equation (7-3) and write it as $c_{sol} \cdot K_{T,CEM}^*$.

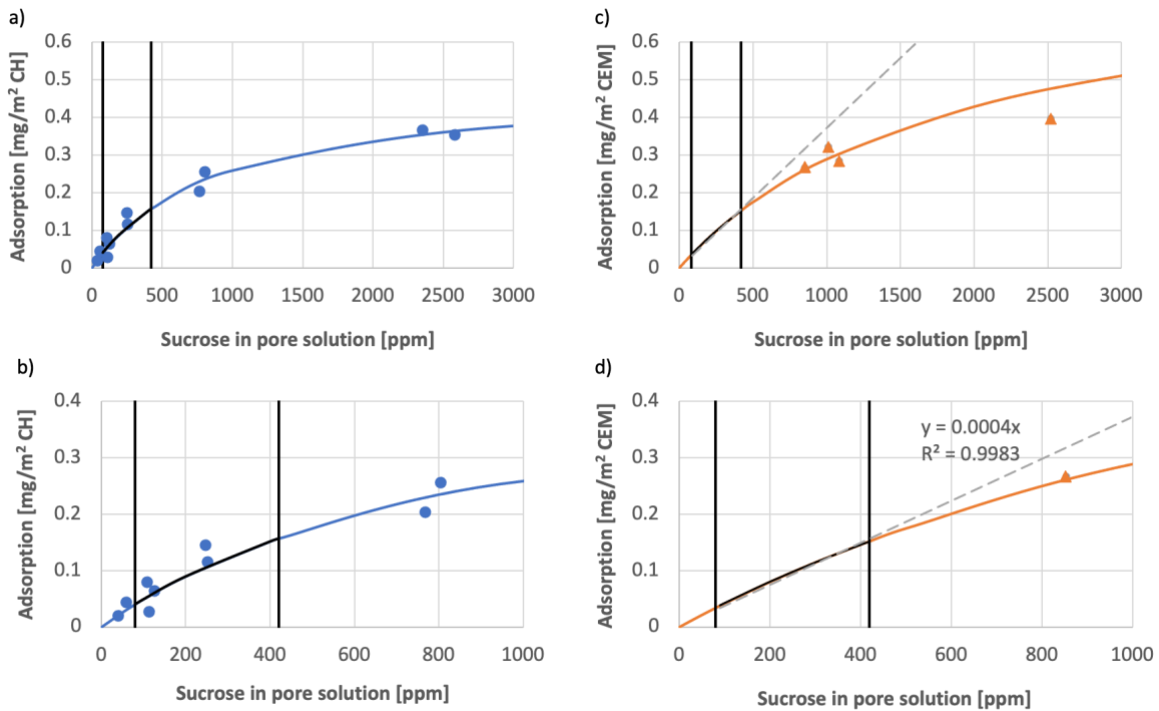


Figure 7.4. Illustration the linearity of adsorption in the solution concentration range being solved numerically. a) and b) refer to the sucrose adsorption on CH. c) and d) refer to sucrose adsorption on OPC. b) and d) are the same plots from a) and c) respectively, but with narrower range on the two axes. In each graph, solid points are the adsorption measurements data from TOC; solid curve is the fitting curve with Langmuir equation; vertically lines are the lower and upper limits for solution concentrations obtained from numerical solving. Discontinuous line in graph c) and d) represent the linear regression line in the concentration range of interest based on the Langmuir fitting curve.

Equation (7-3) can therefore be expressed as:

$$\frac{m}{S_{CEM}} = c_{sol} \cdot \left(\frac{L}{S_{CEM}} + K_{T,CEM}^* \cdot c_{\infty,CEM} + \frac{K_{T,CH}^* \cdot c_{\infty,CH}}{1 + K_{T,CH}^* \cdot c_{sol}} \cdot \frac{S_{CH}}{S_{CEM}} \right) \quad (7-4)$$

and rearranged to the following second order equation:

$$\begin{aligned} c_{sol}^2 K_{T,CH}^* \left(\frac{L}{S_{CEM}} + K_{T,CEM}^* c_{\infty,CEM} \right) \\ + c_{sol} \left(K_{T,CEM}^* c_{\infty,CEM} + \frac{L}{S_{CEM}} + K_{T,CH}^* c_{\infty,CH} \frac{S_{CH}}{S_{CEM}} \right. \\ \left. - K_{T,CH}^* \frac{m}{S_{CEM}} \right) - \frac{m}{S_{CEM}} = 0 \end{aligned} \quad (7-5)$$

The solution of this quadratic equation gives the expression of c_{sol} as:

$$\begin{aligned} c_{sol} \\ = \frac{- \left(K_{T,CEM}^* c_{\infty,CEM} + \frac{L}{S_{CEM}} + K_{T,CH}^* c_{\infty,CH} \frac{S_{CH}}{S_{CEM}} - K_{T,CH}^* \frac{m}{S_{CEM}} \right) + \sqrt{\Delta}}{2 K_{T,CH}^* \left(\frac{L}{S_{CEM}} + K_{T,CEM}^* c_{\infty,CEM} \right)} \end{aligned} \quad (7-6)$$

with

$$\begin{aligned} \Delta = \left(K_{T,CEM}^* c_{\infty,CEM} + \frac{L}{S_{CEM}} + K_{T,CH}^* c_{\infty,CH} \frac{S_{CH}}{S_{CEM}} - K_{T,CH}^* \frac{m}{S_{CEM}} \right)^2 \\ + 4 \frac{m}{S_{CEM}} K_{T,CH}^* \left(\frac{L}{S_{CEM}} + K_{T,CEM}^* c_{\infty,CEM} \right) \end{aligned} \quad (7-7)$$

To check the accuracy of this approximation, we plot the sucrose coverages obtained by numerical solution versus those from the above approximation. Figure 7.5 shows that both methods give similar results both for OPC and CH, thereby validating the simplified analytical solution.

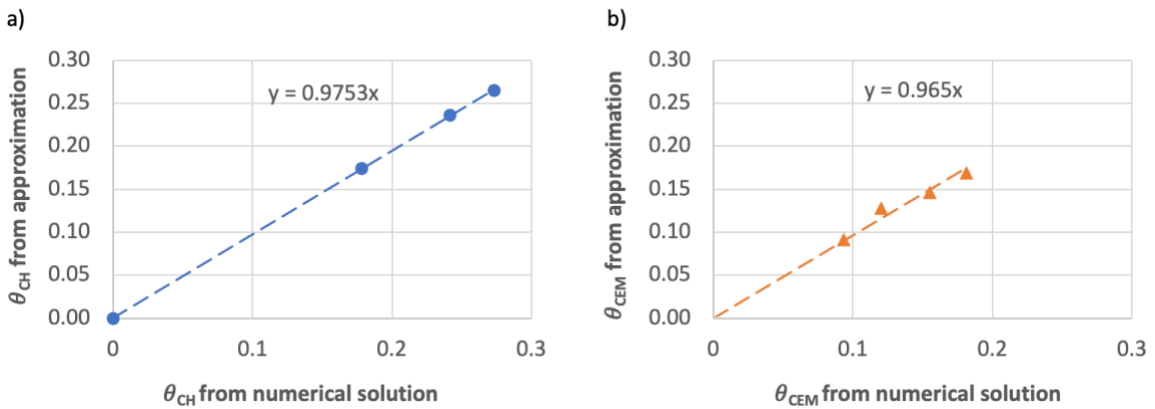


Figure 7.5. Comparison of surface coverage of sucrose on a) CH and on b) OPC obtained by using the equations and from the numerical solutions.

7.2.4 Impact of CH on the maximum slope of the acceleration period

Based on the calorimetry curves, the slope in each acceleration period (R_{max}) is extracted as described in the previous chapters. As shown in Figure 7.6, sucrose does not cause significant differences in R_{max} for OPC hydration with different dosages of CH. As to the impact of CH, R_{max} remains almost unchanged up to CH dosages of about 0.15 g/m² CEM. For the highest CH dosage (0.36 g CH/m² CEM), the slopes are clearly higher no matter whether sucrose is present or not.

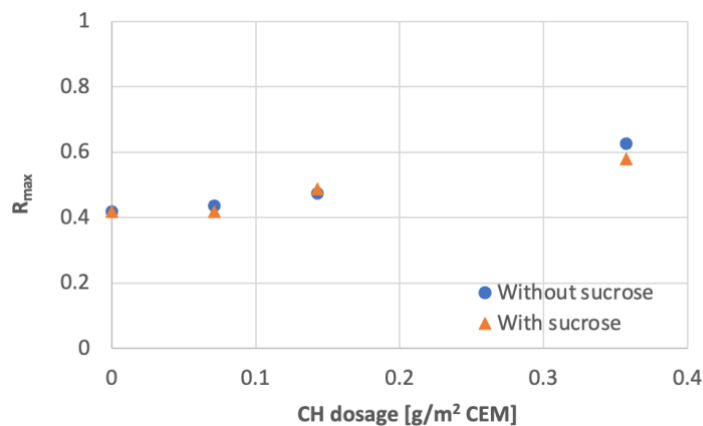


Figure 7.6. Slopes of the calorimetry curves. (Circles: OPC hydration without sucrose but with CH; triangles: OPC hydration with sucrose and CH).

7.2.5 Impact of CH on the hydration rate in induction period

When examining the impact of CH on the induction period rate in mixed CEM and CH systems, the definition of onset becomes more problematic in presence of CH. To address, this issue we use two ways of determining the hydration onset:

- using the intersection of the maximum rate of the acceleration period with the abscissa
- also using the maximum rate of the acceleration rate but considering its time at the minimum rate of the induction period.

Unfortunately, as in the part of the work a baseline correction is needed, the minimum of the induction period does not have a true physical meaning. Therefore, the onset is simply defined as the intersection of the maximum rate with the abscissa, as shown in Figure 7.7.

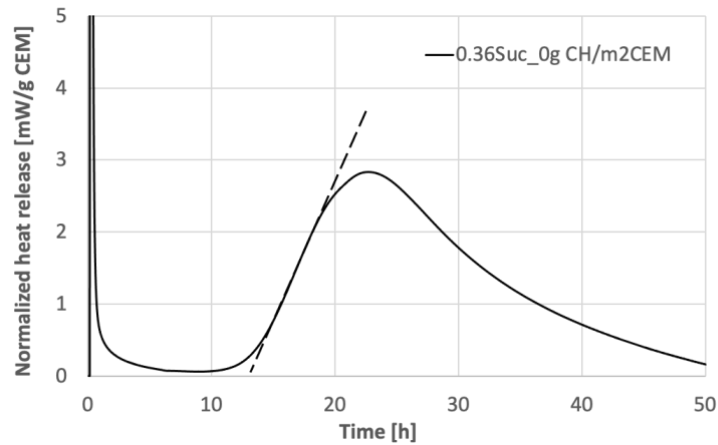
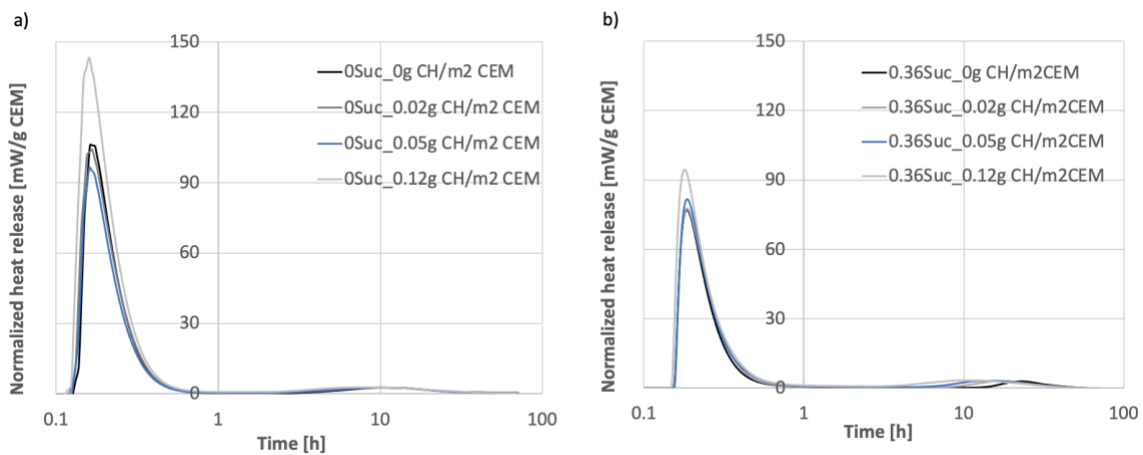


Figure 7.7. Defining the onset by using the crossing point of the tangent in the linear range in acceleration period with the abscissa.

Beside of onset time, another important parameter is the degree of hydration at the onset. As discussed in the previous chapter, the heat release caused by the aluminate reaction in the first hour is much more pronounced than that of the silicate. So, when looking at the degree of hydration of alite at the onset, the contribution from this aluminate reaction should be discarded. For this, as in the previous chapter, we first re-plot the calorimetry curves from linear-linear scale to log-linear scale as shown in Figure 7.8 to have a clearer insight into the aluminate peak. Based on this, we define the end of the aluminate peak as the moment when all curves coincide. For experiments without and with sucrose, this specific time is 0.65 h and 1.35 h, respectively.



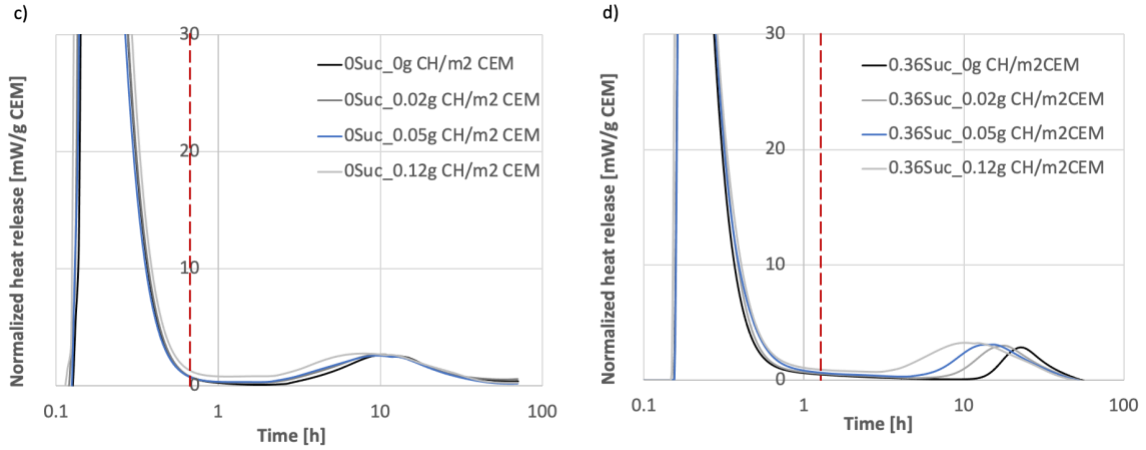


Figure 7.8. Re-plot the calorimetry curves for system a) without sucrose and b) with sucrose in log-linear scale. c) and d) are the same plot from a) and b) respectively, with y-axis limited to 30 mW/g CEM.

From the heat release curve, we could easily read the cumulative heat at the onset (H_{tOS}) in J/g CEM and the cumulative heat at the end of aluminat peak (H_{Al} , in J/g CEM). Corresponding heats are shown in Figure 7.9 versus CH dosage. No matter the presence or absence of sucrose, H_{tOS} and H_{Al} remain stable regardless of CH dosage. So, in what follows we use average values shown by the discontinuous lines in Figure 7.9.

The cumulative heat at the onset produced by alite phases $\overline{H_{alite}}$ is then:

$$\overline{H_{alite}} = \overline{H_{tOS}} - \overline{H_{Al}} \quad (7-8)$$

and the velocity in the induction period is defined as

$$v_{ind} = \frac{\overline{H_{alite}}}{t_{OS}} \quad (7-9)$$

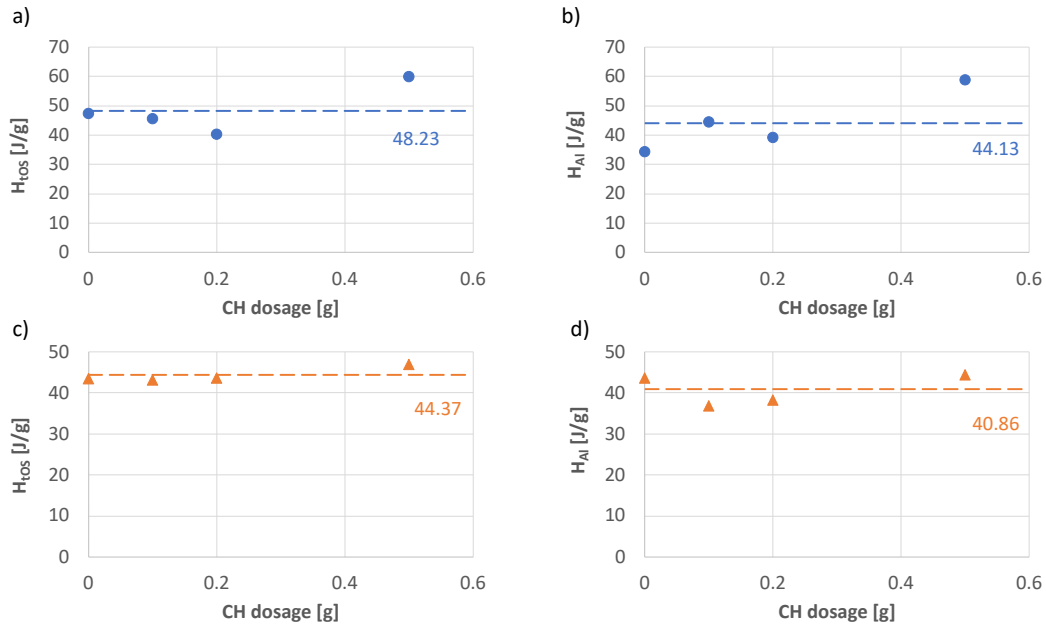


Figure 7.9. a) Cumulative heat at the hydration onset and b) cumulative heat at the end of aluminat peak for experiments without sucrose. c) Cumulative heat at the hydration onset and d) cumulative heat at the end of aluminat peak for experiments with sucrose. The discontinuous line represents the average value for each series of data.

In Figure 7.10, we plot v_{ind} versus CH dosage. It shows that the effect CH on hydration kinetics is similar with and without sucrose. Both data series increase linearly and with similar slopes as a function of the CH surface.

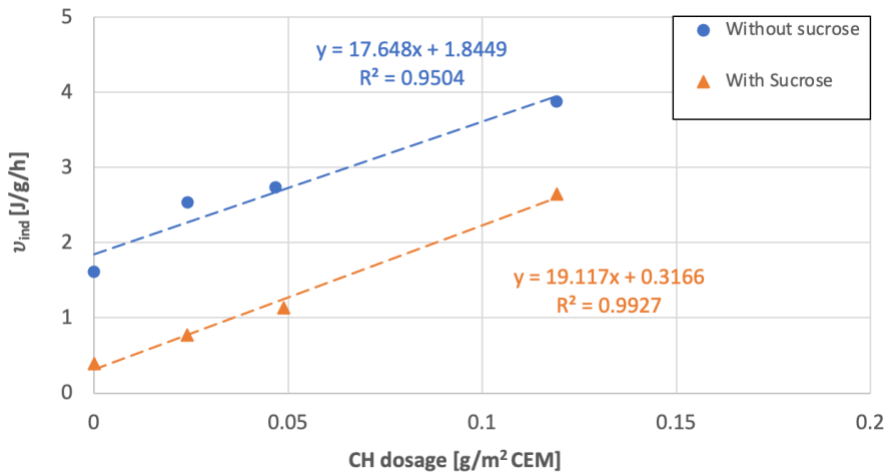


Figure 7.10. Evolution of the velocity in induction period versus CH dosage. Discontinuous lines are the regression lines for different data series.

7.3 Discussion

7.3.1 Impact of CH on OPC induction period without sucrose

Let us first look at the impact of CH in terms of the maximum rate of the acceleration period. Figure 7.6 shows that for most CH dosages, this is constant, meaning that whatever mechanism causes the induction period rate to shorten, it is no more active in the acceleration period. This finding is the same as for blended C₃S/CH system in chapter 5.

Similarly, to chapter 5, we now examine whether the shortening of the induction period is linked to an increase surface to liquid ratio when CH is added. As a reminder, in that analysis for C₃S and CH, we had introduced an effective surface:

$$S_L^\# = \frac{m_{C_3S} \cdot SSA_{C_3S} + f_{CH} \cdot m_{CH} \cdot SSA_{CH}}{V_L} \quad (7-10)$$

where the term f_{CH} expresses a difference in efficiency of CH surfaces versus C₃S ones.

Thereby, the reference surface in absence of both sucrose and CH was

$$S_L^0 = \frac{m_{C_3S} \cdot SSA_{C_3S}}{V_L} \quad (7-11)$$

For this chapter, as we are concerned with the hydration kinetics of alite in OPC, it makes sense to account separately for the alite and non-alite surfaces in OPC. For this we note ϕ_{alite} the volume fraction of alite in cement (taken equivalent to the mass fraction that is 63%) and redefine $S_L^\#$ as:

$$S_L^\# = \frac{\phi_{alite} \cdot m_{Cem} \cdot SSA_{Cem} + f_{Rest-Cem} \cdot (1 - \phi_{alite}) \cdot m_{Cem} \cdot SSA_{Cem}}{V_L} + \frac{f_{CH} \cdot m_{CH} \cdot SSA_{CH}}{V_L} \quad (7-12)$$

where the term $f_{Rest-Cem}$, accounts for the different efficiency of phases other than alite in OPC.

With the above approach, we can consider two extreme situations.

In the first situation, no hydrates deposit on the non-alite surfaces, so that those surfaces would not contribute to accelerating hydration. The term $f_{Rest-Cem}$ would then be zero, so that:

$$S_L^\# = \frac{\phi_{alite} \cdot m_{Cem} \cdot SSA_{Cem} + f_{CH} \cdot m_{CH} \cdot SSA_{CH}}{V_L} \quad (7-13)$$

And the reference surface in absence of both sucrose and CH would be given by:

$$S_L^0 = \frac{\phi_{alite} \cdot m_{cem} \cdot SSA_{cem}}{V_L} \quad (7-14)$$

The second situation is that the deposition factor for non-alite surfaces is the same as for CH ($f_{Rest-cem} = f_{CH}$), which gives:

$$S_L^{\#} = \frac{m_{cem} \cdot SSA_{cem} \cdot (\phi_{alite} + f_{CH} \cdot (1 - \phi_{alite})) + f_{CH} \cdot m_{CH} \cdot SSA_{CH}}{V_L} \quad (7-15)$$

With the reference surface being:

$$S_L^0 = \frac{m_{cem} \cdot SSA_{cem} \cdot (\phi_{alite} + f_{CH} \cdot (1 - \phi_{alite}))}{V_L} \quad (7-16)$$

Our analysis of both situations suggests that the second is more realistic, which is why it is further developed below. This represents the case where $f_{Rest-cem} = f_{CH}$. We however reported the analysis and conclusions of the first situation in the Appendix A to this chapter for completeness.

Let us plot the normalized velocity versus the normalized surface, using the expression for S_L^0 given in equation (7-16). The effective surface is then calculated with equation (7-15). Figure 7.11a shows that this gives a slope very close to 1, meaning that no correction factor is needed for CH. Thus, all surfaces behave equivalently. An efficiency factor f_{CH} of 1.05 leads to a slightly better fit and then gives a slope of 1 in Figure 7.11b. As both the slope in Figure 7.11a and the efficiency factor are very close to 1, we could infer that the hydrates deposit similarly on all surfaces, including CH surface. This appears to be a reasonable situation and explains why we select it for further analysis.

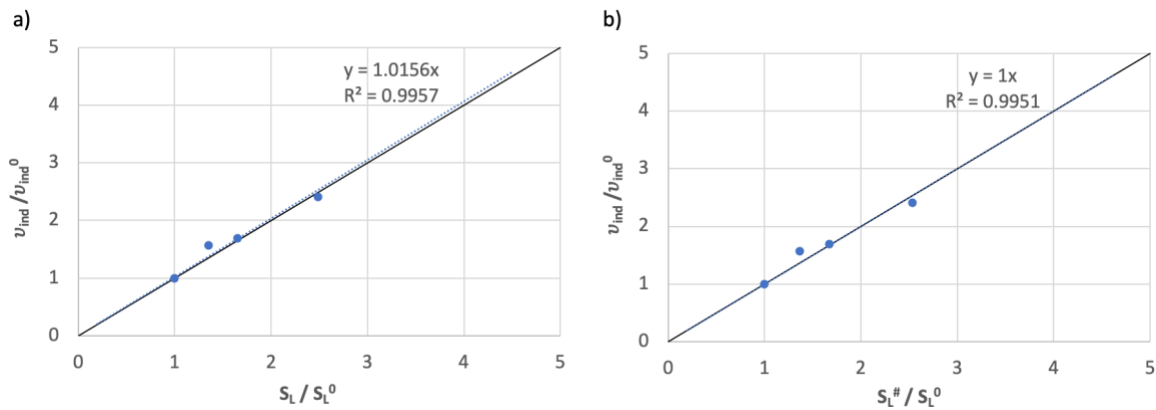


Figure 7.11. Change of relative velocity in the induction period with respect to the total surface area in absence of sucrose. The reference values of v_{ind}^0 and S_L^0 are taken for the pastes without CH. a) total solid surfaces, b) effective surfaces as defined in equation (7-13) with a value of 1.05 for $f_{Rest-cem} = f_{CH}$.

7.3.2 Impact of CH on the OPC induction period with sucrose

We now turn to cases where sucrose is introduced in the blend of OPC/CH. Two important effects are hindering dissolution of alite and modifying the available surface for hydrate deposition.

Let us begin with the impact on dissolution. This will be linked to the surface coverage of alite in OPC, in agreement with our conclusion from chapter 5. Unfortunately, that surface coverage is not trivial to define, because as explained in that chapter, it appears that sucrose first adsorbed on alite and then on other surfaces, where it can adsorb more but with a lower affinity. The impact on dissolution can be written as and represents the second term in equation (7-18). To be able to calculate it, we must define the distribution of sucrose between the different surfaces in our present system (OPC-alite, OPC-non alite and CH).

For simplicity we will consider that the OPC-non alite surfaces behave as CH, not only for adsorption, but also for their impact on the available surface for hydrated deposition (equation (7-12)).

This means that with respect to that equation we are considering a situation where $f_{Rest-Cem} = f_{CH}$. This, along with surface coverages of sucrose on OPC ($\theta_{alite-OPC}^*$), as well as on non-alite and CH (both given by θ_{CH}^*) leads to writing the total available surface in the system as:

$$\begin{aligned}
 S_L^* &= \frac{\phi_{alite} \cdot m_{Cem} \cdot SSA_{Cem} \cdot (1 - \theta_{alite-OPC}^*)}{V_L} \\
 &+ \frac{f_{CH} \cdot (1 - \theta_{CH}^*) \cdot (m_{CH} \cdot SSA_{CH} + (1 - \phi_{alite}) \cdot m_{Cem} \cdot SSA_{Cem})}{V_L}
 \end{aligned} \tag{7-17}$$

The above-mentioned surface coverages are estimated using the equations presented in section 7.2.3, with an adsorption plateau of 0.22 mg/m² for alite in OPC rather than the value of 0.83 mg/m² CEM from the Langmuir isotherm.

With this in hand, we replot data in Figure 7.11b, adding data with sucrose as triangles in Figure 7.12. The filled triangles that show the good alignment with the original data are obtained with the above assumptions concerning surface coverages. The open triangles are in contrast obtained if saturation plateau on OPC is used to estimate surface coverages. Their clearly different behaviors underline the importance of choosing an adsorption behavior of sucrose on C₃S surface, which is consistent with our findings from chapter 6.

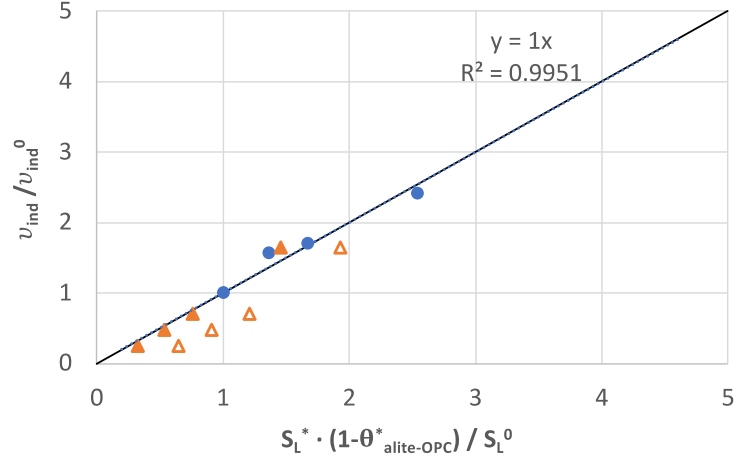


Figure 7.12. Addition of data obtained with sucrose to Figure 7.11b. Filled triangles show result of analysis considering that sucrose adsorption on OPC-non alite surface is similar to sucrose adsorption on CH surface, and that the adsorption happens on OPC- alite surface has a plateau consistent with the one inferred for OPC-alite as reported in chapter 6. Open triangles are obtained without those consideration on the difference of adsorption in OPC between alite and other surfaces.

In summary, our results show that the normalized velocity of OPC hydration in the induction period can be written as:

$$\frac{v_{ind}}{v_{ind}^0} = \frac{S_L^X}{S_L^0} (1 - \theta_{alite-OPC}^X) \quad (7-18)$$

where v_{ind}^0 is the hydration rate without CH sucrose, S_L^0 is ratio of the total solid surface to the liquid volume in absence of both CH and sucrose, as given in equation (7-16) for case $f_{Rest-Cem} = f_{CH}$.

7.3.3 Considerations on possible transfer from OPC to CH

In chapter 5, we found that when we assume that sucrose only adsorbs on C_3S surface, the correlation between experimental and theoretical relative velocity is very good. This suggest that sucrose has a higher affinity for C_3S surfaces than for CH surfaces. Consequently, the displacement of sucrose from C_3S surface to CH surface is not favored.

In contrast, for OPC hydration with CH and sucrose, Reiter et al. [72] proposed that sucrose adsorbs preferably on CH surface and that a transfer from OPC surface to CH is highly favored. In the next section we will discuss those results more directly, but first, in this section, we must evaluate in OPC, the role played by addition of CH on hydration rates and how this is affected by sucrose adsorption.

Indeed, in our experiments, the surface of CH impacts hydration kinetics substantially, even in absence of sucrose, contrary to what was reported by Reiter et al. Therefore, the effect of CH

does not only concern a possible sequestration of sucrose from C₃S surfaces, but also the increased deposition rate of hydrates. Adding to this complication, the available surface for deposition can be modified by sucrose adsorption. Our objective here is therefore to determine the relative importance of the change in deposition surface, term S_L^X/S_L^0 in equation (7-18), versus the change in C₃S dissolution rate, the term $(1 - \theta_{alite-OPC}^X)$ in equation (7-18).

To analyze the relative importance of these terms for increasing amounts of CH, we report the ratio of v_{ind}/v_{ind}^0 for the case with both sucrose and CH, over the case with the same sucrose dosage but no CH. The same is done for S_L^X/S_L^0 and for $(1 - \theta_{alite-OPC}^X)$. Results in Figure 7.13 clearly show that the change in velocity when adding CH is dominated by the surface deposition term.

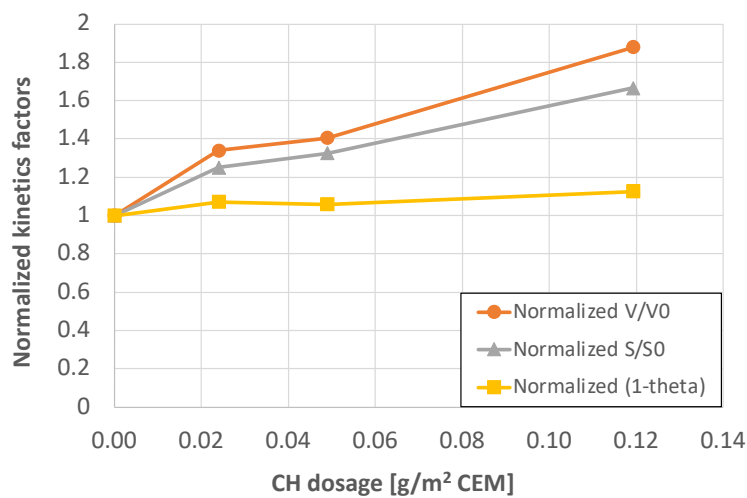


Figure 7.13. Illustration the contributions of total effective surface and surface coverage to the hydration velocity. Sucrose is considered to adsorb on OPC-alite, OPC-non alite and CH surfaces. Factors for the deposition of hydrates on OPC-non-C₃S surface and CH surface are the same. Circles: Normalized relative velocities, triangles: normalized relative total effective surface and squares: normalized $(1 - \theta_{alite-OPC}^*)$ at each CH dosage.

7.3.4 Comparison with Reiter's results

A previous work from Reiter [73] in our group showed that the retardation of OPC (CEM I 52.5R) hydration can be cancelled by addition of CH, and this cancellation was proportional to the total CH surface in hydration system (Figure 7.14). He proposed that sucrose adsorbs preferably on CH surface comparing to other phases in OPC, which reduced the retardation by reducing the surface coverage of sucrose on OPC. He also observed a 80% initial adsorption of sucrose on OPC for low sucrose dosages (Figure 7.15), while in our case, this value is only 30% but stronger retardation is obtained with the same sucrose dosage (in mg/m² CEM) as he used.

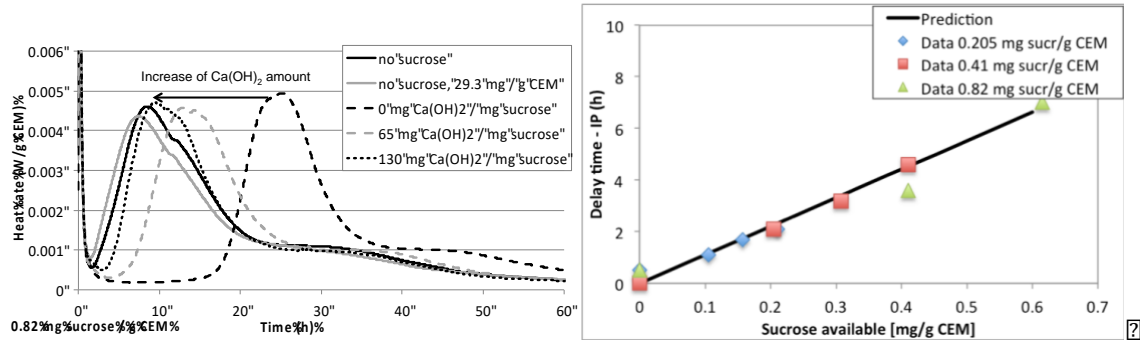


Figure 7.14. (left) Heat rate in cement pastes containing both sucrose and CH. The addition of portlandite reduces the retardation caused by sucrose, the addition of CH alone accelerates hydration to a minor extent. (right) Delay of hydration onset for combinations of sucrose and CH, subtracting the quantity of sucrose adsorbed on CH calculated from the plateau of the adsorption isotherm of sucrose and CH. (Adapted from Reiter [73]).

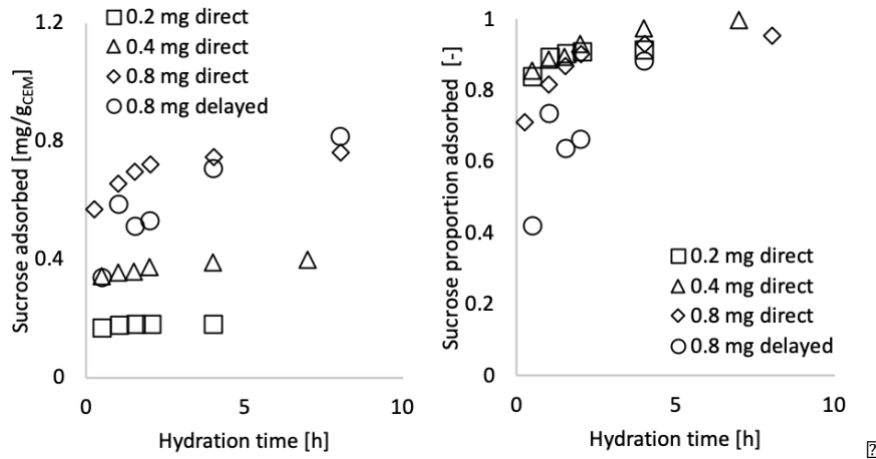


Figure 7.15. (left) Heat Adsorption of sucrose in Portland cement pore solution, increasing over time (left) absolute adsorption (right) adsorption relative to added sucrose indicating almost full adsorption. (Adapted from Reiter [73]).

Considering the definition of hydration velocity given in section 7.2.5, the $\overline{H_{alite}}$ is temperature dependent but it is independent to sucrose dosages. We can write

$$\frac{v_{ind}^0}{v_{ind}} = \frac{t_{os}}{t_{os}^0} = 1 + \frac{\Delta t_{os}}{t_{os}^0} = \frac{S_L^0}{S_L^X \cdot (1 - \theta_{alite-OPC}^X)} \quad (7-19)$$

And we have

$$\frac{\Delta t_{os}}{t_{os}^0} = \frac{\Delta S_L^X}{S_L^X \cdot (1 - \theta_{alite-OPC}^X)} + \frac{\theta_{alite-OPC}^X}{1 - \theta_{alite-OPC}^X} \quad (7-20)$$

Assuming adsorption on C₃S follows a Langmuir adsorption, we have:

$$\frac{\Delta t_{os}}{t_{os}^0} = \frac{\Delta S_L^X}{S_L^X \cdot (1 - \theta_{alite-OPC}^X)} + K_T^{alite-OPC} \cdot c_{sol} \quad (7-21)$$

If sucrose preferably covers CH surface and CH reaches its adsorption plateau, the solution concentration of sucrose c_{sol} would be depleted by an amount $S_L^{CH} \cdot c_{\infty}^{CH}$. So, we can defined an effective dosage of sucrose:

$$c_{dos}^* = c_{dos} - S_L^{CH} \cdot c_{\infty}^{CH} \quad (7-22)$$

Moreover, if adsorption onto cement lies in the linear range, the solution concentration is proportional to dosage, in this case the effective dosage c_{dos}^* , so:

$$\frac{\Delta t_{os}}{t_{os}^0} = \frac{\Delta S_L^X}{S_L^X \cdot (1 - \theta_{alite-OPC}^X)} + \alpha K_T^{OPC} \cdot c_{dos}^* \quad (7-23)$$

If the surface effect is negligible, the term ΔS_L^X can be neglected and we get:

$$\frac{\Delta t_{os}}{t_{os}^0} \cong \alpha K_T^{OPC} \cdot c_{dos}^* \quad (7-24)$$

which is the result reported by Reiter.

In our case, the hydration velocity is dominated by surface effect. But in Reiter's work, this effect was either not pronounced or being cancelled for some reasons. This may be caused by the fractions difference of varies phases in clinker, and/or the content of other chemical components in OPC. Table 7.2 presents the main active components of different OPC used in this thesis and in Reiter's work.

Table 7.2. Main active components of different OPC used in this thesis and in Reiter's work.

	Alite (%)	Belite (%)	C ₃ A (%)	C ₄ AF (%)	Hemihydrate (%)	Anhydrate (%)	Gypsum (%)
CEM I 52.5R*	64.6	9.2	5.2	11.6	5.2	-	3.0
CEM I 52.5R	62.1	9.7	4.5	18.3	-	0.2	3.1
CEM I 42.5R	63.0	4.1	2.7	21.4	-	2.4	1.1

* OPC used in Reiter's work.

7.4 Conclusions

The addition of CH modifies the kinetics of OPC hydration no matter whether sucrose is present or not. Without sucrose, the OPC hydration is accelerated and the extent of acceleration in the induction period is proportional to the total available surface in the system after applying an efficiency factor for CH. This value is much lower than 1 when assuming no hydrates deposit on non-alite surfaces, while it is almost equal to 1 when considering the hydrates deposit the same way on non-alite surface as on CH surface. Comparing to C₃S hydrating only with CH (efficiency factor 1.27), the efficiency factor in the second case for CH hydrating with OPC appears to have a similar value, suggesting that the ability of CH for consuming ions from OPC pore solution is similar than from C₃S.

In C₃S/CH system, the sucrose adsorption isotherm is linear for CH in the dosage range of interest, but not for C₃S. However, this behavior is inverted for OPC/CH system. Additionally, the proper adsorption plateau should be used for calculating the total effective surface in the system. Consistently with this finding, we take the alite fraction into account for the total effective surface, with a value of 0.22 mg/m² for the sucrose adsorption plateau on alite surfaces contained in OPC.

Regarding to the sucrose distribution in blended OPC/CH system, we notice that sucrose more likely to adsorbs on both alite and CH surface. The surface effect dominates the change in hydration velocity when CH is added, whereas the change in surface coverage of alite by sucrose resulting from CH addition does not substantial impact the hydration rate. This behavior is globally consistent with what we found in C₃S/CH system, but contrasts with previous reports by Reiter et al. [72]. The systems studies differ with regard to the impact of CH on hydration kinetics in absence of sucrose for reasons that remain unclear.

7.5 Acknowledgements

Support for Ms. Weiqing Xu was provided by the SNF project (No. 172481) titled "Molecular control of cement hydration through tailored chemical admixtures".

7.6 Appendix A

This appendix presents the analysis from section 7.3.1 for which $f_{Rest-Cem} = 0$.

In Figure 7.16a, we plot velocity versus surface where the velocity is normalized by its value in absence of CH and the surface is normalized by S_L^0 calculated with equation (7-14). By doing so, we expect a slope of 1 on the plot, which is clearly not the case. This reflects the fact that OPC and CH have different abilities in consuming ions from solution and/or favoring the deposition of hydrates. As in chapter 5, an efficiency factor f_{CH} is thereby introduced to account for this. The effective surface is then be calculated with equation (7-13).

A value of 0.64 for the factor f_{CH} gives a good linear regression with a slope of 1 between v_{ind}/v_{ind}^0 and $S_L^{\#}/S_L^0$ (Figure 7.16b). This supports our hypothesis that for OPC hydrating with CH and without sucrose, the velocity in the induction period is proportional to the free surface, probably reflecting a consumption of ions from the solution and/or hydrate deposition.

In chapter 5, for C₃S hydrating with CH and without sucrose, we obtained an efficiency factor f_{CH} of 1.27, meaning that the efficiency of C₃S is lower than that of CH. In contrast, here OPC appears more efficient than CH in depositing hydrates. In both cases however, the consideration of an efficiency factor leads to a linear relation between the normalized velocity and the normalized surface, which a priori makes physical sense. However, the case assuming similar deposition on all surfaces appears even more realistic, which is why it was favored in our main analysis.

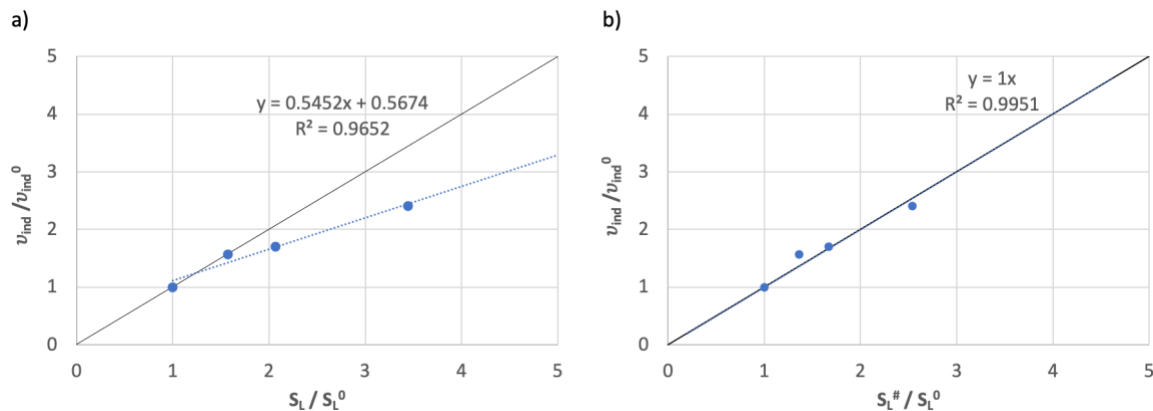


Figure 7.16. For the case $f_{Rest-Cem} = 0$, change of relative velocity in the induction period with respect to the total surface area in absence of sucrose. The reference values of v_0 and S_0 are taken for the pastes without CH. a) real surfaces, b) effective surfaces as defined in equation (7-13) with a value of 0.64 for f_{CH} .

8 Conclusions and outlook

In this chapter, we firstly summarize main outcomes from this work. Then, we develop our thoughts regarding to the remaining questions for this research topic and develop an outlook for future work.


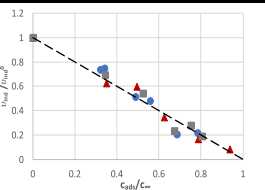
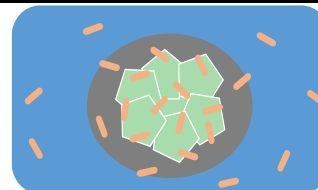
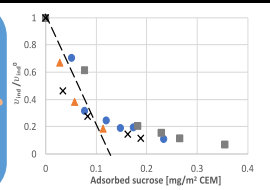

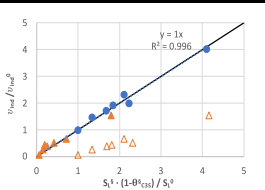
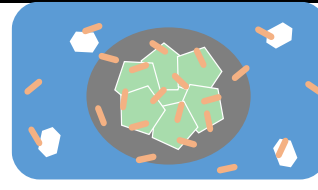
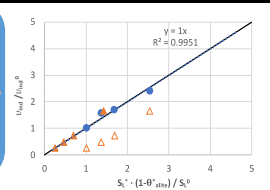
8.1 Conclusions

The objective of this thesis was to better understand the mechanisms of hydration retardation caused by sucrose, and we focused specifically on the impact of sucrose dosage and temperature on hydration kinetics in the induction period. One of our main focuses was on the mechanisms controlling the rate of hydration in that period and how they are modified by sucrose. Secondly, since sucrose adsorption is an important phenomenon, we additionally investigated this topic and in particular the ability of sucrose adsorption to inhibit the dissolution of C_3S by adding CH to single reactant system. This action was applied based on the assumption that CH may “sequester” sucrose from system and lead to its release from C_3S surfaces to reduce the hindrance of dissolution caused by adsorbed sucrose on C_3S surface.

Due to the complexity of clinker composition and coupled chemical reactions happening during hydration of OPC, we started our research with the most abundant clinker phase in its pure form: C_3S . With understanding based on this phase, we then moved to real OPC systems. It was significant to see that most of our analytical methods in C_3S systems are equally applicable to OPC. We also obtained good results that illustrated the similitudes and differences between C_3S as pure phase and alite in OPC hydration in presence of sucrose. Importantly, we gained fundamental understanding on the impact of sucrose on the rate of hydration as well as role of CH in the induction period.

In Table 8.1, we summarize the key results from chapters 4-7 respectively with schematic demonstrations of each reaction system. In graphs, green pentagons represent either C_3S as individual particles in the pure systems or alite within cement grains of industrial cement. Orange bars are sucrose molecules and white hexagons are the CH particles based on a possible shape of these crystals. The first column summarizes results obtained with C_3S , with C_3S alone in the first line and C_3S/CH in the second. The second column is organized similarly, but presents results obtained with the industrial cement. The shape in grey represents a cement particle which contains more than 60% of alite phase.

Table 8.1 A summary of main outcomes from this PhD work, with schematic demonstration of different reaction systems

  <ul style="list-style-type: none"> • Temperature dependent adsorption with 87% initial adsorption at 23 °C. • $v_{ind} = DOH_{t_{OS}}/t_{OS}$ • 2 valid models to predict sucrose adsorptions from dosages • $v_{ind} = v_{ind}^0(1 - \theta)$ • $c_{\infty} = 0.22 \text{ mg/m}^2 \text{ C}_3\text{S}$ • $E_a = 36 \text{ kJ/mol}$ 	  <ul style="list-style-type: none"> • Temperature independence adsorption with 30% initial adsorption • $v_{ind} = \overline{H_{alite}}/t_{OS}$ • 2 models valid to predict sucrose adsorptions from dosages • $c_{\infty} = 0.13 \text{ mg/m}^2 \text{ CEM} \Rightarrow c_{\infty} = 0.22 \text{ mg/m}^2 \text{ alite}$ • $E_a = 47 \text{ kJ/mol}$, similar to E_a for alite dissolution in saturated CH system[102]
  <ul style="list-style-type: none"> • Linear adsorption of sucrose on CH but not on C₃S • 2 methods to calculate θ_{C_3S} and θ_{CH} • $v_{ind} = DOH_{t_{OS}}/t_{OS}$ • Total effective surface affects hydration kinetics • Deposition factor $f_{CH} = 1.27$ • $\frac{v_{ind}}{v_{ind}^0} = \frac{S_L^s}{S_L^0} (1 - \theta_{C_3S}^s)$ • Preferential adsorption on C₃S surfaces, no sucrose transfer to CH surfaces • E_a not determined because experiments only done at 23°C 	  <ul style="list-style-type: none"> • Linear adsorption of sucrose on OPC but not on CH • 2 methods to calculate θ_{alite} and θ_{CH}, with $c_{\infty} = 0.22 \text{ mg/m}^2$ of alite surface in OPC • $v_{ind} = \overline{H_{alite}}/t_{OS}$ • Two cases for deposition factors, $f_{Rest-Cem} = f_{CH} = 1.05$ is considered • $\frac{v_{ind}}{v_{ind}^0} = \frac{S_L^s}{S_L^0} (1 - \theta_{alite}^s)$ • No Sucrose transfers from surface of alite to CH, surface effect dominates hydration kinetics • E_a not determined because experiments only done at 23°C

Green pentagons: C₃S particles.
 Orange bars: sucrose molecules.
 White hexagons: CH particles.
 Grey oval: cement particle.
 Blue background: water/pore solution.

8.1.1 Main results for systems with pure C₃S phase

For hydration of pure C₃S with sucrose, studies on hydration kinetics were focused on the induction period because the effect of sucrose on retardation can be directly reflected by the changing of length of this period. By well defining the onset (h) for the acceleration period, which is also the end of induction period, we found that the degree of hydration at the onset ($DOH_{t_{OS}}$) is independent to sucrose dosages. This emphasises **that acceleration takes place**

once C₃S hydration reaches a critical level that is independent of sucrose dosage. The rate in induction period (v_{ind}) is then taken as the average $DOH_{t_{os}}$ for each temperature divided by the onset time. To obtain a rate of hydration expressed in a reasonable way with respect to parameters as surface coverage, represented a key step in our rationalization hydration kinetics. The importance of this step is illustrated by our work with OPC systems. Here, with careful data analysis, **we demonstrate for the first time that v_{ind}/v_{ind}^0 decreases linearly with c_{ads}/c_{∞} with a slope of 1. In other words, the rate of hydration depends on the fraction of C₃S surface not occupied by sucrose.**

Apart from obtaining elegant expressions for the role of key factors, another critical aspect is to link between sucrose dosage and adsorption. With ¹H detected INEPT NMR, the sucrose concentration in the induction period of C₃S hydration is shown to be unchanged. This allows us to develop a model to estimate the sucrose adsorption from its dosage based on Langmuir adsorption isotherm and mass balance in the system. Additionally, another model serving the same purpose was built presented. **Both models work similarly well, but the second one is even better at estimating adsorption at other temperatures without support from Langmuir isotherms.**

The ability of sucrose to hinder C₃S dissolution is further investigated by addition of CH. Definitions of v_{ind} and $DOH_{t_{os}}$ remains valid, but the estimation model based on Langmuir isotherm with needs to be extended to account for more than one surface. In this case, the empirical model lost its validity, so that we resorted to numerical solutions to obtain surface coverage of sucrose (θ) on each surface.

A challenge with CH additions is that they modified the hydration rate even in absence of sucrose. This was accounted for by considering the total effective surface for the deposition of hydrates and/or adsorption of other ions. The value of v_{ind} is found to be not only controlled by the surface coverage of sucrose on C₃S, but also by the total effective surface in the system. Regarding to the ability of CH to sequester sucrose, we concluded that this does not take place. Our results imply that **the transfer of sucrose from C₃S surface to CH surface is not favoured** in our system, which is consistent with the high affinity of sucrose for C₃S at low dosage (about 87% adsorbs) at 23 °C.

8.1.2 Main results for systems with OPC

Our experiments with OPC followed the same strategies as for pure C₃S. For OPC, v_{ind} is defined differently due to the important contribution of aluminate reactions to $DOH_{t_{os}}$. From this aspect, we focus on v_{ind} of alite phase in OPC by removing the cumulative heat of aluminate reactions from the cumulative heat at the onset. This provides an estimation of the cumulative heat coming from C₃S at the onset ($\overline{H_{alite}}$). The hydration velocity of alite phase in OPC in the induction period is then defined as $v_{ind} = \overline{H_{alite}}/t_{OS}$.

In terms of sucrose adsorption, this is found to be temperature independent with much lower initial adsorption (about 30%) on OPC when compared to pure C₃S. We also found that the empirical model worked better in this case for predicting adsorption in relation to dosage.

Different from C₃S, the correlation of v_{ind}/v_{ind}^0 with sucrose adsorption on OPC presents two regimes. It decreases rapidly and linearly with sucrose adsorption in the low dosage range. Then, above a critical dosage, the decrease of hydration rate slows down. The first regime is well described by a linear regression giving a maximum adsorption of 0.13 mg/m² CEM, which is much lower than the Langmuir adsorption plateau. However, if the fraction of alite in clinker is considered, this maximum adsorption corresponds to a value of 0.22 mg/m² of alite surface in OPC, which was found in pure C₃S. Besides, the activation energy we obtained for OPC in this period is also very close to the one for alite dissolution in saturated CH systems [102]. We did not determine the activation energy for systems containing CH, whether for C₃S or for OPC, because those measurements were only performed at one temperature. In any case, **for the first time this thesis demonstrates that the rate of hydration for alite phase in OPC only depends on the surface coverage of sucrose on alite when sucrose dosage is low. Once alite is fully saturated or at least extensively covered, adsorption on other phases becomes significant and the effectiveness of sucrose at delaying hydration decreases.**

The ability of sucrose to hinder the dissolution of alite phase in OPC is also studied by addition of CH. The rate of hydration for alite in OPC is analysed in relation to surface coverage by sucrose of the alite present in OPC (θ_{alite}) and of CH (θ_{CH}). However, special attention on the choice of adsorption plateau is required for the calculations of θ_{alite} and θ_{CH} . With low sucrose dosage used here, the hydration velocity of alite phase in OPC is governed by θ_{alite} . Therefore, the sucrose adsorption plateau on alite rather than the overall plateau on cement (similarly to the OPC without CH) should be considered. Regarding non-alite surfaces, they are best handled as behaving similarly to CH rather than to alite. As a result, we prove that **although sucrose adsorbs on both alite and CH surfaces in this system, the rate of hydration is dominated by the total effective surface. Stated differently, the change of sucrose coverage on alite caused by the addition of CH only has a minor contribution on hydration kinetics.** This finding is similarly to what we concluded for the C₃S/CH system.

As a summary of this thesis, studying the impact of sucrose on hydration first with pure C₃S phase helped to recognize the most essential factors and/or procedures to focus on. This enabled a gradual increase in complexity leading to explaining the impact of sucrose on OPC and blended systems in a way that would not have been possible otherwise. However, although we expect the unravelled principles to be broadly valid, their application in systems of growing complexity as blended cements may become non-trivial. Clarifying such questions is an important new horizon for research, that should hopefully now be in easier reach thanks to the results of this thesis.

8.2 Outlook

During this work, we mainly focused on the impact of sucrose on hydration kinetics in the induction period. We have also looked at the slope of the linear regression of acceleration period in a heat release curve. This slope explains the maximum rate (R_{max}) at which the rate of heat release increases. It corresponds to the second derivative of the heat rate being zero, which may be affected by any change in kinetic factors taking place during the acceleration period, such as specific surface area and ionic concentrations. As these factors may also be temperature dependent, the problem becomes more complicated. By assuming the reaction follows Avrami type kinetics in the acceleration period, the slope of an Arrhenius plot is E_a/n where n is the exponent in the Avrami equation. We noted that this slope is about to be 72 kJ/mol for C₃S and 78 kJ/mol for OPC, which are similar to each other. Further investigations on mathematic description of the hydration velocity in this period and even the analysis on the rate controlling step can be done based on these results. It may not be easy to analyse them from experimental data alone, but combining with modelling may be successful.

Moreover, in chapter 6 we observed for OPC, that v_{ind}/v_{ind}^0 decreases with sucrose adsorption with two distinct regimes. In this work, we focussed on understanding the hydration kinetics in first regime. The second regime that is less effective in terms of retardation caused by additional sucrose adsorption still remains unclear. Our thoughts about this second part of the problem are as follows. Once alite approaches saturation, consumption of sucrose by other clinker phase increases substantial, with C₄AF probably playing an important role therein. This would explain the much higher adsorption plateau for sucrose on OPC than on pure C₃S, as well as the incremental reduction in hydration rate at high dosages. Further research on this is however needed.

Focusing on this work, our transfer of knowledge from the hydration kinetics of pure C₃S to that of alite phase in OPC system works very well, but it is still limited to CEM I which contains more than 95% of clinker. As supplementary cementitious materials are widely used to replace clinker for lowering the CO₂ emission, it would be valuable to see whether our findings on the impact of sucrose on hydration kinetics are still valid for the hydration induction period of blended cements.

We well understand from this work that the retardation induced by sucrose is proportional to the surface not occupied by sucrose. As an interesting topic, we tried to “see” this adsorption interaction at molecular level with advanced NMR techniques. ¹H{¹³C} 2D HETCORE NMR succeed in detecting ¹³C labelled sucrose (dosage 0.12 mg/m² ²⁹Si enriched C₃S) in highly hydrated ²⁹Si enriched C₃S system. However, detecting adsorbed sucrose with ¹H{²⁹Si} 2D HETCORE NMR failed. It was impossible to distinguish ¹H of sucrose from ¹H of -Si-OH from hydrated ²⁹Si enriched C₃S system in the spectrum, because the broadness of that ¹H signal peak overlapped the region where ¹H signal from sucrose should appear. This failure may be due to the low sensitivity of this technique on sucrose with low dosage.

A special pulse sequence was tried to map directly ¹³C-²⁹Si in 2 dimensions. This NHHC (or CHHC) pulse sequence received its success in protein NMR. It helps to detect the proton

connected carbon (H-C) next to the proton connected nitrogen (H-N) with the result of a 2D ^{15}N - ^{13}C spectrum, and it also provides encoded information on the distance between two protons [110]. With a freeze-dried sample of ^{29}Si enriched C_3S shortly contacted with sucrose solution (20 min, sucrose dosage 0.20 mg/m^2 ^{29}Si enriched C_3S), we tried to setup the NHHC pulse sequence. The sample should have a hydroxylated surface without formation of hydrates. In our case, NHHC should be written as SiHHC, we expected it to transfer the magnetization from ^1H in sucrose molecule to ^{13}C in sucrose molecule via cross polarization. In three successive steps, the magnetization would be firstly transferred back to sucrose ^1H , then to other ^1H nuclei nearby (at the hydrated surface), and finally onto ^{29}Si on hydrated C_3S surface for detection. The chemical shift should be evolved on the ^{13}C nuclei following the initial cross polarization and detection on the ^{29}Si nuclei [110]. This was supposed to give a 2D ^{13}C - ^{29}Si spectrum which directly shows the adsorption of sucrose on C_3S surface. However, the transfer of magnetization for individual step succeeds, but the overall transfer failed in getting signal. This was very likely also caused by the low sucrose dosage.

Based on these experiences, stronger signal enhancement is needed as sucrose has low adsorption plateau on C_3S . DNP surface enhanced NMR is an option to try, but the effect of using radicals and solvent during sample preparation on sucrose adsorption should be checked to ensure the reliability of results. If successful, such experiments would add welcome molecular insight to the type of interpretation proposed in this thesis and that relies on interpretation of more macroscopic results.

9 References

- [1] J. H. Sharp, E. M. Gartner, and D. E. Macphee, “Novel cement systems (sustainability),” *Advances in Cement Research*, vol. 22, no. 4, pp. 195–202, Oct. 2010.
- [2] R. J. Flatt, N. Roussel, and C. R. Cheeseman, “Concrete: An eco material that needs to be improved,” *J Eur Ceram Soc*, vol. 32, no. 11, pp. 2787–2798, Aug. 2012, doi: 10.1016/j.jeurceramsoc.2011.11.012.
- [3] P. C. Nkinamubanzi, S. Mantellato, and R. J. Flatt, *Superplasticizers in practice*. Elsevier Ltd, 2016. doi: 10.1016/B978-0-08-100693-1.00016-3.
- [4] P. C. Aïtcin, “Accelerators,” *Science and Technology of Concrete Admixtures*, pp. 405–413, 2016, doi: 10.1016/B978-0-08-100693-1.00019-9.
- [5] P. C. Aïtcin, “Retarders,” *Science and Technology of Concrete Admixtures*, pp. 395–404, 2016, doi: 10.1016/B978-0-08-100693-1.00018-7.
- [6] R. Gagné, *Shrinkage-reducing admixtures*. Elsevier Ltd, 2016. doi: 10.1016/B978-0-08-100693-1.00023-0.
- [7] R. Gagné, *Air entraining agents*. Elsevier Ltd, 2016. doi: 10.1016/B978-0-08-100693-1.00017-5.
- [8] D. Marchon, “Controlling cement hydration through the molecular structure of comb copolymer superplasticizers,” 2016.
- [9] J. W. Bullard *et al.*, “Mechanisms of cement hydration,” *Cement and Concrete Research*, vol. 41, no. 12, pp. 1208–1223, Dec. 2011. doi: 10.1016/j.cemconres.2010.09.011.
- [10] E.J. Gartner, J.F. Young, D.A. Damidot, and I. Jawed, “Chapter 3: hydration of Portland Cement,” 2001.
- [11] D. Marchon and R. J. Flatt, *Mechanisms of cement hydration*. Elsevier Ltd, 2016. doi: 10.1016/B978-0-08-100693-1.00008-4.
- [12] K. Scrivener, A. Ouzia, P. Juilland, and A. Kunhi Mohamed, “Advances in understanding cement hydration mechanisms,” *Cem Concr Res*, vol. 124, no. June, p. 105823, 2019, doi: 10.1016/j.cemconres.2019.105823.
- [13] H. N. Stein and J. M. Stevels, “Influence of silica on the hydration of 3 CaO,SiO₂,” *Journal of Applied Chemistry*, vol. 14, no. 8, pp. 338–346, May 2007, doi: 10.1002/jctb.5010140805.
- [14] H. M. Jennings and P. L. Pratt, “An experimental argument for the existence of a protective membrane surrounding portland cement during the induction period,” 1979.
- [15] H. M. JENNINGS, “Aqueous Solubility Relationships for Two Types of Calcium Silicate Hydrate,” *Journal of the American Ceramic Society*, vol. 69, no. 8, pp. 614–618, 1986, doi: 10.1111/j.1151-2916.1986.tb04818.x.
- [16] E. M. GARTNER and H. M. JENNINGS, “Thermodynamics of Calcium Silicate Hydrates and Their Solutions,” *Journal of the American Ceramic Society*, vol. 70, no. 10, pp. 743–749, 1987, doi: 10.1111/j.1151-2916.1987.tb04874.x.
- [17] P. Barret and D. Ménétrier, “FILTER DISSOLUTION OF C3S AS A FUNCTION OF THE LIME CONCENTRATION IN A LIMITED AHOUNT OF LIME WATER,” 1980.
- [18] P. Barret, D. Ménétrier, and D. Bertrandie, “MECHANISM OF C3S DISSOLUTION AND PROBLEM OF THE CONGRUENCY IN THE VERY INITIAL PERIOD AND LATER ON,” 1983.
- [19] S. Garrault and A. Nonat, “Hydrated layer formation on tricalcium and dicalcium silicate surfaces: Experimental study and numerical simulations,” *Langmuir*, vol. 17, no. 26, pp. 8131–8138, Dec. 2001, doi: 10.1021/la011201z.

- [20] S. Garrault, T. Behr, and A. Nonat, "Formation of the C-S-H layer during early hydration of tricalcium silicate grains with different sizes," *Journal of Physical Chemistry B*, vol. 110, no. 1, pp. 270–275, Jan. 2006, doi: 10.1021/jp0547212.
- [21] S. Garrault-Gauffinet and A. Nonat, "Experimental investigation of calcium silicate hydrate (C-S-H) nucleation," 1999.
- [22] E. Pustovgar *et al.*, "Understanding silicate hydration from quantitative analyses of hydrating tricalcium silicates," *Nat Commun*, vol. 7, Mar. 2016, doi: 10.1038/ncomms10952.
- [23] P. Juilland, E. Gallucci, R. Flatt, and K. Scrivener, "Dissolution theory applied to the induction period in alite hydration," *Cem Concr Res*, vol. 40, no. 6, pp. 831–844, Jun. 2010, doi: 10.1016/j.cemconres.2010.01.012.
- [24] P. Juilland and E. Gallucci, "Morpho-topological investigation of the mechanisms and kinetic regimes of alite dissolution," *Cem Concr Res*, vol. 76, pp. 180–191, Jun. 2015, doi: 10.1016/j.cemconres.2015.06.001.
- [25] L. Nicoleau, E. Schreiner, and A. Nonat, "Ion-specific effects influencing the dissolution of tricalcium silicate," *Cem Concr Res*, vol. 59, pp. 118–138, 2014, doi: 10.1016/j.cemconres.2014.02.006.
- [26] L. Nicoleau and A. Nonat, "A new view on the kinetics of tricalcium silicate hydration," *Cem Concr Res*, vol. 86, pp. 1–11, Aug. 2016, doi: 10.1016/j.cemconres.2016.04.009.
- [27] F. Bellmann, T. Sowoidnich, H. M. Ludwig, and D. Damidot, "Dissolution rates during the early hydration of tricalcium silicate," *Cem Concr Res*, vol. 72, pp. 108–116, 2015, doi: 10.1016/j.cemconres.2015.02.002.
- [28] V. Robin, B. Wild, D. Daval, M. Pollet-Villard, A. Nonat, and L. Nicoleau, "Experimental study and numerical simulation of the dissolution anisotropy of tricalcium silicate," *Chem Geol*, vol. 497, pp. 64–73, Oct. 2018, doi: 10.1016/j.chemgeo.2018.08.023.
- [29] P. Juilland, L. Nicoleau, R. S. Arvidson, and E. Gallucci, "Advances in dissolution understanding and their implications for cement hydration," *RILEM Technical Letters*, vol. 2, pp. 90–98, Sep. 2017, doi: 10.21809/rilemtechlett.2017.47.
- [30] L. Nicoleau, A. Nonat, and D. Perrey, "The di- and tricalcium silicate dissolutions," *Cem Concr Res*, vol. 47, pp. 14–30, 2013, doi: 10.1016/j.cemconres.2013.01.017.
- [31] L. Nicoleau and M. A. Bertolim, "Analytical Model for the Alite (C3S) Dissolution Topography," *Journal of the American Ceramic Society*, vol. 99, no. 3, pp. 773–786, Mar. 2016, doi: 10.1111/jace.13647.
- [32] K. Scrivener, A. Ouzia, P. Juilland, and A. Kunhi Mohamed, "Advances in understanding cement hydration mechanisms," *Cement and Concrete Research*, vol. 124. Elsevier Ltd, Oct. 01, 2019. doi: 10.1016/j.cemconres.2019.105823.
- [33] E. Pustovgar *et al.*, "Influence of aluminates on the hydration kinetics of tricalcium silicate," *Cem Concr Res*, vol. 100, no. June, pp. 245–262, 2017, doi: 10.1016/j.cemconres.2017.06.006.
- [34] S. Mantellato, M. Palacios, and R. J. Flatt, "Relating early hydration, specific surface and flow loss of cement pastes," *Materials and Structures/Materiaux et Constructions*, vol. 52, no. 1, Jan. 2019, doi: 10.1617/s11527-018-1304-y.
- [35] J. J. Thomas, "A new approach to modeling the nucleation and growth kinetics of tricalcium silicate hydration," *Journal of the American Ceramic Society*, vol. 90, no. 10, pp. 3282–3288, Oct. 2007, doi: 10.1111/j.1551-2916.2007.01858.x.
- [36] J. J. Thomas, H. M. Jennings, and J. J. Chen, "Influence of nucleation seeding on the hydration mechanisms of tricalcium silicate and cement," *Journal of Physical Chemistry C*, vol. 113, no. 11, pp. 4327–4334, Mar. 2009, doi: 10.1021/jp809811w.

- [37] J. J. Thomas, A. J. Allen, and H. M. Jennings, “Hydration kinetics and microstructure development of normal and CaCl₂-accelerated tricalcium silicate pastes,” *Journal of Physical Chemistry C*, vol. 113, no. 46, pp. 19836–19844, 2009, doi: 10.1021/jp907078u.
- [38] J. W. Bullard and R. J. Flatt, “New insights into the effect of calcium hydroxide precipitation on the kinetics of tricalcium silicate hydration,” *Journal of the American Ceramic Society*, vol. 93, no. 7, pp. 1894–1903, Jul. 2010, doi: 10.1111/j.1551-2916.2010.03656.x.
- [39] H. M. Jennings, “A model for the microstructure of calcium silicate hydrate in cement paste,” 2000.
- [40] H. M. Jennings, J. J. Thomas, J. S. Gevrenov, G. Constantinides, and F. J. Ulm, “A multi-technique investigation of the nanoporosity of cement paste,” *Cem Concr Res*, vol. 37, no. 3, pp. 329–336, Mar. 2007, doi: 10.1016/j.cemconres.2006.03.021.
- [41] H. M. Jennings, J. W. Bullard, J. J. Thomas, J. E. Andrade, J. J. Chen, and G. W. Scherer, “Characterization and Modeling of Pores and Surfaces in Cement Paste: Correlations to Processing and Properties,” 2008. [Online]. Available: http://infoscience.epfl.ch/record/200217/files/EPFL_TH6296.pdf
- [42] E. M. Gartner, “A PROPOSED MECHANISM FOR THE GROWTH OF C-S-H DURING THE HYDRATION OF TRICALCIUM SILICATE,” 1997.
- [43] D. L. Kantro, S. Brunauer, C. H. Weise, and V. 66, “DEVELOPMENT OF SURFACE IN THE HYDRATION OF CALCIUM SILICATES. II. EXTENSION OF INVESTIGATIONS TO EARLIER AND LATER STAGES OF HYDRATION.” [Online]. Available: <https://pubs.acs.org/sharingguidelines>
- [44] J. F. YOUNG, H. S. TONG, and R. L. BERGER, “Compositions of Solutions in Contact with Hydrating Tricalcium Silicate Pastes,” *Journal of the American Ceramic Society*, vol. 60, no. 5–6, pp. 193–198, 1977, doi: 10.1111/j.1151-2916.1977.tb14104.x.
- [45] J. D. Birchall, A. J. Howard, and J. E. Bailey, “On the hydration of Portland cement,” *Proceedings of the Royal Society A*, 360, pp. 445–453, 1978.
- [46] S. Bishnoi and K. L. Scrivener, “Studying nucleation and growth kinetics of alite hydration using μ ic,” *Cem Concr Res*, vol. 39, no. 10, pp. 849–860, Oct. 2009, doi: 10.1016/j.cemconres.2009.07.004.
- [47] Bazzoni.A, “Study of early hydration mechanisms of cement by means of electron microscopy,” *Thèse EPFL n°6296*, 2014, [Online]. Available: http://infoscience.epfl.ch/record/200217/files/EPFL_TH6296.pdf
- [48] W.A. Corstanje, H.N. Stein, and J.M. Stevels, “Hydration reactions in pastes C3S + C3A + CaSO₄·2aq + H₂O at 25°C.I,” *Cem Concr Res*, vol. 3, no. 6, pp. 791–806, 1973.
- [49] W. A. Corstanje, H. N. Stein, and J. M. Stevels, “HYDRATION REACTIONS IN PASTES C3S + C3A + CaSO₄·2aq + water AT 25°C.III z),” Pergamon Press, Inc, 1974.
- [50] E. Breval and H. F. W. Taylor, “C3A HYDRATION,” Pergamon Press, Inc, 1976.
- [51] S. Joseph, J. Skibsted, and Ö. Cizer, “A quantitative study of the C3A hydration,” *Cem Concr Res*, vol. 115, pp. 145–159, Jan. 2019, doi: 10.1016/j.cemconres.2018.10.017.
- [52] A. Quennoz and K. L. Scrivener, “Hydration of C 3A-gypsum systems,” *Cem Concr Res*, vol. 42, no. 7, pp. 1032–1041, 2012, doi: 10.1016/j.cemconres.2012.04.005.
- [53] A. C. Lasaga, *KINETIC THEORY IN THE EARTH SCIENCES*. Princeton University Press, 1998.
- [54] H. Minard, S. Garrault, L. Regnaud, and A. Nonat, “Mechanisms and parameters controlling the tricalcium aluminate reactivity in the presence of gypsum,” *Cem Concr Res*, vol. 37, no. 10, pp. 1418–1426, Oct. 2007, doi: 10.1016/j.cemconres.2007.06.001.

- [55] G. Geng *et al.*, “Synchrotron X-ray nanotomographic and spectromicroscopic study of the tricalcium aluminate hydration in the presence of gypsum,” *Cem Concr Res*, vol. 111, pp. 130–137, Sep. 2018, doi: 10.1016/j.cemconres.2018.06.002.
- [56] S. Pourchet, L. Regnaud, J. P. Perez, and A. Nonat, “Early C3A hydration in the presence of different kinds of calcium sulfate,” *Cem Concr Res*, vol. 39, no. 11, pp. 989–996, Nov. 2009, doi: 10.1016/j.cemconres.2009.07.019.
- [57] K. L. Scrivener, P. Juilland, and P. J. M. Monteiro, “Advances in understanding hydration of Portland cement,” *Cement and Concrete Research*, vol. 78. Elsevier Ltd, pp. 38–56, Dec. 01, 2015. doi: 10.1016/j.cemconres.2015.05.025.
- [58] D. Marchon and R. J. Flatt, *Mechanisms of cement hydration*. Elsevier Ltd, 2016. doi: 10.1016/B978-0-08-100693-1.00008-4.
- [59] N. Tenoutasse, “The hydration mechanism of C3A and C3S in the presence of calcium chloride and calcium sulfate,” in *Proceedings of the 5th International Symposium on the Chemistry of Cement*, 1968, pp. 372–378.
- [60] N. Robeyst, G. De Schutter, C. Grosse, and N. De Belie, “Monitoring the effect of admixtures on early-age concrete behaviour by ultrasonic, calorimetric, strength and rheometer measurements,” *Magazine of Concrete Research*, vol. 63, no. 10, pp. 707–721, Oct. 2011, doi: 10.1680/mac.2011.63.10.707.
- [61] J. Cheung, A. Jeknavorian, L. Roberts, and D. Silva, “Impact of admixtures on the hydration kinetics of Portland cement,” *Cem Concr Res*, vol. 41, no. 12, pp. 1289–1309, Dec. 2011.
- [62] D. Marchon and R. J. Flatt, *Impact of chemical admixtures on cement hydration*. Elsevier Ltd, 2016. doi: 10.1016/B978-0-08-100693-1.00012-6.
- [63] N. L. Thomas and J. D. Birchall, “The retarding action of sugars on cement hydration,” *Cem Concr Res*, vol. 13, no. 6, pp. 830–842, 1983.
- [64] L. Zhang, L. J. J. Catalan, R. J. Balec, A. C. Larsen, H. H. Esmaili, and S. D. Kinrade, “Effects of saccharide set retarders on the hydration of ordinary portland cement and pure tricalcium silicate,” *Journal of the American Ceramic Society*, vol. 93, no. 1, pp. 279–287, Jan. 2010, doi: 10.1111/J.1551-2916.2009.03378.X.
- [65] G. Gelardi, S. Mantellato, D. Marchon, M. Palacios, A. B. Eberhardt, and R. J. Flatt, *Chemistry of chemical admixtures*. Elsevier Ltd, 2016. doi: 10.1016/B978-0-08-100693-1.00009-6.
- [66] J. M. de Bruijn, A. P. G. Kieboom, and H. van Bekkum, “Alkaline degradation of monosaccharides III. Influence of reaction parameters upon the final product composition,” *Recueil des Travaux Chimiques des Pays-Bas*, vol. 105, no. 6, pp. 176–183, 1986, doi: 10.1002/recl.19861050603.
- [67] J. F. Young, “A REVIEW OF THE MECHANISMS OF SET-RETARDATION IN PORTLAND CEMENT PASTES CONTAINING ORGANIC ADMIXTURES,” *Cem Concr Res*, vol. 2, pp. 415–433, 1972.
- [68] B. Lina, L. Barbara, F. M. Alejandro, and L. Christophe, “Portlandite solubility and Ca²⁺ activity in presence of gluconate and hexitols,” *Cem Concr Res*, vol. 149, Nov. 2021, doi: 10.1016/j.cemconres.2021.106563.
- [69] K. I. Popov *et al.*, “¹³C NMR and electrospray ionization mass spectrometric study of sucrose aqueous solutions at high pH: NMR measurement of sucrose dissociation constant,” *Food Chem*, vol. 96, no. 2, pp. 248–253, 2006, doi: 10.1016/j.foodchem.2005.02.025.
- [70] R. ; Käser *et al.*, “Further Reduction of CO₂-Emissions and Circularity in the Cement and Concrete Industry,” in *The 16th International Congress on the Chemistry of Cement (ICCC)*, 2023, pp. 117–120. doi: 10.3929/ethz-b-000636065.

- [71] C. Nalet and A. Nonat, "Ionic complexation and adsorption of small organic molecules on calcium silicate hydrate: Relation with their retarding effect on the hydration of C3S," *Cem Concr Res*, vol. 89, pp. 97–108, 2016, doi: 10.1016/j.cemconres.2016.08.012.
- [72] L. Reiter, M. Palacios, T. Wangler, and R. J. Flatt, "Putting Concrete to Sleep and Waking It Up with Chemical Admixtures," *AMC Special Publication*, pp. 145–154, 2015.
- [73] L. Reiter, "Structural Build-up for Digital Fabrication with Concrete-Materials, Methods and Processes", doi: 10.3929/ethz-b-000456199.
- [74] C. Nalet and A. Nonat, "Effects of functionality and stereochemistry of small organic molecules on the hydration of tricalcium silicate," *Cem Concr Res*, vol. 87, pp. 97–104, Sep. 2016, doi: 10.1016/J.CEMCONRES.2016.06.002.
- [75] C. Nalet and A. Nonat, "Retarding effectiveness of hexitols on the hydration of the silicate phases of cement: Interaction with the aluminate and sulfate phases," *Cem Concr Res*, vol. 90, pp. 137–143, 2016, doi: 10.1016/j.cemconres.2016.09.018.
- [76] M. C. Garci Juenger and H. M. Jennings, "New insights into the effects of sugar on the hydration and microstructure of cement pastes," *Cem Concr Res*, vol. 32, no. 3, pp. 393–399, Mar. 2002, doi: 10.1016/S0008-8846(01)00689-5.
- [77] P. Juilland and E. Gallucci, "Hindered Calcium Hydroxide Nucleation and Growth as Mechanism Responsible for Tricalcium Silicate Retardation in Presence of Sucrose," in *Superplasticizers and Other Chemical Admixtures in Concrete Proceedings Twelfth International Conference, Beijing, China*, American Concrete Institute, 2018, pp. 143–154. doi: 10.14359/51711210.
- [78] A. Kumar *et al.*, "The Atomic-Level Structure of Cementitious Calcium Silicate Hydrate," *Journal of Physical Chemistry C*, vol. 121, no. 32, pp. 17188–17196, 2017, doi: 10.1021/acs.jpcc.7b02439.
- [79] K. L. Scrivener, T. Matschei, F. Georget, P. Juilland, and A. K. Mohamed, "Advances in hydration and thermodynamics of cementitious systems," *Cem Concr Res*, vol. 174, p. 107332, Dec. 2023, doi: 10.1016/j.cemconres.2023.107332.
- [80] B. J. Smith *et al.*, "Origins of saccharide-dependent hydration at aluminate, silicate, and aluminosilicate surfaces," *Proceedings of the National Academy of Sciences*, vol. 108, no. 22, pp. 8949–8954, 2011, doi: 10.1073/pnas.1104526108.
- [81] B. J. Smith, L. R. Roberts, G. P. Funkhouser, V. Gupta, and B. F. Chmelka, "Reactions and surface interactions of saccharides in cement slurries," *Langmuir*, vol. 28, no. 40, pp. 14202–14217, 2012, doi: 10.1021/la3015157.
- [82] R. P. Sangodkar *et al.*, "Influences of Dilute Organic Adsorbates on the Hydration of Low-Surface-Area Silicates," *J Am Chem Soc*, vol. 137, no. 25, pp. 8096–8112, 2015, doi: 10.1021/jacs.5b00622.
- [83] P. Suraneni and R. J. Flatt, "Micro-reactors to Study Alite Hydration," vol. 1641, pp. 1634–1641, 2015, doi: 10.1111/jace.13472.
- [84] M. Bishop and A. R. Barron, "Cement hydration inhibition with sucrose, tartaric acid, and lignosulfonate: Analytical and spectroscopic study," *Ind Eng Chem Res*, vol. 45, no. 21, pp. 7042–7049, Oct. 2006, doi: 10.1021/ie060806t.
- [85] L. M. Meyer and W. F. Perenchio, "Theory of concrete slump loss as related to the use of chemical admixtures," *Concrete International*, pp. 36–43, 1979.
- [86] E. Pustovgar *et al.*, "Influence of aluminates on the hydration kinetics of tricalcium silicate," *Cem Concr Res*, vol. 100, no. June, pp. 245–262, 2017, doi: 10.1016/j.cemconres.2017.06.006.
- [87] X. Li, A. Ouzia, and K. Scrivener, "Laboratory synthesis of C3S on the kilogram scale," *Cem Concr Res*, vol. 108, no. September 2017, pp. 201–207, 2018, doi: 10.1016/j.cemconres.2018.03.019.

- [88] E. Pustovgar, "Passivation Mechanism of Aluminates on the Hydration of Tricalcium Silicate," no. 23764, 2016.
- [89] M. Mercedes, C. Fernandez Thèse,) École, P. Fédérale, and D. E. Lausanne, "Effect of Particle Size on the Hydration Kinetics and Microstructural Development of Tricalcium Silicate," 2008.
- [90] N. C. Collier, J. H. Sharp, N. B. Milestone, J. Hill, and I. H. Godfrey, "The influence of water removal techniques on the composition and microstructure of hardened cement pastes," *Cem Concr Res*, vol. 38, no. 6, pp. 737–744, Jun. 2008, doi: 10.1016/j.cemconres.2008.02.012.
- [91] S. Mantellato, M. Palacios, and R. J. Flatt, "Impact of sample preparation on the specific surface area of synthetic ettringite," *Cem Concr Res*, vol. 86, pp. 20–28, Aug. 2016, doi: 10.1016/j.cemconres.2016.04.005.
- [92] S. Brunauer, P. H. Emmett, and E. Teller, "Adsorption of Gases in Multimolecular Layers," 1938. [Online]. Available: <https://pubs.acs.org/sharingguidelines>
- [93] S. Mantellato, "FLOW LOSS IN SUPERPLASTICIZED CEMENT PASTES," 2017. doi: 10.3929/ethz-b-000265510.
- [94] S. Mantellato, M. Palacios, and R. J. Flatt, "Reliable specific surface area measurements on anhydrous cements," *Cem Concr Res*, vol. 67, pp. 286–291, 2015, doi: 10.1016/j.cemconres.2014.10.009.
- [95] "Sucrose NMR spectrum," *Biological Magnetic Resonance Data Bank*.
- [96] I. J. Lowe, "INDUCTION DECAYS OF ROTATING SOLIDS," *Phys. Rev. Lett*, vol. 2, no. 7, pp. 285–287, 1959.
- [97] R. Freeman and G. A. Morris, "Enhancement of Nuclear Magnetic Resonance Signals by Polarization Transfer," *J Am Chem Soc*, vol. 101, no. 3, pp. 760–762, 1979, [Online]. Available: <https://pubs.acs.org/sharingguidelines>
- [98] G. Gemmecker and H. Kessler, "Chapter 2: Methodology and Applications of Heteronuclear and Multidimensional ¹³C NMR to the Elucidation of Molecular Structure and Dynamics in the Liquid State," 1995.
- [99] T. D. W. Claridge, "One-Dimensional Techniques," in *High-Resolution NMR Techniques in Organic Chemistry*, Elsevier, 2016, pp. 133–169. doi: 10.1016/b978-0-08-099986-9.00004-x.
- [100] B. Irvinq Langmuir, "THE ADSORPTION OF GASES ON PLANE SURFACES OF GLASS, MICA AND PLATINUM," *J Am Chem Soc*, vol. 40, no. 9, pp. 1291–1460, 1918, [Online]. Available: <https://pubs.acs.org/sharingguidelines>
- [101] D. Marchon, S. Mantellato, A. B. Eberhardt, and R. J. Flatt, *Adsorption of chemical admixtures*. Elsevier Ltd, 2016. doi: 10.1016/B978-0-08-100693-1.00010-2.
- [102] P. Juilland and E. Gallucci, "Morpho-topological investigation of the mechanisms and kinetic regimes of alite dissolution," *Cem Concr Res*, vol. 76, pp. 180–191, Oct. 2015, doi: 10.1016/J.CEMCONRES.2015.06.001.
- [103] J. J. Thomas, "The instantaneous apparent activation energy of cement hydration measured using a novel calorimetry-based method," *Journal of the American Ceramic Society*, vol. 95, no. 10, pp. 3291–3296, Oct. 2012, doi: 10.1111/j.1551-2916.2012.05396.x.
- [104] S. Joseph, J. Skibsted, and Ö. Cizer, "A quantitative study of the C3A hydration," *Cem Concr Res*, vol. 115, pp. 145–159, Jan. 2019, doi: 10.1016/j.cemconres.2018.10.017.
- [105] K. Luke and G. Luke, "Effect of sucrose on retardation of Portland cement," *Advances in cement research*, vol. 12, no. 1, pp. 9–18, Jan. 2000.
- [106] E. V Ivanova, E. P. Andreeva, and N. P. Stukalova, "ADSORPTION INTERACTIONS IN HYDRATION OF INDIVIDUAL BINDERS IN CARBOHYDRATE SOLUTIONS," 1978.

- [107] E. V. Ivanova, E. P. Andreeva, N. P. Stukalova, and O. V. Tikhonova, "Ivanova et al, Sucrose and aluminoferrite, Journal of applied chemistry of the USSR copy," *Journal of applied chemistry of the USSR copy*, vol. 53, no. 1, pp. 181–185, 1978.
- [108] P. W. Brown, "Kinetics of Tricalcium Aluminate and Tetracalcium Aluminoferrite Hydration in the Presence of Calcium Sulfate," *Journal of the American Ceramic Society*, vol. 76, no. 12, pp. 2971–2976, 1993, doi: 10.1111/j.1151-2916.1993.tb06597.x.
- [109] P. W. BROWN, "Early Hydration of Tetracalcium Aluminoferrite in Gypsum and Lime-Gypsum Solutions," *Journal of the American Ceramic Society*, vol. 70, no. 7, pp. 493–496, 1987, doi: 10.1111/j.1151-2916.1987.tb05682.x.
- [110] A. Lange, S. Luca, and M. Baldus, "Structural constraints from proton-mediated rare-spin correlation spectroscopy in rotating solids," *J Am Chem Soc*, vol. 124, no. 33, pp. 9704–9705, Aug. 2002, doi: 10.1021/ja026691b.